The impact of smooth muscle cell ageing upon actin cytoskeleton organisation, adhesion and motility

Porter, Lauren Jade

Awarding institution:
King's College London

The impact of smooth muscle cell ageing upon actin cytoskeleton organisation, adhesion and motility

Lauren Porter
0859666

Thesis submitted for the degree of Doctor of Philosophy
2013

Supervisors: Dr Derek Warren & Professor Cathy Shanahan

King's College London
BHF Centre of Research Excellence
Division of Cardiovascular Medicine
James Black Centre

Declaration

I declare that the work undertaken in this thesis is my own original work, except where acknowledged in the text.

Lauren Porter

King's College London

This thesis is dedicated to my whole family for simply being brilliant and for their constant support, encouragement and understanding

xxx

Acknowledgements

First and foremost, I thank my supervisors Derek Warren and Cathy Shanahan for their continual support and guidance throughout the past 3 years, for which I am extremely grateful. I would especially like to thank Derek for putting up with me on a daily basis and always providing great supervision with the utmost enthusiasm and patience. I couldn't have wished for better supervisors, Derek and Cathy are inspirational people and I feel very fortunate to have known and worked with them. My gratitude also extends to Daniel Soong and Mark Holt from the Randall Division for dedicating their time towards my project and assisting with all microscopy techniques and data analysis. I would also like to acknowledge the British Heart Foundation and King's College London for financial support.

I would also like to give a big thanks to Rosie Minaisah (my partner in crime in 'Team Derek') and the entire Shanahan lab who were always on hand to offer their advice and expertise as well as making the time throughout my PhD enjoyable and extremely entertaining. From day one I have relied on the experience and invaluable advice from those in the laboratory. In particular, Dipan Rajgor, Daniel J Brayson, Anne Jacob and Aisling Williams have been crucial to the success of my project. Huge thanks also go to my friends and colleagues at the James Black Centre, especially Hannah Tomlins, Roshni Molls and all of the hot desk dwellers, it has been an absolute pleasure to have worked here and I feel very privileged to have met you all.

I would like to take this opportunity to thank Karolina for being such an amazing friend and husband, I couldn't have wished to meet a better person to undergo this journey with. I would also like to thank all my friends and family for keeping me sane and smiling throughout my studies. To my closest friends, Steph, Nicholl, Rach and Lynds, your friendship and encouragement has helped more than you know. To my family, thank you for keeping me grounded and always providing a loving home away from London. Last but not least, a special thank you goes to my little one, Dr Simpson, for being amazing in so many ways.

To all of you, without all of your support and encouragement this would not have been possible. Thank you x

Glossary of Abbreviations

ACAFA	Actin cap associated focal adhesion
Arp	Actin-related protein
BSA	Bovine serum albumin
CH	Calponin homology
DAPI	4’,6’-Diamidino-2-Pheylindoledihydrochloride
DMEM	Dulbecco's modified eagle medium
DNA	Deoxyribose nucleic acid
ECM	Extracellular matrix
EDMD	Emery-Dreifuss muscular dystrophy
ER	Endoplasmic reticulum
ERK	Extracellular signal-regulated kinase
FAK	Focal adhesion kinase
F-actin	Filamentous actin
FBS	Foetal bovine serum
FRAP	Fluorescence recovery after photobleaching
FTI	Farnesyltransferase inhibitor
GAPs	GTPase-activating proteins
GDIs	Guanine nucleotide dissociation inhibitors
GEFs	Guanine nucleotide exchange factors
GFP	Green fluorescent protein
HGPS	Hutchinson-Gilford progeria syndrome
INM	Inner nuclear membrane
KASH	Klarsicht, Anc-1, Syne-1 homology
LAP	Lamina-associated protein
LIMK	LIM kinase
LINC	Linker of the nucleoskeleton and cytoskeleton

MAPK	Mitogen-activated protein kinase
MEF	Mouse embryonic fibroblast
MKL1	Megakaryoblastic leukaemia 1
MLC	Myosin light chain
MMP	Matrix metalloproteinase
NE	Nuclear envelope
Nesprin	Nuclear envelope, spectrin repeat-containing protein
NPC	Nuclear pore complex
ONM	Outer nuclear membrane
PAK	P21-activated protein kinase
PBS	Phosphate buffered saline
PDT	Population doubling time
PNS	Perinuclear space
PDGF	Platelet-derived growth factor
qPCR	Quantitative polymerase chain reaction
ROCK	Rho-associated protein kinase
ROI	Region of interest
ROS	Reactive oxygen species
RT	Room temperature
SaβG	Senescence-associated β-galactosidase
SDS	Sodium dodecyl sulphate
siRNA	Small interfering RNA
SUN	Sad1p-UNC84
VSMC	Vascular smooth muscle cell
WASP	Wiskott-Aldrich Syndrome protein
WAVE	WASP family verprolin homology

Abstract

Vascular smooth muscle cell (VSMC) phenotypic switching, from a contractile to a migratory phenotype, is essential for vascular repair and is compromised in ageing. Phenotypic transition involves dramatic actin reorganisation which is regulated by the linker of the nucleoskeleton and cytoskeleton (LINC) complex that spans the nuclear envelope (NE). The LINC complex physically anchors cytoskeletal filaments to the nucleoplasm via nesprin-SUN-nuclear lamina connections which enable rapid biophysical signalling between the nuclear interior and exterior. The nuclear lamina consists of A and B-type lamins that maintain nuclear architecture, however, the lamin A precursor protein, prelamin A, is a biomarker of VSMC ageing and this project investigates the impact of prelamin A upon LINC complex function.

During VSMC ageing *in-vitro*, prelamin A accumulates at the presenescent growth phase which is associated with cellular elongation and focal adhesion reorganisation. Interference reflection imaging (IRM) and time-lapse microscopy revealed that presenescent VSMCs exhibit increased focal adhesion turnover with enhanced migratory speed and persistence. Importantly, prelamin A accumulation induced by siRNA-mediated knockdown of its processing enzyme, FACE-1, reiterates these morphological changes and enhances migratory persistence. Moreover, RhoA and Rac1 are well-established regulators of cell motility and their expression and activity diminishes in presenescent and FACE-1 depleted VSMCs. Fluorescence recovery after photobleaching (FRAP) also revealed that nuclear lamina disruption increases nesprin-2 dynamics at the nuclear exterior. Thus, we suggest that prelamin A impacts on actin-regulated processes including cell shape and motility via the LINC complex.

We utilised an siRNA-mediated approach to investigate the importance of other LINC complex components in regulating cell morphology and migration. Interestingly, SUN2 levels decrease during *in-vitro* VSMC ageing and SUN2 knockdown enhances the migratory speed of VSMCs and fibroblasts similarly to presenescent VSMCs. The role of nesprins in regulating cell phenotype varies between different cells, highlighting that LINC complex organisation and function is flexible and cell-type specific.

Together, our data reveal that the LINC complex is a versatile structure that is specialised to cell function and is an important regulator of cellular morphology, focal adhesion organisation, Rho GTPase activity and migration. VSMC ageing is associated with prelamin A accumulation and loss of SUN2 expression which consequently deregulates LINC complex organisation and functioning. Therefore, LINC complex disruption gives rise to an aged VSMC phenotype which we predict may underlie cardiovascular diseases such as atherosclerosis.

In addition, IRM captured the release of adhesion-like structures, termed cell traces, from the rear of migrating VSMCs that outline their migratory path. Cell traces form physical tracks that enhance the speed and migrational directionality of neighbouring VSMCs. Therefore, we predict that cell traces support VSMC migration to injury sites and are important for vessel repair.

Table of Contents

Chapter 1: Introduction 11
1.1 The vessel wall: in health and disease 12
1.2 Vascular smooth muscle cell phenotypic switching 13
1.3 Actin cytoskeleton remodelling during cell migration 14
1.3.1 The cell migration cycle 15
1.4 The role of focal adhesions in cell migration 17
1.4.1 Integrins: central focal adhesion components 17
1.4.2 Vinculin stabilises focal adhesion complexes 19
1.4.3 Focal adhesions regulate cell signalling pathways 19
1.5 Modes of cell migration 20
1.6 The role of Rho GTPases in cell migration 21
1.6.1 Rho GTPase targets and downstream signalling 22
1.7 Nuclear regulation of cell migration 25
1.7.1 The nuclear envelope 25
1.7.2 The nuclear lamina and prelamin A processing 25
1.7.3 Nesprins 27
1.7.4 The LINC complex 29
1.7.5 LINC complex diversity 29
1.7.6 The LINC complex in human disease: nuclear envelopathies 31
1.8 VSMC ageing 35
1.8.1 VSMC senescence drives the development of atherosclerosis 35
1.8.2 The impact of senescence on VSMC phenotype 36
1.8.3 Progerin and prelamin A drive VSMC ageing 37
1.9 Hypothesis & Project Aims 40
Chapter 2: Materials and Methods 41
2.1 Cell culture 42
2.1.1 Human vascular smooth muscle cells (VSMCs) 42
2.1.2 MRC-5 cells 42
2.1.3 Human osteosarcoma cell line (U2OS) 42
2.1.4 siRNA-mediated interference 43
2.1.5 DNA plasmid transfection 46
2.2 Molecular biology techniques 46
2.2.1 RNA extraction 46
2.2.2 Reverse transcription (cDNA synthesis) 46

2.2.3 Quantitative PCR (qPCR) 47
2.2.4 Generation of competent *E.coli* DH5α 48
2.2.5 Transformation of *E. coli* DH5α and plasmid isolation 48
2.3 Biochemical techniques 49
2.3.1 Whole cell lysate preparation 49
2.3.2 DC protein assay 49
2.3.3 Subcellular fractionation 49
2.3.4 GST pull-down assay 50
2.3.5 Western blot analysis 51
2.4 Cell biology techniques 53
2.4.1 Immunofluorescence microscopy 53
2.4.2 Time-lapse video microscopy 54
2.4.3 Fluorescence recovery after photobleaching (FRAP) 64
Chapter 3: Characterising the impact of *in-vitro* ageing and nuclear lamina disruption on smooth muscle cell and fibroblast phenotype 69
3.1 Introduction 70
3.2 Aim of this chapter 70
3.3 Results 71
3.3.1 Prelamin A accumulation is associated with VSMC ageing 71
3.3.2 FACE-1 downregulation induces prelamin A accumulation 71
3.3.3 Aged VSMCs exhibit alterations to nuclear morphology 72
3.3.4 VSMC ageing and prelamin A accumulation alters cell morphology 73
3.3.5 VSMC ageing and nuclear lamina disruptions alter focal adhesion organisation 74
3.3.6 *In-vitro* ageing and nuclear lamina disruptions affect cell migration 75
3.3.7 The impact of *in-vitro* ageing and nuclear lamina disruption on directional VSMC migration 76
3.3.8 VSMC ageing and nuclear lamina disruptions hinder Rho GTPase activity 77
3.4 Discussion 109
3.4.1 Characterising the morphological changes associated with VSMC ageing 109
3.4.2 Aged-related changes to focal adhesion formation 109
3.4.3 Age-related changes to VSMC migration 110
3.4.4 Age-related changes to Rho GTPase expression 112
3.4.5 Chapter 3 conclusions 114
3.4.6 Limitations and future work 114
Chapter 4: The role of the LINC complex in regulating cell motility 117
4.1 Introduction 118

4.2 Aim of this chapter 118
4.3 Results 119
4.3.1 VSMC ageing alters LINC complex organisation 119
4.3.2 Prelamin A accumulation disrupts LINC complex organisation 119
4.3.3 SUN2 is an important regulator of cell morphology and migration 120
4.3.4: Nesprin knockdown differentially effects VSMC and fibroblast speed 121
4.3.5 Nesprin-2 dynamics at the NE following LINC complex disruption 122
4.4 Discussion 141
4.4.1 SUN proteins regulate cellular morphology and migratory behaviour 141
4.4.2 Nesprins regulate cell migratory speed 142
4.4.3 Nuclear lamina disruption affects nesprin-2 dynamics at the ONM 142
4.4.4 Chapter 4 conclusions 143
4.4.5 Limitations and future work 144
Chapter 5: Characterising the role of cell traces in VSMC migration 145
5.1 Introduction 146
5.2 Aim of this chapter 146
5.3 Results 147
5.3.1 Migrating VSMCs *in-vitro* release traces at their trailing end 147
5.3.2 VSMCs migrate over pre-laid cell-derived traces 147
5.3.3 Cell traces provide a cell-derived matrix to assist VSMC migration 148
5.3.4 The impact of ROCK inhibition on VSMC migration 149
5.4: Discussion 160
5.4.1 VSMCs release traces at the rear during migration 160
5.4.2 Recreating cell-derived traces 161
5.4.3 ROCK inhibition prevents rear-end retraction of VSMCs 162
5.4.4 Chapter 5 conclusions 162
5.4.5 Limitations and future work 162
Chapter 6: General Discussion & Conclusions 164
6.1 Ageing and NE remodelling impacts on cell migration 165
6.2 Pathological VSMC migration 170
6.3 Cell-derived traces 173
6.4 Final conclusions 175
Reference list 176

Chapter 1: Introduction

1.1 The vessel wall: in health and disease

The human vasculature comprises of a vast, organised network of blood vessels that deliver oxygen and nutrients to tissues whilst removing metabolic waste; processes that are essential for maintaining tissue homeostasis. The blood vessel wall consists of 3 distinct layers known as tunics. The *tunica intima* is the innermost layer comprising of endothelial cells that line the vessel lumen to form a physical barrier between blood and extravascular tissues. Endothelial cells also control vessel tone by the production and release of vasoactive substances such as nitric oxide.[1] The middle layer or *tunica media* is primarily made up of vascular smooth muscle cells (VSMCs) that are arranged transversally to the longitudinal axis of the vessel.[2] This is the thickest arterial layer and determines vessel diameter and blood flow via vasoconstriction/vasodilation. The outermost *tunica adventitia* contains fibroblasts embedded within an extracellular matrix (ECM) of collagen and elastic fibres.[2, 3] The adventitial layer structurally supports the vessel, anchors nerve endings and produces reactive oxygen species (ROS) as well as numerous growth factors that regulate vascular remodelling.[2, 4, 5] Additionally, fibroblasts play an important role in vessel repair as they are able to transform into myofibroblasts in response to injury.[6] **Figure 1.1** illustrates the vessel wall composition.

In addition to providing structural integrity, the endothelium, VSMCs and fibroblasts collectively regulate vessel tone, counteract changes in blood flow and protect the vessel against damage. This involves alterations in cell proliferation, cell migration, cell death and ECM production/degradation; all of which contribute towards remodelling of vessel size and composition.[7] However, when these cellular processes are impaired, inappropriate vessel remodelling drives the pathogenesis of cardiovascular diseases including atherosclerosis and restenosis.[8]

Atherosclerosis is a complex, age-related disease arising from mild inflammation in the arterial wall that progressively worsens over time due to irregularities in blood flow, lipid overload or hypertension.[9] Atherosclerotic lesions are intimal thickenings of medium to large arteries that consist of a necrotic cell core, lipids and numerous cell types including monocyte-derived macrophages, neutrophils, endothelial cells and VSMCs.[10] Continual exposure to atherosclerotic risk factors enhances macrophage and lymphocyte infiltration into the lesion and the release of hydrolytic enzymes, chemokines, cytokines and growth factors that further induce damage and necrosis.[11] This inflammatory response stimulates VSMC proliferation and

migration from the vessel media into the intima. Intimal VSMC invasion is essential for vascular repair in early stages of atherosclerosis as increased collagen, elastin, proteoglycan and ECM deposition restructures the lesion and forms a fibrous cap to surround and stabilise the atherosclerotic plaque.[12-14] However, as the atherosclerotic cap ages, it thins due to reduced VSMC, collagen and ECM content, thus increasing the likelihood of plaque rupture and thrombosis.[15]

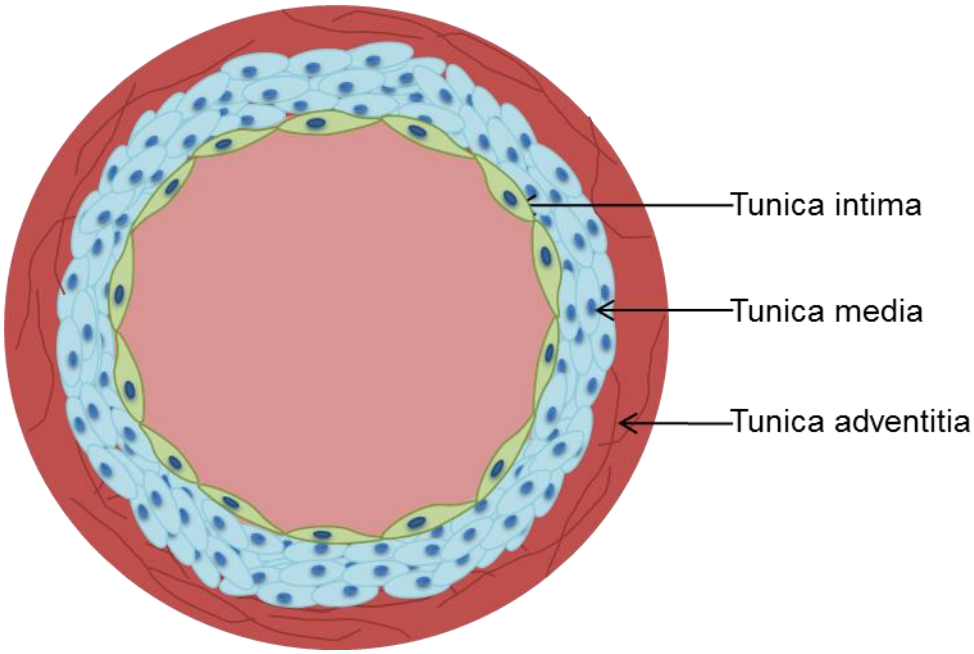

Figure 1.1: Schematic illustration of the 3 vessel wall layers. The tunica intima is comprised of a single endothelial cell layer that lines the vessel lumen. The tunica media mostly consists of VSMCs arranged circumferentially around the vessel wall and is important for maintaining vessel diameter and tone. The tunica adventitia lies in the outermost vessel layer and is comprised of fibroblasts embedded within an ECM of thick collagen bundles and elastic fibres.

1.2 Vascular smooth muscle cell phenotypic switching

As the major component of the arterial wall, VSMCs normally exist in a contractile, differentiated state to regulate vascular tone, blood pressure and blood flow.[16] VSMCs in adult vessels are normally characterised by a low proliferation rate and the expression of numerous contractile markers including α-smooth muscle actin (α-SMA), smooth muscle-myosin heavy chain (SM-MHC), SM-22α and calponin.[17] A

unique characteristic of VSMCs, distinguishing them from skeletal and cardiac muscle is their ability to transiently switch phenotype. This phenomenon, referred to as 'phenotypic modulation' or 'phenotypic switching' is regulated by external physiological cues such as growth factors, mechanical stimuli from blood flow and pressure, cell matrix interactions and inflammatory mediators.[17, 18] This is essential during vessel development and wound repair via modulation of cellular functions such as migration, proliferation and ECM production.[19] For example, in response to vascular injury, VSMCs dedifferentiate from a contractile to a synthetic phenotype, whereby cells lose expression of contractile marker genes, become more migratory, proliferative and synthesise ECM components to aid the repair of vessel damage.

However, VSMC plasticity can be detrimental to the vasculature as changes to physiological cues, such as hypertension, deregulate phenotypic switching leading to inappropriate VSMC migration and pathological vessel remodelling. This is a key event in the development of atherosclerosis as inefficient VSMC migration within the vessel wall reduces atherosclerotic plaque stability and increases the likelihood of plaque rupture.[12] As atherosclerosis is a primary indicator of stroke and peripheral artery disease, improved understanding of the molecular mechanisms underlying VSMC phenotypic switching will benefit the development of therapeutics for cardiovascular disease.[18, 20, 21] This is critical as atherosclerosis is ranked by the National Health Service (NHS) as the leading cause of death in the developed world.[22]

1.3 Actin cytoskeleton remodelling during cell migration

VSMC phenotypic transition from a contractile to a synthetic (proliferative and migratory) phenotype is associated with cytoskeletal reorganisation. The cell cytoskeleton is composed of an interconnected network of actin filaments, microtubules, intermediate filaments and a plethora of regulatory proteins. The cytoskeleton is characterised by three main functions: i) spatial organisation of intracellular organelles, ii) connection of the cell, physically and biochemically, to the external environment, and iii) control of cell shape change during cell movement.[23, 24] Therefore, the cytoskeleton and its structural organisation is fundamental to cell behaviour and its mechanical properties.

1.3.1 The cell migration cycle

Filamentous actin (F-actin) is the key constituent of the actin cytoskeleton and occurs in cross-linked aggregates, linked to more than 150 actin-binding proteins.[25] This actin-rich framework supports the cell membrane and is dynamically remodelled via actin polymerisation (assembly) and depolymerisation (disassembly) to control cell shape and generate movement.[26] Upon activation by pro-migratory stimuli, actin polymerisation at the cell leading edge produces actin-rich, finger-like extensions of cell membrane, termed filopodia, and large, broad, sheet-like protrusions, known as lamellipodia.[27] Next, small, nascent focal adhesions assemble immediately behind the leading edge to attach cell membrane to the underlying ECM. Once matured, stable focal adhesions form anchors which the cell uses to pull itself over the ECM.[28] Actin-myosin crosslinking within the cell body generates contractile force to propel the cell forwards whilst the cytoskeleton remodels and mature focal adhesions at the cell rear disassemble to detach from the ECM.[19, 28] **Figure 1.2** depicts the stages involved in cell migration.

In a migratory cell, focal adhesions are rapidly turned over; new focal adhesions continuously form at the leading edge whilst mature adhesions are disassembled at the rear.[29] However, the mechanisms of rear-end detachment and processes involved in adhesion disassembly are not clearly defined. Breaking cell-ECM contact requires a combination of high contractile force and proteolytic degradation of localised ECM by matrix metalloproteinases (MMPs) and cathepsins.[30] Contractility-promoted release occurs when actin-myosin interactions generate forces exceeding the adhesive strength of focal adhesions which directly detaches them from the substrate. In fish keratocytes, transient increases in cell tension activate stretch-activated calcium channels, leading to sudden influxes of extracellular calcium that further generate actin-myosin contractile forces and promote rear-end retraction.[31] In addition, the small Rho GTPases and their downstream signalling targets mediate cell contraction and retraction. In various cell types, Rho inhibition blocks stress fibre assembly and prevents rear-end release during cell migration.[32-34] Calpains are calcium-dependent cysteine proteases that are also implicated in rear-end detachment as they destabilise focal adhesions and reduce VSMC adhesiveness by cleavage of several focal adhesion proteins.[35] Calpain-deficient embryonic fibroblasts exhibit impaired rear-end retraction, increased tail length and reduced cell migration.[36]

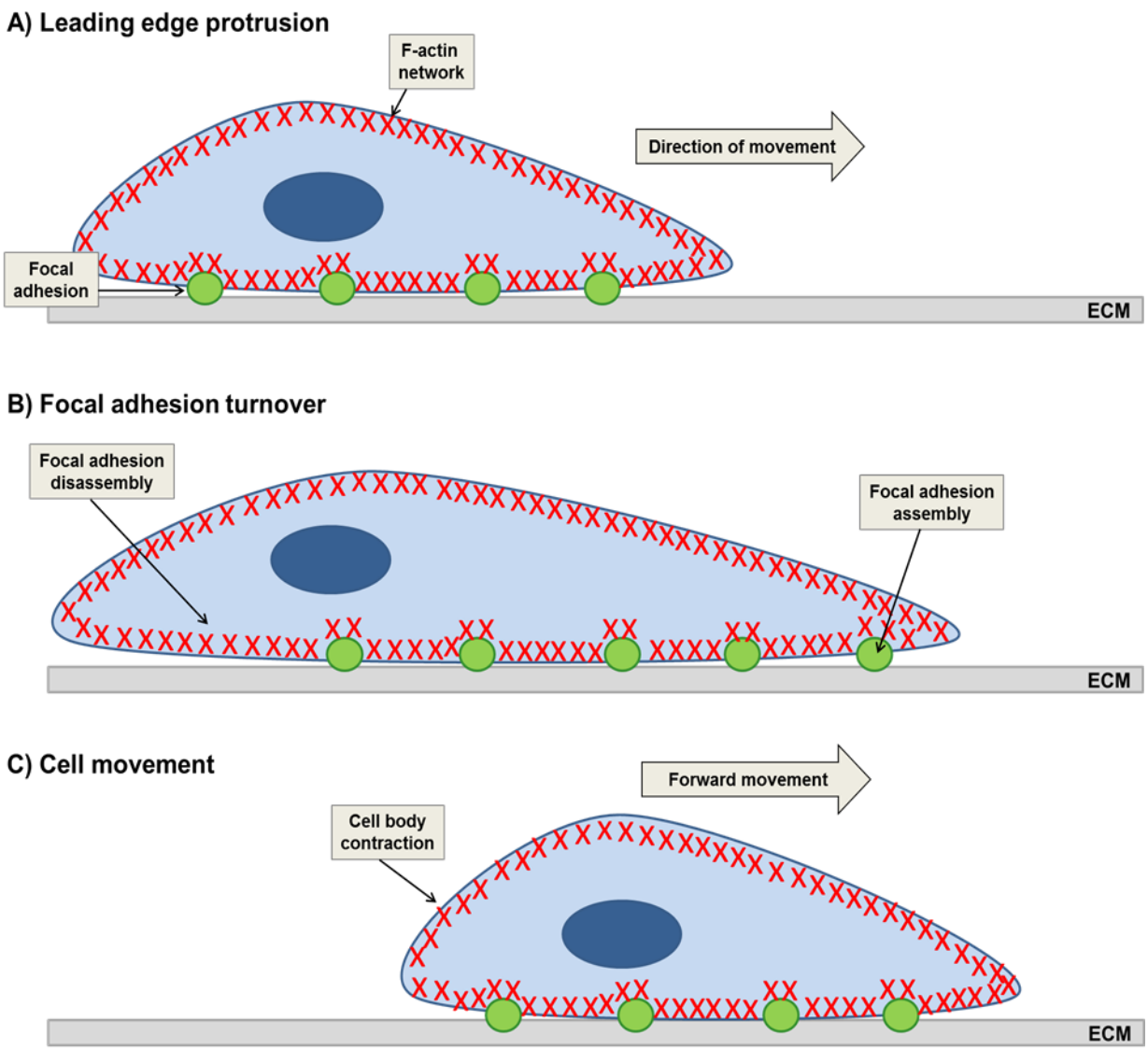

Figure 1.2: A schematic representation of the cell migration cycle. (A) Actin polymerisation at the leading edge extends cell membrane protrusions, lamellipodia and filopodia, in the direction of movement. **(B)** Focal adhesions simultaneously assemble at the leading edge to attach the cell to the ECM and disassemble at the rear to detach the cell from the ECM. **(C)** Actin-myosin crosslinking in the cell body generates contractile force to drive forward movement. Figure modified from Ananthakrishnan & Ehrlicher, 2007.[28]

1.4 The role of focal adhesions in cell migration

Focal adhesions are specialised protein complexes at the basal surface of adherent cells that serve as traction points during cell migration. Fundamentally, focal adhesions physically link the actin cytoskeleton to the ECM and their formation is closely coupled with actin polymerisation and actin-myosin-generated tension.[37, 38] The focal adhesion complex contains over 125 structural and regulatory proteins, many of which exhibit multiple protein-protein interactions, indicating considerable functional diversity.[39-41] Hence, this structure forms a 'bidirectional signalling hub' through which chemical (growth factors, hormones, cytokines) and mechanical (tension, stretch, compression) signals are exchanged between the ECM and cell cytoskeleton.[42-44] This communication between the extracellular environment and cell interior is essential for regulating cell behaviours including cytoskeletal remodelling, cell morphology, adhesion, spreading and motility.[42, 45, 46]

Focal adhesions are mechanosensitive and past studies illustrate that focal adhesions form and enlarge under intense force and disassemble when force subsides.[38] Initially, small (1-2 μm), nascent focal adhesions form in response to internal or external stress. Subsequent increases in intracellular contractility causes focal adhesions to develop into relatively large (2-6 μm), mature focal adhesions.[38] Small focal adhesions at the cell leading edge are highly dynamic and change their morphology, protein composition and phosphorylation state to promote cell migration, whereas, mature focal adhesions reside centrally within the cell and serve primarily as anchors to the ECM.[47, 48] The ability of focal adhesions to continually remodel in response to mechanical cues makes them crucial for modifying cell behaviour according to their local surroundings.[48, 49]

1.4.1 Integrins: central focal adhesion components

Integrins are a family of transmembrane glycoprotein receptors that are composed of a large, ligand-binding extracellular domain and a short, cytoplasmic domain.[50] Heterodimers of α-integrin and β-integrin form the core component of focal adhesions and in response to ligand binding, integrin activation and clustering subsequently recruits a plethora of proteins to the cytoplasmic surface of the cell membrane.[51, 52] Talin directly binds β-integrin and indirectly binds F-actin via a hierarchical cascade of proteins including vinculin, paxillin, α-actinin and focal adhesion

kinase (FAK) (**Figure 1.3**).[53-56] Therefore, activated integrins promote focal adhesion formation and provide structural linkage between the ECM, intracellular signalling machinery and actin cytoskeleton.

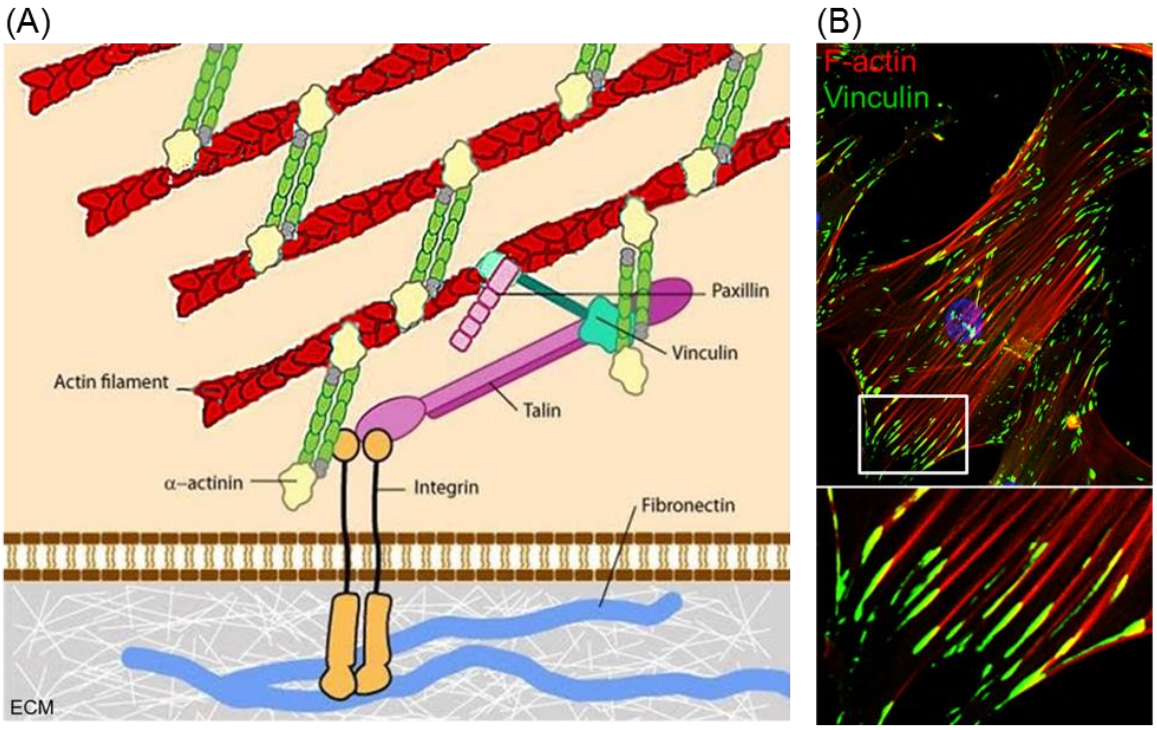

Figure 1.3: Focal adhesions link the ECM to the actin cytoskeleton. (A) Schematic representation of a focal adhesion complex. Transmembrane integrins form the core component of focal adhesions and upon integrin activation, talin directly binds integrin on the cytoplasmic face of the cell membrane. This subsequently leads to the recruitment of a hierarchical chain of adaptor proteins including vinculin, paxillin and α-actinin that indirectly link the ECM and actin cytoskeleton. Image modified from Rao & Winter, 2009.[57] **(B)** Immunofluorescence image illustrating vinculin (*green*) at the cell membrane connected to rhodamine phalloidin-stained F-actin (*red*). Insert below displays image at a higher magnification.

1.4.2 Vinculin stabilises focal adhesion complexes

Recent evidence reveals that vinculin is fundamental for focal adhesion formation. Under high tension, vinculin induces focal adhesion assembly and enlargement, whereas, at the rear of migrating cells, focal adhesion disassembly occurs when vinculin is under low tension.[58] Vinculin directly interacts with F-actin and contains binding sites for numerous regulators of cytoskeletal dynamics.[59] Furthermore, vinculin directly binds talin to promote integrin clustering, contractile force generation and focal adhesion stabilisation.[54] Vinculin lies between integrin-talin and the actin cytoskeleton where it is pivotal for force transmission between the ECM and cell interior and regulates cellular tension.[60] Therefore, vinculin is regarded as a mechanosensing protein that mediates mechanical signals between cell surface integrins and the cell cytoskeleton. In addition, studies demonstrate that contractile force exerted to the matrix is diminished in the absence of vinculin or enhanced when vinculin is present.[61] Vinculin's role is further implicated in mechanotransduction, as vinculin-deficient cells are less stiff, exert lower traction forces and exhibit impaired cell spreading and migration.[62-64] Recent evidence also shows that intercellular forces coincide with vinculin accumulation at cell-cell adhesion contacts and vinculin is responsible for potentiating cadherin mechanosensory responses.[65] Vinculin knockout mouse embryonic fibroblasts (MEFs) also have reduced adhesion to ECM proteins and possess smaller and fewer focal adhesions compared with control cells.[62, 66-68] Therefore, force transmission across a cell is dependent on stable integrin-cytoskeletal connections that are mediated by the focal adhesion component, vinculin.

1.4.3 Focal adhesions regulate cell signalling pathways

Focal adhesions indirectly scaffold paxillin, a multi-domain protein that provides a platform for numerous structural and signalling proteins that regulate cytoskeletal organisation, cell adhesion and motility.[69, 70] Force-dependent integrin activation also leads to the activation of FAK, Src family protein tyrosine kinases and $p130^{cas}$.[71] Auto-phosphorylation of FAK promotes the binding of Src to further phosphorylate other sites present on FAK, ensuring full activation of its kinase activity.[72] This subsequently activates the Rho GTPase or mitogen-activated protein kinase (MAPK) superfamily including extracellular signal-regulated kinases (ERK1/2), c-Jun amino-terminal kinases (JNK 1-3) and p38 kinases (α, β, γ, δ). This triggers the upregulation and activation of nuclear transcription factors such as the activator protein 1 (AP-1) and nuclear factor kappa B (NFKB) that regulate gene expression and protein synthesis.[73] Thus, focal

adhesions play a critical role in various intracellular processes including cell proliferation, differentiation, migration and cell survival.

1.5 Modes of cell migration

Two distinct modes of cell migration exist that are classified into i) single (amoeboid or mesenchymal) and ii) collective (multicellular or streaming) cell migration.[74] Cells migrate individually or collectively depending on their physiological purpose. Collective cell migration involves numerous cells that remain connected during movement and is relevant for tissue remodelling and repair as well as being implicated in cancer invasion and metastasis.[75-77] Single cell migration is more dispersive, allowing cells to migrate over long distances which is important during development, immune cell trafficking and cancer metastasis.[78-80]

Amoeboid migration occurs in single, rounded cells that lack focal adhesions and stress fibres and exhibit low polarity, whereas, mesenchymal migration is dependent on high focal adhesion-ECM interactions and high cell contractility.[81-84] Conversely, multicellular migration involves a group of cells that migrate simultaneously in whole, coordinated clusters of strands or sheets.[76, 77] This is reliant on stable cell-cell contact between leading cells and successive cells at the rear and lateral regions, enabling them to communicate and migrate as a single unit.[85] VSMC cell-cell contacts are mediated by N-cadherin which is essential for VSMC survival, however, the role of N-cadherin in VSMC migration is controversial at present.[86, 87] One study demonstrates that downregulation of N-cadherin enhances VSMC migration, whereas others illustrate that inhibition of N-cadherin significantly reduces VSMC migration.[88] Alternatively, cell streaming or chain-like migration refers to cells following each other in a loose, head-to-tail fashion along a narrow common track.[89, 90] This requires less stable and short-lived cell-cell contacts that are continuously disassembled and reproduced.[91, 92] This mode of collective cell migration is important for long-range communication between cells and is mediated by cell-cell contacts as well as filopodial and lamellipodial extensions.[92]

1.6 The role of Rho GTPases in cell migration

Rho GTPases are a G protein subfamily of the Ras superfamily, with Rho, Rac and Cdc42 being the most important regulators of actin cytoskeleton organisation and cell motility.[93] Rho GTPases undergo conformational changes and cycle between a GDP-bound (inactive) form and GTP-bound (active) form (**Figure 1.4**). This is regulated by numerous cellular proteins including guanine nucleotide exchange factors (GEFs) that promote the exchange of GDP to GTP to activate GTPases and GTPase-activating proteins (GAPs) that negatively regulate the switch by enhancing the intrinsic GTP hydrolysing activity of GTPases.[94-96] Guanine nucleotide dissociation inhibitors (GDIs) sequester GDP-bound GTPases in the cytoplasm and prevent GDP nucleotide exchange to hinder their activation.[97, 98] In the GTP-bound form, Rho GTPases phosphorylate and activate over 40 downstream effectors to mediate actin organisation, gene transcription, cell-cycle progression, cell adhesion and cell migration.[99]

Rac and Cdc42 are activated during early migratory events and localise actin polymerisation to the cell leading edge where cell membrane protrudes forwards in lamellipodial and filopodial extensions. More specifically, Rac controls lamellipodial and focal adhesion formation, whereas, Cdc42 generates filopodia and maintains cell polarity.[19, 45] During cell migration, Cdc42 positions microtubules and Golgi towards the direction of travel.[100] Golgi-derived vesicles at the cell leading edge provide membrane and associated proteins required for forward protrusion.[100] Studies demonstrate that Cdc42 inhibition prevents Golgi reorganisation and polarity is lost in these cells, resulting in protrusions around the entire cell periphery, not just at the leading edge.[34] Later, Rho activation is required for focal adhesion maturation and regulates actin bundling into stress fibres for cell body contraction and rear-end retraction.[101]

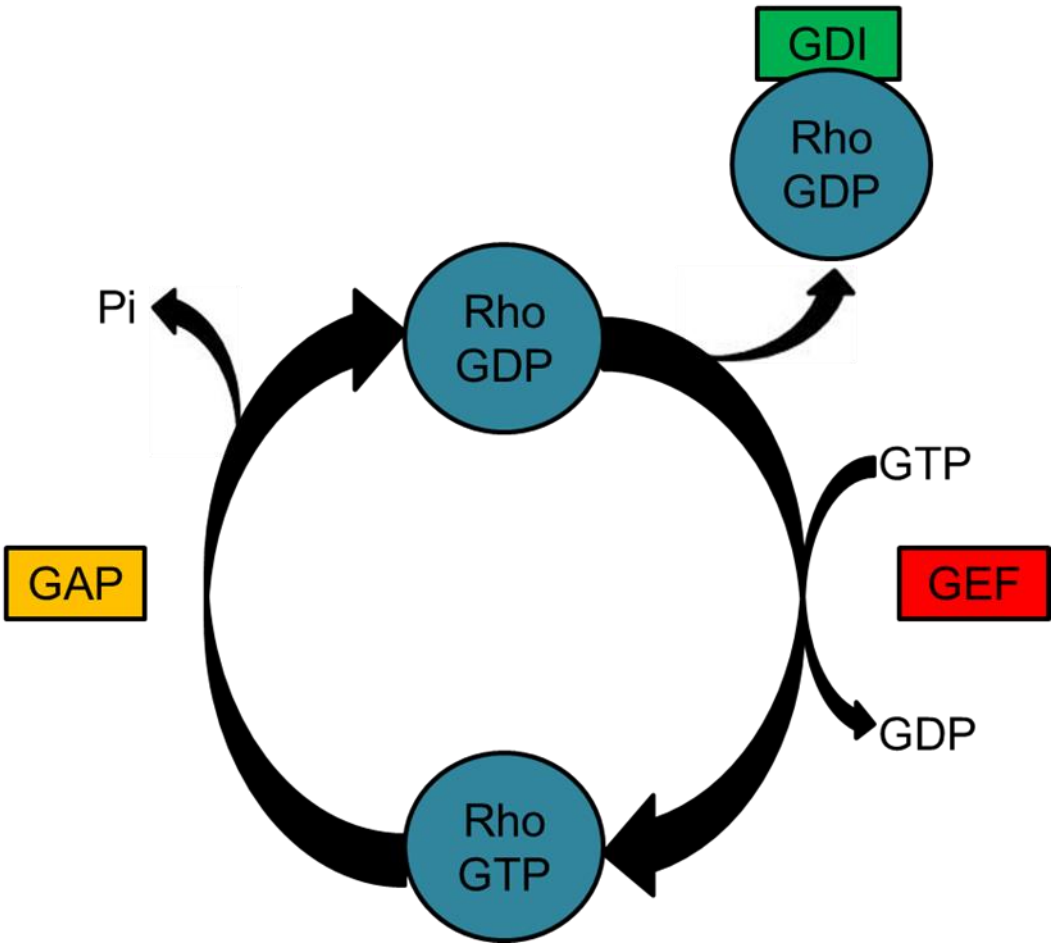

Figure 1.4: The Rho GTPase switch. Rho GTPases cycle between a GDP (inactive) and GTP (active) form. Guanine nucleotide exchange factors (GEFs) activate GTPases, GTPase-activating proteins (GAPs) inactivate GTPases by enhancing GTP hydrolysis and guanine nucleotide dissociation inhibitors (GDIs) prevent activation by sequestering GTPases in the cytoplasm. Figure modified from Raftopoulou & Hall, 2004.[19]

1.6.1 Rho GTPase targets and downstream signalling

The Rho GTPase signalling molecules, Cdc42, Rac and Rho have numerous downstream effectors that elicit a variety of responses involved in actin organisation. As illustrated in **Figure 1.5**, these mainly include the Wiskott-Aldrich Syndrome protein (WASP) family, the WASP family verprolin homology (WAVE) complex, P21-activated protein kinase (PAK) and Rho-associated protein kinase (ROCK).

1.6.1.1 The WASP Family

The WASP family of proteins are downstream targets of Cdc42. Cdc42 exposes a domain near the WASP C-terminus able to interact and subsequently activate components of the actin-related protein (Arp2/3) complex.[102] The highly conserved Arp2/3 complex is a stable assembly of two actin-related proteins (Arp 2 and 3) and once activated, Arp2/3 mimics the fast-growing, barbed end of the actin filament.[103] This supports the addition of globular, monomeric actin and filament elongation into filopodia, whilst also capping the nascent filament at its slow-growing, pointed end.[102-104]

Rac binds and activates the WAVE complex, a family of WASP-related proteins that also activates Arp2/3.[105] This complex adjoins to the side of pre-existing F-actin to initiate filament branching at 70 degrees from host filaments, characteristic of the lamellipodium.[26] Actin polymerisation continues within the lamellipodium until growth is terminated by capping proteins.[105, 106]

1.6.1.2 PAK

PAK is a downstream effector of both Rac and Cdc42 that regulates actin cytoskeletal dynamics and cell adhesion during migration. The primary function of PAK is phosphorylation and activation of LIM kinase (LIMK) which subsequently phosphorylates cofilin.[107] Unphosphorylated cofilin depolymerises F-actin, whilst phosphorylation by LIMK disrupts cofilin-actin interactions, enabling actin polymerisation.[107] PAK also directly phosphorylates myosin light chains to activate actin-myosin crosslinking.[107] It has also been reported that PAK phosphorylates the actin-binding protein, I-caldesmon (the dominant form expressed in VSMCs), and its phosphorylation is necessary for stress fibre disassembly.[108] In addition, PAK-mediated phosphorylation of cortactin reduces its binding to actin and reduces actin branching.[109] Therefore, PAK impacts on actin cytoskeleton remodelling and regulates actin-myosin contractility.

1.6.1.3 Formins

The formin family of proteins are the largest group of Rho GTPase effectors and are activated by Rho and Cdc42 to promote the extension of unbranched actin filaments. Formins contain a highly conserved formin homology 2 (FH2), sufficient to promote actin assembly alone and a FH1 domain that binds profilin-actin to accelerate actin filament extension. Upon activation, formins dimerise, adopting a hoop-like

conformation, which binds the F-actin barbed end to obstruct capping proteins that usually prevent elongation. G-actin is inserted between the formin cap and the barbed end of the filament to polymerise actin at the leading edge into long parallel bundles of straight filaments characteristic of filopodia.[110, 111] Formins also function alongside adenomatous polyposis coli (APC) protein that also shapes the actin cytoskeleton by binding to actin filaments and sequestering G-actin to aid filament extension. Synergistically, formins deter capping proteins and APC rapidly assembles actin filaments.[112]

1.6.1.4 ROCK

Rho-activated ROCK phosphorylates the myosin-binding subunit of myosin light chain (MLC) phosphatase rendering it inactive.[113] This indirectly increases MLC phosphorylation and stimulates the ATPase activity of myosin II to promote actin-myosin interactions and generate contractile force for forward cell movement.[113] Tension exerted across the cell also induces conformational changes within adhesion proteins which regulates focal adhesion maturation and stability.[114] Moreover, ROCK directly phosphorylates MLC and LIMK to inhibit cofilin, as described above.[115, 116]

1.6.1.5 Other effectors of smooth muscle cell contractility

In addition to GTP-binding proteins, arachidonic acid and protein kinase C (PKC) have also been linked to smooth muscle contraction *in-vitro*. These compounds mediate calcium sensitisation by inhibiting myosin phosphatase activity. Independently of Rho, arachidonic acid directly activates ROCK by releasing its autoinhibitory mechanism.[117, 118] Both ROCK and PKC also phosphorylate and activate CPI-17, a phosphorylation-dependent inhibitor of myosin phosphatase activity.[119, 120] In addition, calponin binding to F-actin exerts an inhibitory effect on actin-activated myosin ATPase activity and ROCK phosphorylates calponin to reduce the binding activity of calponin to F-actin.[121] This accumulative evidence suggests that the Rho/ROCK pathway and their associated downstream targets are particularly important for regulating smooth muscle contraction. Numerous studies have also demonstrated the importance of ERK1/2 as mediators of VSMC contraction.[122-125] ERK1/2 most likely regulate contractility via phosphorylation and inactivation of the myosin ATPase inhibitory protein caldesmon.[126]

1.7 Nuclear regulation of cell migration

So far, I have described the importance of the Rho GTPase family of proteins and their respective downstream signalling molecules in regulating actin remodelling, focal adhesion dynamics and cell migration. However, emerging evidence suggests that there is a direct, mechanical aspect to actin and focal adhesion organisation via the nucleus.[127-130] Recent work highlights that physical interactions between the nucleus, intracellular cytoskeleton and cell membrane facilitate direct biophysical signalling throughout the cell which is important for efficient mechanotransduction; the translation of mechanical forces into biochemical signals.[131] Mechanotransduction is a homeostatic process whereby deviations in local mechanical stimuli rapidly modulate cell behaviour to ensure tissue maintenance. Mechanical signals sensed by focal adhesion complexes are translated to the cell interior to subsequently regulate actin cytoskeleton organisation, gene expression, motility, proliferation and survival.[132]

1.7.1 The nuclear envelope

The nuclear envelope (NE) is a highly organised structure that physically divides the nucleoplasm and cytoplasm and plays an important role in regulating nuclear activity. It is composed of an inner nuclear membrane (INM) separated, by perinuclear space (PNS), from an outer nuclear membrane (ONM) that is continuous with nuclear pore complexes (NPCs) and endoplasmic reticulum (ER).[133] The INM contains more than 70 transmembrane proteins, including lamina-associated proteins (LAPs), chromatin-binding proteins and emerin.[134] These proteins are initially inserted into the ER and move through NPCs to the INM where they maintain their localisation by binding chromatin or tethering to the nuclear lamina.[135-137]

1.7.2 The nuclear lamina and prelamin A processing

The nuclear lamina is a filamentous meshwork lying beneath the INM that mainly consists of the type V intermediate filament proteins, A- and B-type nuclear lamins. These are encoded by the *LMNA* and *LMNB* genes, respectively. The *LMNA* gene encodes four A-type lamins (A, AD10, C & C2) with lamins A and C being the major isoforms of the nuclear lamina. Prelamin A is the precursor of lamin A that contains a nuclear localisation signal (NLS) required for direct transport into the

nucleus and a C-terminal CAAX motif that undergoes a series of post-translational modifications to form mature lamin A. The cysteine residue of CAAX is first farnesylated by farnesyl transferase, AAX is then removed by endoproteolytic cleavage and the farnesyl-cysteine residue is carboxymethylated by an isoprenylcysteine methyltransferase (ICMT). Further cleavage by the zinc metalloproteinase, FACE-1/Zmpste24, removes 15 additional C-terminal amino acids, including the farnesylated/carboxymathylated cysteine, to release mature lamin A.[138-141] (**Figure 1.6**) Mature A-type lamins are incorporated into the nuclear lamina where they maintain NE structure and stability as well as scaffolding important protein complexes for the regulation of DNA synthesis, DNA damage responses, chromatin organisation, gene transcription, cell-cycle progression and cell migration.[142, 143]

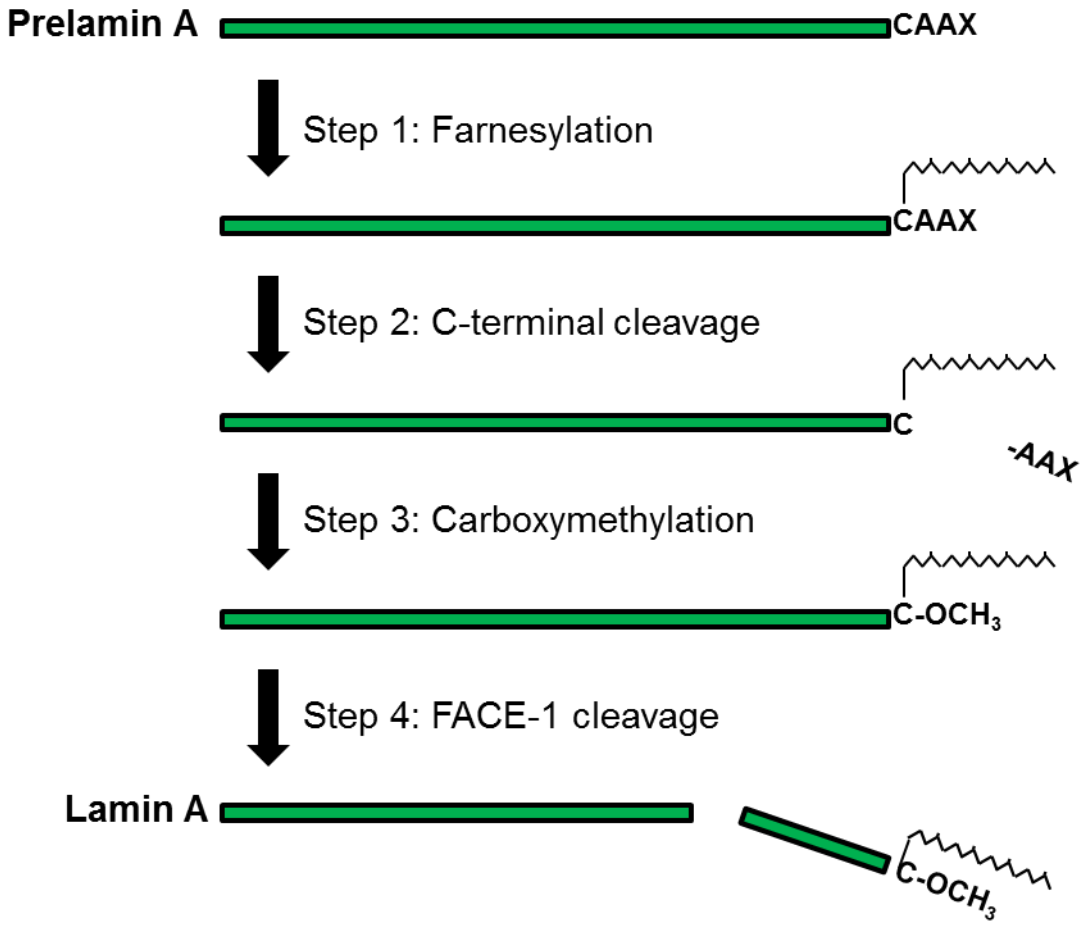

Figure 1.6: Schematic representation of prelamin A processing. A-type lamins are generated from the precursor protein, prelamin A, by four post-translational modifications. **Step 1:** Farnesylation of a cysteine residue on the C-terminal CAAX motif. **Step 2:** Endoproteolytic cleavage of the 3 terminal amino acids, AAX. **Step 3:** Carboxymethylation of farnesyl-cysteine. **Step 4:** Cleavage of 15 additional C-terminal amino acids by FACE-1/Zmpste24 produces mature lamin A. Image adapted from Kudlow *et al*., 2007.[141]

1.7.3 Nesprins

Nesprins (nuclear envelope spectrin repeat-containing proteins) are a ubiquitously expressed family of multi-isomeric spectrin repeat proteins that are highly conserved throughout evolution. They are the only spectrin repeat proteins to be identified at the NE and were originally discovered as VSMC differentiation markers in a cDNA library screen.[144, 145] However, the role of nesprins as intracellular scaffolds and linkers is ever-expanding, with newly identified roles beyond those at the NE. Four nesprin genes (*SYNE* 1-4) have been identified to date, which encode proteins with distinct cellular functions. The largest nesprin proteins, nesprin-1 and -2, consist of a pair of N-terminal calponin homology (CH) domains, a central rod domain composed of multiple spectrin repeats and a C-terminal Klarsicht, Anc-1, Syne homology (KASH) transmembrane domain.[146] After titin (3MDa), nesprin-1 and -2 are the largest proteins encoded by the human genome (approximately 1MDa and 800kDa, respectively) whereas nesprins-3 and -4 are much smaller (approximately 110kDa and 42kDa, respectively) and lack N-terminal CH domains (**Figure 1.7**).[147-149]

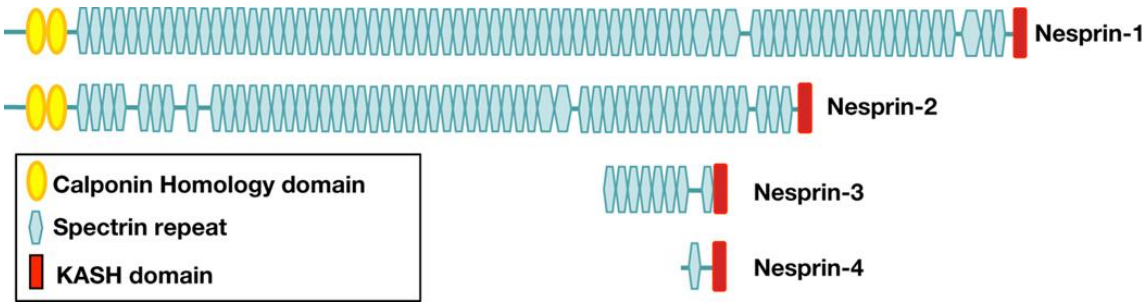

Figure 1.7: Published nesprin genes (1-4). The giant isoforms (nesprin-1 and -2), consist of a pair of N-terminal calponin homology (CH) domains, a central rod domain composed of multiple spectrin repeats and a C-terminal Klarsicht, Anc-1, Syne-1 homology (KASH) transmembrane domain. Nesprin-3 and -4 are much smaller and lack the N-terminal CH domains yet retain their NE-targeting KASH domain. Image from Rajgor & Shanahan, 2013.[146]

Giant nesprin isoforms localise to the ONM where they extend beyond the NE to form a filamentous network surrounding the nuclear surface.[129] Via their spectrin repeats, nesprins provide platforms to facilitate protein-protein interactions that are important for maintaining nuclear integrity and function.[145] Patients with Emery-Dreifuss muscular dystrophy (EDMD) exhibit nesprin mutations and present with mislocalised, reduced, or no NE nesprins and subsequently defective nuclear morphology.[150] Recent

evidence indicates that nesprin-1 and -2 exhibit multiple initiation and termination sites allowing the generation of alternative N and C-terminally spliced isoforms.[151, 152] These include shorter isoforms such as nesprin-1α and -2α as well as KASH-less nesprins that localise to multiple sub-cellular compartments, including the nucleoplasm and focal adhesions, with roles beyond the NE that have yet to be explored.[153-155] The diversity of nesprin isoforms may be important for scaffolding variable protein complexes between cell types and maintaining tissue-specificity. The identified NE-localising nesprin-1 and -2 isoforms identified to date are illustrated in **Figure 1.8**.

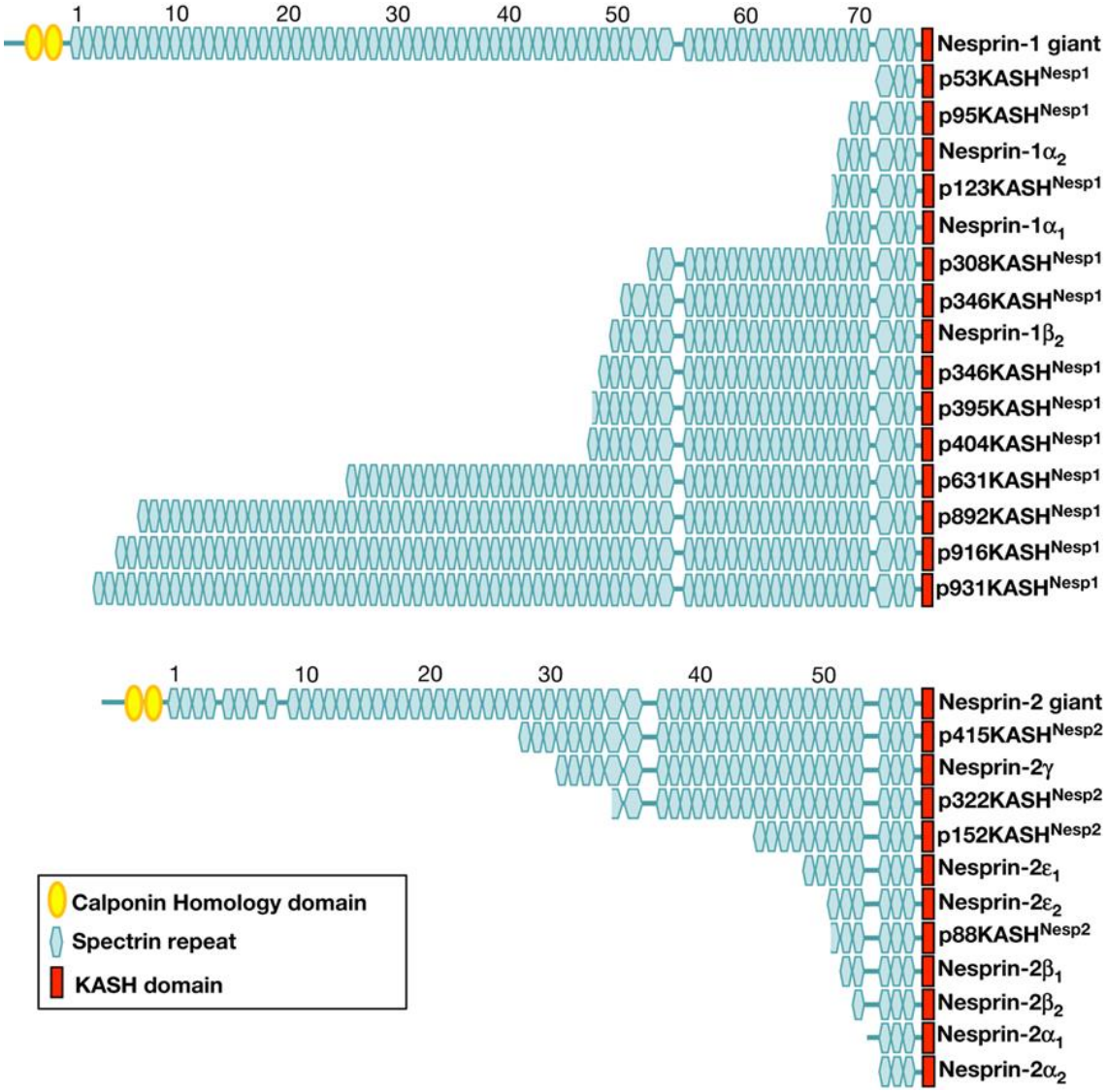

Figure 1.8: Published nesprin-1 and -2 isoforms. This figure illustrates KASH-containing nesprin-1 and -2 isoforms that localise to the NE. Diverse nesprin-1 and -2 isoforms are generated by alternative initiation and termination of transcription that represent smaller portions of the giant proteins. Image from Rajgor & Shanahan, 2013.[146]

1.7.4 The LINC complex

The linker of the nucleoskeleton and cytoskeleton (LINC) complex is a unique NE-spanning structure that physically anchors the nuclear lamina to cytoskeletal filaments creating a continuum between the nuclear exterior and interior. The KASH domain of nesprin-1/2 specifically targets them to the ONM via interactions with the C-terminus of Sad1p-UNC84 (SUN) proteins, SUN1 and SUN2, located in the PNS.[127, 156] In turn, the nucleoplasmic N-terminus of SUN1/2 tethers lamin A/C, emerin and chromatin on the INM surface.[145] In addition, INM-associated nesprin isoforms have been identified as nucleoplasmic binding partners of lamin A/C, emerin and SUN1/2 that further stabilise the LINC complex.[150, 157] Data show that SUN1/2 depletion or dominant-negative overexpression leads to the displacement of endogenous nesprins from the NE to the ER and expansion of the PNS, highlighting that SUN proteins are integral for nesprin localisation and normal segregation of the INM and ONM.[128, 158] SUN1/2 proteins serve as scaffolds to maintain nuclear architecture, chromatin dynamics and genomic stability but more crucially, SUN-KASH bridging between the nuclear lamina and cell cytoskeleton appears to be essential for mechanotransduction.[159, 160] In support of this theory, recent data also highlights the role of nuclear lamins as important force-transmitting filaments to molecules inside the nucleoplasm.[161] This implicates a pivotal role of the LINC complex in intracellular communication between the cytoskeleton and genome. Many studies are now attempting to further elucidate the importance of the LINC complex in cellular functioning such as mechanotransduction signalling, gene regulation, cell proliferation and migration.[146, 162-165]

1.7.5 LINC complex diversity

Variable N-terminal motifs enable nesprins in the ONM to interact with different cytoskeletal components including plectin, F-actin or microtubules.[147-149] Nesprin-1/2 contain N-terminal CH domains that interact directly with F-actin and indirectly with focal adhesions.[147, 153, 166] Evidence demonstrates that that F-actin depolymerisation induces nuclear morphology changes and mislocalises nesprin-2 from the NE into actin-rich foci.[167] Nesprin-3 contains a plectin-binding motif that facilitates interactions with cytoplasmic intermediate filaments and nesprin-4 has a kinesin-binding function that supports interactions with microtubules to regulate cell polarity.[148, 149] Evidence suggests that nesprins 1-3 also physically and functionally interact with one another creating a lattice surrounding the NE.[168] Furthermore, recent studies illustrate that SUN2 forms a trimeric structure that interacts with 3 independent KASH proteins in a

3:3 ratio, thus suggesting that SUN can associate with more than one nesprin variant at once.[156] This highlights the complexity of the LINC complex and suggests that diverse nesprin isoforms and their varying interactions with SUN allow the LINC complex to specifically tailor itself according to different cell functions. At present it is unknown whether SUN1 and 2 form homodimeric or heterodimeric structures. Nesprins also undergo isoform switching during phenotypic modulation, suggesting that nesprin and LINC adaptability could be essential for VSMC switching.[169] **Figure 1.9** provides a schematic representation of the LINC complex.

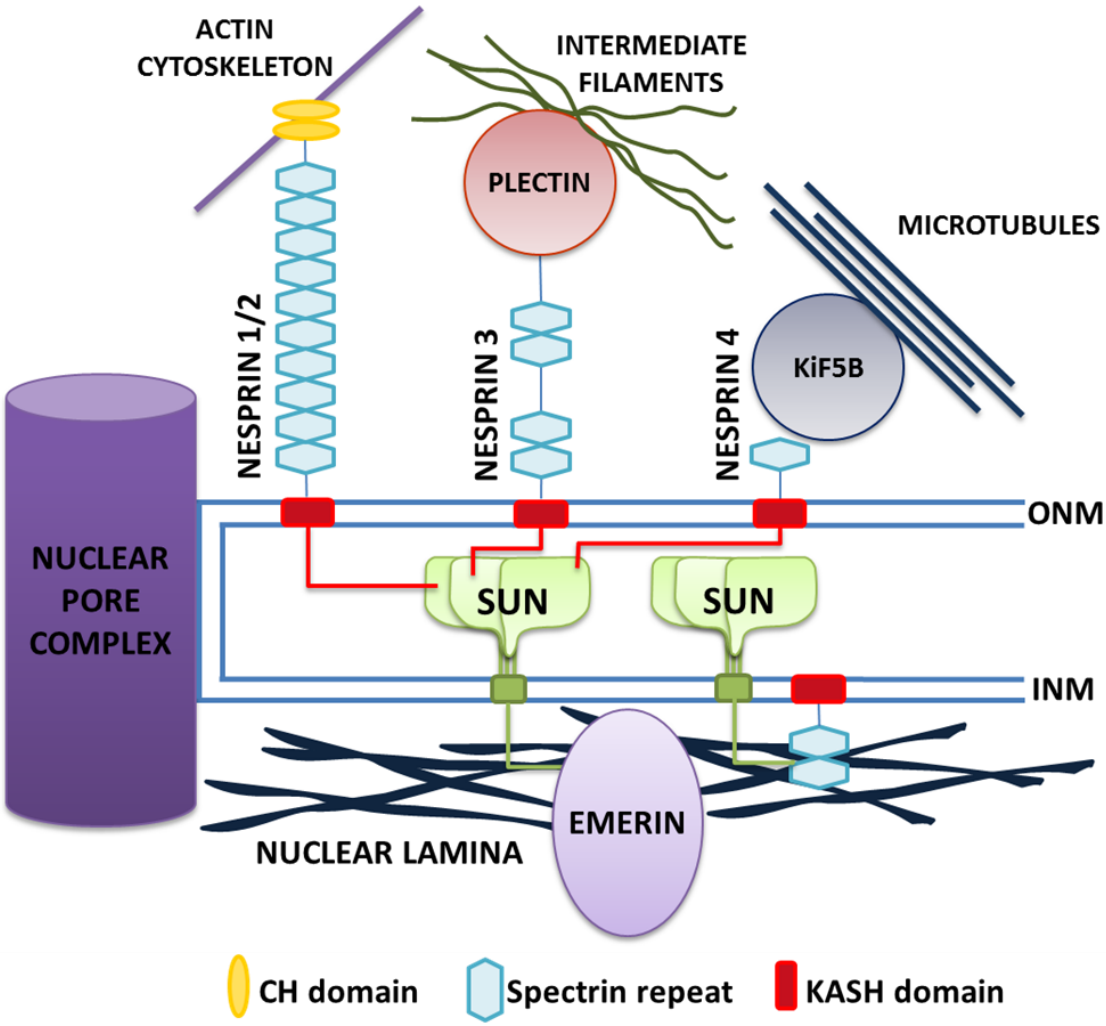

Figure 1.9: The LINC complex physically anchors the nuclear lamina to cytoskeletal filaments. The LINC complex spans the NE and consists of nesprins, SUN and nuclear lamina proteins. KASH targets nesprin to the ONM via interactions with trimeric SUN structures in the PNS, which in turn interact with lamin A/C and emerin on the INM. Nesprins form a protein scaffold that connects intranuclear structures, via this bridging complex at the NE, to cytoplasmic actin filaments, intermediate filaments and microtubules. Image from Rajgor & Shanahan, 2013.[146]

1.7.6 The LINC complex in human disease: nuclear envelopathies

The importance of the LINC complex is highlighted by evidence associating mutations in NE proteins with a group of human diseases termed 'nuclear envelopathies' or 'laminopathies'. These are a family of early-onset degenerative disorders caused by mutations in the genes encoding nesprin (*SYNE*), lamin (*LMNA*), emerin (*EMD*) and, more recently, SUN proteins (*SUN*).[150, 157, 170] Such mutations are associated with diseases including EDMD, Hutchinson-Gilford progeria syndrome (HGPS), atypical Werner syndrome (WS), dilated cardiomyopathy (DCM) and Dunnigan-type familial partial lipodystrophy (FPLD) that are clinically characterised by premature ageing, ataxia, atherosclerosis, cardiomyopathy, muscular dystrophy and lipodystrophy (see **Table 1.1**).[171] Therefore, nuclear envelopathy/laminopathy models are commonly used to gain mechanistic insight into ageing and interrogate the importance of the LINC complex on cellular functions. Increasing evidence illustrates that LINC complex disruption by these genetic mutations severely impacts upon mechanotransduction and cell motility as described below.

Table 1.1: Clinical characteristics of nuclear envelopathies. Nuclear envelopathies occur as a result of mutations in LINC complex components. The table below illustrates the mutations associated with each disease and the clinical phenotypes arising from these mutations.

Nuclear Envelopathies	Gene mutation	Clinical Characteristics	Reference
Hutchinson-Gilford progeria syndrome (HGPS)	*LMNA*	Premature ageing, hair loss, loss of subcutaneous fat, premature atherosclerosis, myocardial infarction	172-175
Atypical Werner syndrome (WS)	*LMNA*	Premature ageing, premature atherosclerosis, cataracts, muscle wasting	176, 177
Emery-Dreifuss muscular dystrophy (EDMD)	*LMNA*, *EMD*, *SYNE*-1/2 or *SUN1/2*	Early contractures of the neck/elbows/Achilles tendons, muscle weakening and wasting, cardiac conduction defects	150, 157, 170, 172, 178-180
Dilated cardiomyopathy (DCM)	*LMNA* or *SYNE1*	Ventricular dilatation, systolic dysfunction, arrhythmias, conduction defects	181-183
Dunnigan-type familial partial lipodystrophy (FPLD)	*LMNA*	Dramatic absence of adipose tissue in the limb/trunk and accumulation in the neck/face, increased susceptibility to atherosclerosis/diabetes	184, 185

1.7.6.1 LINC complex disruption impairs cell migration

Mutations in NE proteins have been shown to impact on actin cytoskeleton organisation and actin-mediated cellular processes, as described below. Studying the implications of nuclear lamina disruption on cell structure and migrational behaviour reveals that cell motility is defective in laminopathic cells.[186] More recent evidence shows that fibroblasts from EDMD patients exhibit nuclear shape defects and alterations in cell adhesion and migration.[162] Lamin A/C deficient MEFs have a dysfunctional cytoskeleton, diminished ability to polarise at the edge of a wound and significantly reduced migration into a wound healing assay.[187] Furthermore, cells derived from HGPS and EDMD mouse models are defined by cytoplasmic elasticity, weakened cell adhesion and slow wound closure.[172] On the contrary, skin fibroblasts from EDMD patients are associated with enhanced cell polarity and migration speed.[188] Overall, these data indicate that NE mutations impact on LINC complex integrity and compromise actin organisation, adhesion formation and cell migration.

1.7.6.2 LINC complex disruption impairs mechanotransduction signalling

Emerging evidence indicates that direct linkage between the cell cytoskeleton and nucleus by the LINC complex facilitates mechanotransduction signalling throughout the cell. Cytoskeletal structures normally withstand mechanical stresses and maintain their integrity independent of dynamic remodelling at the molecular level, however, LINC complex alterations disturb actin architecture and severely affect the mechanical properties of the cell.[187] Cells derived from HGPS and EDMD mice have significantly weakened cytoplasmic stiffness, most likely resulting from disrupted actin organisation.[172] Also, lamin A/C deficient MEFs exhibit nuclear fragility and reduced mechanical stiffness, thus, hindering their ability to respond to mechanical stress.[189] Impaired nesprin functionality reduces cellular tension and induces defects in mechanical force transmission between the cytoplasm and nucleus.[182, 190, 191] Moreover, overexpressing dominant-negative nesprin-2 and SUN protein mislocalises endogenous nesprin from the NE and weakens intracellular force transmission.[165] This detailed study also revealed that strain-induced nuclear deformations are reduced in LINC complex disrupted cells and cytoskeleton organisation, cell polarisation and migration are also impaired.[165] Mechanically-induced actin polymerisation normally facilitates nuclear import of the mechanosensitive transcription factor, megakaryoblastic leukaemia 1 (MKL1, also known as MRTF-A) to activate regulatory genes of cell motility and contractility.[192] Recent evidence demonstrates that lamin mutant cells have altered actin organisation and dynamics, resulting in diminished

nuclear translocation and downstream signalling of MKL1.[193] Collectively, this evidence emphasises that the LINC complex is crucial for efficient mechanotransduction and implicates LINC complex weakening in the progression of nuclear envelopathies.

1.7.6.3 LINCing the cell membrane, actin cytoskeleton and nuclear lamina

Accumulating evidence implicates both focal adhesions at the cell membrane and the LINC complex at the NE in mechanical signal transmission throughout the cell as both vinculin and nesprin interact with and regulate F-actin. This suggests that the LINC complex extends beyond the NE, creating a mechanically-coupled system between the cell membrane, actin cytoskeleton and nucleus (**Figure 1.10**).[42, 147] The actin cap is a unique structure of thick F-actin bundles tightly covering the apical surface of the nucleus via direct connection to LINC complexes.[194] A recent study identifies a subset of focal adhesions terminating in the actin cap termed actin cap associated focal adhesions (ACAFAs) that are composed of vinculin, paxillin, talin, zyxin and talin; proteins that are thought to be important mechanosensors.[195] LINC complex disruption, by dominant-negative KASH expression, subsequently disrupts actin cap structure, reduces ACAFA number and impairs mechanosensing responses, suggesting that the LINC complex creates a physical pathway between the cell membrane and nucleus.[195] In support of this, force application to the cytoskeleton or cell membrane subsequently induces nuclear deformations and activation of mechanosensitive genes.[164] Moreover, lamin A deficient cells exhibit reduced mechanosensitive gene expression and reduced nuclear rigidity in response to mechanical distortion.[186] Lamin mutant cells also have diminished vinculin expression and fewer focal adhesions compared with wild-type cells.[193] Studies also demonstrate that uncoupling of the nucleus from the actin cytoskeleton diminishes the cellular tension required for mechanical signal propagation and consequently impairs focal adhesion stability and cell motility.[172, 196] Earlier studies demonstrate that pulling cell membrane integrins using a microneedle distorts the nucleus, whereas pulling on metabolic receptors has no effect.[197] This body of evidence indicates that a continuous connection exists between focal adhesions and the nucleus, most likely via the LINC complex, which is crucial for actin organisation, mechanotransduction signalling and cell migration.

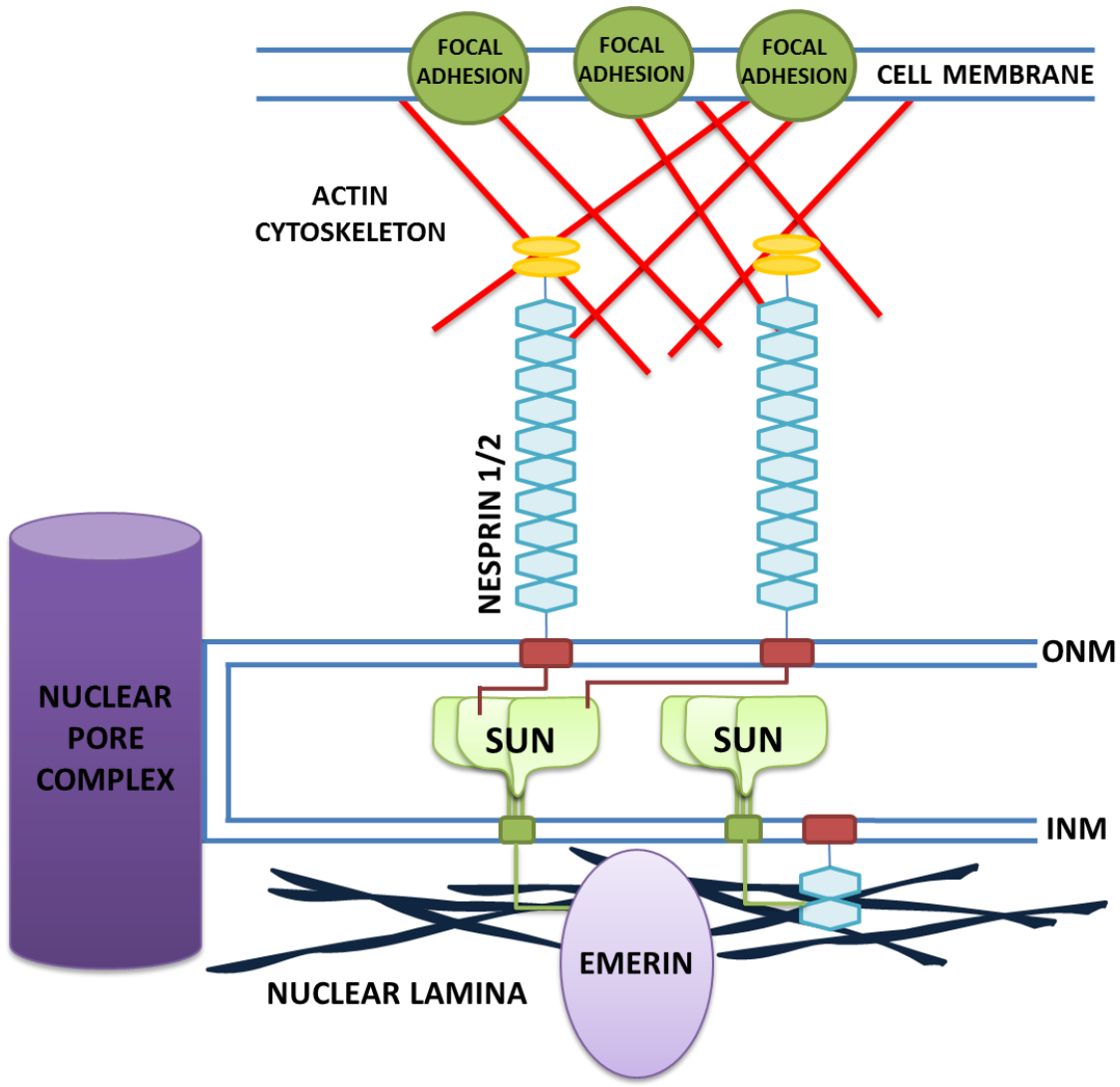

Figure 1.10: The LINC complex physically connects the cell membrane, actin cytoskeleton and nucleus. Proposed model of the LINC complex based on current literature. Focal adhesions at the cell membrane bind F-actin that subsequently connects to the nucleus via nesprin-SUN-nuclear lamina interactions across the NE. This is important for structurally linking the cell surface to the nuclear interior and mediating mechanotransduction throughout the cell. Figure modified from Rajgor & Shanahan, 2013.[146]

1.8 VSMC ageing

Ageing progressively impairs cell function and is a major risk factor for cardiovascular disease, the most prominent cause of morbidity and mortality in the elderly.[198, 199] After the age of 50, the number of human life years remaining is determined predominantly by ageing which results from a complex interaction of genetic and environmental factors.[200, 201] Ultimately, system failure occurs due to a loss of physiological response to stress, including physical and chemical insults, infections, tumours and trauma.[202]

It is well established that human cells have a finite lifespan and as cells age they lose their proliferative capacity, leading to a state of irreversible cell-cycle arrest and altered functionality, a phenomenon referred to as 'cellular senescence'.[203] *In-vitro,* VSMCs exhibit limited growth potential; they are initially highly proliferative at early passage numbers and, following serial passaging, proliferation rate declines when cells enter a phase termed 'presenescence'. Following further passaging, VSMCs ultimately become senescent and are terminally differentiated.[204] Furthermore, VSMCs from old donors reach replicative senescence earlier than those from younger donors.[204] Therefore, senescent VSMCs increase with age and these cells are associated with a large, flattened appearance, reduced telomere length, reduced Ki67-positive staining and increased senescence-associated β-galactosidase (SAβG) activity.[205, 206] There is also an increased expression of negative cell cycle regulators such as p53 and p16 that promote growth arrest and senescence.[205] As the senescent phenotype is characterised by growth arrest, resistance to apoptosis and altered gene expression, it is believed to be a protective mechanism against tumorigenesis.[207] However, VSMC senescence is also associated with adverse vascular modifications and VSMCs derived from atherosclerotic plaques exhibit slower proliferation rates and undergo senescence earlier than normal cells.[205] Much research now focuses on defining the VSMC ageing process and how senescence is implicated in cardiovascular diseases such as atherosclerosis, hypertension, stroke and heart failure.

1.8.1 VSMC senescence drives the development of atherosclerosis

The inflammatory response associated with atherosclerotic plaque development stimulates VSMC dedifferentiation, resulting in enhanced VSMC proliferation and migration from the vessel media into the intima. As previously described, VSMC-

derived collagen, elastin, proteoglycans and other ECM components are essential for the formation of a fibrous cap that stabilises the atherosclerotic plaque.[13] However, cap thinning occurs during ageing due to fewer intimal VSMCs and loss of ECM production.[12-15] Studies demonstrate that VSMCs in advanced atherosclerotic plaques exhibit a decline in proliferative capacity compared with early lesions, suggesting that the predominance of senescent VSMCs within the plaque contribute to age-associated cap thinning and plaque instability.[13, 208, 209] Furthermore, senescent cells demonstrate an age-related upregulation of genes that promote plaque instability including plasminogen activator inhibitor-1 (PAI-1) and MMPs.[210, 211] Plaque instability ultimately leads to sudden plaque rupture, a precursor of myocardial infarction and strokes, thus illustrating the urgency for improved understanding of the mechanisms underlying cellular senescence.

VSMC-derived ECM provides tensile strength to the vessel wall and ECM modifications normally enable the vessel to accommodate hemodynamic forces. However, age-associated ECM destabilisation, resulting from an overproduction of collagen and diminished elastin, increases vessel rigidity, reduces vessel compliance and leads to thickening of the vessel wall.[198, 212, 213] VSMC ageing is also associated with vessel calcification which contributes towards aortic stiffness and is a prominent feature of atherosclerosis.[214] This body of evidence suggests that VSMC ageing is associated with numerous structural and functional changes to the vessel wall, including loss of vessel elasticity, luminal enlargement and intimal thickening, all of which favour atherosclerotic plaque formation.[215, 216] Therefore, VSMCs can be regarded as both protective and detrimental in vessel homeostasis; they play an essential role in cap stability which prevents plaque rupture whilst facilitating arterial thickening that enhances the severity of atherosclerosis.

1.8.2 The impact of senescence on VSMC phenotype

Traditionally, VSMC ageing is associated with a progressive decline in proliferative and migratory capacity.[13, 15, 208, 209] However, more recent work suggests that ageing promotes VSMC phenotypic switching and enhances VSMC proliferation and intimal migration, leading to remodelling of the vasculature.[217] This emphasises a gap within the current literature that does not clearly delineate the impact of ageing on VSMC phenotype.

Previous *in-vitro* studies reveal an age-related reduction in the proliferative activity of human VSMCs which corresponds with a decline in their migrational ability.[218] This was supported in a recent study illustrating that induced human VSMC senescence by serum response factor (SRF) depletion inhibits proliferation, reduces F-actin formation and compromises cell migration.[219] Conversely, a study comparing aortic explants from young and old rats, reveals that aged VSMCs exhibit greater proliferative capacity with a 59.3% higher migration rate than that of younger counterparts.[220] *In-vitro* studies comparing early-passage and presenescent VSMCs also demonstrate that proliferation rates increase with age.[221] Moreover, VSMCs isolated from aged rats dedifferentiated more substantially and replicated more actively than those from new-born or young adult rats.[222] [223] Therefore, a growing body of literature illustrates that ageing induces VSMC proliferation and migration within the vessel and contributes to the progression of atherosclerosis.[10, 224, 225]

Due to conflicting evidence, the impact of ageing on VSMC proliferative and migratory capacity remains undefined. These differences may be a result of studies using a variety of experimental systems to define and measure cell migration. Above I have collated literature from both human and rodent studies. Although rodents have been used to model VSMC behaviour, species variation exists and may account for the observed differences in VSMC migration during ageing. Whether helpful or harmful, VSMCs are heavily implicated in atherosclerosis and improved knowledge of the relationship between ageing and VSMC phenotype is crucial to understanding the role of VSMCs in this disease.

1.8.3 Progerin and prelamin A drive VSMC ageing

Amongst the myriad of factors that contribute towards the onset and progression of vascular ageing, it has come to light that progerin and prelamin A are causal of premature ageing and are associated with advanced atherosclerosis. The laminopathic disease, HGPS is one of the most severe forms of progeria affecting 1 in 4 million people worldwide.[175] HGPS patients have a toxic accumulation of progerin, a prelamin A splice variant, that undergoes normal farnesylation but lacks the FACE-1 cleavage site to generate mature lamin A.[174, 226] This results in permanently farnesylated progerin which exhibits high hydrophobicity and greater affinity for the nuclear membrane than lamin A.[138, 143, 227] Moreover, HGPS is also induced by FACE-1 mutations, which cause the NE accumulation of permanently farnesylated prelamin A.[228, 229] Studying HGPS provides an insight into the molecular mechanisms underlying

cellular ageing as progerin accelerates senescence by inducing telomere shortening, laminal thickening and disrupting nuclear integrity.[230-232] This consequently alters the nuclear position of chromosome territories that normally interact with lamin A, resulting in a loss of chromatin and disrupted transcriptional activity.[233] Progerin accumulation at the NE also impairs mitosis and cell cycle progression.[234] Treatment with farnesyltransferase inhibitors (FTIs) blocks progerin targeting the NE and reduces the abundance of nuclear morphology defects that are associated with HGPS.[235] HGPS grossly affects VSMCs, the primary targets for progerin accumulation, suggesting that VSMCs are especially sensitive to ageing.[236, 237] Furthermore, HGPS patients develop premature atherosclerosis due to profound VSMC dysfunction and usually die of myocardial infarction or stroke in their second decade of life.[143, 173, 238]

Normally, prelamin A is efficiently converted to lamin A in a number of processing steps that are outlined in **section 1.7.2**. However, in the absence of FACE-1, prelamin A processing is defective and lamin A production is hindered.[239] Recent studies in our laboratory identify prelamin A as a novel biomarker of normal VSMC ageing that mirrors progerin accumulation at the NE.[204] Significant prelamin A accumulation was detected in both *in-vitro* and *in-vivo* aged, but otherwise healthy, VSMCs and human vessels (**Figure 1.11**), as well as atherosclerotic lesions, suggesting that lamin A processing is hindered during ageing.[204] As illustrated in **Table 1.2**, prelamin A accumulates in presenescent VSMCs that maintain proliferative capacity, suggesting that prelamin A is a driving force behind VSMC senescence and does not accumulate as a consequence of it.[204] Data from our laboratory also reveal that increased prelamin A induces defective DNA damage repair and nuclear dysmorphologies that are characteristic of ageing.[204] Therefore, the accumulation of prelamin A at the NE disrupts nuclear integrity and accelerates cellular senescence, ageing and age-related pathologies.

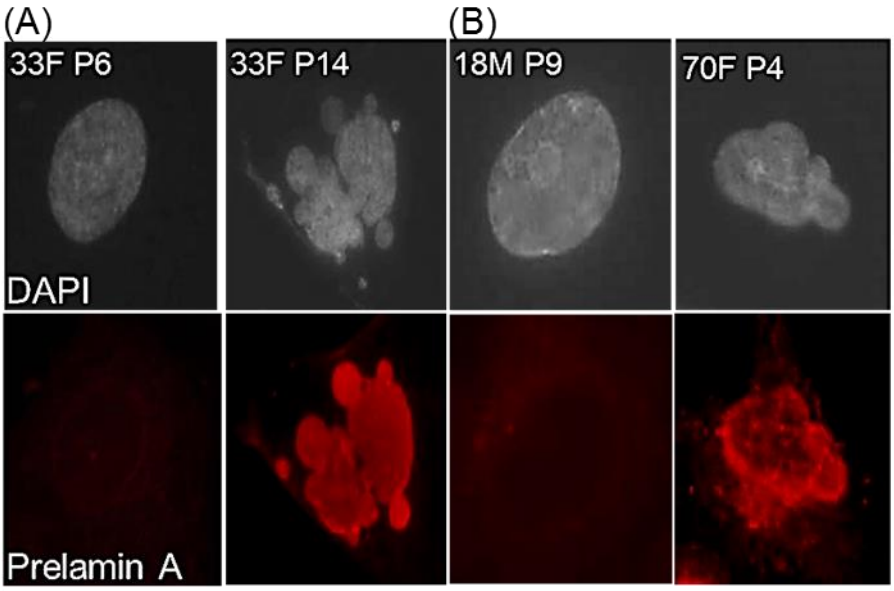

Figure 1.11: Prelamin A accumulates during *in-vitro* and *in-vivo* VSMC ageing. (A) Immunofluorescent images illustrating the absence of prelamin A in early-passage VSMCs (passage 6) derived from a 33-year-old female (33F). Following *in-vitro* passaging (passage 6-14), prelamin A (*red*) accumulates at the NE. **(B)** Aged VSMCs derived from a 70-year-old female (70F) positively stained for prelamin A, which was absent in young, healthy VSMCs from an 18 year-old male donor (18M). Figure modified from Ragnauth *et al*., 2010.[204]

Table 1.2: Stages of VSMC growth *in-vitro*. At early passage numbers, VSMCs are highly proliferative (2-3 day population doubling time) and stain positively for proliferation marker Ki67. Following serial *in-vitro* passaging, VSMCs become presenescent; they stain positively for Ki67, yet proliferation rate is reduced (3-7 day population doubling time). Also, DNA damage marker and prelamin A accumulates. Finally, VSMCs become senescent at late passage numbers when they cease to proliferate and have increased DNA damage, prelamin A and SaβG staining. Data unpublished from Shanahan group (Warren *et al*).

	Proliferative VSMCs	Presenescent VSMCs	Senescent VSMCs
Ki67	✓	✓	x
Prelamin A	X	✓	✓
DNA damage	X	✓	✓
SaβG	X	X	✓
Population doubling time	2-3 days	3-7 days	-

1.9 Hypothesis & Project Aims

Prelamin A accumulates at the NE during VSMC ageing and induces nuclear dysmorphology.[204] Increasing evidence illustrates that loss of nuclear integrity alters LINC complex organisation at the NE, subsequently leading to defective cell adhesion, migration and mechanotransduction.[162, 165, 172, 188] Therefore, a fully-functional LINC complex is fundamental for cell functioning however prelamin A accumulation is thought to compromise LINC complex organisation. We hypothesise that prelamin A accumulation will impact on:

- F-actin organisation and cytoskeletal remodelling
- Focal adhesion organisation and dynamics
- Migrational capacity

My specific objectives were:

1) To characterise VSMC morphological changes associated with *in-vitro* ageing and prelamin A accumulation, specifically actin cytoskeleton and focal adhesion formation.

2) To investigate the impact of *in-vitro* VSMC ageing and prelamin A accumulation on LINC complex organisation in VSMCs and other cell types.

3) To determine whether *in-vitro* ageing or prelamin A accumulation affects the activity of classical signalling pathways (Rho GTPases) involved in regulating cell motility.

4) To study VSMC migration *in-vitro* and characterise any motility changes associated with ageing, prelamin A accumulation or other LINC complex alterations.

Clarifying our understanding of prelamin A and the phenotypic modulations associated with VSMC ageing is important in identifying future therapeutic targets for age-related vascular diseases, primarily atherosclerosis.

Chapter 2: Materials and Methods

2.1 Cell culture

2.1.1 Human vascular smooth muscle cells (VSMCs)

VSMCs were originally isolated from medial explants of human aortic tissue. VSMCs from 3 patients (35-year-old female (35F), 52-year-old male (52M), 54-year-old male (54M)) were cultured in M199 medium complemented with 20% foetal bovine serum (FBS), 1% penicillin/streptomycin and 200 µM L-Glutamine. VSMCs were washed using Earle's balanced salt solution (EBSS) and passaged at a 1:2 split ratio when 60-70% confluent. The VSMC isolate used for each experiment is described within the Figure legend, Mostly 35F VSMCs were used due to their accessibility and time restraints, In the future, experiments will be conducted using all 3 VSMC isolates.

2.1.2 MRC-5 cells

Human embryonic lung fibroblast (MRC-5) cells were purchased from the European cell collection of cell cultures (ECACC) and cultured in Dulbecco's modified eagle medium (DMEM) complemented with 10% FBS, 1% penicillin/streptomycin and 200 µM L-Glutamine. MRC-5 cells were washed using phosphate buffered saline (PBS) and passaged at a 1:3 split ratio when 80-90% confluent.

2.1.3 Human osteosarcoma cell line (U2OS)

Human osteosarcoma (U2OS) cells were purchased from the American Type Culture Collection (ATCC). This cell line was cultured in DMEM complemented with 10% FBS, 1% penicillin/streptomycin and 200 µM L-Glutamine. U2OS cells were washed using PBS and passaged at a 1:10 split ratio when 80-90% confluent.

All cells were cultured in a humidified incubator at 37°C with a 4% $C0_2$ atmosphere. At 60-90% confluency, culture medium was aspirated and cells were washed thoroughly using a balanced salt solution. Trypsin (0.02%) was added for 3-5 min at 37°C to detach cells from the flask surface during passaging. Serum-containing medium was used to inactivate trypsin and cells were seeded into fresh culture flasks (Corning Life Sciences). For storage, cell stocks were initially frozen in freezing medium at -80°C before being transferred to liquid nitrogen.

2.1.4 siRNA-mediated interference

MRC-5 cells (25,000 cells/well of a chamber slide or 200,000 cells/T75 culture flask) or VSMCs (10,000 cells/well of 24-well plate or 200,000 cells/T75 culture flask) were seeded at a medium density and incubated overnight. The next day, for each mL of medium, 0.5 µL siRNA oligo (20 µM stock; sequences shown in **Table 2.1**) was added to 108 µL serum-free medium in an eppendorf tube with 7 µL Hiperfect reagent. The transfection mix was vortexed for 5 sec and incubated for 10 min at room temperature (RT) to allow transfection complex formation. During this time, cells were washed twice and fresh medium (12 mL/T75 culture flask, 4 mL/T25 culture flask, 1 mL/chamber slide well, 500 µL/well of 24-well plate) reapplied. The transfection mix was then added and incubated for 72 hours before cells were prepared for immunofluorescence microscopy or Western blot analysis.

2.1.4.1 siRNA strategy

In these experiments, ON-TARGET plus reagent (Thermo Scientific Dharmacon) combining multiple siRNAs to target distinct regions of the same target gene was used. Because single siRNA reduces target gene expression by less than 50%, this pooling strategy increases the chance of reducing target gene expression. To overcome problems associated with multiple siRNAs increasing the chances of off-target effects , ON-TARGET plus reagent has 2 important modifications i) the sense strand is modified to prevent nitration with RISC and favour antisense strand uptake and ii) the antisense strand seed region is modified to minimise seed-related off-targeting. Evidence has shown that compared to a single siRNA, ON-TARGET plus significantly reduces off-target effects with unmatched potency and specificity.[240] However, contradicting evidence shows that combination siRNAs do not function synergistically to affect target gene expression and suggests that less active siRNAs interfere with the efficiency of higher efficacy siRNAs. Because more potent siRNAs share sequence characteristics, recent evidence demonstrates that single algorithm-designed siRNAs (Cenix BioScience) are more potent and more effective (>85% reduction in target gene expression). Studies directly comparing the alternative strategies show that both single and pooled siRNAs provided false negative/positive results and variable off target effects.[241] It is suggested that several individual siRNAs per target gene in individual transfections is the most effective approach to confirm that obtained results are specific to reduction of gene expression and not off-target effects of single or siRNA pools.[241] Therefore, this approach may be better suited to experiments in the future.

Table 2.1: Oligonucleotides used for siRNA-mediated knockdown

siRNA oligo	Source	Sequence (5' to 3')
Control	Qiagen	AAACCCUCUGAACAGACGACGUU
Human FACE-1/ ZMPSTE24 (ON-TARGETplus, smart pool)	Thermo Scientific Dharmacon	CGGCAGAGAAGGAUAAUA UGGGAAGGCUAAAGACUUA GGUCAGGACUCUAUUCAGA GAUCAUGGAUUCUGAAACA
Lamin A (ON-TARGETplus, smart pool)	Thermo Scientific Dharmacon	CGUGUGCGCUCGCUGGAAA UGAAAGCGCGCAAUACCAA UCACAGCACGCACGCACUA GAAGGAGGGUGACCUGAUA
Nesprin-1 calponin homology 2 (N1CH2) (**Figure 2.1A**)	Thermo Scientific Dharmacon	UGAACGAGGCCGAGAGAGAUU
Nesprin-2 calponin homology 5 (N2CH5) (**Figure 2.1B**)	Thermo Scientific Dharmacon	GCCUUCACGUGCUGGAUAAUU
Human Rac1 (ON-TARGETplus, smart pool)	Thermo Scientific Dharmacon	GUGAUUUCAUAGCGAGUUU GUAGUUCUCAGAUGCGUAA AUGAAAGUGUCACGGGUAA GAACUGCUAUUUCCUCUAA
Human RhoA (ON-TARGETplus, smart pool)	Thermo Scientific Dharmacon	CGACAGCCCUGAUAGUUUA GACCAAAGAUGGAGUGAGA GCAGAGAUAUGGCAAACAG GGAAUGAUGAGCACACAAG
Human UNC 84A (SUN1) (ON-TARGETplus, smart pool)	Thermo Scientific Dharmacon	GAAAAGACCCGACGACACA GCGCUCAGUUCCAGCUAUU GGUACCAGUUUGUUACUUU GGUAACUGCUGGGGCAUUUA
Human UNC 84B (SUN2) (ON-TARGETplus, smart pool)	Thermo Scientific Dharmacon	AGAGCUCGGUGGCGGAAGA GGAAACUGCUGCUCGCAUC CCUGAGGGCCUUCGACAAA CCAGAGACUCAUCGCCACA

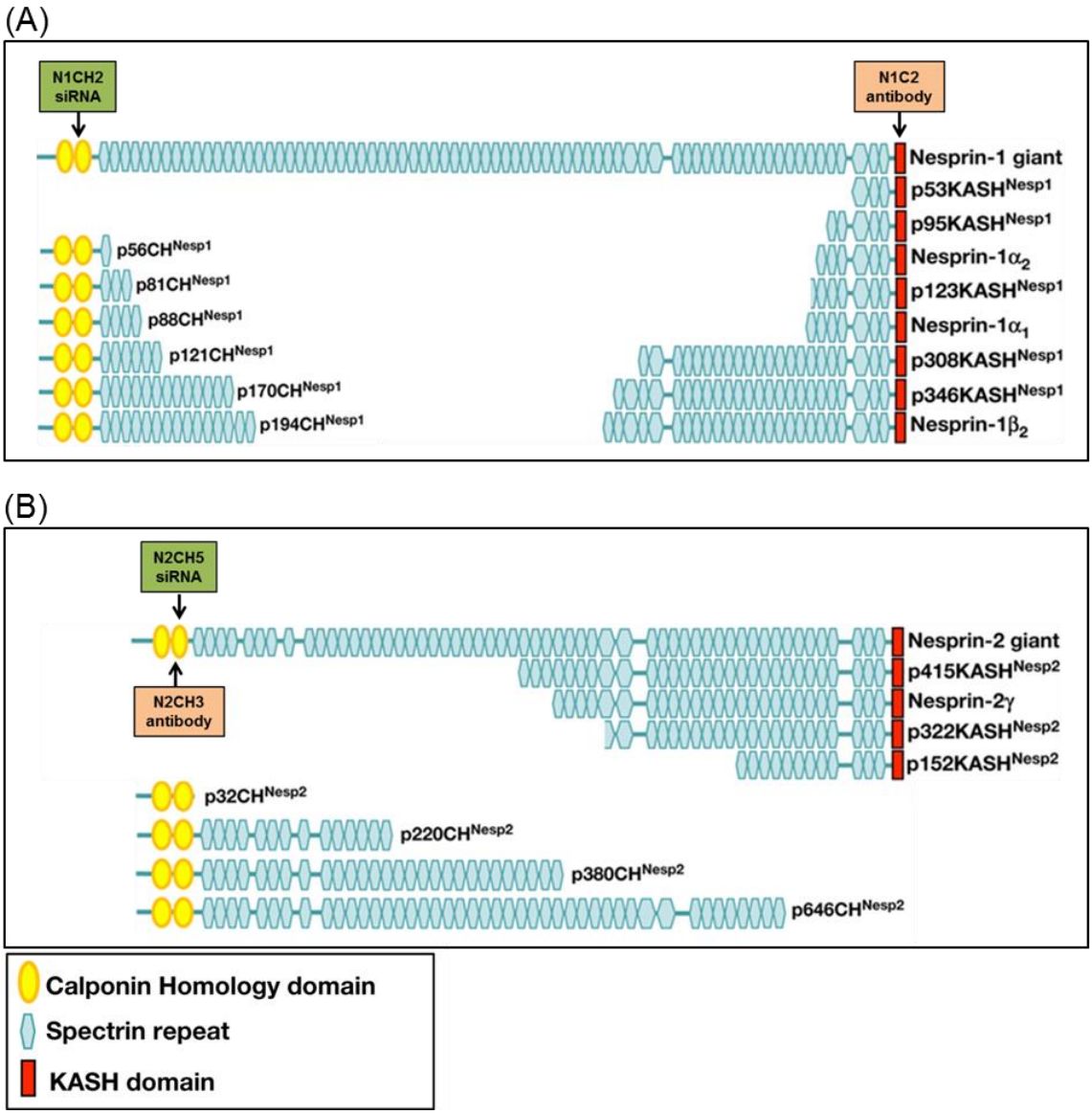

Figure 2.1 Nesprin-1 and -2 siRNA and antibody target sites. Schematic representation of nesprin-1 and -2 giant isoforms. Figure includes examples of their potential N-terminal calponin homology domain and C-terminal KASH domain variants that have been recently published by Rajgor & Shanahan, 2013.[146] Due to their sequence homology and the lack of isoform-specific tools, the exact nesprin content of VSMCs at present is unknown. Arrows indicate where **(A)** nesprin-1 and **(B)** nesprin-2 siRNA and polyclonal antibodies are designed to target.

2.1.5 DNA plasmid transfection

U20S cells, seeded at a medium density, were transfected with DNA plasmid using the following protocol. For each mL of media, 1.5 µg plasmid was added to 75 µL Opti-MEM and vortexed for 5 sec before adding 5 µL Fugene HD transfection reagent. The transfection mix was vortexed for 10 sec and incubated for 15 min at RT to allow transfection complex formation. U20S cells were washed with PBS and incubated for 16-24 hours with transfection mix before cells were prepared for immunofluorescence microscopy or fluorescence recovery after photobleaching (FRAP).

2.2 Molecular biology techniques

2.2.1 RNA extraction

Initially, all surfaces and labware were decontaminated using RNase away reagent. Cells from a confluent T75 culture flask were lysed using 1 mL RNA STAT-60™ and incubated for 5 min at RT to allow complete dissociation of nucleoprotein complexes. Following the addition of 200 µL chloroform, samples were shaken vigorously by hand for 20 sec and incubated for 10 min at RT. This was followed by centrifugation for 15 min/10,500 rpm/4°C and the upper aqueous phase was transferred to an RNase-free microcentrifuge tube with 500 µL isopropanol for 10 min at RT. Total RNA was pelleted by centrifugation for 15 min/10,500 rpm/4°C and the supernatant removed. The pellet was washed with 1 mL 75% ethanol solution in diethylpyrocarbonate (DEPC)-treated water and centrifuged for 5 min/8,250 rpm/4°C. The supernatant was removed and the RNA pellet air-dried for 10 min before being resuspended in ~20 µL DEPC-treated water and stored at -80°C for subsequent analysis.

2.2.2 Reverse transcription (cDNA synthesis)

Total RNA (1 µg) was incubated with 0.5 µL Oligo (dT) primers, 0.5 µL random primers and 2 µL dNTP for 5 min at 65°C. 4 µL 5x buffer and 1 µL RNase inhibitor were added and incubated for a further 3 min at 37°C. 1 µL Promega Avian Myeloblastosis Virus–RT (AMV-RT) was added and reverse transcription performed using the

following protocol in a thermal cycler 2720 (Applied Biosystems); 10 min at 25°C, 50 min at 37°C and 5 min at 95°C. Total cDNA was diluted to the required concentration using nuclease-free water.

2.2.3 Quantitative PCR (qPCR)

Prior to qPCR, primer sets were examined using *Taq* based PCR. Purified products were diluted to generate a 0.5 pmol stock which was serially diluted to create 0.05, 0.005, 0.0005, 0.00005 and 0.000005 pmol standards.

cDNA was diluted 100 ng/µL and 900 ng was used per 20 µL reaction containing 1x SYBR green qPCR master mix and 5 µmol of each primer (**Table 2.2**). PCRs were performed at 95°C for 10 min followed by 40 cycles at 95°C for 5 sec and 60ºC for 1 min using a RotorGene-3000 thermal cycler (Corbett Research). The cycle threshold (CT) for each sample was automatically determined (RG-3000 software) as the first cycle at which a significant increase in optical signal, above an arbitrary base line, was detected. mRNA expression was quantified using standard curves for each primer set and normalised to the internal control, GAPDH, from the same sample. All samples were tested in triplicate and fold changes were calculated using the delta-delta CT method.

Table 2.2: Primers used for qPCR

Primer	Primer sequence
Nesprin-1 CH domain forward	AGAGTCTCTTGGTGTTGGCTTCGT
Nesprin-1 CH domain reverse	TCTCTTGCTCATCTTGCAGCCTCT
Nesprin-2 KASH 2 domain forward	AGAGCAGTGAGAACTACAGAAGGC
Nesprin-2 KASH 2 domain reverse	AGTGCAGCTGTAGTCTTCTTCGGA
GAPDH forward	CGACCACTTTGTCAAGCTC
GAPDH reverse	CAAGGGTCTACATGGCAAC
FACE-1	Ordered from Qiagen

2.2.4 Generation of competent *E.coli* DH5α

E.coli strains DH5α were cultured overnight in antibiotic-free LB medium at 37°C in a shaking incubator. The next morning the culture was centrifuged for 10 min/4,000 rpm/4°C and the bacterial pellets stored at 4°C for 1 hour before being resuspended in 20 mL sterile ice cold 100 mM $CaCl_2$. Bacteria were then re-pelleted for 10 min/3,500 rpm/4°C and treated again with ice cold 100 mM $CaCl_2$ before repeating centrifugation as above. Pelleted bacteria were stored at -80°C in 100 µL aliquots as 15% glycerol stocks.

2.2.5 Transformation of *E. coli* DH5α and plasmid isolation

After thawing on ice, glycerol stocks of competent bacteria were incubated with 1 µL plasmid DNA on ice for 20 min. Bacteria were submerged in a water bath at 42°C for 40 sec to heat shock, then immediately cooled on ice for 2 min. Bacteria were then added to 500 µL antibiotic-free LB medium and incubated in a shaking incubator for 1 hour at 37°C. 50 µL transformed bacteria were plated out on an appropriate antibiotic-treated LB agar plate and cultured overnight at 37°C for antibiotic-resistant gene expression. The next morning, a selected colony was cultured in 3 mL antibiotic-treated LB for a further 8-10 hours. At this point, bacteria were stored at -80°C as 15% glycerol stocks for future use or 1 mL was added to 100 mL antibiotic-treated LB and incubated overnight at 37°C. The next day, bacteria were pelleted by centrifugation 10 min/4,000 rpm/RT and plasmid was isolated using an Endofree Plasmid Maxiprep kit (Qiagen) as per the manufacturer's instructions. Initially, bacteria were lysed in 10 mL lysis buffer, which was subsequently neutralised by the addition of 10 mL neutralisation solution. Plasmid was separated from cell debris by passing the mixture through a filtered syringe. Plasmid-containing liquid was next incubated with 2.5 mL endotoxin removal buffer for 20 min on ice before the plasmid was captured and washed using a Qiagen-tip column. DNA was eluted in 15 mL elution buffer and precipitated using 10.5 mL isopropanol followed by centrifugation 1 hour/4000 rpm/4°C. The DNA pellet was washed in an ethanol-based wash buffer and re-pelleted by centrifugation for 1 hour/4000 rpm/4°C. Finally, the pellet was air-dried and resuspended in 500 µL TE buffer.

2.3 Biochemical techniques

2.3.1 Whole cell lysate preparation

Cells were washed using PBS and harvested by scraping into IP buffer. Suspended cells were sonicated (Branson Sonifier 150) for 10 sec to lyse and cell debris was pelleted by centrifuging for 5 min/12,000 rpm/4°C. The pellet was discarded and the cell lysate (supernatant) protein concentration determined using a DC protein assay (Bio-Rad). Lysates were added to an equal volume of 2x sample loading buffer, vortexed and heated to 80°C for 5 min before Western blot analysis.

2.3.2 DC protein assay

Purified BSA 1.48 mg/mL was serially diluted to make DC protein assay standards. 2 µL cell lysate, alongside 2 µL standards, were incubated with 25 µL Bio-Rad DC Protein Assay Reagent A in a 96-well plate for 5 min at RT. Next, 200 µL Bio-Rad DC Protein Assay Reagent B was added to each well for 5 min at RT. Protein concentrations were determined spectrophotometrically (Tecan GENios pro) at 710 nm by comparing to BSA standards.

2.3.3 Subcellular fractionation

A confluent T75 culture flask was washed with PBS and cells scraped into 400 µL extraction buffer A (for all buffer recipes please refer to table 2.4). Homogenates were incubated on ice for 15 min to lyse. Centrifugation for 3 min/14,000 rpm/RT pelleted the nucleus and the supernatant was collected as the cytosolic fraction. The pellet was resuspended in 100 µL extraction buffer B and incubated for 30 min at 37°C. Centrifugation for 3 min/14,000 rpm/RT pelleted the nuclear insoluble fraction and supernatant was collected as nuclear soluble fraction. The nuclear insoluble fraction was resuspended in 1% sodium dodecyl sulphate (SDS), heated for 10 min at 100°C and sonicated for 10 sec. Each fraction was then added to an equal volume of 2x sample loading buffer, vortexed and heated to 80°C for 5 min before Western blot analysis.

2.3.4 GST pull-down assay

PAK is an immediate downstream effector of stimulated Rac1 and was used in this experiment as a measure of Rac1 activity. *E.coli* BL-21 were transformed with GST-PAK1-PBD (p21-binding domain) plasmid (Addgene #12217) and cultured overnight on an ampicillin agar plate at 37°C. A single colony was selected, diluted into 5 mL ampicillin-LB medium and incubated in a shaking incubator overnight at 37°C. The next day, 500 µL culture was diluted into 200 mL fresh ampicillin-LB medium and grown for ~2 hours in a shaking incubator at 37°C. GST-protein expression was induced with 1 mM Isopropyl β-D-1-thiogalactopyranoside (IPTG) for ~2 hours at 37°C and bacteria were harvested by centrifuging for 15 min/2,500 rpm/RT. Pellets were then resuspended in 5 mL PBS with protease inhibitors (2 µL/mL) and sonicated for 10 sec. Proteins were solubilised by incubating with 1% Triton-X for 1 hour at 4°C before bacterial debris was pelleted (15 min/2,500 rpm/RT). Supernatant was collected and recombinant protein was purified by adding 500 µL glutathione-sepharose beads (50% slurry) and rotating for 30 min at RT. Beads were washed (3 x 5 min) with PBS at 4°C and GST-protein expression was visualised by SDS-PAGE and coomassie staining.

GST-protein beads (50 µL of 50% slurry) were mixed with 200 µg cell lysate on a rotator for 2 hours at 4°C. Beads were then pelleted by centrifugation for 2 min/2000 rpm/4°C and washed with 200 µL lP buffer (3 x 5 min). Bound protein was eluted following the addition of 50 µL 2x sample buffer and boiling for 5 min at 95ºC. Pulled-down proteins were analysed by SDS-PAGE and Western blot analysis.

2.3.4.1 Quantification of GTPase activity

To determine Rac1 activity, Western blotting utilised anti-Rac1 antibody followed by densitometric analysis. Band intensity was measured using the Gel Analyser function of Image J software. GST-PAK1-PBD (active Rac1) lysates were loaded alongside control lysates of the same cell sample (retained to measure total Rac1). Active Rac1 intensities were normalised to control lysates, which then allowed us to compare active Rac1 between experimental samples i.e. proliferative vs presenescent VSMCs.

2.3.5 Western blot analysis

10% resolving gels were set in gel casting kits (Bio-Rad) before 4% stacking gel was poured on top, using combs to create wells within the gel for sample loading (for solution details see **Table 2.4**). Gels were submerged in running buffer and cell lysate samples loaded into individual wells, alongside a protein standard. Protein samples were then subjected to SDS-PAGE using a Mini PROTEAN 3 system (Bio-Rad). Gels were initially resolved at 80 V, until protein samples passed through the stacking gel, then increased to 120 V until samples reached the end of the resolving gel. Next, the resolving gel was laid on methanol-activated polyvinylidene difluoride (PVDF) membrane and sandwiched between blotting paper (3 layers on each side) soaked in 1x transfer buffer. Proteins were transferred from the gel to PVDF membrane using a semi-dry transfer cell (Bio-Rad Trans-Blot® SD) for 1 hour at 25 V. Gels were stained with coomassie and membranes were blocked using 5% milk solution for 1 hour at RT on an orbital shaker. Membranes were then incubated with primary antibodies (**Table 2.3**) diluted in 5% milk solution overnight at 4°C. After briefly washing with TBS-T, membranes were incubated with secondary antibody conjugated to horseradish peroxidase (HRP) (**Table 2.3**) diluted in 5% milk solution for 1 hour at RT. Membranes were further washed with TBS-T (15 min x 3), processed using an enhanced chemiluminescent (ECL) kit and developed (Compact X4 Automatic Processor) to visualise protein bands.

All commercially available antibodies were validated at the beginning of each experiment: individual protein bands were detected at the correct molecular weight (see Table 2.3). Nesprin-1 and -2 antibodies were produced in-house and different nesprin isoforms at varying molecular weights (~20, 80 and 220kDa).

Table 2.3: Antibodies used for immunofluorescence microscopy (IF) and Western blot analysis (WB).

Primary antibodies & molecular weight	Source & order number	Dilution (WB)	Dilution (IF)
α-tubulin (55 kDa)	Sigma-Aldrich (T9026)	1:10,000	1:1000
β-actin (42 kDa)	Sigma-Aldrich (A2228)	1:10,000	-
Emerin (NCL) (34 kDa)	Leica Biosystems (6012130)	1:500	1:50
FACE-1 (ZMPSTE24) (54 kDa)	Novus Biologicals (100-2387)	1:200	-
Lamin A/C (N-18) (70 kDa)	Santa Cruz Biotechnology (6215)	1:1,000	-
Nesprin-1 (N1C2) (multiple bands)	Made in-house (**Figure 2.1A**)	1:1000	-
Nesprin-2 (N2CH3) (multiple bands)	Made in-house (**Figure 2.1B**)	1:1000	1:100
Prelamin-A (C-20) (74 kDa)	Santa Cruz Biotechnology (H1312)	1:250	1:250
Rac1 (21 kDa)	Millipore (05-389)	1:1000	-
Rac2 (21 kDa)	Millipore (07-604)	1:1000	-
RhoA (22 kDa)	Abcam (54835)	1:100	-
Smooth muscle α-actin (SM-actin) (43 kDa)	Sigma-Aldrich (75228)	1:1000	-
SUN1 (90 kDa)	Abcam (74758)	1:100	-
SUN2 (80 kDa)	Abcam (65447)	1:1000	1:100
Vinculin (116 kDa)	Sigma-Aldrich (V9264)	1:10,000	1:1000
Secondary antibodies	**Source & order number**	**Dilution (WB)**	**Dilution (IF)**
Anti-mouse IgG, HRP-conjugated	GE healthcare (NA931)	1:5000	-
Anti-goat IgG HRP-conjugated	Sigma-Aldrich (A9452)	1:5000	-
Anti-rabbit IgG HRP-conjugated	GE healthcare (NA934)	1:5000	-
Donkey-anti-mouse Alexa flour 488	Invitrogen (A21202)	-	1:500
Donkey-anti-goat Alexa fluor 488	Invitrogen (A11055)	-	1:500
Goat-anti-rabbit Alexa fluor 488	Invitrogen (A11011)	-	1:500

2.4 Cell biology techniques

2.4.1 Immunofluorescence microscopy

VSMCs cultured on 13 mm glass cover slips in 24-well plates or MRC-5 cells on chamber slides were washed with PBS and fixed for 5 min in 4% paraformaldehyde at RT. Cells were then washed in PBS x 2 and cell membranes permeabilised using 0.5% Nonidet P-40 (NP-40) alternative for 2 min at RT. To reduce non-specific background staining, cells were incubated with PBS containing 1% BSA for 1 hour at RT prior to incubation with primary antibody solution overnight at 4°C. The next day, cells were washed with PBS and incubated in fluorescence-conjugated secondary antibody solution or rhodamine phalloidin (1:2,000) for 1 hour at RT (see **Table 2.3** for all primary and secondary antibodies used). Cell nuclei were stained using 4',6'-Diamidino-2-Pheylindoledihydrochloride (DAPI; 1:10,000) and subsequently washed in PBS x 3. Cells were mounted onto slides using Mowiol/Dabco mounting media and visualised using a Zeiss Axioplan 2 light microscope (20 or 40x objective) or Leica SP5 confocal microscope, with an x63, 1.2NA oil emersion lens attached to a Hamamatsu Orca-R2 cooled CCD camera. Volocity software (Perkin Elmer, USA) was used to control exposure time and gain/offset measurements before storing captured images. Initially, all antibodies were tested individually to confirm antibody specificity. We also confirmed that dual antibody staining did not affect protein localisation.

2.4.1.1 Analysing cell morphology

Acquired images were exported from Volocity as TIFF files. Image J software was used to manually draw around individual cells and measure morphological parameters such as area (arbitrary value) and circularity/shape factor. Circularity is defined as 4π (area)/(perimeter) whereby values approaching 1 signify a rounded cell and 0 represents an elongated cell. During my project, I converted to Volocity software for image analysis as this automatically measures the same parameters by fluorescence detection. Rhodamine phalloidin (F-actin stain) and DAPI (DNA stain) were used to determine cell shape and nuclear shape, respectively. Additionally, anti-vinculin was used to measure focal adhesion number, size and shape. Student's *t*-tests were performed using GraphPad Prism software for statistical analysis.

2.4.2 Time-lapse video microscopy

Time-lapse microscopy was used to monitor different modes of cell migration *in-vitro.* Firstly, single cell migration was captured to determine the intrinsic capacity of cells to migrate without the influence of external factors. We also recorded the migration of cells towards a scratch in an attempt to imitate wound healing. Finally, a chemotactic assay was used to represent cell migration during injury responses. The Dunn chamber was used to capture directional cell movement towards a serum gradient. All time-lapse microscopy was conducted using an Olympus IX81 microscope attached to a Hamamatsu Photonics Orca-R2 cooled CCD camera maintained at 37°C with constant CO_2 supply. Shutters were set for maximum sample protection against phototoxic damage during filming. Volocity software was used to control time-lapse image acquisition and for the compilation of time-lapse movies from which cell migration was analysed.

2.4.2.1 Random single cell migration

Cells were sparsely seeded (50-60% confluency) onto a 24-well plate 24 hours prior to time-lapse microscopy. The next day, cells were washed and medium replaced prior to filming. Multiple positions across each well were selected and phase contrast images at these x-y positions were captured using a motorised stage (LUDL Electronic products) every 5 min for 16-24 hours. A 4x objective was used for VSMC imaging and 10x objective for MRC-5 cells. Images were compiled to generate time-lapse movies of random cell migration without chemoattractant influence.

2.4.2.1.1 Image processing and analysis

Time-lapse movies were exported from Volocity as TIFF files and cell tracking was conducted using Image J software (manual tracking plugin). Single cells were manually tracked by clicking on the centre of cell nuclei throughout consecutive frames (**Figure 2.2A**). Tracking was terminated upon cell-cell contact or during cell division as these influence migratory behaviour. Finally, a static artefact from each movie was tracked to correct for background drift that may have occurred during recording. Each movie was saved as a comma separated value (.CSV) file.

Using these x-y coordinates, Mathematica 6.0 (Wolfram Research Ltd, USA) measured migrational velocity (distance/time) and persistence (calculated as the linear

displacement of the cell divided by total distance migrated; values approaching 1 define persistent cell migration in a linear fashion and 0 defines deviation from a straight line). This was achieved using custom-written Mathematica notebooks (Professor Graham Dunn & Daniel Soong, King's College London) that were created for the analysis and statistical comparison of cell migration. Initially, .CSV files were converted to .CEL format and each movie corrected using static artefact coordinates. .CEL files were then imported into the Chemotaxis Analysis Notebook V1.6 and tracks plotted using the Track Plotter, Analyser and Editor (**Figure 2.2B**). This also generated histograms of velocity and persistence profiles (**Figure 2.3**). A Two Sample Tester was used to statistically compare cell migration between datasets.

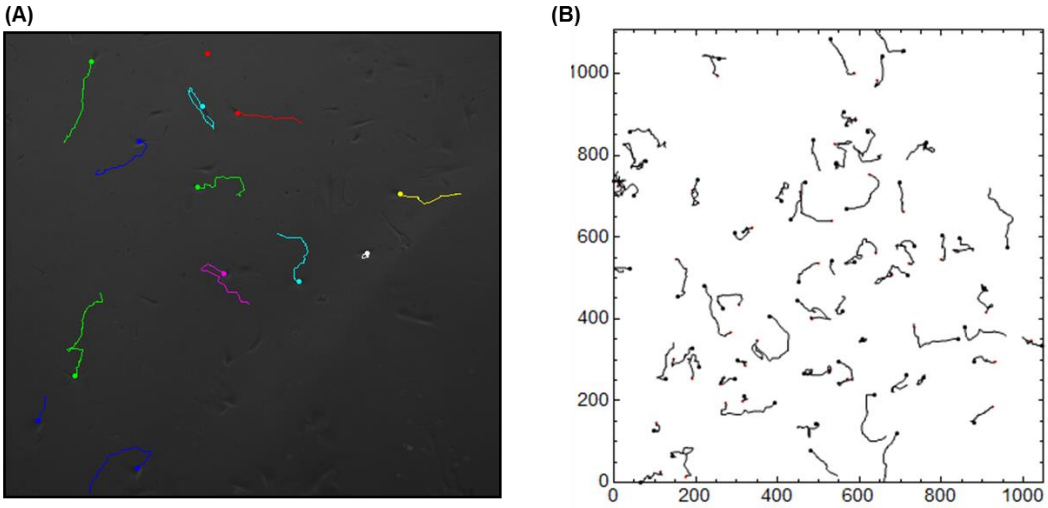

Figure 2.2: Tracking random single cells. (A) Individual cells were tracked throughout consecutive frames of a time-lapse movie using the Image J manual tracking plugin. **(B)** Coordinates from each movie were combined using Mathematica to visualise the migratory path of numerous cells.

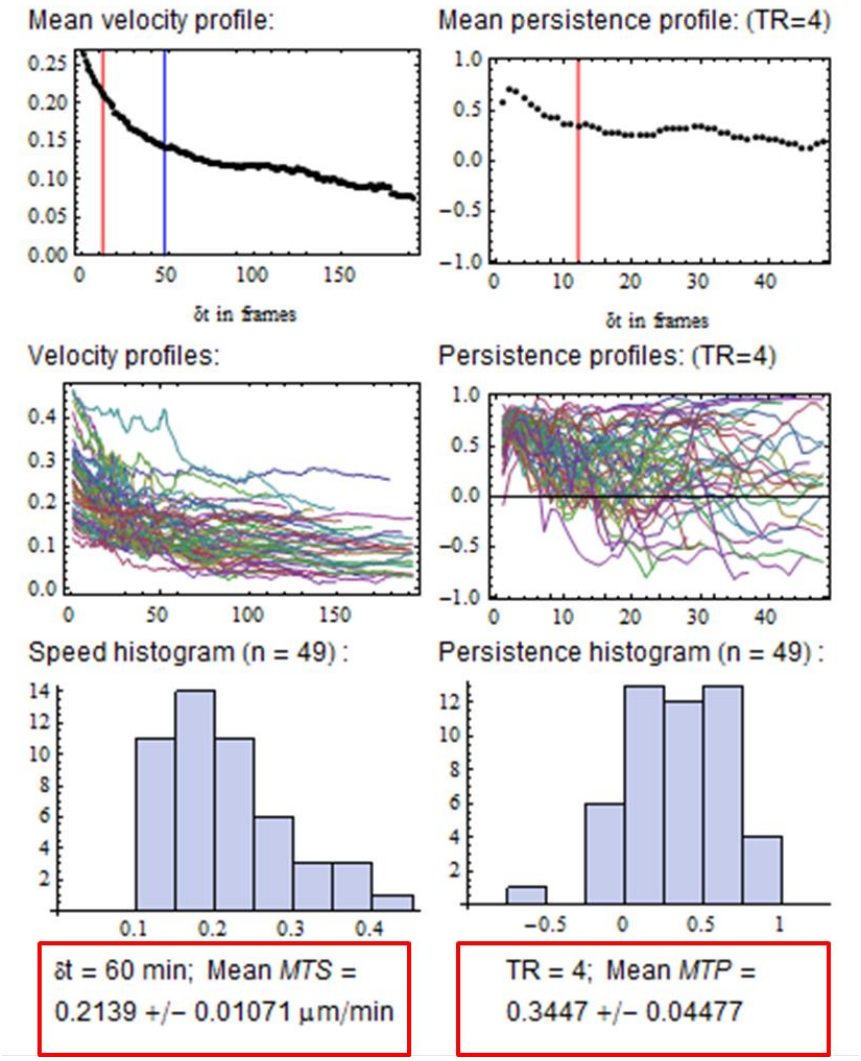

Figure 2.3: Analysing cell migration. Mathematica software was used to generate mean velocity and persistence profiles of cell migration. Histograms illustrate the mean track speed (*MTS*) and mean track persistence (*MTP*) of a selected sampling time.

2.4.2.2 Scratch assay

VSMCs were seeded onto a 24-well plate and cultured until dense (90-100% confluency). A 200 µL pipette tip was used to scratch the centre of each well to simulate a wound, excess cells were removed with PBS and the culture medium replaced prior to filming. Multiple positions across each well were selected and phase contrast images were captured every 5 min for 16 hours using a 4x objective. Images were compiled to generate a time-lapse movie of collective cell migration into the scratch area. A limitation of this assay is that it does not account for proliferation that will also increase the cell number in the scratch assay. To overcome this, future studies

will use a proliferation inhibitor (mytomysin C for VSMCs) prior to filming, to ensure that migration alone is captured.

2.4.2.2.1 Image processing and analysis

Images exported from Volocity as TIFF files were subjected to a series of processing steps using Image J software to compare scratch size at T=0 compared with T=16 hours (**Figure 2.4**). Initially, the edge of the scratch was defined (process-find edges, process-sharpen). To increase contrast between the scratch and cell front, an appropriate threshold was applied to each image to generate a binary image (image-adjust-threshold, process-find edges). Each image was then inverted (image-lookup tables-invert LUT) and scratch area was measured from the area fraction value (analyse-analyse particles). The fraction size change between T=0 and T=16 hours determined scratch closure (%).

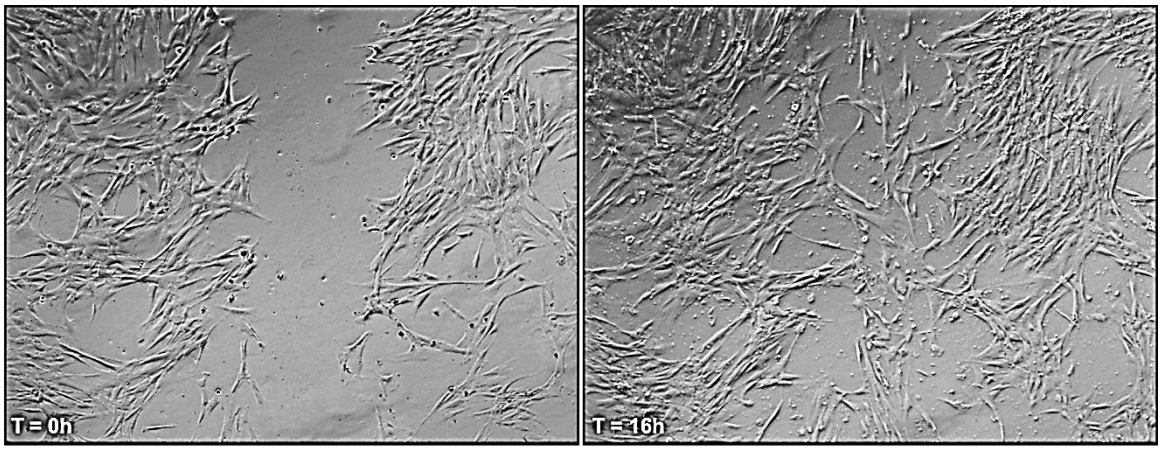

(A) Phase contrast scratch images after 0 and 16 hours of time-lapse microscopy

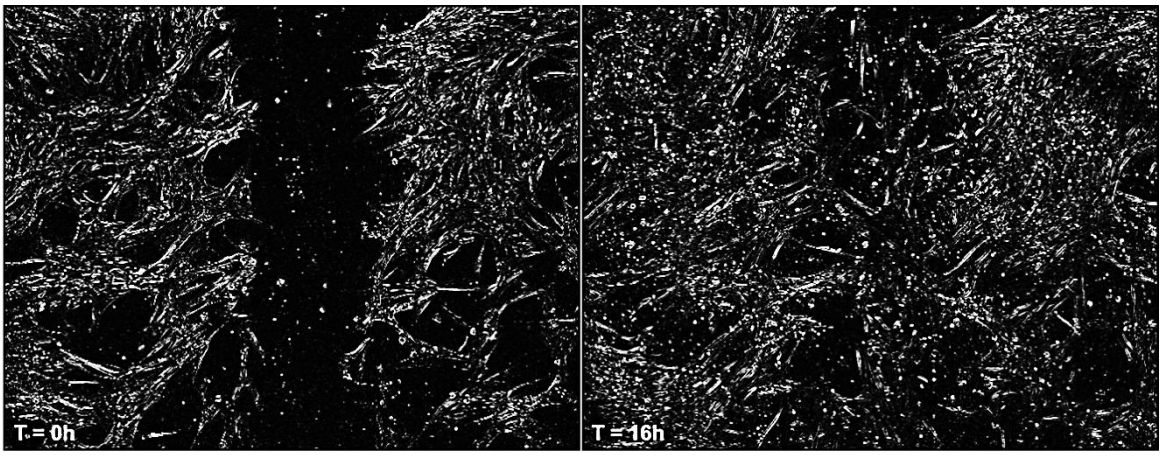

(B) The scratch edge was defined using Image J software (process image-find edges, process-sharpen)

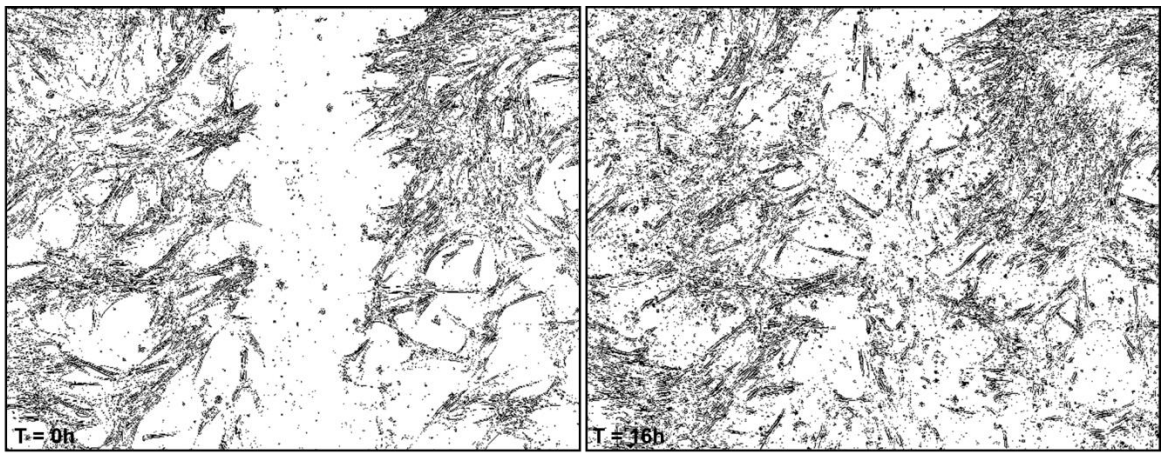

(C) Binary images were produced (image-adjust-threshold, process-find edges)

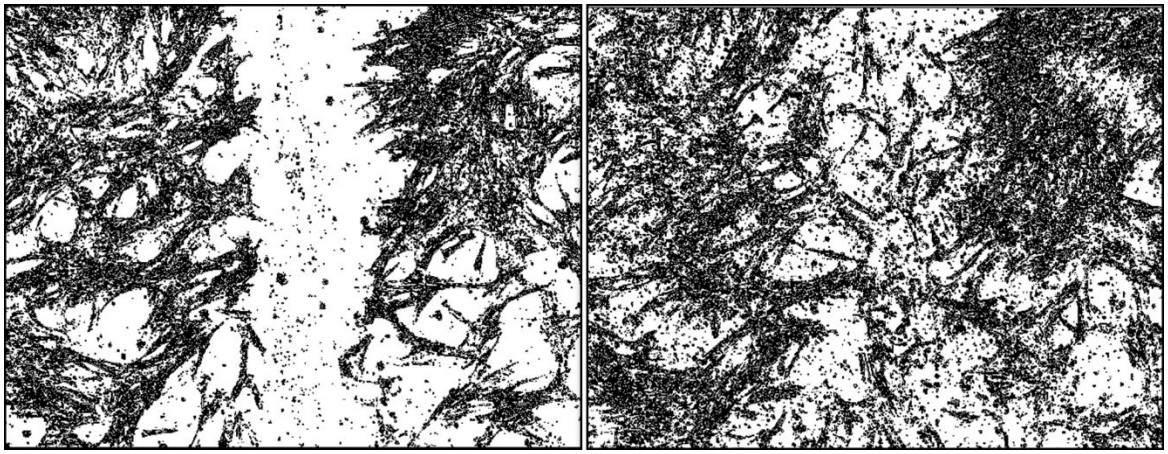

(D) Images were inverted to increase contrast (image-lookup tables-invert LUT) and scratch area was measured (analyse-analyse particles)

Figure 2.4: Image processing steps using Image J software for scratch closure analysis

2.4.2.3 Interference reflection microscopy (IRM)

IRM is used to image cell-substrate interactions and is a widely used technique for quantifying the focal adhesion dynamics of live cells in culture. Initially, cells were sparsely seeded (50-60% confluency) onto a glass-bottom culture dish (MatTek Ltd) for 24 hours. The next day, cells were washed using PBS and the culture medium replaced prior to filming. Multiple positions (5-10) across the dish were selected, focussing on the leading edge of cells. Images were captured every 2 min for 1 hour using an incident light fluorescence attachment and a 63x oil immersion objective.

2.4.2.3.1 Principles of IRM

When cells are very close to the glass surface, reflected light from the cell membrane shifts out of phase with reflected light from the glass. This causes 'interference' which manifests as a dark pixel against the cell-free background. When cell membrane is not attached to the glass, reflected beams will not interfere, resulting in a bright pixel in the image (**Figure 2.5**).[242] Therefore, IRM enables clear imaging of the focal adhesion pattern at the base of the cell and can be used to measure focal adhesion turnover.

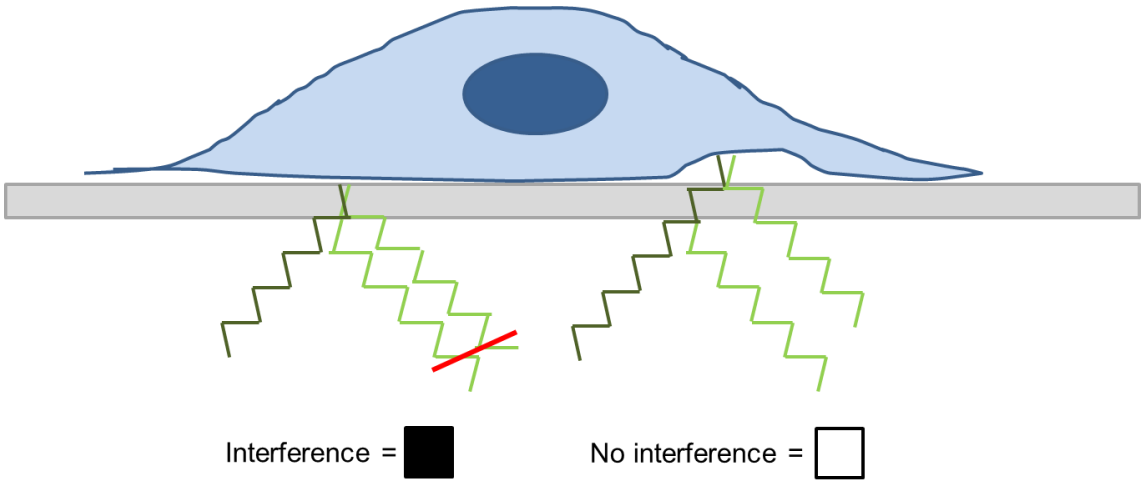

Figure 2.5: Principles of interference reflection microscopy. Dark green waves represent emitted light from the fluorescence source and pale green waves represent reflected light. If the cell membrane is too close to the glass, reflected light from the cell membrane shifts half a wavelength. This interferes with waves reflected from the glass, resulting in a dark pixel in the image. A greater distance between the glass and cell membrane does not cause interference and results in a bright pixel.

2.4.2.3.2 Image processing and analysis

In our study, focal adhesion formation at the leading edge of VSMCs and MRC-5 fibroblasts was analysed after 20 min and 1 hour of filming, respectively. Time-separated images (t=0, t=20/60 min) were exported from Volocity as TIFF files and subject to a series of processing steps to increase contrast between focal adhesions and image background (**Figure 2.6**). This was achieved using Image J software in a method modified from previous studies.[243] Firstly, an FFT bandpass filter was applied to each image (process-FFT-bandpass filter) and an appropriate threshold was

selected (image-adjust-threshold) to generate binary images, making focal adhesions strikingly obvious against the background. Any artefacts, not representing focal adhesions, were removed manually by selecting and inverting to colour-match the background. The cell leading edge was selected and Image J measured the pixel count of each focal adhesion (analyse-analyse particles-show outlines). Next, a composite image was created (image-colour-merge channels) to highlight newly formed focal adhesions (t=20/60; red) against original focal adhesions (t=0; green). The pixel count of newly formed focal adhesions were then was expressed as a percentage of the total number of original pixels to give focal adhesion assembly (%).

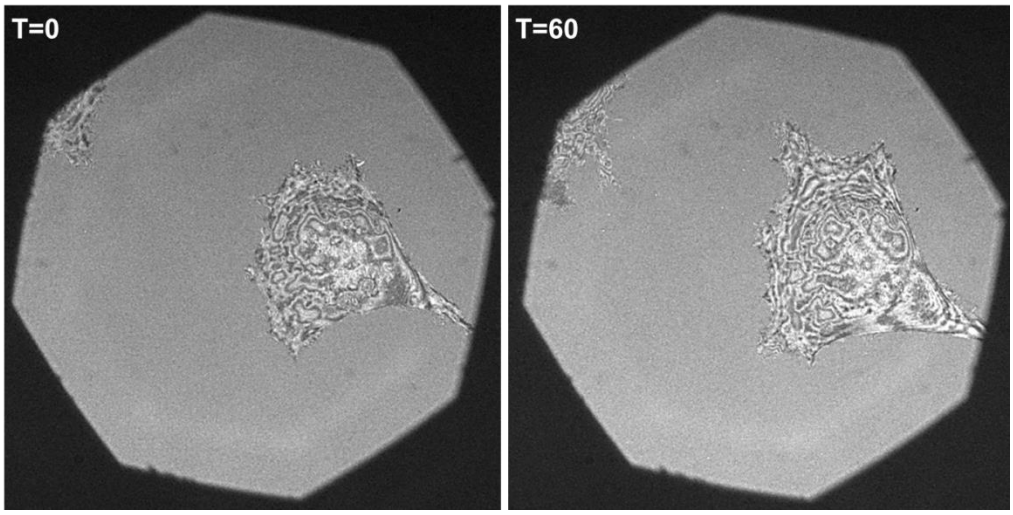

(A) IRM images of MRC-5 fibroblasts captured at 0 and 60 min

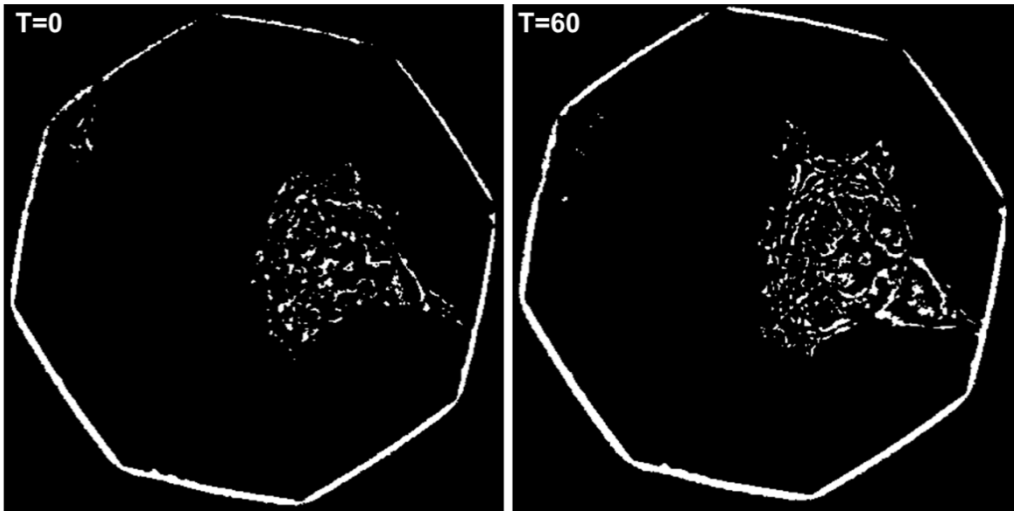

(B) Images were subject to numerous processing steps to increase the contrast between focal adhesions and the image background (process-FFT-bandpass filter, image-adjust-threshold)

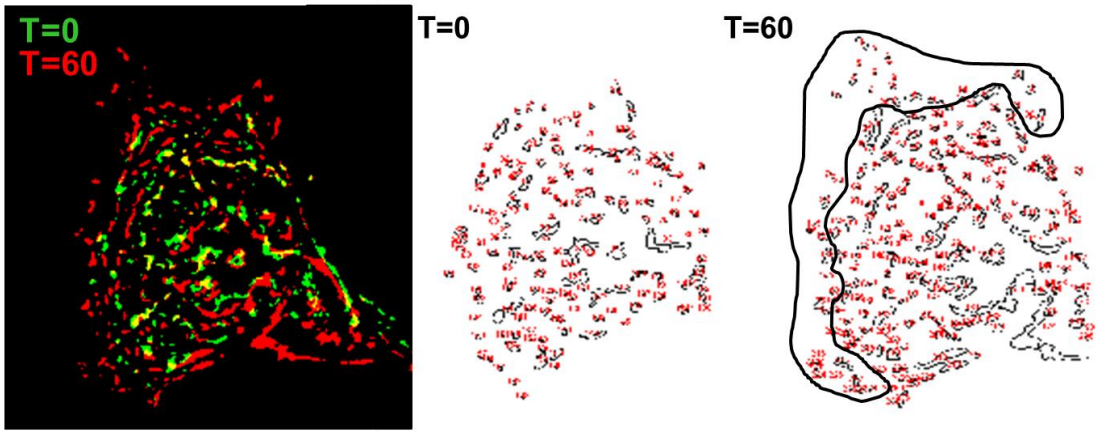

(C) A composite image (image-colour-merge channels) distinguishes newly-formed focal adhesions (red) against those in the original image (green). The pixel count of new adhesions (T=60) was compared with the total number of original pixels (T=0) to provide a percentage of focal adhesion assembly (analyse-analyse particles-show outlines)

Figure 2.6: IRM image processing and analysis

2.4.2.4 Chemotaxis assay

Chemotaxis describes the movement of cells in response to spatial gradients of chemical cues. In our studies, Dunn chemotaxis chambers (Hawksley Technology, Lancing, UK) were used to determine VSMC migration towards a serum gradient. Initially, VSMCs were seeded onto glass coverslips (22x22 mm, 1.5 mm thickness) for 8 hours in culture medium containing 20% FBS. Cells were then serum-starved overnight in culture medium containing 2% FBS before setting up Dunn chambers as described below.

2.4.2.4.1 Principles of the Dunn chamber assay

The Dunn chamber is a glass microscope slide into which two concentric annular wells are cut at a depth approximately half the thickness of the slide. These two wells are separated by a bridge. Filling the outer well with chemoattractant creates a gradient across the bridge and triggers cell migration into this area (see **Figure 2.7**).[244] In our experiments, the Dunn chamber slide was covered with 2% FBS culture medium containing 20 µm HEPES to maintain a physiological pH throughout filming. A glass coverslip was then inverted onto the Dunn chamber, just off-centre to leave a small filling slit at one edge. Surplus medium was removed and the edges, apart from the filling slit, were sealed using hot wax mixture (Vaseline: paraffin: beeswax 1:1:1). A gradient was created by placing 20% FBS culture medium (containing 20 µm HEPES) in the outer well via the filling slit before this slit was sealed. On the time-lapse microscope, multiple fields were selected and VSMC migration from the inner to the outer well was recorded every 10 min for 16 hours.

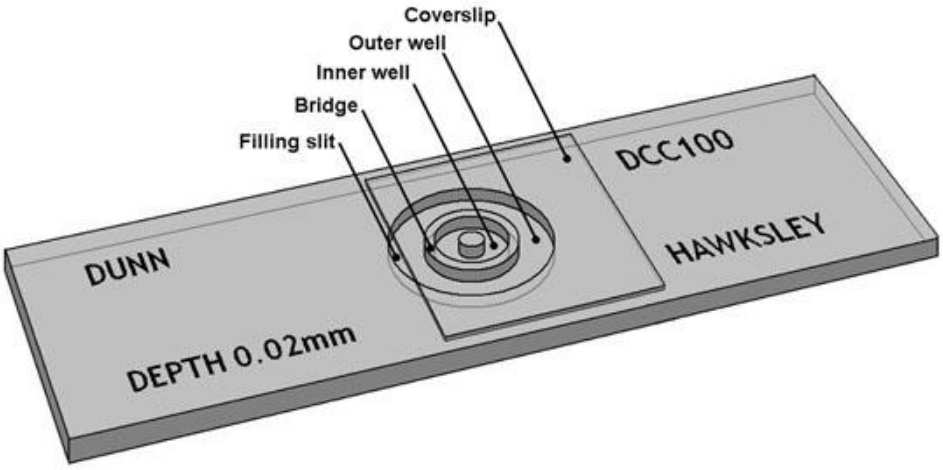

Figure 2.7: The Dunn chamber. The Dunn chamber is a glass microscope slide with an inner and outer well that are separated by a bridge. Cells are cultured on coverslips that are then inverted onto the slide. Applying a chemoattractant source to the outer well, via the filling slit, creates a chemotactic gradient across the bridge and cell migration from the inner to outer well is recorded using time-lapse microscopy.[244]

2.4.2.4.2 Image processing and analysis

Time-lapse movies were exported from Volocity as TIFF files and VSMCs were manually tracked using Image J software as previously described. These migratory coordinates were imported into Mathematica and .CEL files were subsequently analysed using the Chemotaxis Analysis Notebook V1.6. The angle at which each movie was captured was also used to normalise migrational directionality.

A Rose plot (circular histogram) displayed distributions of VSMC trajectories relative to their gradient orientation (0°). Rayleigh tests assessed whether clustering of VSMC track directionality occurred and determined whether a significant chemotactic response was stimulated. A significant chemotactic response is indicated on Rose plots by a red arrow facing the mean angle of migration. The green section highlights the 95% confidence interval.

2.4.3 Fluorescence recovery after photobleaching (FRAP)

All FRAP experiments were conducted at the Randall Division of Cell and Molecular Biophysics by Dr Daniel Soong (King's College BHF Centre Light microscopy research officer). FRAP is a non-invasive method of measuring protein mobility and dynamics within a living cell. FRAP uses a high-powered laser beam to irreversibly photobleach fluorescently-tagged protein within a small region of interest (ROI). Subsequently, fluorescence recovery occurs from the diffusion of surrounding unbleached molecules into the bleached area until a steady state is reached. This is monitored by capturing a series of images post-bleach and results in a characteristic recovery curve which is used to determine protein mobility and turnover.

2.4.3.1 Cell preparation

U2OS cells were seeded into T25 culture flasks at a medium density (50-60%) and incubated overnight. The next day, siRNA transfection mix was added as previously described (see **section 2.1.4**). After 48 hours, DNA transfection mix was prepared into 3 mL phenol red-free medium (see **section 2.1.5**) using GFP-mini-nesprin-2G construct (kindly donated from Gregg Gunderson, Columbia University). During this time, U2OS cells were washed twice with PBS and trypsinised using phenol red-free trypsin. Trypsinised cells were then resuspended in DNA transfection mix and seeded onto glass-bottom dishes (MatTek Ltd) for 16-24 hours prior to FRAP experiments.

2.4.3.2 FRAP imaging

FRAP images were acquired on a Ti Eclipse A1R laser scanning confocal microscope (Nikon, Tokyo, Japan) using a 60x 1.4 NA oil-immersion objective. A 488 nm 40 mW diode laser (Coherent, Santa Clara, USA) was used for excitation and emitted light was collected via a 505/550 nm bandpass filter. Images were captured every second for 20 seconds before a circular ROI was bleached for 25 iterations at full laser power (100% transmission). FRAP was subsequently monitored for a further 300 sec, again with images acquired approximately every second. In addition, a background ROI monitored the amount of non-bleached fluorescent signal lost during imaging.

2.4.3.3 FRAP analysis

FRAP analysis was conducted by Dr Daniel Soong who specifically created a programme to determine the mobile fraction as well as binding rate constants (k_{on} and k_{off}) of bleached GFP-mini-nesprin-2G. Briefly, intensity curves were fit to an equation using Mathematica in accordance with published data determining FRAP rate fittings.[245] All intensity plots we recorded were found to adhere most closely to the formula for a reaction dominant FRAP curve, in which the rate of diffusion is very small compared to the intensity increase (recovery) in the bleach region. This is caused by the release of bleached molecules from within and binding of unbleached molecules from outside of the beach region. The reaction dominant formula allows calculation of mobile fraction from the plateau of the curve, whilst the fit can extract values for K_{on} and K_{off} rates by rearranging the formulae:

1) $$\text{intensity} = 1 - C_{\text{eq}} \times e^{(-k_{\text{off}} \times t)}$$

2) $$C_{\text{eq}} = \frac{k_{\text{on}}}{k_{\text{off}} + k_{\text{on}}}$$

This experiment was repeated numerous times to optimise this technique. Final analysis was performed by Dr Daniel Soong on data collated from 20-30 cells imaged during 4 independent experiments. Using GraphPad Prism, statistical significance was determined with a paired Student's *t* test.

Table 2.4: Solutions used for experiments

Solutions	Solution components
Extraction buffer A	50 mM HEPES pH 7.5, 150 mM NaCl, 1 mM EDTA, 0.1% Triton, 10 mM NaF, 10 mM ß-glycerophosphate, 1 mM Na_3VO_4, 2 µL/mL protease inhibitors
Extraction buffer B	50 mM HEPES pH 7.5, 150 mM NaCl, 1 mM EDTA, 10 mM NaF, 10 mM ß-glycerophosphate, 1 mM Na_3VO_4, 5 mM MnCl2, 300 µg/mL DNase 1, 2 µL/mL protease inhibitors
Freezing medium (tissue culture)	1 mL DMSO, 1 mL FBS, 8 mL growth medium containing 20% FBS
IP buffer	10 mM Tris-HCl pH7.5, 150 mM NaCl, 1 mM EDTA, 1% Triton, 2 µL/mL protease inhibitors
Milk solution (5%)	5 g dried milk, 100 mL TBS-T
Resolving gel 10% (~20 mL)	7.9 mL H_2O, 6.7 mL 30% acrylamide, 5 mL 1.5 M Tris pH 8.8, 0.2 mL 10% SDS, 0.2 mL APS, 8 µL TEMED
Running Buffer	15 g Glycine, 3 g Tris, 10 mL 10% SDS, 1 L H_2O
Sample loading buffer 2x (20mL)	1 M Tris-HCl pH 6.8, 10% glycerol, SDS, 0.1% bromophenol blue (w/v), 20% ß-mercaptoethanol
Stacking gel 5% (~10 mL)	6.8 mL H_2O, 1.7 mL 30% acrylamide, 2.5 mL 0.5 M Tris pH 6.8, 100 µL 10% SDS, 100 µL 10% APS, 10 µL TEMED
Transfer buffer 10x (1 L)	30 g Tris, 150 g glycine, 20 mL 10% SDS, up to 1L H_2O
Transfer buffer 1x (500 mL)	50 mL 10x transfer buffer, 100mL MeOH, 500mL H_2O
Mowiol/Dabco mounting media	2.4 g Mowiol 4-88, 6 g glycerol, 6 mL H_2O, 12 mL 0.2 M Tris pH 8.5, 2.5% DABCO
TBS (Tris-buffered saline) 10x (1 L)	12.11 g Tris, 87.6 g NaCl, 1 L H_2O, pH 7.6 (HCl)
TBS-T (1 L)	100 mL 10x TBS, 900 mL H_2O, 0.3% tween 20

Table 2.5: Details of laboratory reagents used

Laboratory reagents	Source	Order number
β-Mercaptoethanol (C_2H_6OS, βME)	Sigma-Aldrich	M-6250
ß-glycerophosphate	Sigma-Aldrich	G9422
5x buffer & RNase inhibitor kit	Promega	M1705
30% Acrylamide/Bis solution	BioRad	161-0158
Ammonium Persulfate (APS)	Bio-Rad	161-0700
AMV-RT	Promega	M5101
Bovine Serum Albumin (BSA)	Sigma-Aldrich	A4503
Bromophenol Blue	Sigma-Aldrich	11,439-1
Chamber slides (4 well)	BD Falcon	354114
Chloroform	Sigma-Aldrich	C2432
Coomassie G-250 stain	Bio-Rad	161-0786
DABCO (1,4-diazabicyclo[2.2.2]octane)	Sigma-Aldrich	D-2522
DAPI (4',6'-Diamidino-2-Pheylindoledihydrochloride)	Sigma-Aldrich	D-9542
DC Protein Assay	Bio-Rad	500-0113, 500-0114
DEPC-treated water	Invitrogen	750023
DNase I	Sigma-Aldrich	AMPD1
dNTPs master mix	Promega	NU-0010-10
Dulbecco's Modified Eagle's Medium (DMEM)	Sigma-Aldrich	D5671
Dulbecco's Modified Eagle's Medium (DMEM) Phenol red free	Sigma-Aldrich	D5921
DMSO (dimethyl sulfoxide)	Sigma-Aldrich	D8418
Earl's Balanced Salt solution (EBSS)	Sigma-Aldrich	E6267
Enhanced Chemiluminescent (ECL) kit	Pierce	32106
Ethanol (CH_3CH_2OH, EtOH)	Sigma-Aldrich	E7023
Ethylenediaminetetra-acetic Acid (EDTA)	Sigma-Aldrich	E-5134
FACE-1 primers (ZMPSTE24)	Qiagen	QT00024627
Foetal Bovine Serum (FBS)	Sigma-Aldrich	F-7524
Fugene HD transfection reagent	Promega	E2311
Glycine	Fisher Scientific	BP381-500
HEPES	Sigma-Aldrich	H4034
Hiperfect transfection reagent	Qiagen	301707
Isopropanol (C_3H_8O)	Sigma-Aldrich	I9516
LB Agar	Sigma-Aldrich	L2897

LB Medium	Sigma-Aldrich	L3022
Manganese chloride (MnCl2)	Sigma-Aldrich	244589
Maxiprep kit (endofree)	Qiagen	12362
Methanol (CH_3OH,MeOH)	Sigma-Aldrich	322415
Milk (dried skimmed)	Marvel	
Mowiol	Calbiochem	475904
M199 media	Sigma-Aldrich	M4530
NP-40 alternative	Calbiochem	492016
Oligo (dT) primers	Promega	C1101
Opti-MEM	Invitrogen	11058-21
Paraformaldehyde powder	Sigma-Aldrich	P6148
Penicillin-Streptomycin-Glutamine solution liquid	Invitrogen	10378-016
Phosphate buffered saline (PBS)	Sigma-Aldrich	D1408
Protease Inhibitor Cocktail	Sigma-Aldrich	P8340
Protein standards (Precision Plus Protein™ Dual Colour Standards	Bio-Rad	161-0374
PVDF membrane (Immobilon-P™)	Millipore	IPVH00010
Random Primers	Promega	C1181
Rhodamine Phalloidin	Invitrogen	R415
RNase away	Molecular Bioproducts	7003
RNA STAT-60™	AMS Biotechnology	CS-110
ROCK inhibitor Y27632 dihydrochloride	Sigma-Aldrich	Y-0503
SDS	Fluka Analytical	05030
Sodium Chloride (NaCl)	Sigma-Aldrich	S7653
Sodium fluoride (NaF)	Sigma-Aldrich	201154
Sodium orthovanadate (Na_3VO_4)	Sigma-Aldrich	S-6508
SYBR green qPCR master mix	Eurogentec	RT-SY2X-03+NRWOUB
TEMED	Bio-Rad	161-0801
Triton-X 100	Sigma-Aldrich	X-100
Trizma™ base	Sigma-Aldrich	T6066
Trypsin 1x-EDTA solution	Sigma-Aldrich	T3924
Trypsin (phenol red free) 10x	Invitrogen	15400-054
Tween 20	Sigma-Aldrich	P2287

Chapter 3: Characterising the impact of *in-vitro* ageing and nuclear lamina disruption on smooth muscle cell and fibroblast phenotype

3.1 Introduction

Ageing is the largest risk factor in the development of cardiovascular diseases such as atherosclerosis, however, our understanding of the mechanisms underlying ageing and how ageing impinges upon cell function remains poorly defined.[198, 199] Previous studies conducted in our laboratory discovered prelamin A accumulation as a biomarker of normal VSMC ageing.[204] These studies demonstrate that prelamin A accumulated in VSMCs from aged vessels and atherosclerotic lesions, which did not occur in VSMCs from young, healthy vessels.[204] Furthermore, prelamin A accumulates in presenescent VSMCs and prelamin A overexpression induces premature senescence, indicating that prelamin A drives VSMC senescence rather than accumulating as a consequence of it.[204] However, the precise role of prelamin A in ageing and the pathophysiological implications of prelamin A accumulation have yet to be fully described.

Emerging evidence illustrates that the LINC complex plays an important role in regulating actin organisation and cell motility.[151, 165, 246] This is mediated by nesprin-SUN-nuclear lamina interactions spanning the NE that physically couple the actin cytoskeleton and nuclear interior.[128] Prelamin A accumulation occurs at the NE during ageing and induces nuclear dysmorphology.[204] In light of this, we aimed to determine the impact of prelamin A accumulation upon the LINC complex; its organisation and role in regulating F-actin, focal adhesion dynamics and migration. As the current literature stands, we have a limited understanding of how ageing impacts on VSMC migration and contributes towards the development of cardiovascular diseases such as atherosclerosis.

3.2 Aim of this chapter

This chapter aims to investigate the impact of prelamin A accumulation upon LINC complex organisation and function in VSMCs and MRC-5 fibroblasts. We hypothesise that prelamin A accumulation alters LINC complex stability and disrupts the coupling between the NE and actin cytoskeleton. As a result, we expect this to impinge upon general cell morphology, focal adhesion organisation and migratory behaviour.

3.3 Results

3.3.1 Prelamin A accumulation is associated with VSMC ageing

To model ageing, young and healthy primary human VSMCs were serially passaged *in-vitro* until cell growth ceased. The VSMC growth curve (**Figure 3.1A**) has 3 distinct stages: an initial *proliferative* phase when growth rate is high (population doubling time (PDT) 3-4 days) at early passage numbers (passages 6-12), a *presenescent* phase (passages 12-14) when VSMCs become 'aged' and growth rate is reduced (PDT 6-7 days) and finally, a *senescent* phase when proliferation terminates (passage ~15+). High-passage (aged) and early-passage (healthy) VSMCs were compared to investigate the morphological changes associated with ageing. As illustrated in earlier studies, prelamin A accumulation occurred at the NE of presenescent and senescent VSMCs, with no positive staining in proliferative VSMCs (**Figure 3.1B**).[204] This further supports evidence that prelamin A accumulation occurs during presenescence rather than a result of senescence.

3.3.2 FACE-1 downregulation induces prelamin A accumulation

In healthy VSMCs, prelamin A is continually cleaved by FACE-1 to form lamin A which is incorporated into the nuclear lamina.[140] During VSMC ageing, prelamin A processing is hindered causing prelamin A to accumulate at the NE.[204, 239] In agreement with our previous findings, Western blot analysis comparing proliferative and presenescent VSMCs illustrated a reduction of FACE-1 levels in presenescent VSMCs which expectedly corresponded with prelamin A accumulation (**Figure 3.2A**).

To specifically observe the impact of prelamin A accumulation at the NE, siRNA-mediated knockdown of FACE-1 was performed to artificially accelerate prelamin A accumulation in proliferative VSMCs. Western blot analysis confirmed that FACE-1 siRNA treatment successfully depleted FACE-1 levels leading to a subsequent increase in prelamin A (**Figure 3.2B**). This was further supported by qPCR data showing reduced FACE-1 mRNA expression (68.7 ± 3.680% reduction) in FACE-1 siRNA cells compared with control cells (**Figure 3.2C**). Furthermore, immunofluorescence microscopy confirmed that prelamin A accumulated at the NE of most FACE-1 siRNA treated cells (79.23 ± 2.439%) with none detected in control cells (**Figure 3.3B & D**). This prelamin A staining mirrored that observed in *in-vitro* aged VSMCs. Most presenescent VSMCs stained positive for prelamin A (96.83 ± 1.740%)

which was scarcely detectable in proliferative VSMCs (3.03 ± 0.837%) (**Figure 3.3A & C**). Together, these experiments identified FACE-1 siRNA as a valuable tool to manipulate prelamin A levels at the NE and was used throughout this project to model VSMC ageing.

Fibroblasts were also treated with FACE-1 siRNA to determine whether these cells could accumulate prelamin A and be used to model VSMC ageing. Fibroblasts were used in these experiments to preserve precious VSMC stocks whilst also modelling ageing in a cell type that doesn't naturally accumulate prelamin A. Interestingly, the prelamin A mutant, progerin, is detected in fibroblasts derived from HGPS patients and its accumulation drives defective phenotypic changes. However, the impact of progerin accumulation on fibroblast migration is unknown. Immunofluorescence microscopy revealed that prelamin A accumulated at the NE of 85.39 ± 3.036% FACE-1 depleted fibroblasts to mimic aged VSMCs and no prelamin A was detectable in control cells (**Figure 3.4A & B**). This was reinforced by Western blot analysis and qPCR, illustrating that diminished FACE-1 protein levels correlated with increased prelamin A (**Figure 3.4C**) and FACE-1 mRNA expression was depleted by 69.23 ± 6.558% (**Figure 3.4D**).

3.3.3 Aged VSMCs exhibit alterations to nuclear morphology

Previous studies report that VSMC ageing induces nuclear morphology defects.[204] Serial VSMC passaging *in-vitro* is associated with increased nuclear convolutions and cells from older patients have more dysmorphic nuclei compared with those derived from younger patients.[204] In the current study, early-passage and presenescent nuclei from 3 VSMC isolates (52M, 54M, 35F) were stained with DAPI and immunofluorescence microscopy was used to determine the nuclear changes associated with ageing (**Figure 3.5A**). Volocity software measured nuclear parameters to reveal that presenescent nuclei were 2-fold larger and significantly more elongated than proliferative cell nuclei (**Figure 3.5B & C**). To establish whether prelamin A accumulation was causal for the nuclear changes detected during VSMC ageing, FACE-1 siRNA was used to accelerate prelamin A accumulation. VSMC nuclei were stained using DAPI and immunofluorescence microscopy revealed no change to the nuclear size or shape of FACE-1 depleted VSMCs (**Figure 3.6**).

3.3.4 VSMC ageing and prelamin A accumulation alters cell morphology

Our evidence indicates that VSMC ageing induces alterations to nuclear morphology. As the actin cytoskeleton defines cell morphology, we next investigated the impact of ageing on F-actin organisation. Early-passage and presenescent VSMC actin filaments were stained using rhodamine phalloidin (**Figure 3.7A**). Immunofluorescence microscopy captured images of 3 VSMC isolates (52M, 54M, 35F) and subsequent analysis using Image J software revealed that presenescent cells were 2.8-fold larger and significantly more elongated than proliferative VSMCs (**Figure 3.7B & C**). These morphological changes mimicked those previously detected in aged VSMC nuclei (**Figure 3.5**). Based on our evidence so far, we speculate that prelamin A accumulation at the NE is capable of inducing morphological changes via its impact on the actin cytoskeleton. To ensure that ageing was not affecting the microtubule network, *in-vitro* aged VSMCs were stained at proliferative and presenescent growth stages with α-tubulin antibody. Apart from the morphological changes previously discussed (**Figure 3.7**), immunofluorescence microscopy found no gross change to microtubule organisation during *in-vitro* ageing (**Figure 3.8**).

We next investigated whether the cell shape changes associated with ageing were specifically a result of augmented prelamin A at the NE. VSMCs were treated with control and FACE-1 siRNA and F-actin staining prior to immunofluorescence microscopy revealed that prelamin A accumulation had no impact on cell area but significantly reduced cell circularity (**Figure 3.9**). Therefore, prelamin A plays a part, but is not solely responsible, for driving the morphological changes that occur during VSMC ageing. This experiment was repeated in fibroblasts of 3 different passage numbers (passage 34, 38, 39). Immunofluorescence microscopy revealed that FACE-1 depleted fibroblasts were significantly smaller and more elongated than control cells (**Figure 3.10**). Although these changes do not exactly reflect those detected in aged VSMCs, this data confirms that prelamin A accumulation influences cell architecture.

In addition, confocal microscopy further assessed actin organisation in *in-vitro* aged and artificially aged (FACE-1 depleted) VSMCs. Actin filaments stained using rhodamine phalloidin were imaged at successive optical slices throughout individual VSMCs. This enabled finer-detailed imaging of the actin cytoskeleton and visualisation of the actin cap. The actin cap is a highly organised structure of thick F-actin bundles that tightly covers the apical surface of the nucleus via direct connection to LINC complexes.[194] Because VSMC ageing influences nuclear and cell morphology, we were surprised to find no alterations in actin cap formation in either presenescent or FACE-1

siRNA treated VSMCs when compared to proliferative and control siRNA treated VSMCs, respectively (**Figure 3.11**). This supports more recent findings demonstrating that the actin cap is unaffected in cells possessing various lamin A mutations.[247]

3.3.5 VSMC ageing and nuclear lamina disruptions alter focal adhesion organisation

The actin cytoskeleton is connected to the cell membrane via a plethora of adaptor proteins that make up focal adhesion complexes.[37] As *in-vitro* ageing and prelamin A accumulation significantly impacts upon nuclear and cell morphology, we expanded our study to examine the impact of VSMC ageing upon focal adhesion organisation. Immunofluorescence microscopy of vinculin-stained VSMCs revealed focal adhesions to be abundantly expressed throughout proliferative cells (99.61 ± 5.170 focal adhesions per cell) which were largely reduced in presenescent VSMCs (74.03 ± 4.499 focal adhesions per cell) and redistributed to the cell periphery (**Figure 3.12A & B**). Analysis with Volocity software revealed that focal adhesions were significantly smaller and more circular in presenescent VSMCs compared with proliferative VSMCs (**Figure 3.12C & D**).

After observing that ageing impinges on focal adhesion organisation, we next investigated whether prelamin A accumulation was specifically accountable for these changes. Proliferative VSMCs and MRC-5 fibroblasts were treated with FACE-1 siRNA for 72 hours to accumulate prelamin A and focal adhesions were stained with anti-vinculin. Immunofluorescence microscopy and subsequent analysis with Volocity software revealed that focal adhesions were abundantly expressed throughout control VSMCs and fibroblasts (53.49 ± 3.290 & 58.08 ± 3.420 focal adhesions per cell, respectively), whereas, FACE-1 depletion was associated with a loss of focal adhesions (43.04 ± 2.385 & 40.16 ± 1.710 focal adhesions per cell, respectively) (**Figure 3.13A & B** & **3.14A & B**). Furthermore, focal adhesions primarily localised to the periphery of FACE-1 depleted cells similarly to those observed in presenescent VSMCs (**Figure 3.13A** & **3.14A**). Following FACE-1 depletion, focal adhesions were significantly more spherical in both VSMCs and fibroblasts (**Figure 3.13C** & **3.14C**) and were significantly smaller in VSMCs (**Figure 3.13D**). Fibroblasts showed no change to focal adhesion size (**Figure 3.14D**).

Together, this evidence demonstrates that *in-vitro* VSMC ageing and prelamin A accumulation induce focal adhesion relocalisation to the cell periphery and increase

their circularity, attributes that are indicative of high focal adhesion turnover and cell motility.[248] To study focal adhesion dynamics, interference reflection microscopy (IRM) measured focal adhesion assembly in *in-vitro* aged and FACE-1 depleted VSMCs. The leading edge of presenescent VSMCs was significantly more dynamic, with focal adhesion turnover (23.96 ± 2.615%) doubling that of proliferative (11.6 ± 2.844%) and senescent (15.37 ± 2.901%) VSMCs (**Figure 3.15**).

IRM also illustrated that FACE-1 depletion significantly enhanced focal adhesion dynamics in both VSMCs and MRC-5 fibroblasts. As prelamin A is a dominant negative of lamin A, this experiment was repeated using lamin A siRNA as a positive control. Successful lamin A depletion in VSMCs and fibroblasts (63.07 ± 4.042% & 46.35 ± 6.154% reduction, respectively) was demonstrated using immunofluorescence microscopy and Western blot analysis (**Figure 3.17 & 3.19**). Focal adhesion assembly in FACE-1 (20.44 ± 2.989%) and lamin A (20.47 ± 2.089%) depleted VSMCs nearly doubled that measured in control VSMCs (10.73 ± 1.875%) after 20 min (**Figure 3.16**). Control fibroblasts had little focal adhesion formation in 60 min (9.08 ± 1.677%) which more than doubled in FACE-1 (21.38 ± 2.123%) and lamin A (26.96 ± 5.012%) depleted fibroblasts (**Figure 3.18**). This evidence illustrates that nuclear lamina remodelling is able to influence focal adhesion behavior at the cell membrane and strongly supports the notion that the LINC complex creates a continuously-coupled system throughout the entire cell.

3.3.6 *In-vitro* ageing and nuclear lamina disruptions affect cell migration

Due to accumulating evidence indicating that ageing impacts upon VSMC morphology and focal adhesion dynamics, we next characterised the effect of ageing upon migrational behaviour. Time-lapse video microscopy captured random single cell migration of proliferative, presenescent and senescent VSMCs over a 16 hour period. Individual cells were tracked throughout time-lapse movies using Image J software, x-y coordinates were plotted and migration was analysed using Mathematica software (**Figure 3.20A**).

Presenescent VSMCs (0.180 ± 0.006 μm/min) were significantly faster than early-passage VSMCs (0.140 ± 0.007 μm/min). Once VSMCs reached the senescent growth stage, migration speed slowed (0.144 ± 0.006 μm/min) to match that of early-passage, proliferative cells **(Figure 3.20B**). The increased migratory speed of presenescent VSMCs correlated with enhanced migrational persistence. Presenescent

VSMC persistence (0.406 ± 0.021) was significantly higher than that of proliferative (0.206 ± 0.03) and senescent (0.256 ± 0.027) VSMCs (**Figure 3.20C**). This clearly indicates that fundamental changes to cell migration occur throughout the 3 distinct stages of *in-vitro* ageing.

To study the impact of nuclear lamina disruption on single cell migration, VSMCs and MRC-5 fibroblasts were treated with FACE-1 and lamin A siRNA for 72 hours prior to time-lapse microscopy. As described above, Mathematica software plotted individual VSMC and fibroblast migration tracks before analysing migratory behaviour (**Figure 3.21A & 3.22A**). FACE-1 (0.193 ± 0.006 µm/min) and lamin A (0.185 ± 0.006 µm/min) depleted VSMCs exhibited no change to migrational velocity when compared with control siRNA-treated VSMCs (0.196 ± 0.007 µm/min) (**Figure 3.21B**). However, FACE-1 (0.235 ± 0.018 µm/min) and lamin A (0.251 ± 0.023 µm/min) depleted fibroblasts were significantly faster than control fibroblasts (0.154 ± 0.009 µm/min) (**Figure 3.22B**). FACE-1 depleted VSMCs (0.595 ± 0.019) were significantly more persistent than lamin A (0.55 ± 0.019) and control (0.501 ± 0.023) VSMCs (**Figure 3.21C**). Moreover, FACE-1 (0.266 ± 0.033) and lamin A (0.273 ± 0.038) knockdown increased the migratory persistence of fibroblasts compared with control cells (0.102 ± 0.029) (**Figure 5.22C**). Together, this evidence suggests that the nuclear lamina contributes to the migratory behaviour of both cell types studied.

3.3.7 The impact of *in-vitro* ageing and nuclear lamina disruption on directional VSMC migration

After observing the impact of ageing and nuclear lamina disruption on single VSMC migration, we next employed a scratch assay to study migration more closely in these cells. A scratch was engraved into a confluent monolayer of VSMCs and time-lapse captured migration into the scratch area over 16 h. Scratch closure was significantly higher in presenescent (15.28 ± 1.897%) and senescent (12.2 ± 0.835%) VSMCs compared with proliferative VSMCs (8.897 ± 1.417%) (**Figure 3.23**). Furthermore, scratch closure was significantly more efficient in FACE-1 (15.45 ± 1.159%) and lamin A (14.79 ± 1.113%) depleted VSMCs than control siRNA-treated VSMCs (9.346 ± 0.8623%) (**Figure 3.24**).

We also investigated the impact of *in-vitro* ageing on the ability of VSMCs to undergo chemotaxis. A Dunn chamber assay combined with time-lapse microscopy compared proliferative, presenescent and senescent VSMC migration towards a serum

gradient. Proliferative and presenescent VSMCs migrated directionally towards the serum gradient (mean direction; -20.637 ± 28.8962° & -17.5024 ± 43.338°, respectively). Rayleigh tests revealed that clustering in the direction of these gradients was significant in both proliferative ($p < 0.0001$, $n = 119$) and presenescent ($p = 0.0035$, $n = 87$) VSMCs. However, senescent VSMCs were unable to sense and migrate directionally towards the gradient ($p = 0.3902$, $n = 122$) (**Figure 3.25**). Thus, proliferative and presenescent VSMCs were able to effectively chemotax, and only when cells reached senescence was chemotaxis impaired.

3.3.8 VSMC ageing and nuclear lamina disruptions hinder Rho GTPase activity

After observing the migratory changes associated with presenescence and prelamin A accumulation, we next explored the molecular changes underlying VSMC ageing, in particular, the impact of VSMC ageing on Rho GTPase proteins. Rho GTPases are well-established regulators of the actin cytoskeleton, cell motility and cell proliferation.[45] Western blot analysis comparing proliferative and presenescent VSMC lysates revealed that total levels of Rac1 and RhoA were attenuated in presenescent VSMCs (**Figure 3.26**).

To specifically assess the impact of ageing on Rac1 activity, proliferative and presenescent cell lysates were prepared for a GST pull-down assay. GST-PAK1-PBD (p21-binding domain) beads were used to specifically precipitate Rac1 in its GTP-bound form. Western blotting revealed that Rac1 activity was significantly inhibited in presenescent VSMCs (66.21 ± 0.066% reduction) compared with proliferative VSMCs (**Figure 3.27**). Next, this experiment was repeated in nuclear lamina disrupted VSMCs. Control, FACE-1 and lamin A siRNA-treated VSMC lysates were prepared for GST-pull down with Rac1-GST. Western blotting revealed that Rac1 activity was repressed in FACE-1 and lamin A depleted VSMCs by 40 ± 0.079% and 77.11 ± 0.033%, respectively (**Figure 3.28**).

ROCK is a downstream effector of Rho and its activation generates contractile force required to drive cell movement and disassemble focal adhesions at the rear of migrating cells.[113, 114] Time-lapse microscopy captured the effect of ROCK inhibition on random single VSMC migration using Y-27632. Y-27632 is the most widely used selective inhibitor of the ROCK family protein kinases; p160ROCK (ROCK-I) and ROKα/Rho-kinase (ROCK-II). Characterisation studies have revealed that Y-27632

inhibits the ROCK family of kinases with much greater affinity (>200-fold selectivity) than to other kinases, including citron kinase, PKN, PKC, cAMP-dependent protein kinase, and myosin light chain kinase.[249, 250] Y-27632 can abolish stress fibres at low concentrations (10 µM) with little to no off-target effects or impact to the cell cycle or cytokinesis.[250]

ROCK-inhibited VSMCs were significantly faster (0.248 ± 0.013 µm/min) than untreated VSMCs (0.139 ± 0.006 µm/min) (**Figure 3.29A**). ROCK inhibition also significantly increased migrational persistence (0.803 ± 0.020) compared with untreated cells (0.610 ± 0.022) (**Figure 3.29B**). In addition, we further tested the specific impact of Rac1 and RhoA depletion on MRC-5 fibroblast migration. Successful Rac1 and RhoA knockdown using siRNA was confirmed by Western blot analysis (**Figure 3.30A & B**). Time-lapse microscopy captured random single migration, cells were manually tracked using Image J (**Figure 3.30C**) and migration analysed using Mathematica software. Rac1 depletion reduced fibroblast migration speed (0.057 ± 0.007 µm/min), however, this was not significant. Conversely, RhoA-depleted fibroblasts were significantly faster (0.132 ± 0.017 µm/min) than control cells (0.079 ± 0.010 µm/min) (**Figure 3.30D**). No significant change to migratory persistence was detected across the 3 treatment groups (**Figure 3.30E**). These data suggest that RhoA is an important mediator of migration speed and loss of RhoA in aged VSMCs may be causal for their enhanced velocity.

(A)

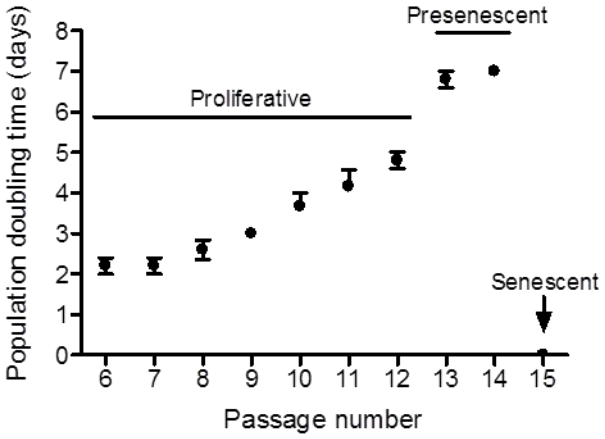

(B)

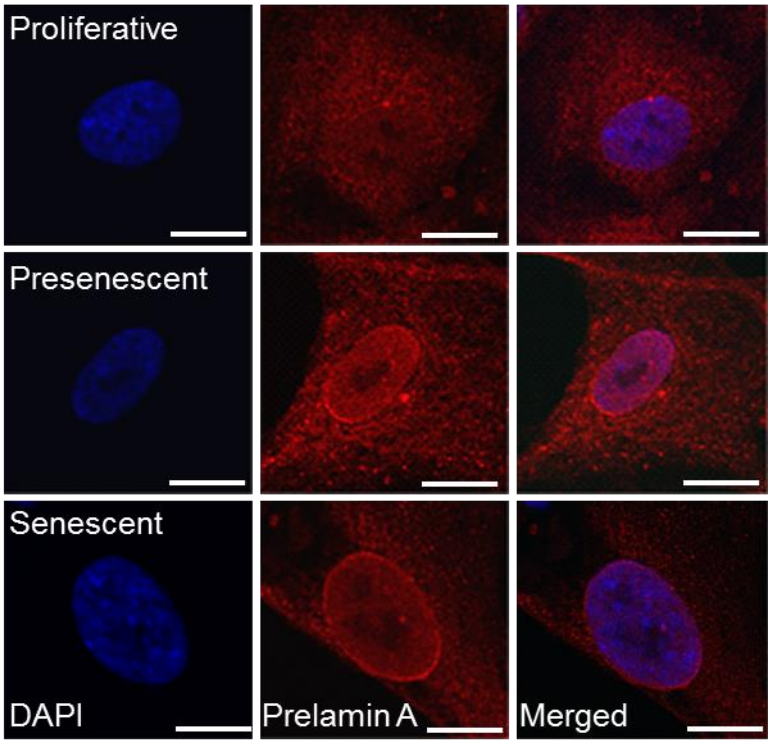

Figure 3.1: Prelamin A accumulation is associated with *in-vitro* VSMC ageing. (A) Graph of VSMC population doubling time during *in-vitro* passaging (n=3, 35F VSMCs). The 3 distinct stages of VSMC growth are highlighted; proliferative, presenescent and senescent. **(B)** Representative immunofluorescence images compare prelamin A staining (*red*) in proliferative, presenescent and senescent VSMCs. DAPI (*blue*) stained VSMC nuclei. Scale bar represents 5 μm.

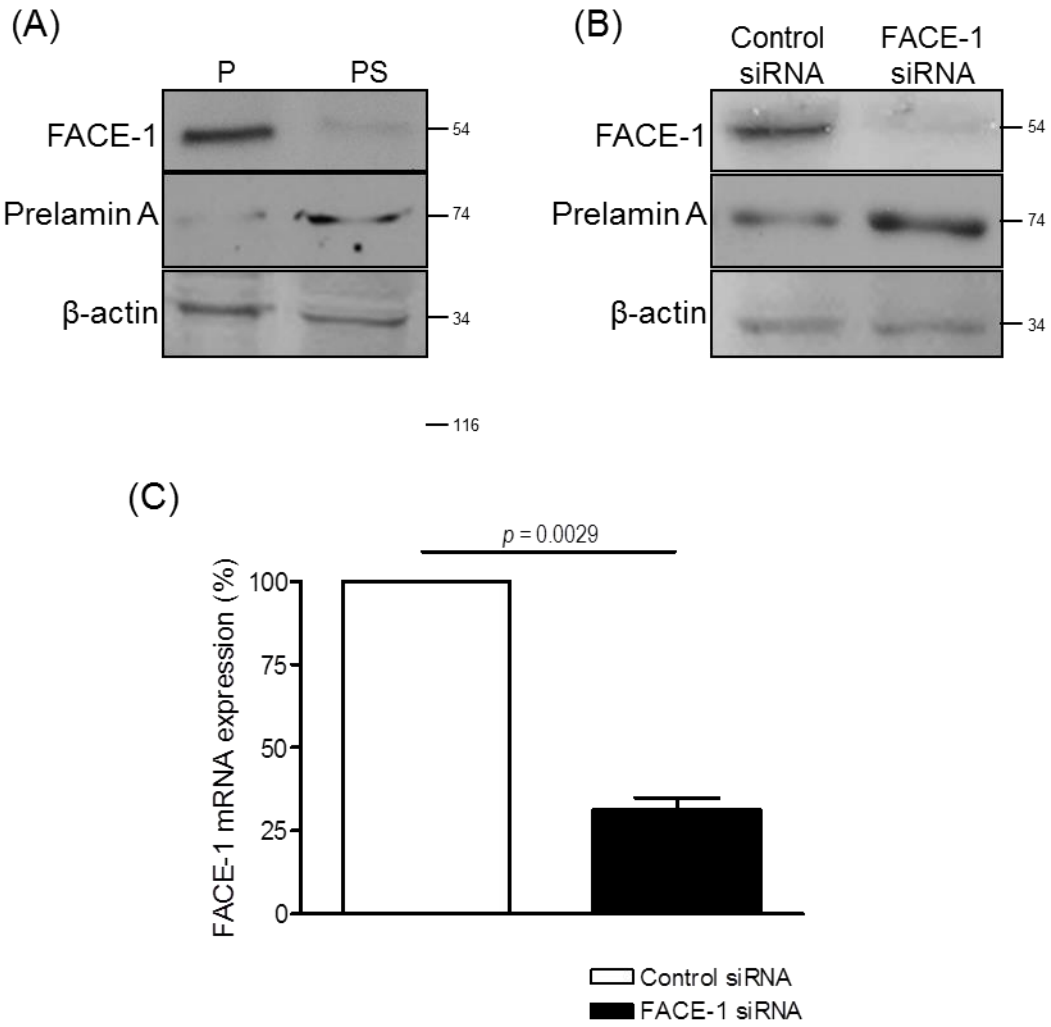

Figure 3.2: FACE-1 depletion corresponds with prelamin A accumulation. Representative Western blot demonstrating prelamin A and FACE-1 levels in **(A)** presenescent (PS) and **(B)** FACE-1 siRNA treated 35F VSMCs when compared with proliferative (P) and control siRNA treated VSMCs, respectively. β-actin indicates equal protein loading (20 µg of each protein lysate was loaded). **(C)** Quantitative PCR revealed reduced FACE-1 expression in FACE-1 siRNA treated 35F VSMCs compared with control cells. Experiments were performed in triplicate and a paired Student's *t* test was used for statistical analysis (control vs treatment).

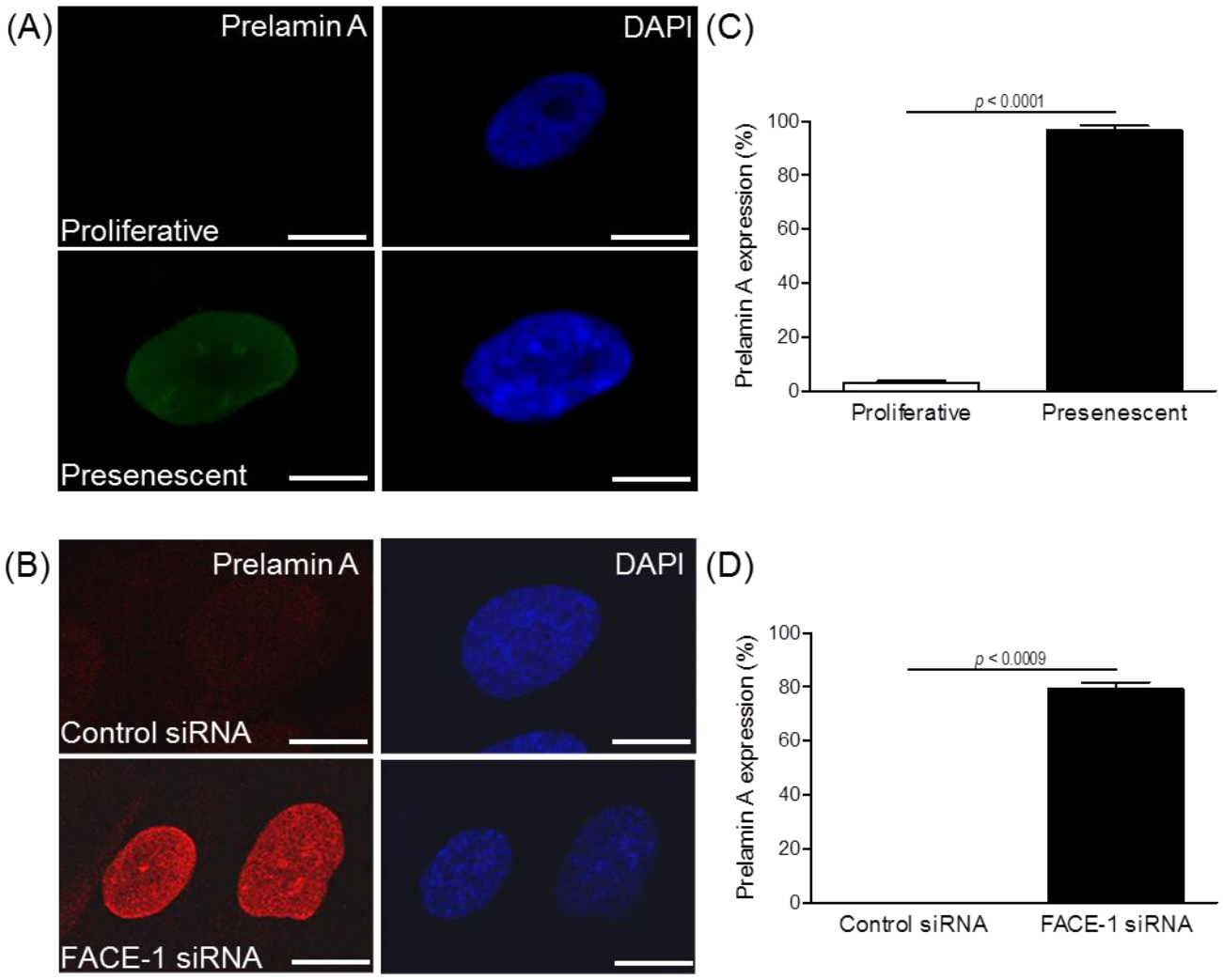

Figure 3.3: FACE-1 siRNA induces prelamin A accumulation in VSMCs. (A & C) Representative immunofluorescence microscopy images of prelamin A (*green*) in presenescent, and proliferative 35F VSMCs. The number of cells positively stained for prelamin A were counted and an unpaired Student's *t* test was used for statistical analysis (proliferative vs presenescent). Data are based on counting >300 cells per group across 3 independent experiments. **(B & D)** Following FACE-1 siRNA treatment for 72 h, 35F VSMCs were positive for prelamin A (*red*). A paired Student's *t* test was used for statistical analysis (control vs treatment). DAPI (*blue*) stained VSMC nuclei. Data are based on counting >300 cells per group across 3 independent experiments. Scale bar represents 5 μm.

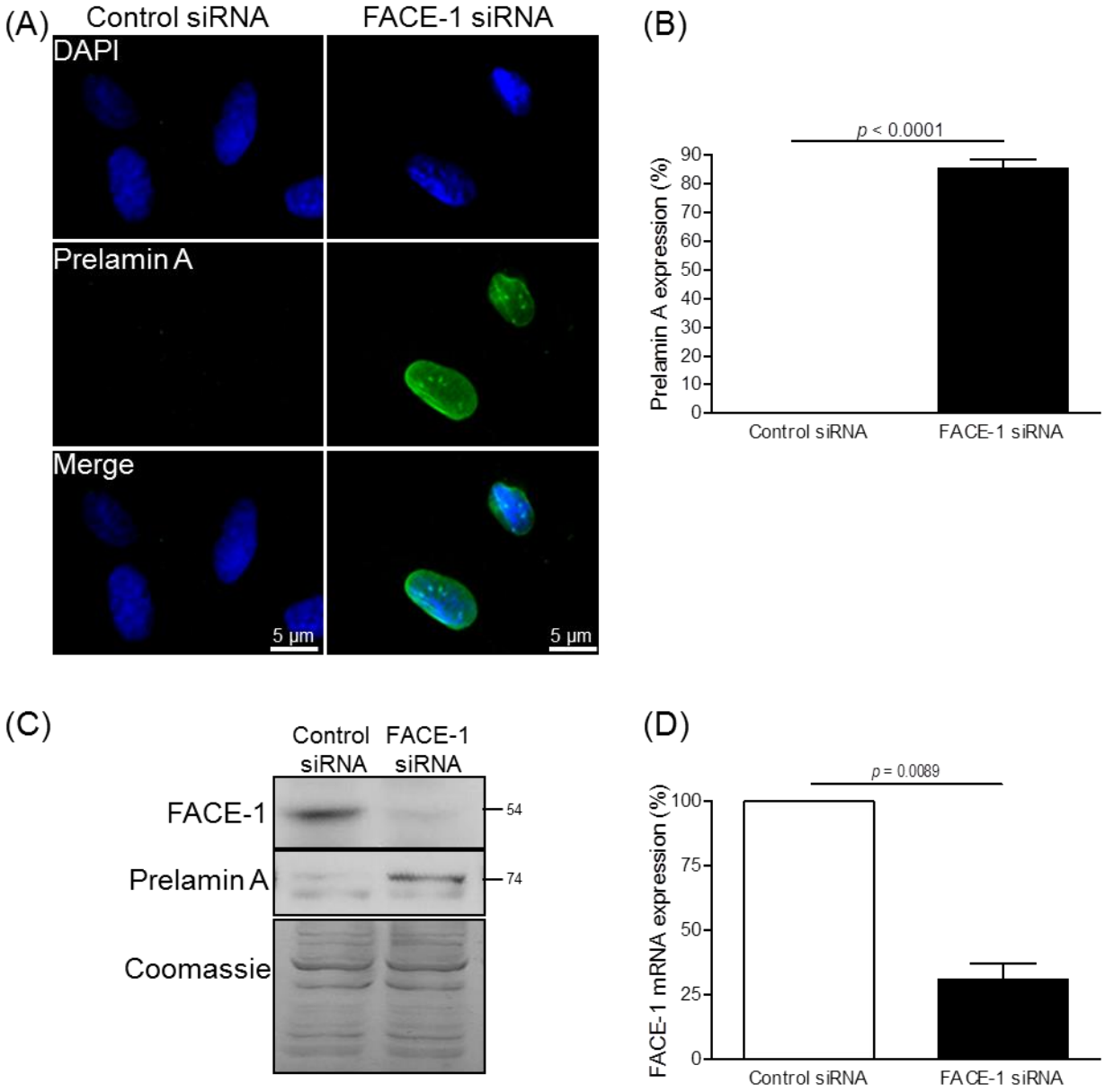

Figure 3.4: Prelamin A accumulates at the nuclear envelope of FACE-1 depleted fibroblasts. MRC-5 fibroblasts were treated with control and FACE-1 siRNA for 72 h. **(A & B)** Representative immunofluorescence microscopy images show prelamin A (*green*) in FACE-1 and control siRNA treated cells. DAPI (*blue*) stained nuclei. The number of cells positively stained for prelamin A were counted and a paired Student's *t* test was used for statistical analysis (control vs treatment). Data are based on counting >300 cells per group across 3 independent experiments. **(C)** Representative Western blot showing FACE-1 and prelamin A levels in control and FACE-1 siRNA treated fibroblasts. Coomassie staining indicates equal protein loading (20 µg of each protein lysate was loaded). **(D)** Quantitative PCR of FACE-1 mRNA expression in FACE-1 and control siRNA-treated MRC-5 fibroblasts. Experiment was performed in triplicate and a paired Student's *t* test was used for statistical analysis (control vs treatment).

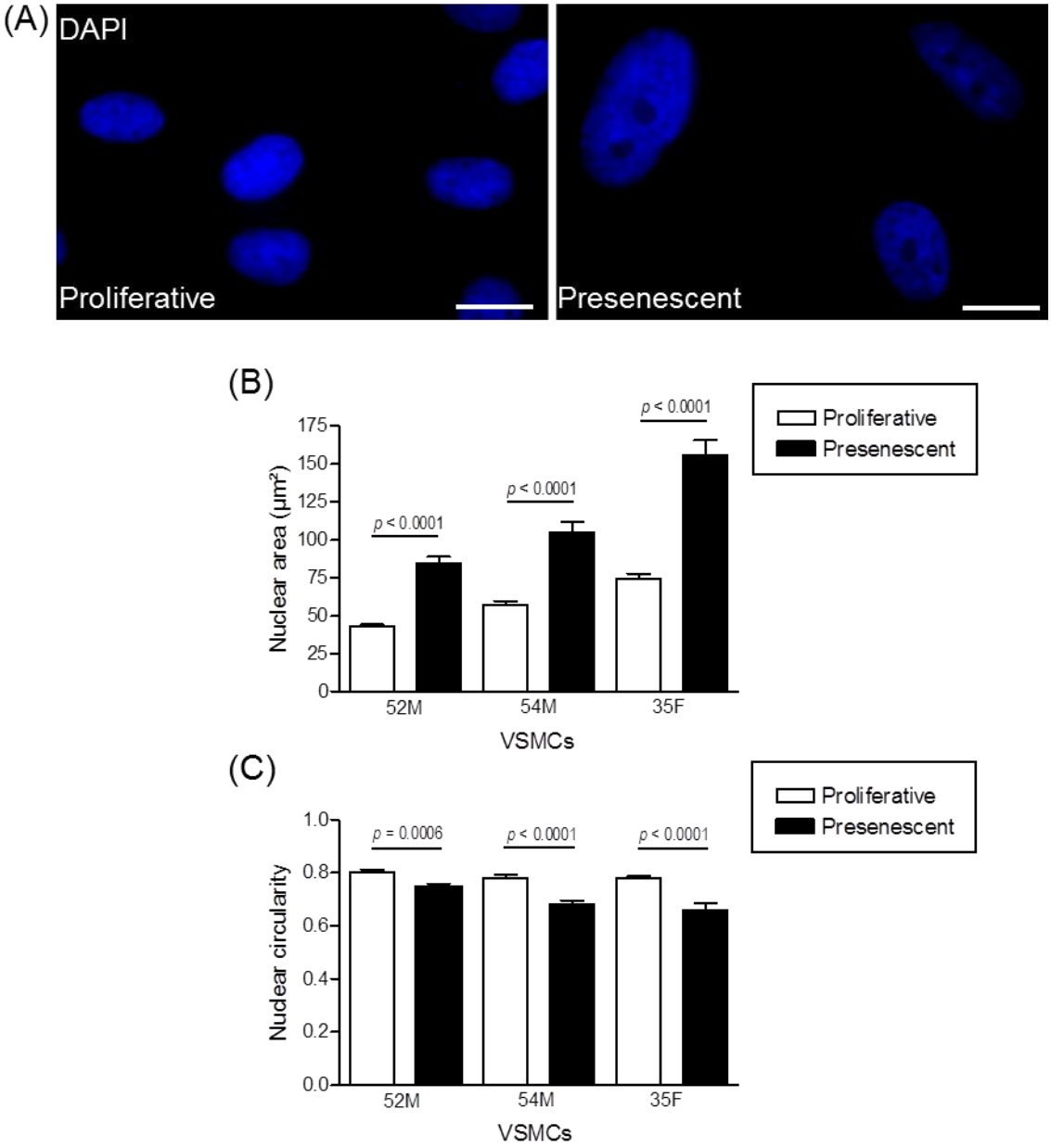

Figure 3.5: VSMC ageing induces nuclear morphology changes. (A) Representative immunofluorescence images of proliferative and presenescent 54M VSMC nuclei, stained using DAPI (*blue*), to visualise nuclear changes associated with *in-vitro* ageing. **(B)** Volocity software was used to measure nuclear area and **(C)** nuclear circularity in presenescent and proliferative VSMC isolates.(52M, 54M, 35F). Data are based on the measurement of 50-100 nuclei from 3 independent experiments.. Statistical significance was calculated using an unpaired Student's *t* test (proliferative vs presenescent nuclei). Scale bar represents 10 µm.

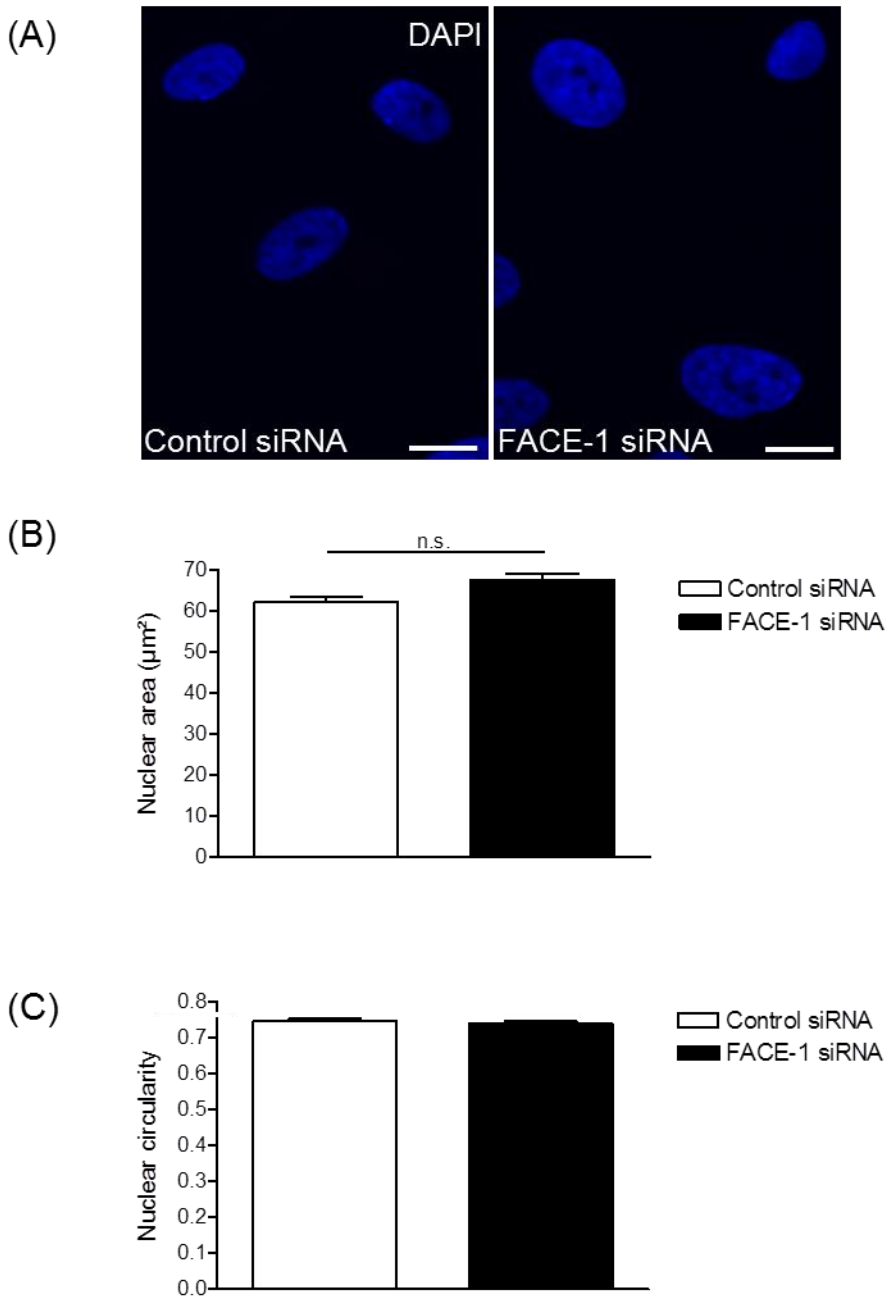

Figure 3.6: Prelamin A accumulation does not impact upon VSMC nuclear morphology. **(A)** Representative immunofluorescence images of control and FACE-1 siRNA treated VSMC nuclei stained using DAPI (*blue*). Scale bar represents 5 µm. Volocity software was used to measure the **(B)** area and **(C)** circularity of 35F VSMC nuclei. Data are based on the measurement of >100 nuclei from 3 independent experiments. Statistical significance was calculated using a paired Student's *t* test (control vs treatment).

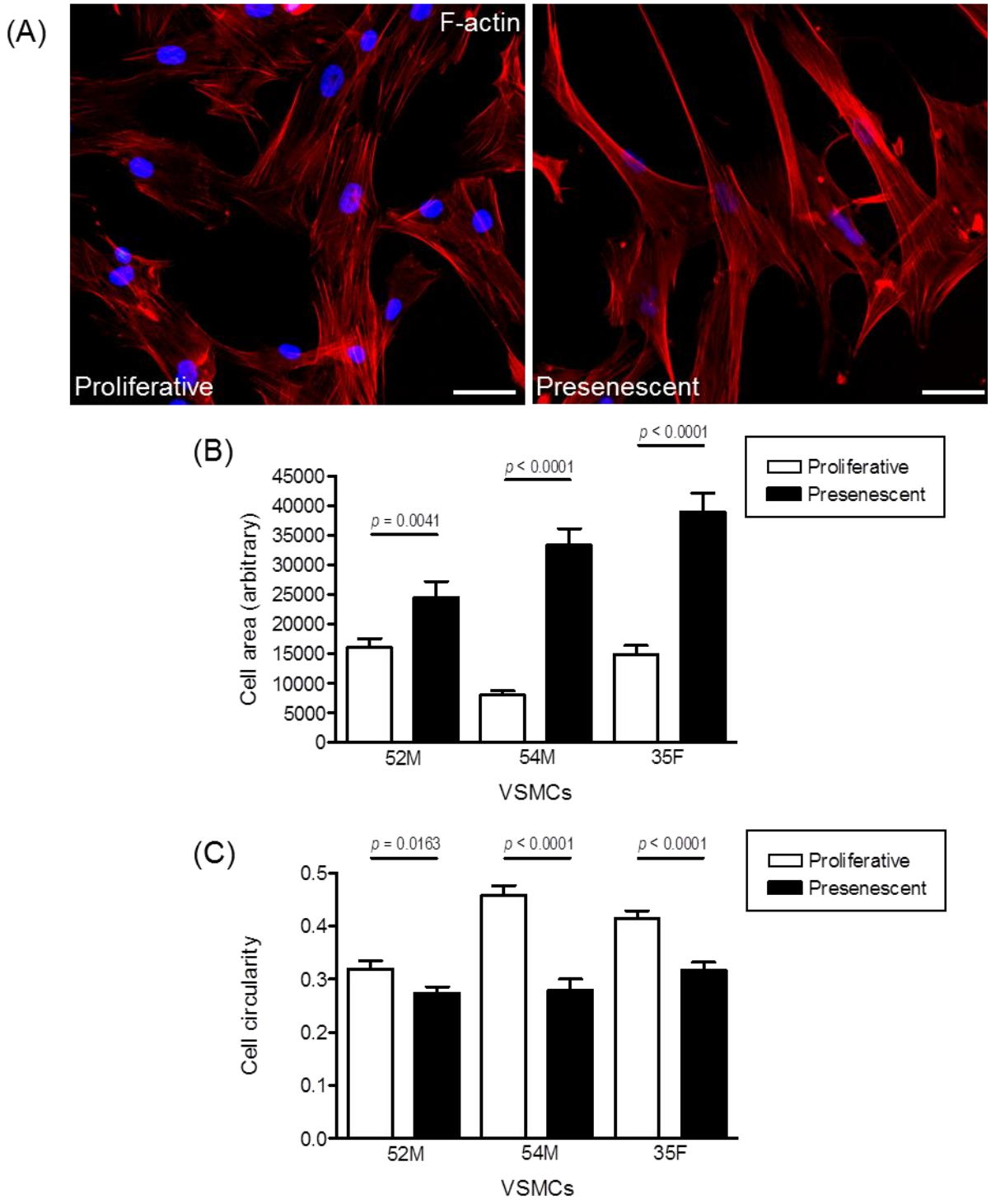

Figure 3.7: *In-vitro* ageing drives VSMC morphology changes. (A) Representative immunofluorescence images showing proliferative and presenescent VSMC actin filaments (F-actin) stained using rhodamine phalloidin (*red*). DAPI (*blue*) stained VSMC nuclei. Scale bar represents 50 µm. Image J software was used to manually measure **(B)** cell area and **(C)** cell circularity in presenescent and proliferative VSMC isolates (52M, 54M, 35F) . Data are based on the measurement of 50-100 VSMCs from 3 independent experiments. Statistical significance was calculated using an unpaired Student's *t* test (proliferative vs presenescent VSMCs).

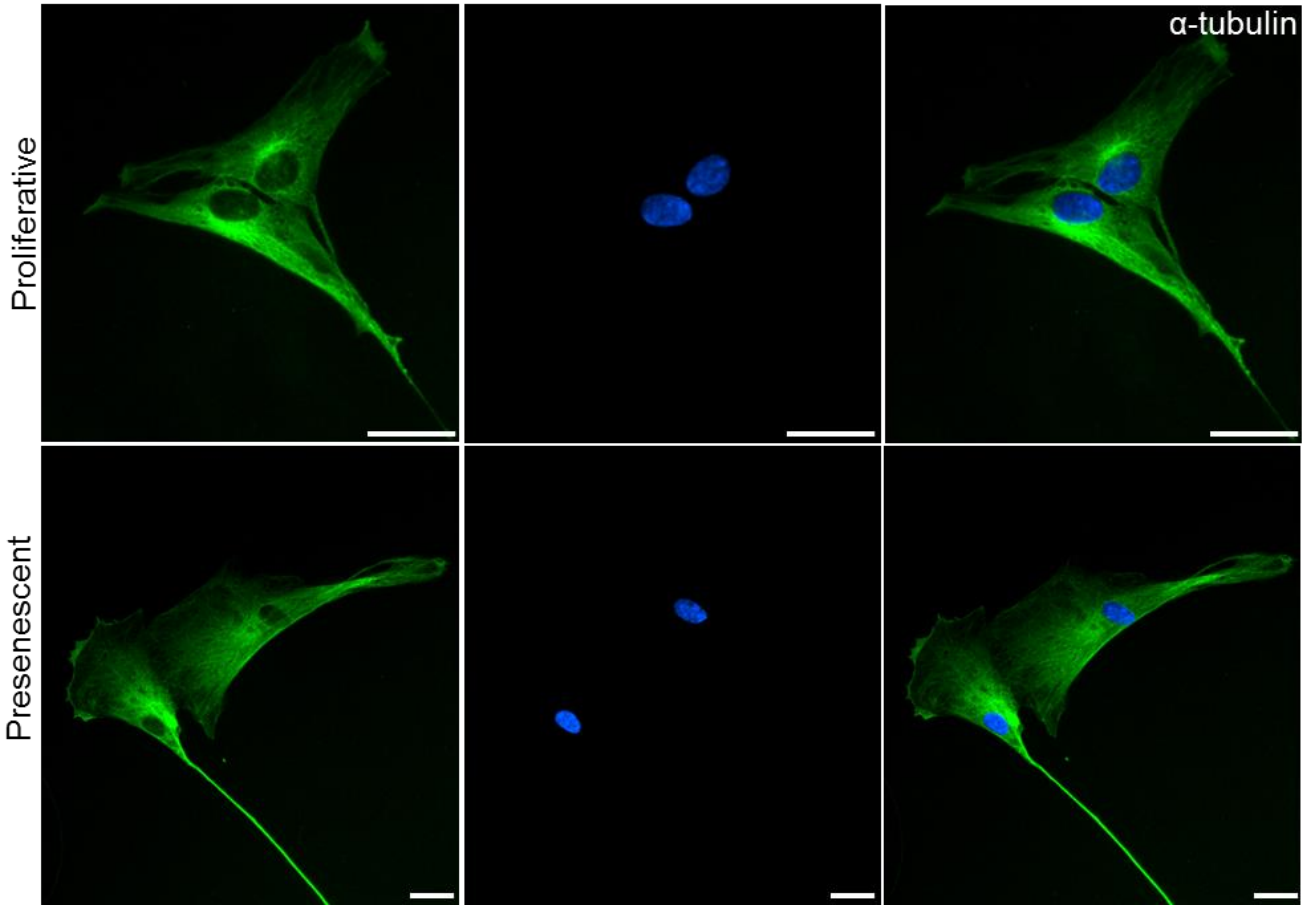

Figure 3.8: *In-vitro* ageing does not affect microtubule organisation. Immunofluorescence microscopy images of proliferative and presenescent 35F VSMC microtubules stained using α-tubulin (*green*). DAPI (*blue*) stained VSMC nuclei. Scale bar represents 50 μm.

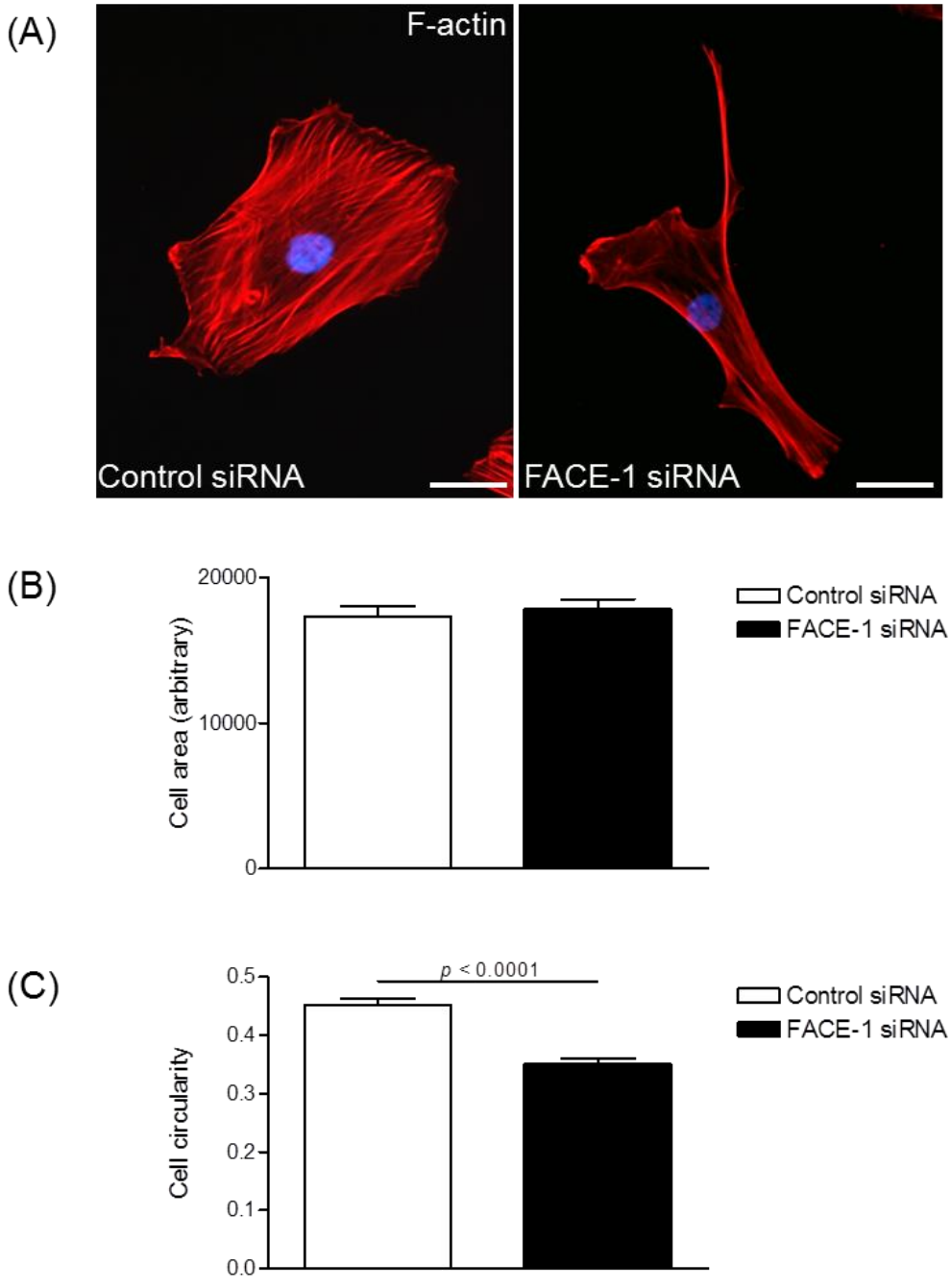

Figure 3.9: The impact of FACE-1 knockdown on VSMC morphology. (A) Representative immunofluorescence images showing control and FACE-1 siRNA treated 35F VSMC actin filaments (F-actin) stained using rhodamine phalloidin (*red*). DAPI (*blue*) stained VSMC nuclei. Scale bar represents 35 µm. Image J software was used to manually measure the **(B)** area and **(C)** circularity of control and FACE-1 siRNA treated 35F VSMCs. Data are based on the measurement of >300 VSMCs from 3 independent experiments. Statistical significance was calculated using a paired Student's *t* test (control vs treatment).

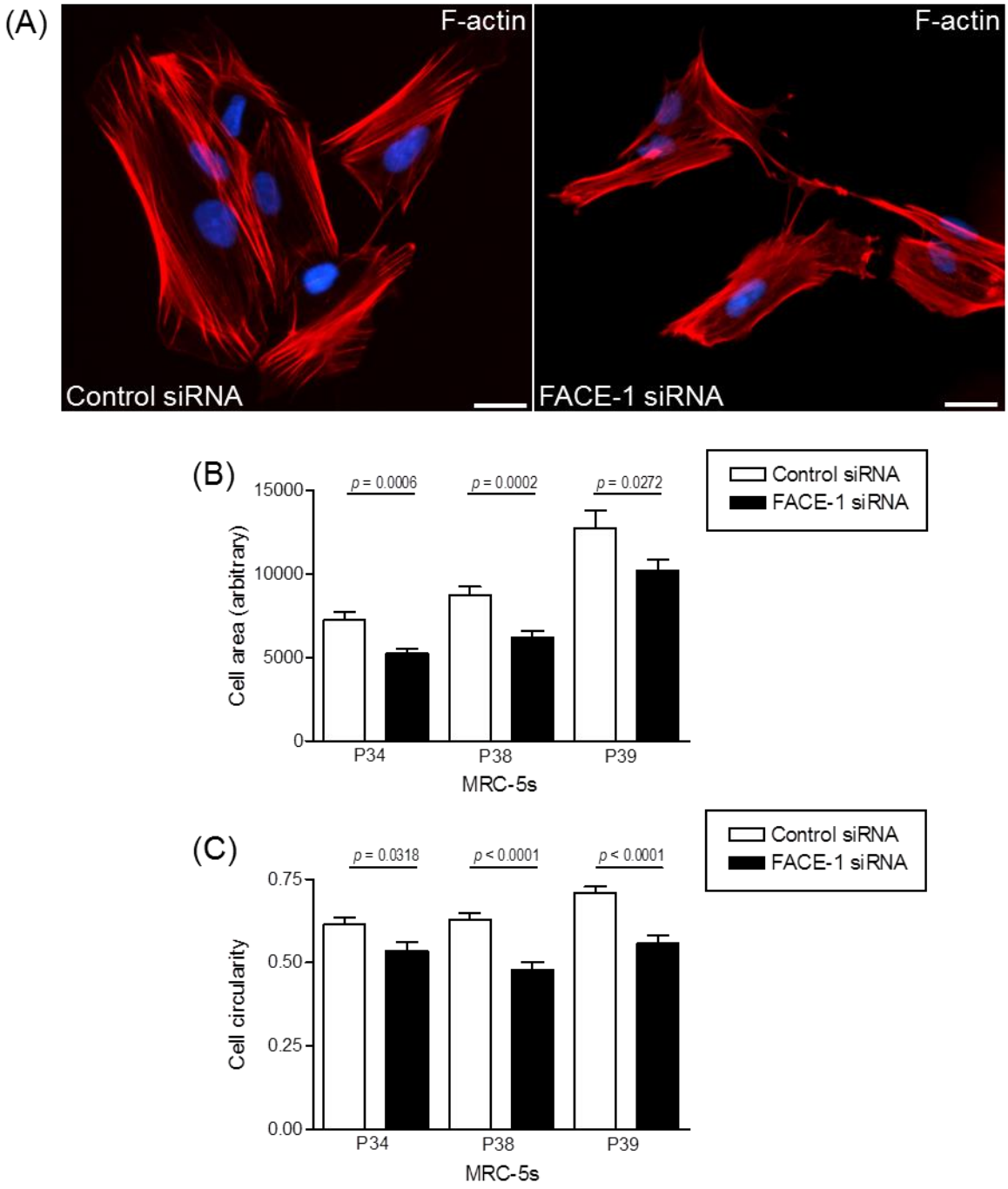

Figure 3.10: The impact of FACE-1 knockdown on actin organisation in fibroblasts. (A) Representative immunofluorescence images of MRC-5 fibroblasts following treatment with control and FACE-1 siRNA for 72 h. Actin filaments (F-actin) were stained using rhodamine phalloidin (*red*) and DAPI (*blue*) stained nuclei. Scale bar represents 10 µm. **(B & C) Image J software was used to manually measure the** cell area and cell circularity of control and FACE-1 siRNA treated fibroblasts (passage 34, 38, 39). Data are based on the measurement of >50 MRC-5 fibroblasts from 3 independent experiments . Statistical significance was calculated using a paired Student's *t* test (control vs treatment).

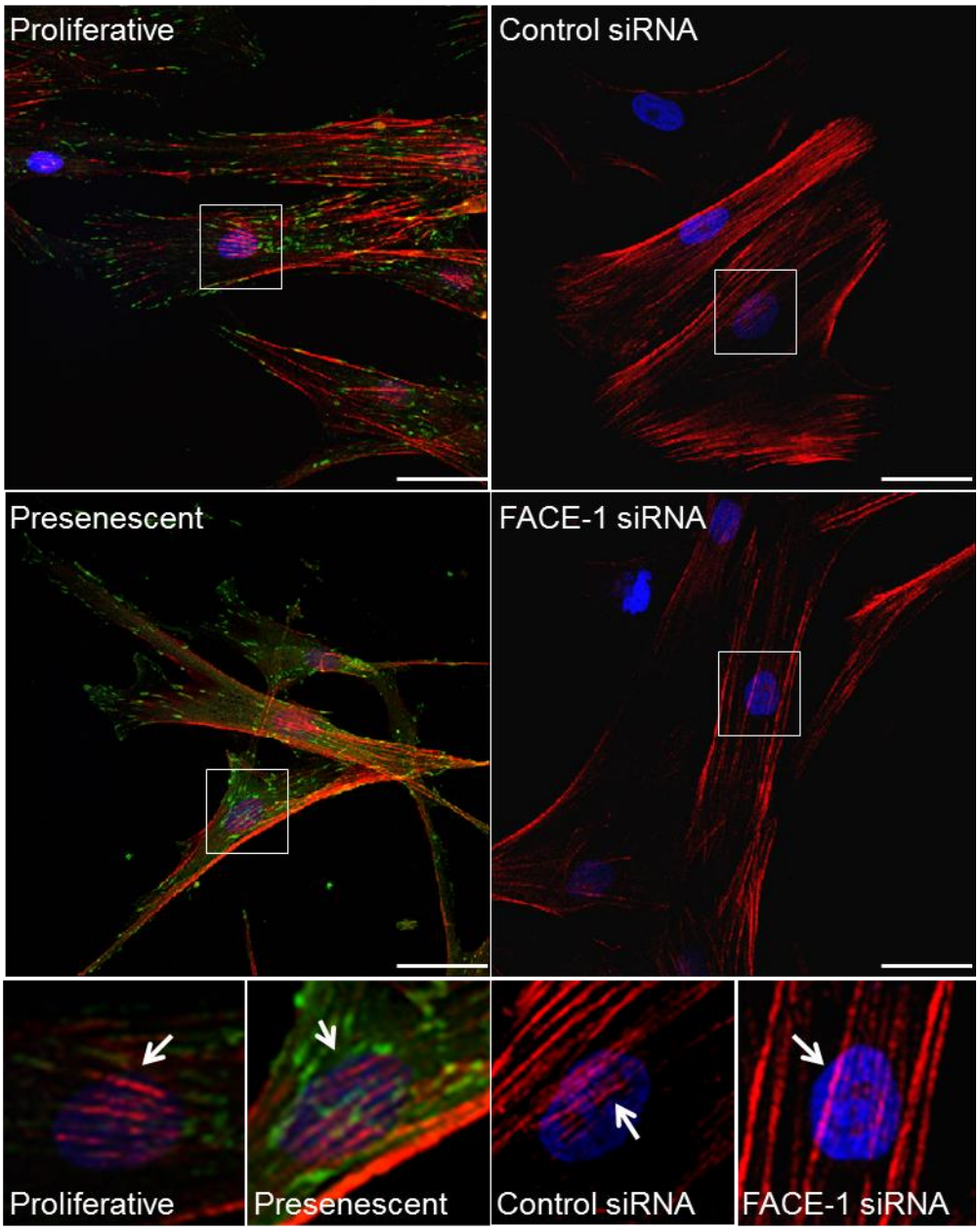

Figure 3.11: *In-vitro* ageing and prelamin A accumulation do not affect actin cap formation. Confocal microscopy shows actin cap formation in presenescent and FACE-1 siRNA treated 35F VSMCs when compared to proliferative and control VSMCs, respectively. Rhodamine phalloidin stained actin filaments (*red*), DAPI stained nuclei (*blue*) and anti-vinculin stained focal adhesions (*green*). Scale bar represents 35 µm. The lower panel displays higher magnification images of the actin cap indicated by arrows.

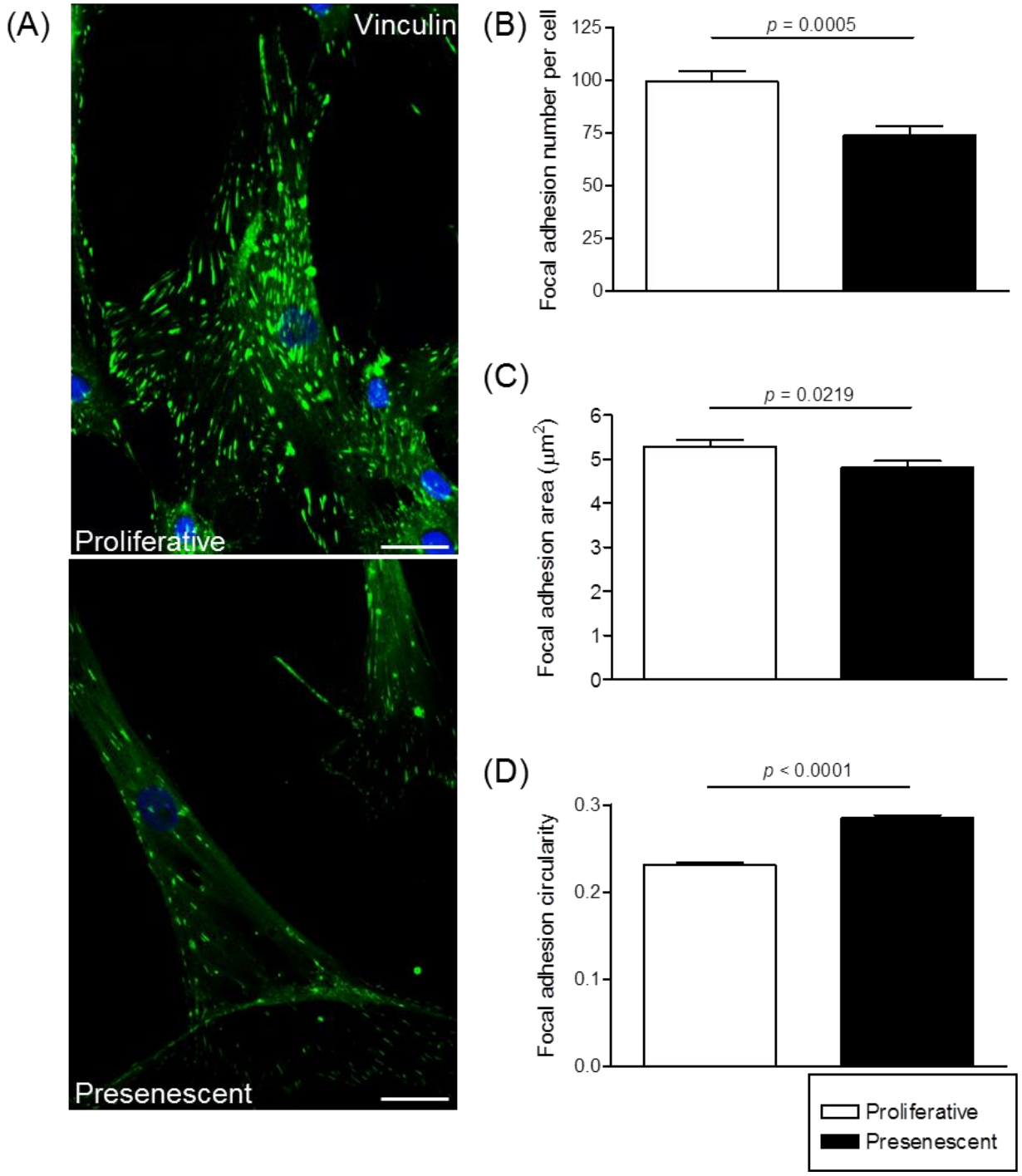

Figure 3.12: VSMC ageing disrupts focal adhesion organisation. (A) Representative immunofluorescence images showing focal adhesions, stained with anti-vinculin (*green*), of proliferative and presenescent 35F VSMCs. DAPI (*blue*) stained VSMC nuclei. Scale bar represents 20 μm. Volocity software was used to measure **(B)** focal adhesion number, **(C)** size and **(D)** circularity in presenescent and proliferative 35F VSMCs.. Data represent the analysis of 500-1000 focal adhesions from >100 cells (n=3). Statistical significance was determined using an unpaired Student's *t* test (proliferative vs presenescent VSMCs).

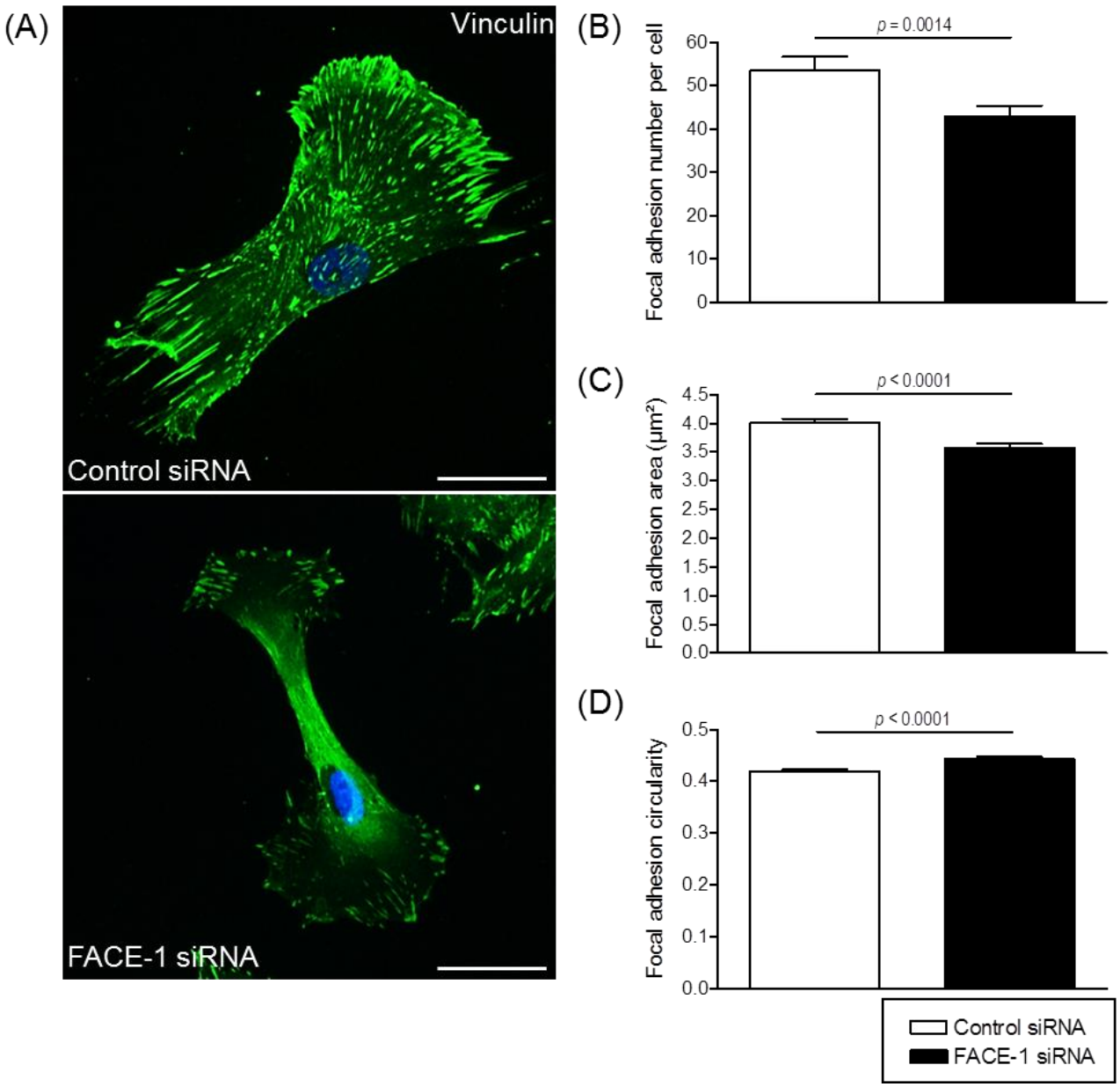

Figure 3.13: The impact of FACE-1 knockdown upon focal adhesion organisation. (A) Representative immunofluorescence images showing focal adhesion staining with anti-vinculin (*green*) of control and FACE-1 siRNA treated 35F VSMCs. DAPI (*blue*) stained VSMC nuclei. Scale bar represents 20 μm. Volocity software was used to measure **(B)** focal adhesion number, **(C)** size and **(D)** circularity in control and FACE-1 siRNA treated 35F VSMCs. Data represent the analysis of 500-1000 focal adhesions from >100 cells (n=3). Statistical significance was determined using a paired Student's *t* test (control vs treatment).

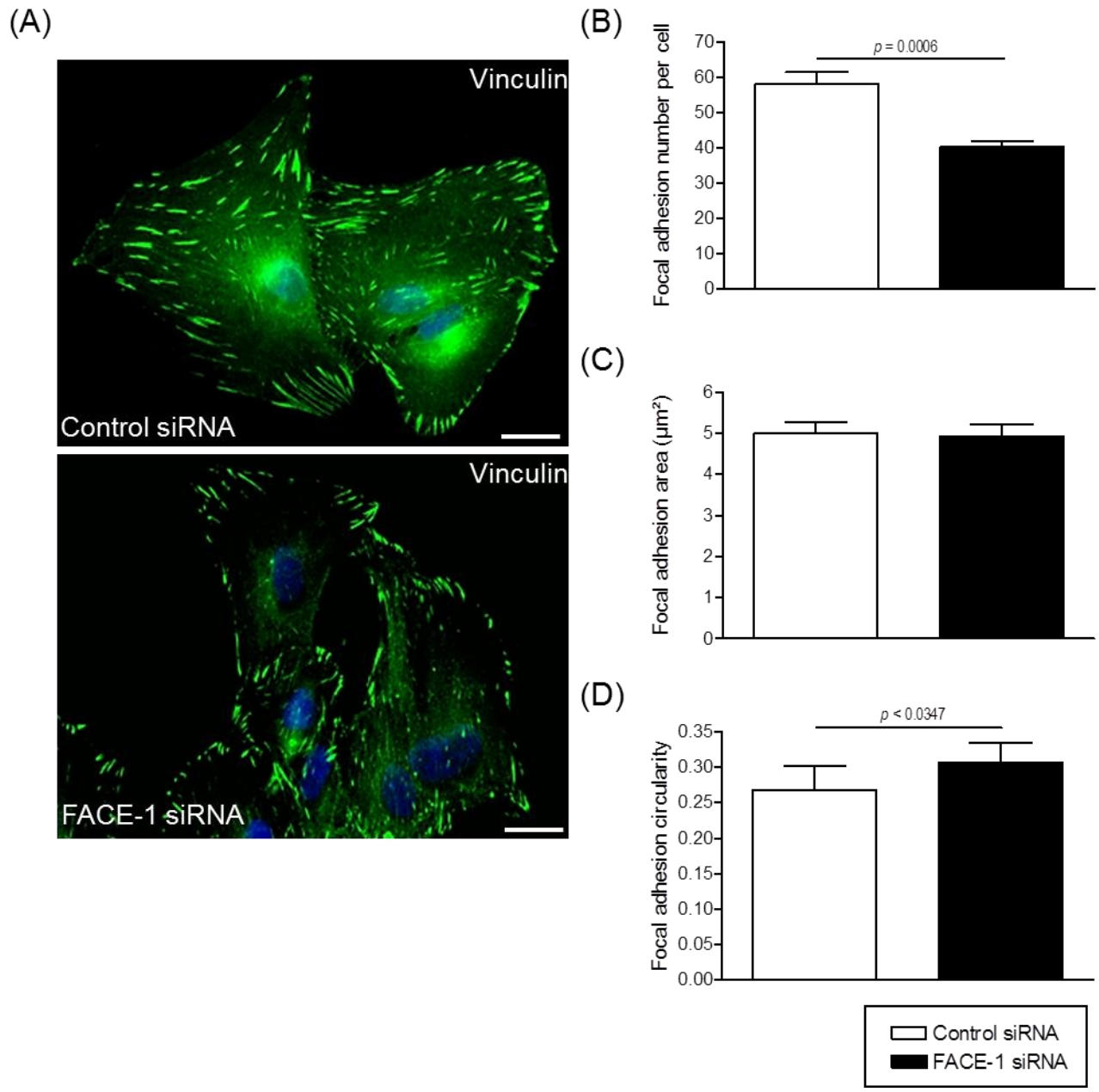

Figure 3.14: FACE-1 knockdown disrupts focal adhesion organisation in fibroblasts. MRC-5 fibroblasts were treated with control and FACE-1 siRNA for 72 h. **(A)** Representative immunofluorescence images show focal adhesion staining with anti-vinculin (*green*) of control and FACE-1 siRNA treated cells. DAPI (*blue*) stained nuclei. Scale bar represents 10 µm. Volocity software was used to measure **(B)** focal adhesion number, **(C)** size and **(D)** circularity in control and FACE-1 siRNA treated fibroblasts. Data represent the analysis of >300 focal adhesions pooled from >50 cells per group (n=3, passage 34, 38, 39). Statistical significance was determined using a paired Student's *t* test (control vs treatment).

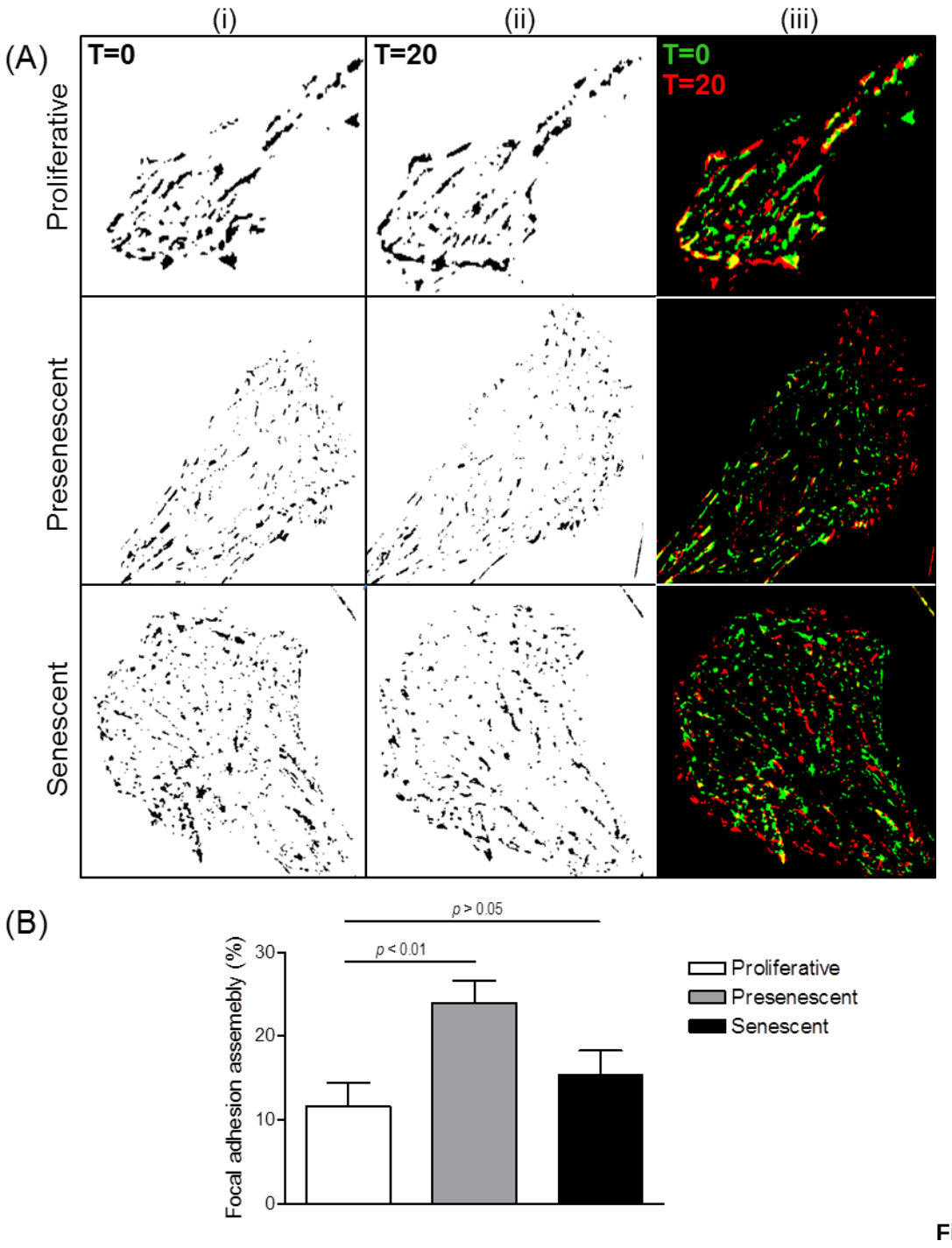

Figure 3.15: Presenescent VSMCs exhibit increased focal adhesion dynamics. (A) Representative binary images of proliferative, presenescent and senescent VSMCs captured during interference reflection microscopy (IRM) at t=0 min **(i)** and t=20 min **(ii)**. Composite images **(iii)** highlight focal adhesion formation at t=20 (*red*) compared with original focal adhesions at t=0 (*green*). **(B)** IRM analysis revealed adhesion turnover in presenescent and senescent 35F VSMCs compared with proliferative cells. Data are based on the analysis of 15-20 cells pooled from 3 independent experiments. Statistical significance was determined using ANOVA to show global differences between the VSMC growth stages (p = 0.0079), followed by a Tukey's multiple comparison test.

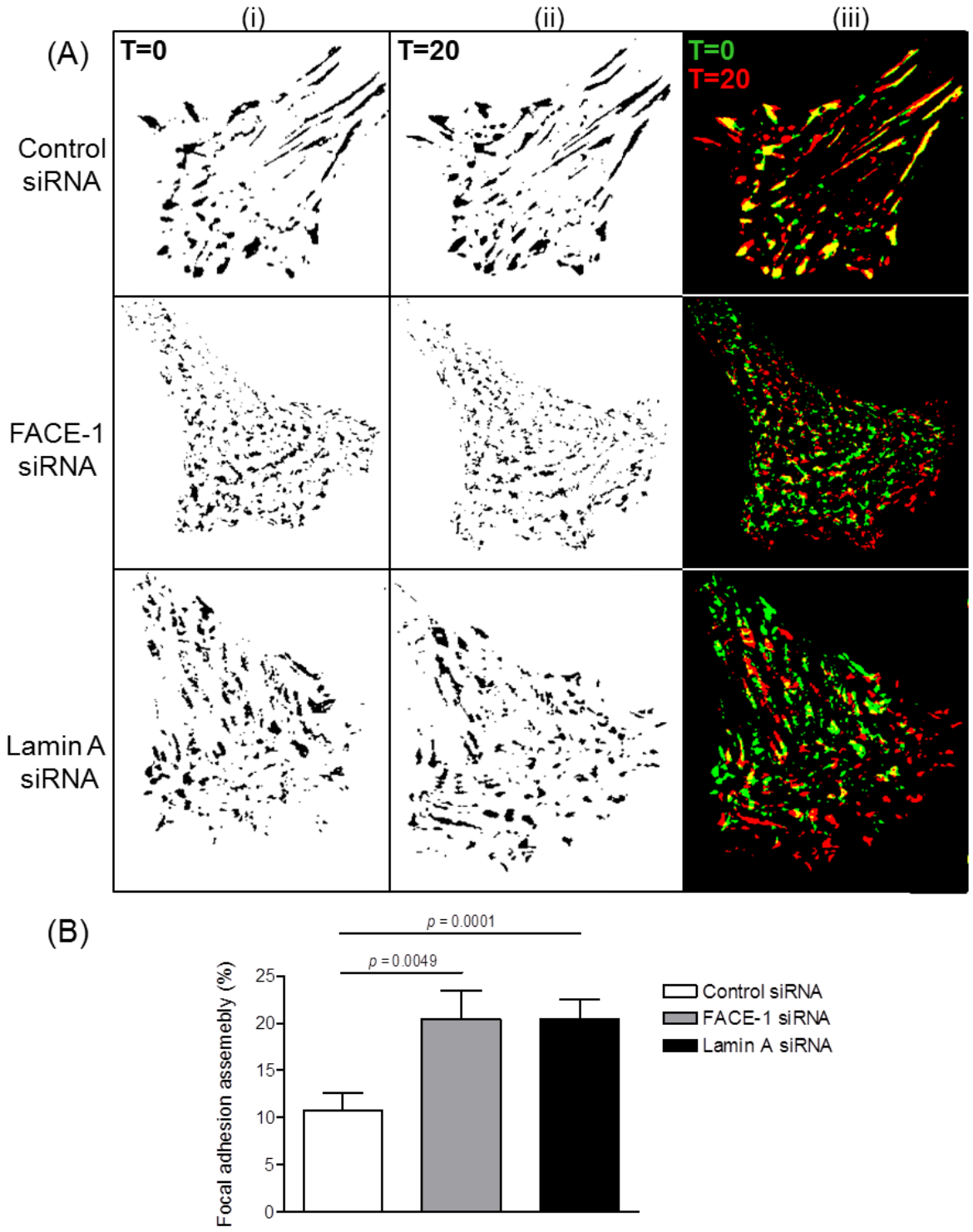

Figure 3.16: Nuclear lamina disruption increases focal adhesion dynamics. (A) Representative binary images of control, FACE-1 and lamin A siRNA treated VSMCs captured during interference reflection microscopy (IRM) at t=0 min **(i)** and t=20 min **(ii)**. Composite images **(iii)** highlight focal adhesion formation at t=20 (*red*) compared with original focal adhesions at t=0 (*green*). **(B)** IRM analysis revealed focal adhesion turnover in FACE-1 and lamin A depleted 35F VSMCs compared with control VSMCs. Data are based on the analysis of 15-20 cells pooled from 3 independent experiments. Statistical significance was determined using a paired Student's *t* test (control vs treatment).

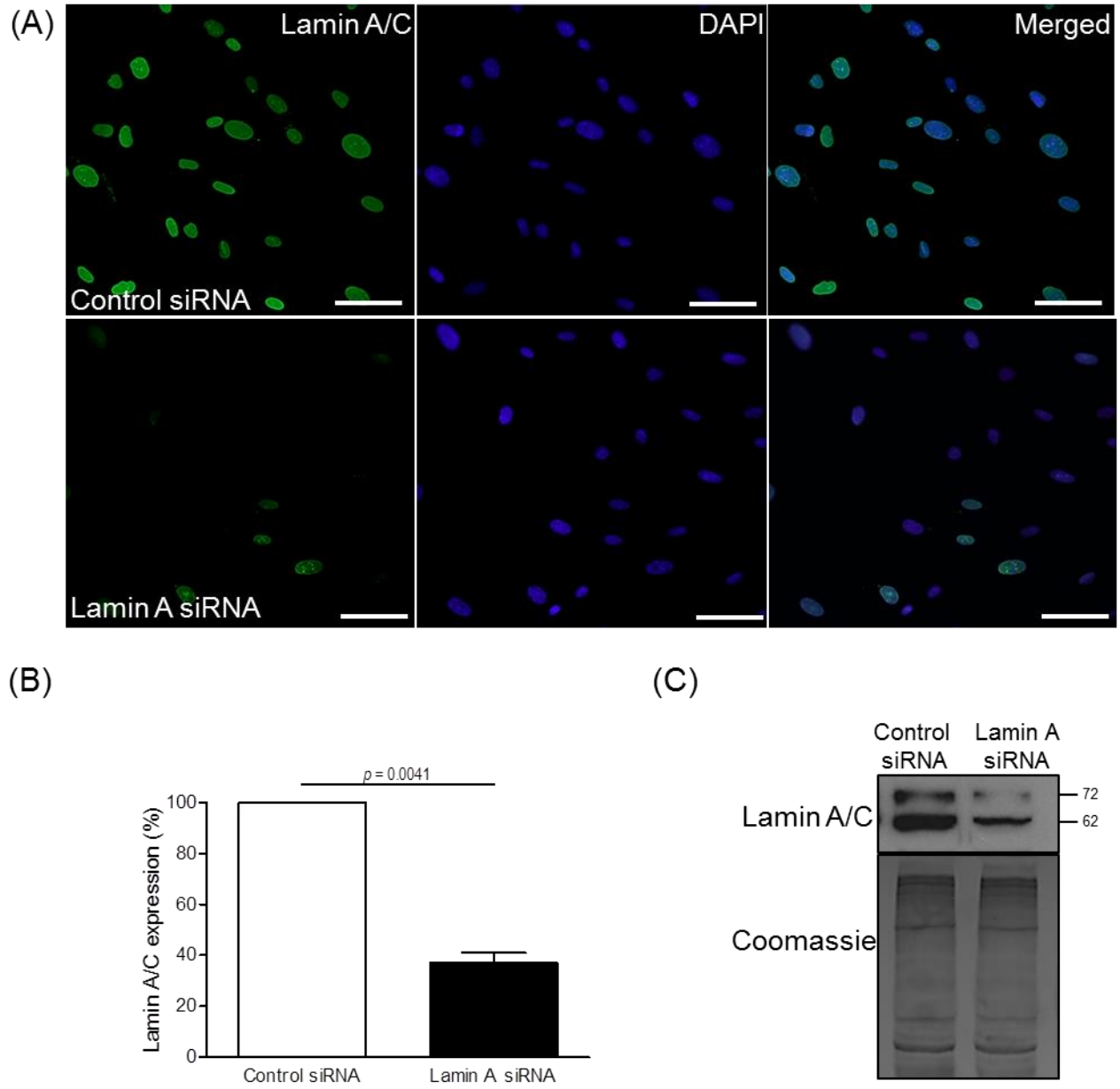

F**igure 3.17: siRNA-mediated lamin A depletion.** VSMCs were treated with lamin A and control siRNA for 72 h prior to experimentation. **(A)** Representative immunofluorescence images showing lamin A (*green*) and DAPI (*blue*) stained 35F VSMC nuclei. Scale bar represents 50 µm. **(B)** The number of cells positively stained for lamin A were counted. Data are based on >300 cells counted across 3 independent experiments and statistical significance was determined using a paired Student's *t* test (control vs treatment). **(C)** Western blot analysis demonstrated lamin A/C levels of control and lamin A siRNA treated cells. Coomassie stain indicated equal loading (20 µg of each protein lysate was loaded).

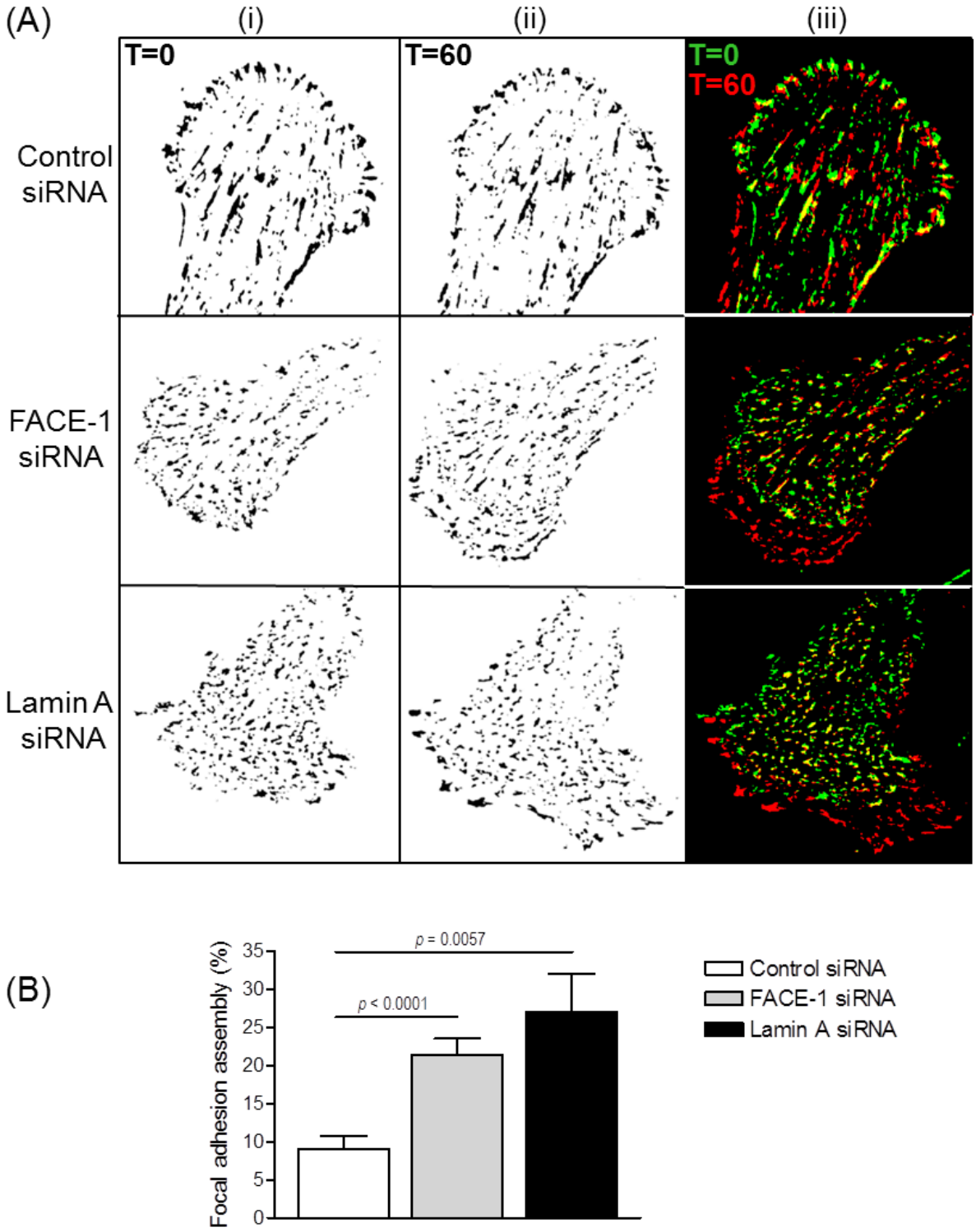

Figure 3.18: Nuclear lamina disruption increases focal adhesion dynamics in fibroblasts. (A) Representative binary images of control, FACE-1 and lamin A siRNA-treated MRC-5 fibroblasts captured during interference reflection microscopy (IRM) at t=0 min **(i)** and t=60 min **(ii)**. Composite images **(iii)** highlight focal adhesion formation at t=60 (*red*) compared with original focal adhesions at t=0 (*green*). **(B)** IRM analysis revealed focal adhesion turnover in FACE-1 and lamin A depleted fibroblasts compared with control fibroblasts. Data are based on the analysis of 13-17 cells pooled from 3 independent experiments. Statistical significance was determined using a paired Student's *t* test (control vs treatment).

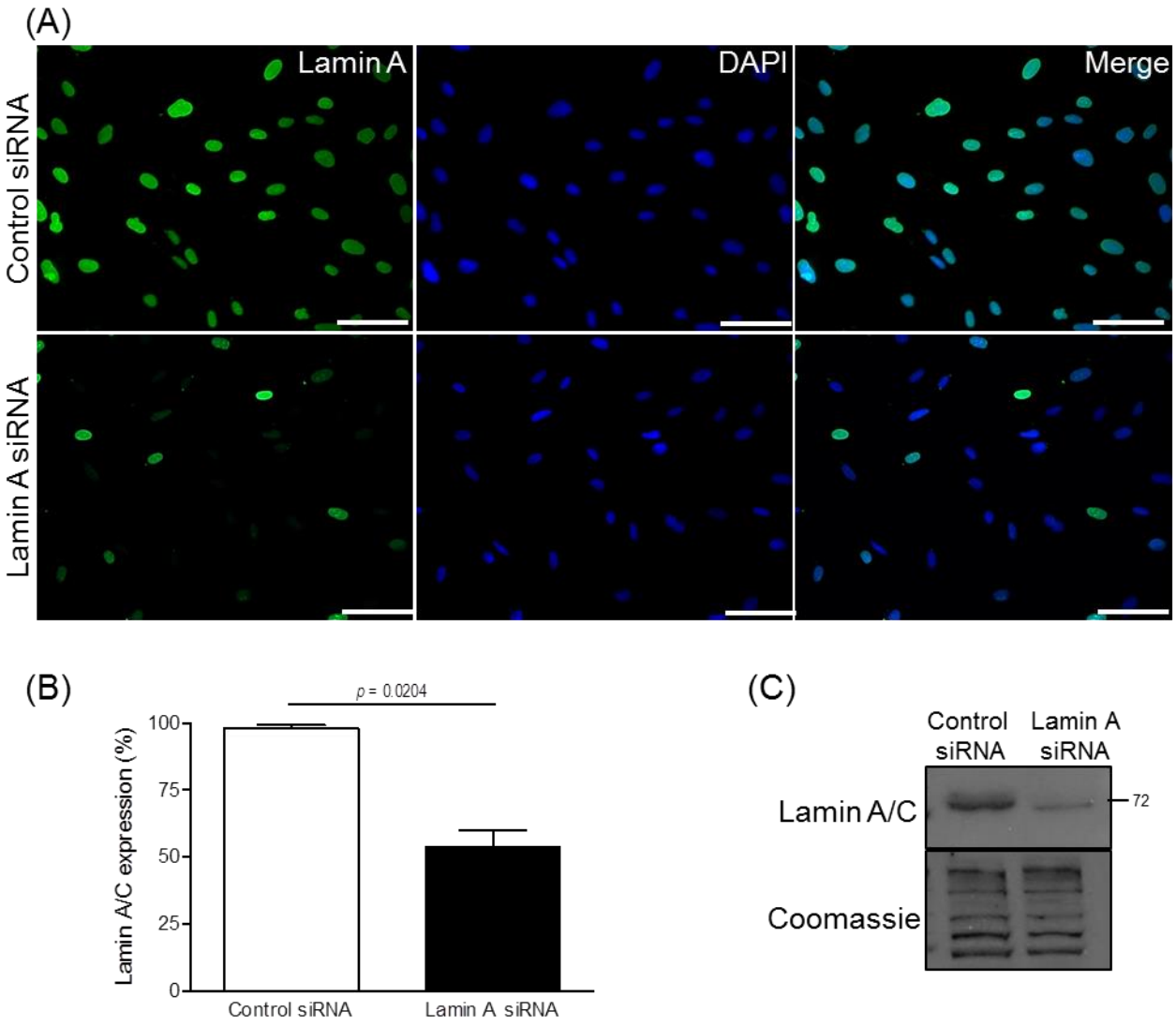

Figure 3.19: Lamin A knockdown in MRC-5 fibroblasts. MRC-5 fibroblasts were treated with lamin A and control siRNA for 72 h prior to experimentation. **(A)** Representative immunofluorescence images show lamin A (*green*) and DAPI (*blue*) stained nuclei. Scale bar represents 50 µm. **(B))** The number of cells positively stained for lamin A were counted. Data are based on >300 cells counted across 3 independent experiments. **(C)** Western blot analysis demonstrated lamin A/C levels of control and lamin A siRNA treated cells. Coomassie stain indicated equal loading (20 µg of each protein lysate was loaded).

.

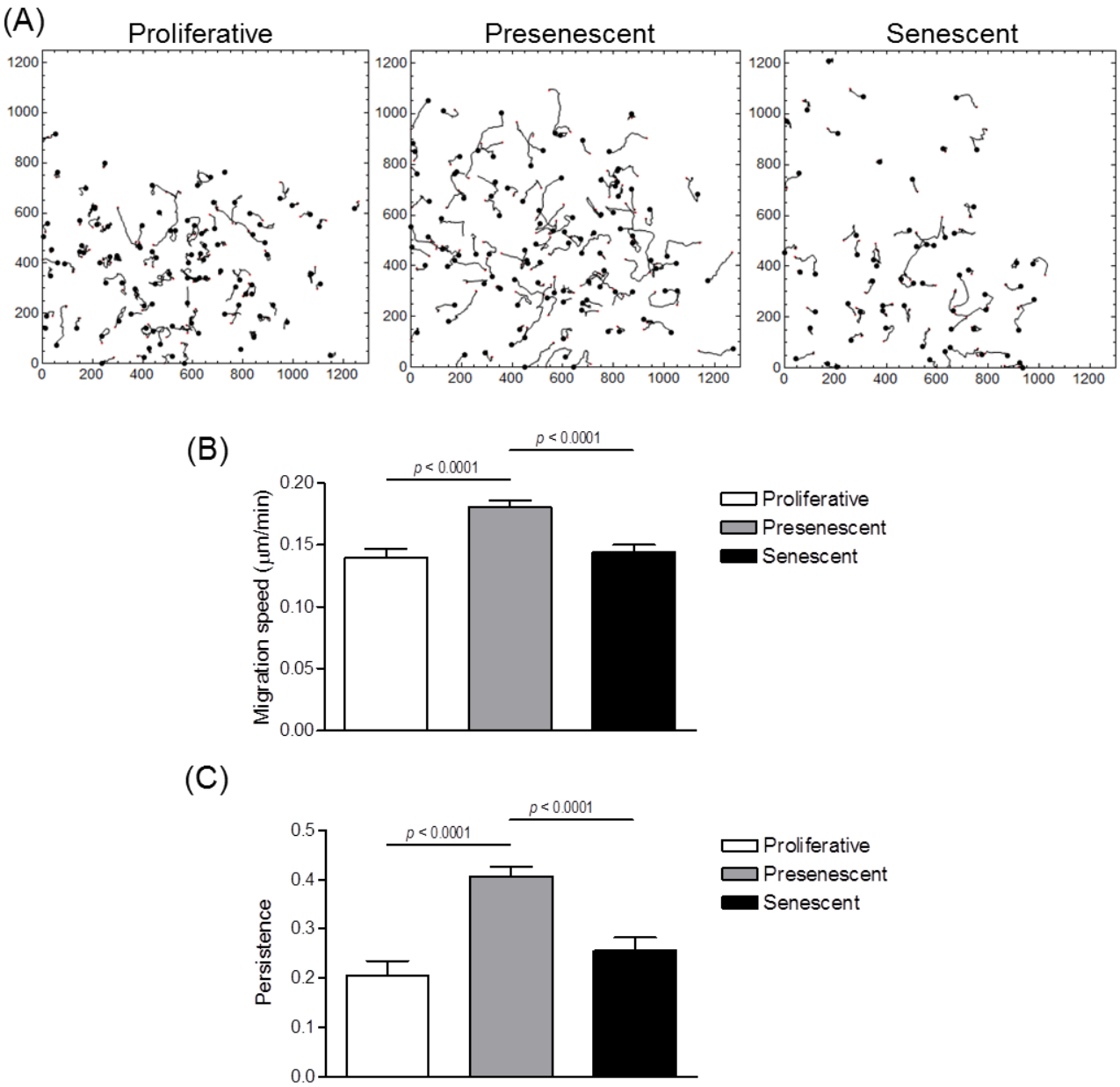

Figure 3.20: Ageing impacts upon single VSMC migrational behaviour. Time-lapse microscopy was used to capture random migration of single proliferative, presenescent and senescent 35F VSMCs. Images were captured every 5 min for 16 h and Mathematica software plotted x-y coordinates to provide **(A)** an overlay of individual cell tracks and analysed **(B)** migratory velocity and **(C)** persistence. Data are based on the analysis of 61 (senescent) and 108 (proliferative & presenescent) individually tracked cells pooled from 3 independent experiments. Statistical significance was calculated using an unpaired Student's *t* test.

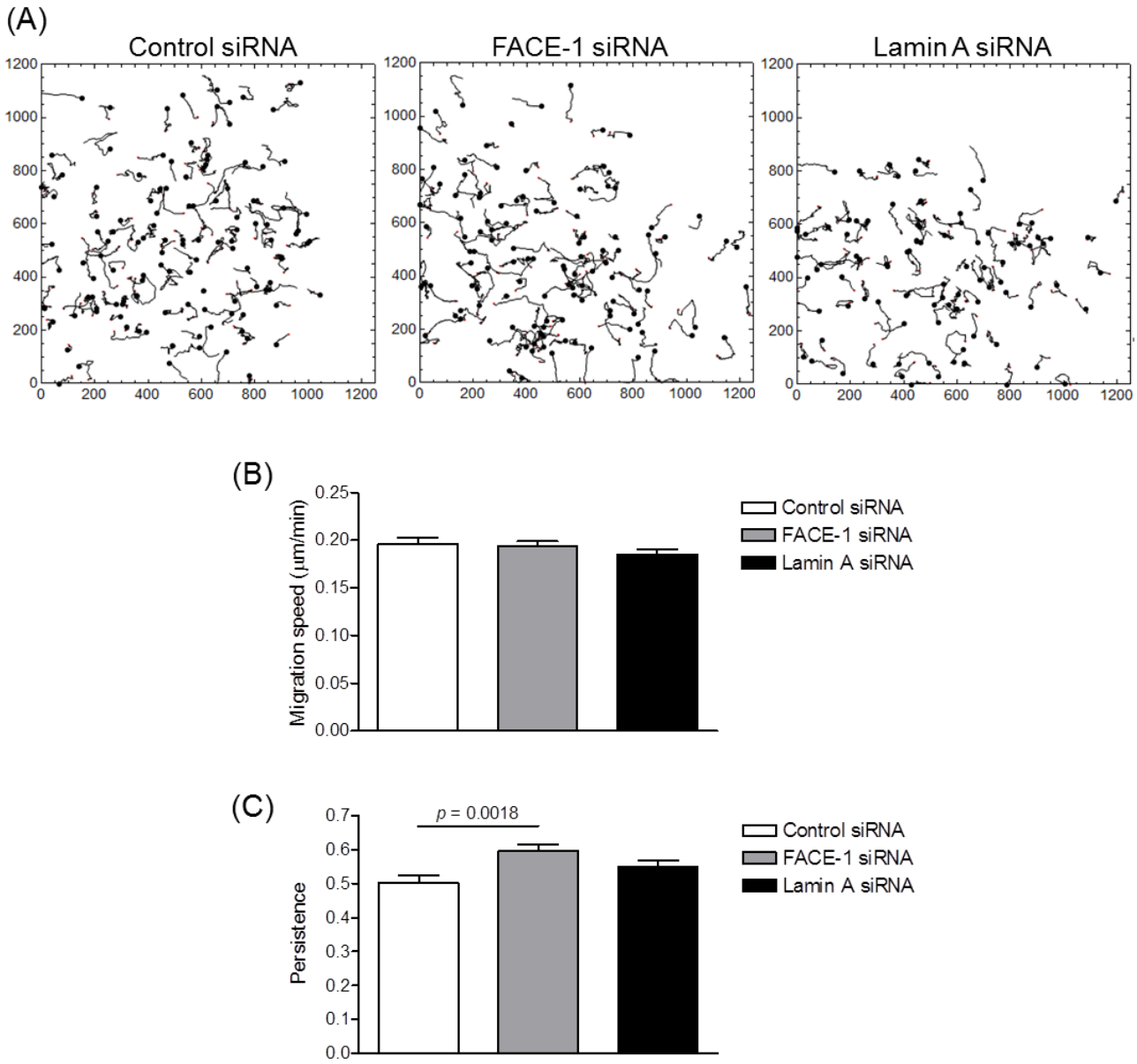

Figure 3.21: The impact of FACE-1 knockdown on VSMC persistence. Time-lapse microscopy was used to capture random migration of single control, FACE-1 and lamin A siRNA treated 35F VSMCs. Images were captured every 5 min for 16 h and Mathematica software plotted x-y coordinates to provide **(A)** an overlay of individual cell tracks and analysed **(B)** migratory velocity and **(C)** persistence. Data are based on the analysis of 121 (control), 118 (FACE-1 siRNA) and 98 (lamin A siRNA) individually tracked cells pooled from 3 independent experiments. Statistical significance was calculated using a paired Student's *t* test (control vs treatment).

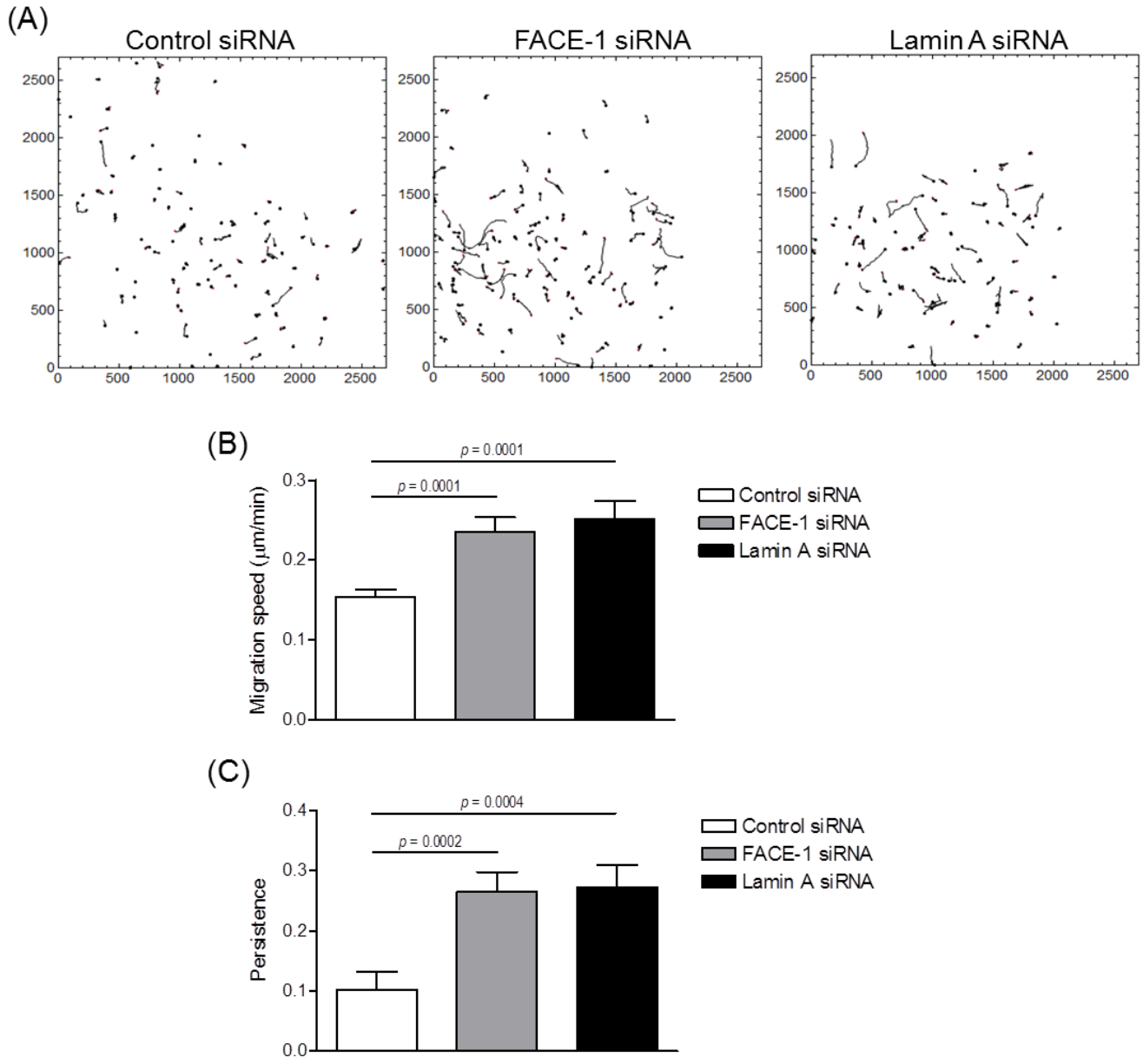

Figure 3.22: Nuclear lamina disruption increases fibroblast migration speed and persistence. Time-lapse microscopy was used to capture random migration of single control, FACE-1 and lamin A siRNA treated MRC-5 fibroblasts. Images were captured every 5 min for 16 h, Image J was used to manually track individual cells and Mathematica software plotted x-y coordinates to provide **(A)** an overlay of individual cell tracks and analysed **(B)** migratory velocity and **(C)** persistence. Data are based on the analysis of 98 (control), 105 (FACE-1 siRNA) and 77 (lamin A siRNA) cells pooled from 3 independent experiments. Statistical significance was calculated using a paired Student's *t* test (control vs treatment).

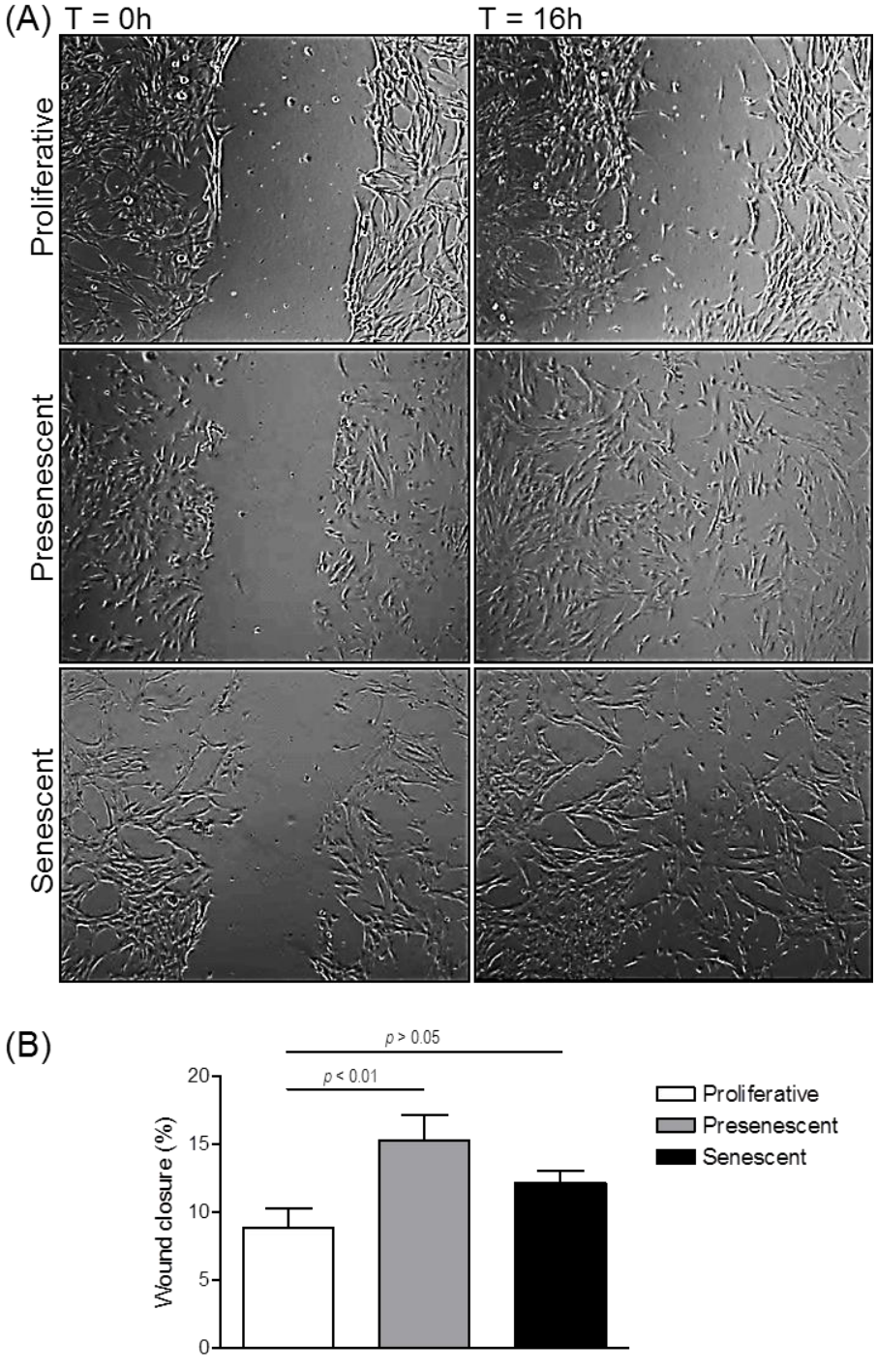

Figure 3.23: The effect of *in-vitro* ageing on VSMC scratch closure. Proliferative, presenescent and senescent 35F VSMCs were seeded onto a 24-well plate and cultured until confluent before being scratched with a pipette tip. Time-lapse microscopy was used to capture VSMC migration into the scratch area. **(A)** Representative phase-contrast images compare scratch closure at 0 and 16 h post-scratch. **(B)** Images were processed and analysed using Image J to reveal the efficiency of scratch closure.. Data are based on the analysis of 10-20 time-lapse movies per group pooled from 3 independent experiments. Statistical significance was determined using ANOVA to show global differences between the VSMC growth stages ($p = 0.0159$), followed by a Tukey's multiple comparison test.

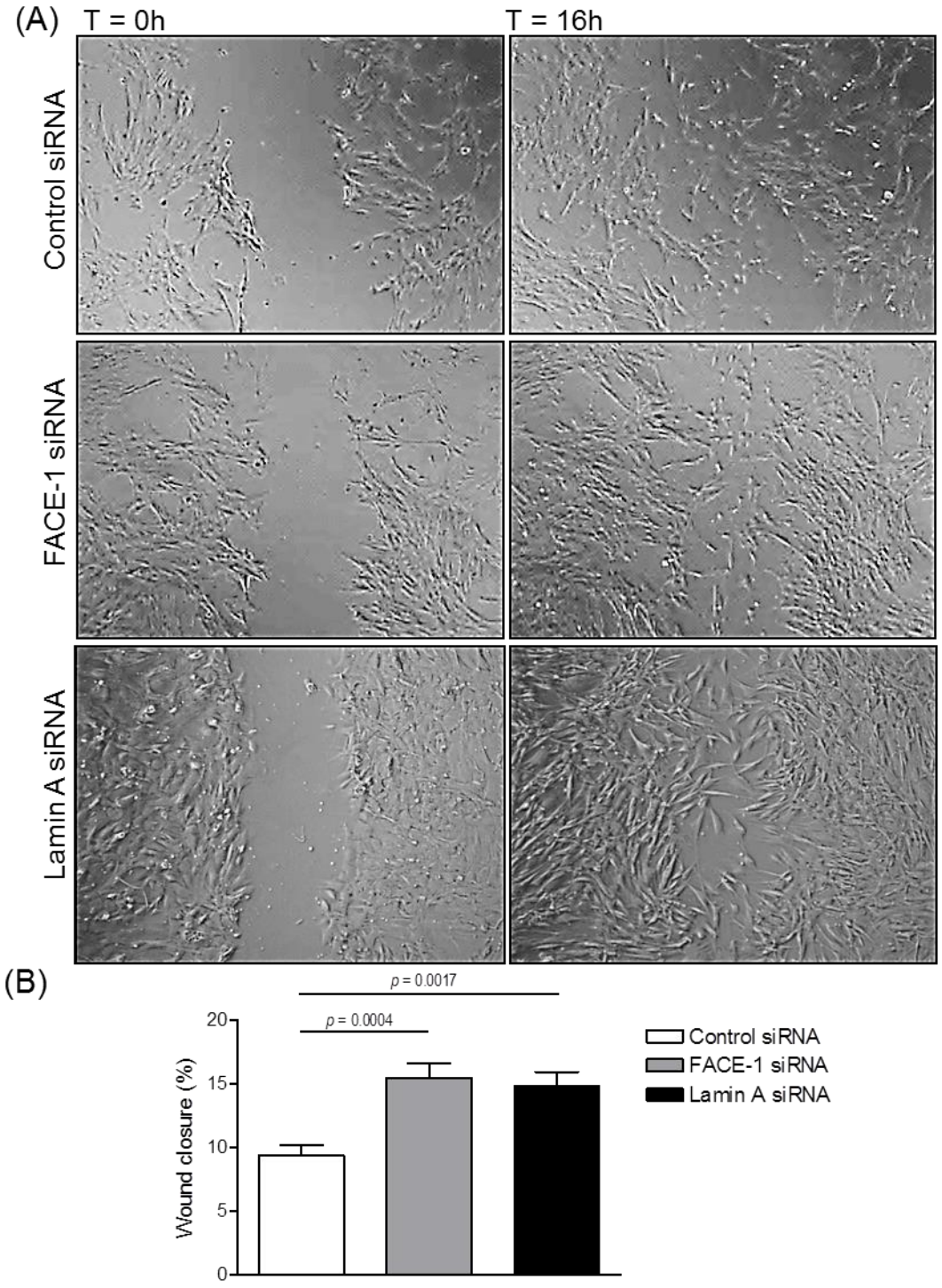

Figure 3.24: The effect of nuclear lamina disruption on VSMC scratch closure. Control, FACE-1 and lamin A siRNA-treated 35F VSMCs were seeded onto a 24-well plate and cultured until confluent before being scratched with a pipette tip. Time-lapse microscopy was used to capture VSMC migration into the scratch area. **(A)** Representative phase-contrast images compare scratch closure at 0 and 16 h post-scratch. **(B)** Images were processed and analysed using Image J to reveal the efficiency of scratch closure. Data are based on the analysis of 15-19 time-lapse movies per group pooled from 3 independent experiments. Statistical significance was determined using a paired Student's *t* test.

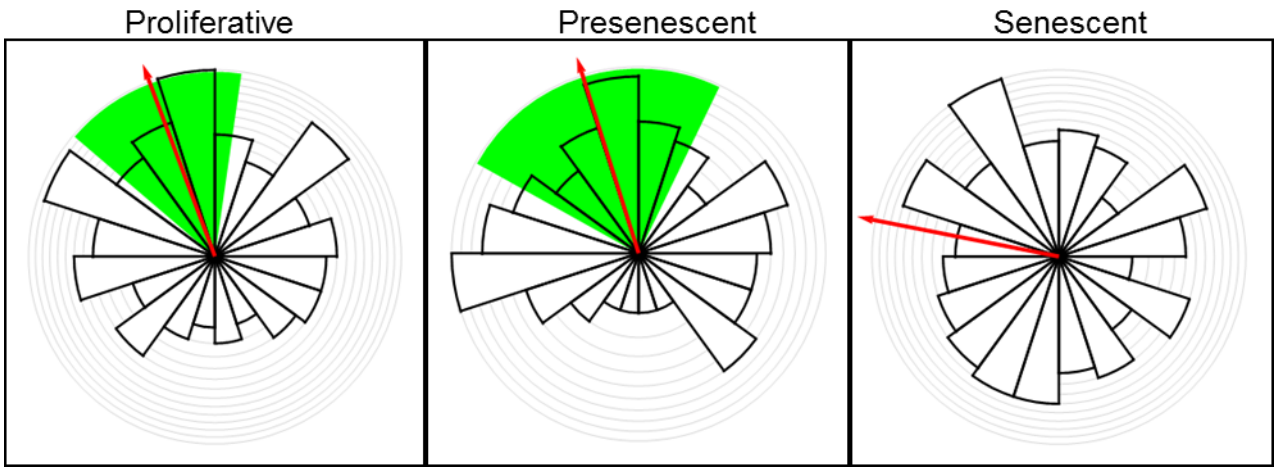

Figure 3.25: The impact of ageing on VSMC chemotaxis. VSMCs (35F) at all 3 stages of growth (proliferative, presenescent, senescent) were seeded on to individual coverslips and incubated in low serum (2% FBS) medium overnight. Cell migration towards high serum (20% FBS) medium was assayed using Dunn chemotaxis chambers and captured using time-lapse microscopy over 16 h. Each segment of the Rose plot (circular histograms) represents the total number of cells with an average angle of migration falling within that particular interval. The Rayleigh test for unimodal clustering determined directional migration. The red arrow indicates the mean migration angle and the 95% confidence interval is highlighted in green. The data presented are based on >80 VSMCs tracked per group and pooled from 2-4 independent experiments.

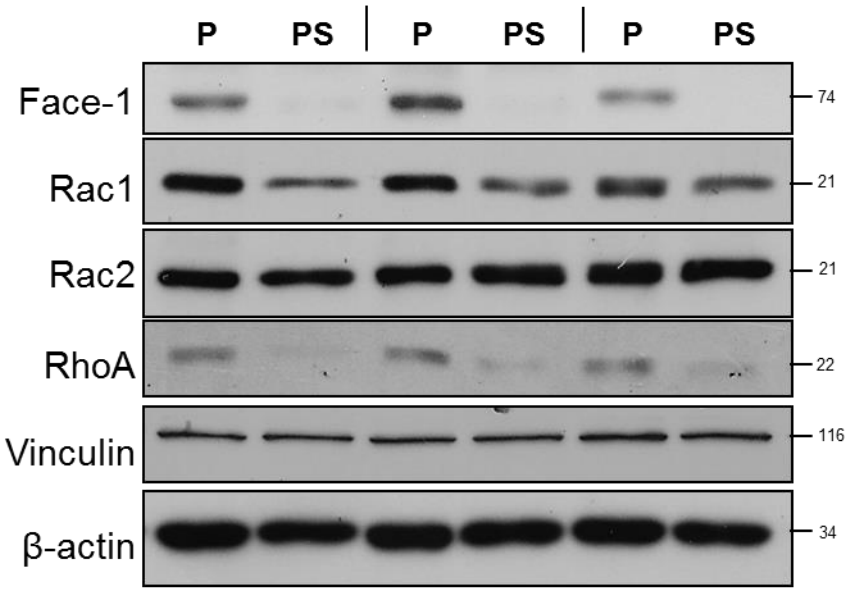

Figure 3.26: VSMC ageing is associated with a loss of Rho GTPases. VSMCs (35F) were cultured *in-vitro* and both proliferative (P) and presenescent (PS) cells were subjected to Western blot analysis to assess Rho GTPase levels, including Rac1, Rac2 and RhoA. FACE-1 was used as presenescence marker and vinculin and β-actin indicated equal protein loading (20 µg of each protein lysate was loaded). This experiment was performed in triplicate. Rac2 is known to be expressed in VSMCs,[251]

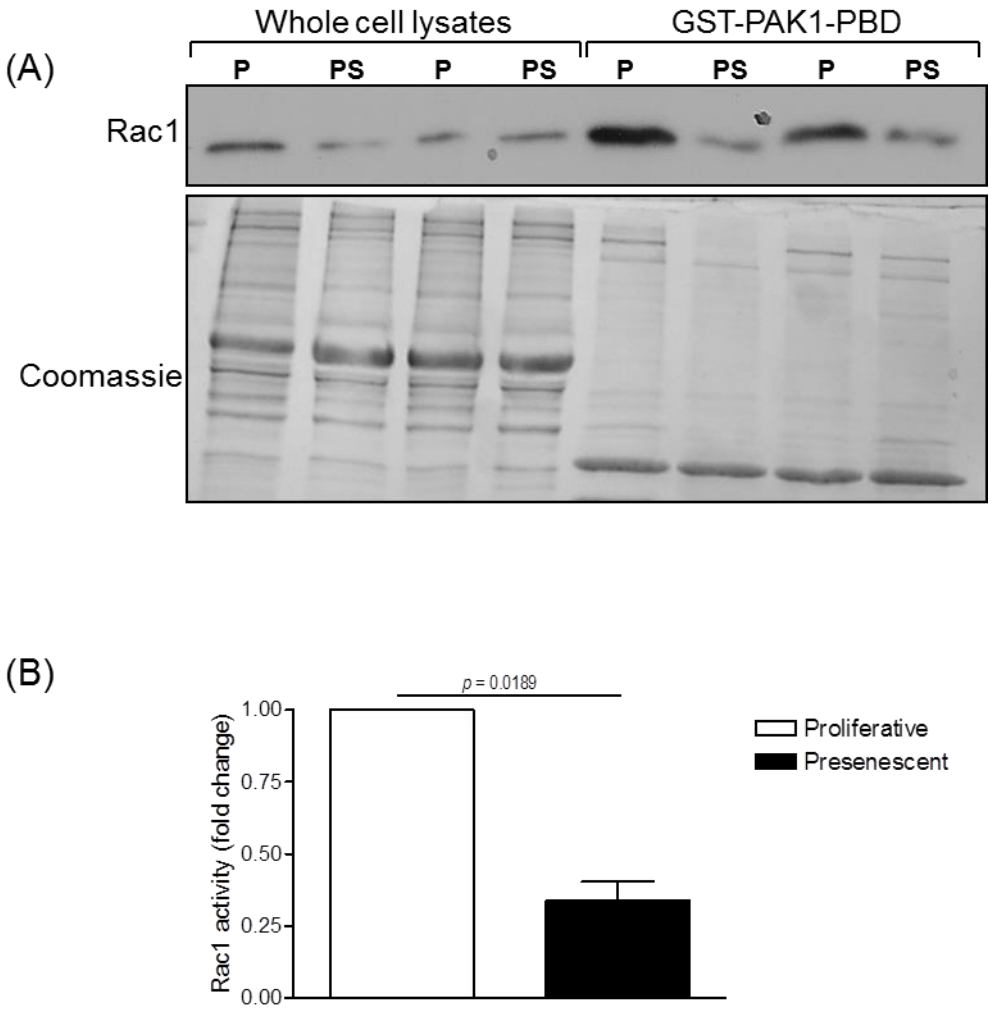

Figure 3.27: Aged VSMCs exhibit reduced Rac1 activity. VSMCs (35F) were passaged *in-vitro* and both proliferative and presenescent VSMCs were lysed for a GST pull-down assay with the GST-PAK1-PBD (p21-binding domain), which specifically precipitates Rac1 in its GTP-bound form. **(A)** Western blot analysis revealed Rac1 activity in presenescent 35F VSMCs compared with proliferative 35F VSMCs (right panel). The left panel represents total Rac1 from whole cell lysates. **(B)** Bar graph representing the fold change in Rac1 activity between proliferative and presenescent VSMCs from 3 independent experiments. Statistical significance was calculated using a paired Student's *t* test.

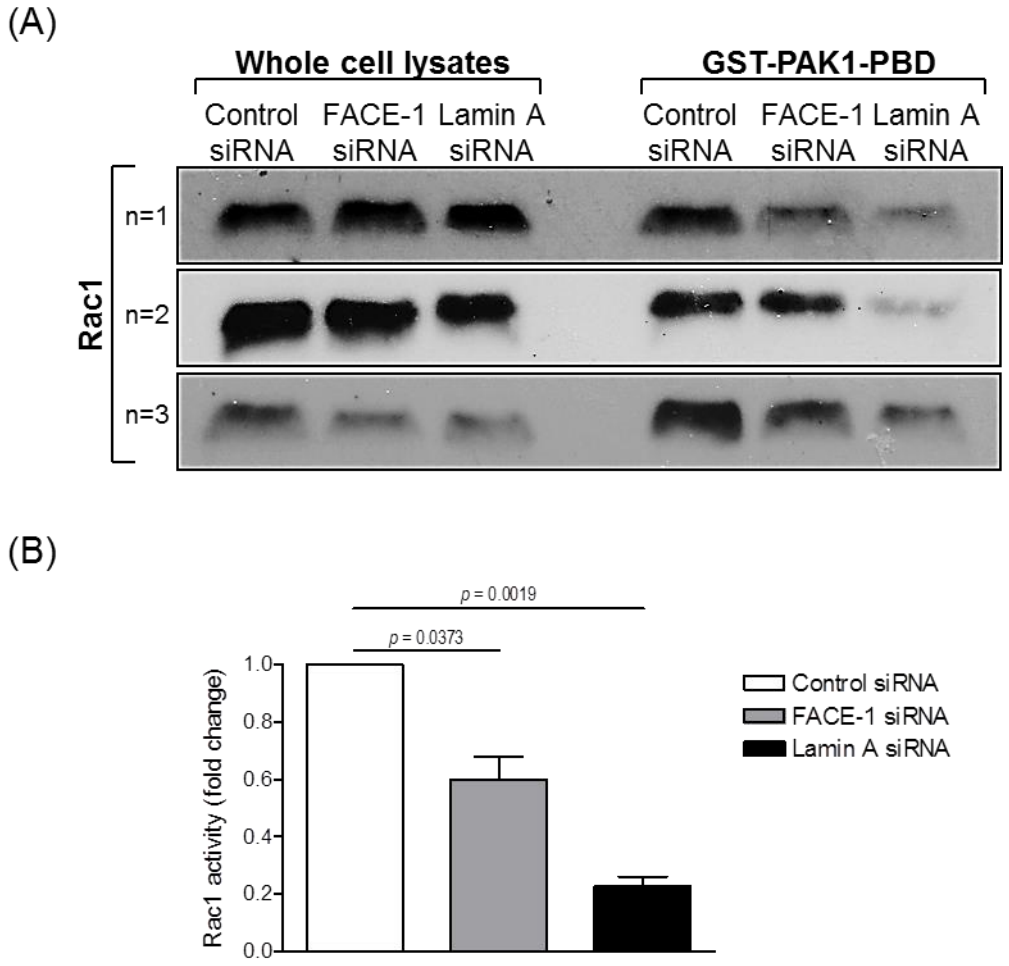

Figure 3.28: Nuclear lamina disruption hinders Rac1 activity in VSMCs. VSMCs were treated with control, FACE-1 and lamin A siRNA for 72 h before being lysed for a GST pull-down assay with the GST-PAK1-PBD (p21-binding domain), which specifically precipitates Rac1 in its GTP-bound form. **(A)** Western blot analysis revealed a significant reduction in Rac1 activity (GST-Rac1) in FACE-1 and lamin A depleted VSMCs when compared with control cells (right panel). The left panel represents total Rac1 from whole cell lysates (n=3). **(B)** The bar graph represents the fold change in Rac1 activity from 3 independent experiments. Statistical significance was calculated using a paired Student's *t* test.

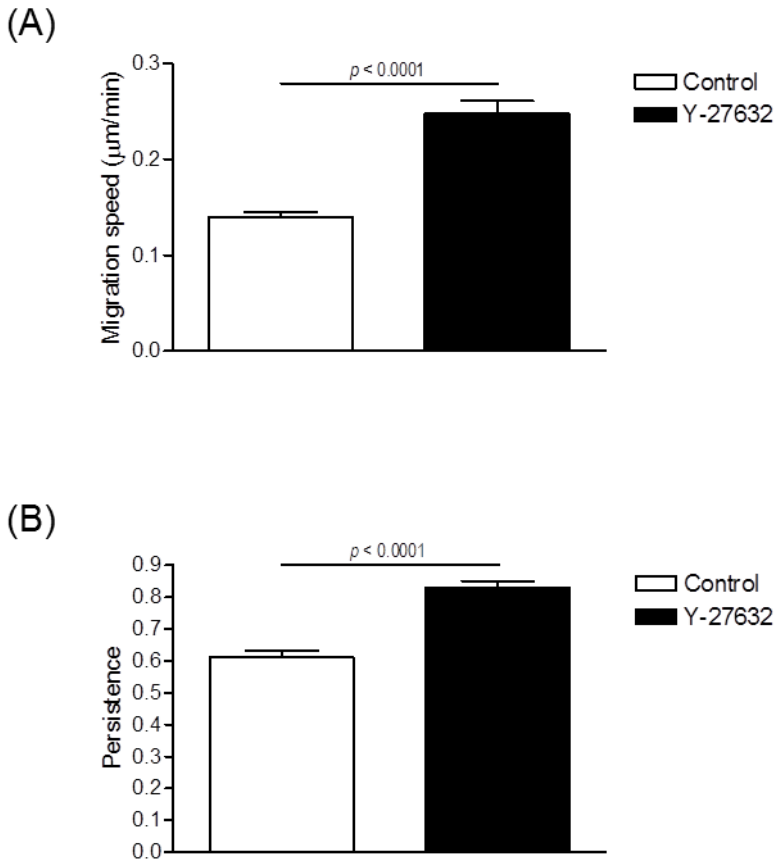

Figure 3.29: ROCK inhibition affects VSMC migration. Time-lapse microscopy recorded the migration of Y-27632 (10 μM) treated and untreated (control) 35F VSMCs for 16 h and individual cells were tracked using Image J software. Mathematica analysed the **(A)** velocity and **(B)** persistence of VSMC migration in the presence and absence of ROCK inhibitor. Data presented are based on >80 VSMCs tracked per group pooled from 3 independent experiments. Statistical significance was calculated using a paired Student's *t* test (control vs treatment).

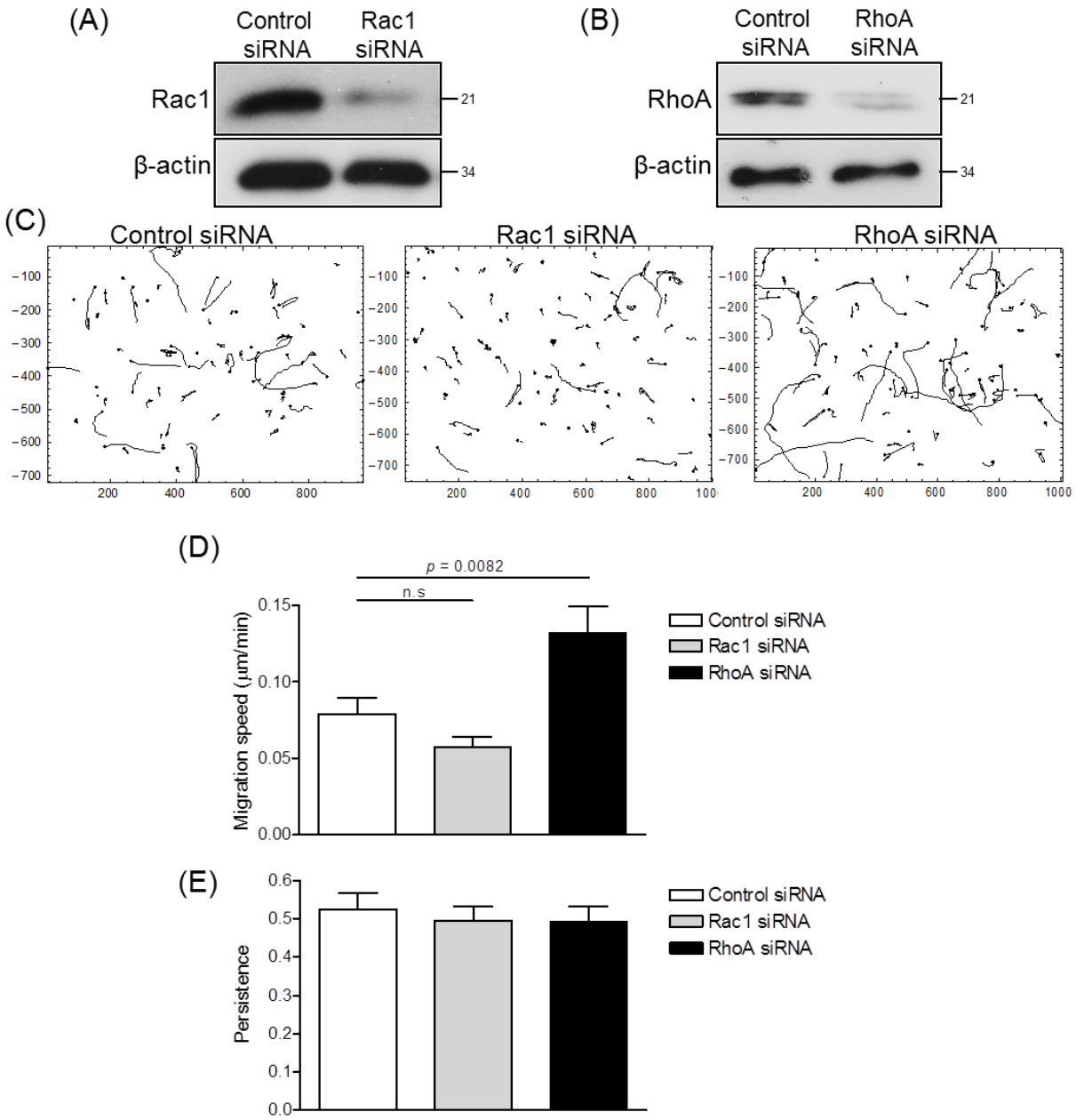

Figure 3.30: RhoA knockdown enhances fibroblast migration speed. MRC-5 fibroblasts were treated with control, Rac1 and RhoA siRNA for 72 h prior to experimentation. **(A & B)** Western blot shows Rac1 and RhoA levels. Coomassie indicates equal protein loading (20 µg of each protein lysate was loaded). Time-lapse microscopy captured images of random cell migration every 10 min for 20 h. Image J software was used to manually track individual cells and Mathematica software plotted x-y coordinates to provide an overlay of migratory tracks and analysed **(D) cell** migration speed and **(E)** migratory persistence. Data are based on the analysis of 69 (control), 82 (Rac1 siRNA) and 82 (RhoA siRNA) cells pooled from 3 independent experiments. Statistical significance was calculated using a paired Student's *t* test (control vs treatment).

3.4 Discussion

It is well-documented that prelamin A accumulates at the NE of VSMCs during ageing, leading to nuclear morphology defects.[204] However, the specific outcome of prelamin A accumulation upon cell function has not yet been extensively reviewed. To better our understanding of prelamin A as a as a driving force of VSMC ageing, this chapter extends on previous findings to characterise the impact of prelamin A upon general cell morphology, focal adhesion organisation and cell migration.

3.4.1 Characterising the morphological changes associated with VSMC ageing

During ageing it is normal for cells to undergo morphological changes. As the actin cytoskeleton defines cell structure and shape, it is heavily implicated in the morphological changes associated with ageing.[23] Furthermore, previous studies demonstrate that cytoskeletal networks are disrupted in cells derived from older patients emphasising that F-actin alterations are an important aspect of the ageing process.[252] In our work, presenescent VSMCs were elongated, with a spindle-like appearance and much larger than proliferative predecessors. This supports previous work illustrating that VSMCs from older donors have a large, flattened appearance compared with those derived from younger patients.[204] Also, VSMCs from atherosclerotic plaques are enlarged and flattened with a stellar shape compared with those from normal arteries.[13] We were able to replicate this spindle-like morphology in young VSMCs and MRC-5 fibroblasts by silencing FACE-1 with siRNA, suggesting that subsequent prelamin A accumulation at the NE is responsible for driving cytoskeletal reorganisation. This is potentially mediated by the LINC complex which tethers actin filaments via nesprins-1/2 to the nucleus.[147] As the actin cytoskeleton regulates numerous cellular processes including contractility, motility and proliferation, age-related alterations to cytoskeletal structure may be detrimental to general VSMC functioning and cell fate.[253, 254]

3.4.2 Aged-related changes to focal adhesion formation

Actin filaments are indirectly connected to the ECM via interactions with focal adhesion proteins at the cell membrane.[147] Therefore, focal adhesions form important bidirectional signalling hubs between the cell interior and its external environment.[44] Our data illustrate that *in-vitro* VSMC ageing and prelamin A accumulation in both

VSMCs and MRC-5 fibroblasts is associated with a loss of focal adhesions per cell. In addition, the few remaining focal adhesions are more circular and primarily distributed at the cell periphery. This focal adhesion phenotype reflects that of motile cells, as focal adhesion number is inversely proportional to cell migration.[248] Previous evidence shows that an overabundance of focal adhesions correlates with reduced fibroblast motility.[255] Large focal adhesions form stable connections between the cell and ECM consequently inhibiting cell movement, whereas smaller and rounder adhesions are characteristic of faster migrating cells as they are rapidly formed and turned over.[47, 48] Smaller focal adhesions at the cell leading edge also exert stronger propulsive tractions and drive more rapid cell migration compared with large and more stable adhesions that mainly serve as anchorage points.[256] Our IRM data also reveals that focal adhesion morphological changes in both *in-vitro* aged and FACE-1 depleted cells are reflected by increased focal adhesion dynamics at the leading edge. Taken together, this evidence suggests that the focal adhesion phenotype we describe in these ageing models is indicative of more migratory cells. We also demonstrate that nuclear lamina disruption, by prelamin A accumulation or lamin A depletion, can impressively drive changes as far as the cell membrane. We predict that this mediated by nesprin-tethered F-actin which strongly supports our hypothesis that focal adhesions provide an extension of the LINC complex, creating a mechanically-coupled system between the cell membrane, actin cytoskeleton and nucleus. This may form an essential bridge between the cell exterior and nuclear interior and supports previous work describing a link between integrin signalling at the cell membrane and gene transcription.[197]

3.4.3 Age-related changes to VSMC migration

Cell migration is normally dictated by pro and anti-migratory cues from the local environment, however, emerging evidence suggests that VSMCs possess an intrinsic steering mechanism and can undergo directional migration independently of external chemotactic cues.[257-260] Collectively, Rho GTPases, polarity signalling machinery, integrin trafficking and ECM architecture determine whether a cell exhibits a random crawl with repeated changes in direction (low intrinsic directionality) or persistent migration in a constant direction (high intrinsic directionality).[261-263] In our study, we monitored single VSMCs throughout *in-vitro* passaging to determine the impact of ageing on their intrinsic migratory capacity. We detected significant differences in migration speed and persistence throughout the 3 distinct VSMC growth stages.

Actin cytoskeleton arrangement is a primary indicator of a cells motile capacity; cells with shorter actin filaments and a rounded shape migrate poorly compared with those possessing long actin filaments and a more polarised shape.[264] As previously described, cell migration rate is also determined by focal adhesion turnover. Consistent with their more rounded morphology and low focal adhesion turnover, time-lapse microscopy revealed that single proliferative VSMCs are relatively slow and lack migratory persistence. This fits with earlier studies demonstrating that VSMCs are slow-moving cells that exhibit random migration patterns and continuously change direction.[265, 266] Rapid and frequent retraction and reformation of the cell rear stimulates directional changes and is associated with less persistent cell migration.[267] Therefore, future work will assess VSMC trailing-end retraction in finer detail as it is emerging as an important determinant of migratory behaviour. Lack of migratory persistence suggests that young, healthy VSMCs within the vessel wall are dispersive with an explorative nature. Interestingly, we uncovered a migratory switch in VSMCs at the presenescent growth stage. Our studies discovered that presenescent VSMCs are significantly faster and more persistent than proliferative VSMCs, suggesting that these cells migrate more efficiently. Moreover, presenescent VSMCs retain their chemotactic ability and display enhanced closure in scratch assays. Ultimately, when VSMCs reach their final stage of growth, migration rate slows, cells cannot chemotax and wound healing is impaired. The inability of senescent VSMCs to respond to chemotactic cues and conduct their migratory functions within the vessel may be detrimental to vascular health.

Within the current literature, the impact of ageing upon cell migration remains undefined. Previous studies have demonstrated the inability of fibroblasts from old mice to complete wound closure when compared with those derived from young mice, whereas, VSMCs from old rats have enhanced migration rates compared with VSMCs from young rats.[220, 268] Although contradictory, the differences in these results may be explained by the brief increase in speed associated with presenescent growth prior to migration subsiding. Therefore, the specific stage of VSMC growth has to be taken into consideration when conducting migration studies.

In support of our notion that cell motility is regulated by the nucleus, we demonstrate that nuclear lamina disruption by FACE-1 or lamin A depletion enhances fibroblast focal adhesion turnover, migratory velocity and persistence, similarly to presenescent VSMCs. This suggests that nuclear lamina adaptations during VSMC ageing influence adhesion dynamics and the cells migratory capacity. However, rapid focal adhesion turnover in FACE-1 depleted VSMCs was not reflected by migratory

speed changes, suggesting that prelamin A accumulation alone does not drive the presenescent phenotype observed in *in-vitro* aged VSMCs. Therefore, alternate age-related modifications, possibly to other LINC complex components such as SUN and nesprin proteins may also define VSMC phenotype. Focal adhesions are signalling hubs that regulate actin dynamics and cell migration, Because prelamin A accumulation induces focal adhesion reorganisation it cannot be ruled out that migratory changes observed are due to these indirect changes in signalling pathways associated with focal adhesions. As VSMC ageing is associated with diminished desmin levels and heightened tubulin, cellular retinol binding protein-1 (CRBP-1), MMP-2 and vascular cell adhesion protein-1 (VCAM-1) expression, these factors may also contribute towards morphological and migrational VSMC changes.[220, 269-271]

3.4.4 Age-related changes to Rho GTPase expression

The Rho GTPase family of signalling molecules regulate the actin cytoskeleton to control cell morphology, motility, polarity and invasion.[272, 273] The three main classes of GTPases include Rho (A, B & C), Rac (1,2 & 3) and Cdc42, however, RhoA, Rac1 and Cdc42 are the most widely studied and play several well-characterised roles in actin reorganisation during cell migration.[274] Interestingly, our study reveals an age-associated reduction in RhoA and Rac1 expression, coupled with reduced Rac1 activity.

Rac1 is the most studied of the Rac subfamily and particularly functions in lamellipodia formation and focal adhesion assembly at the cell leading edge.[263, 275] Our study reveals that Rac1 expression and activity is diminished in presenescent and nuclear lamina disrupted VSMCs. Earlier studies illustrate that Rac1-deficient mouse neutrophils exhibit defects in actin assembly and migration towards chemotactic stimuli.[276] However, more recent data demonstrate that raised Rac1 expression promotes random migration, whereas slightly lowering Rac1 levels by 30-50% enhances the migratory persistence of primary human fibroblasts.[263] This closely supports our work, as low Rac1 expression and activity in *in-vitro* aged and FACE-1 depleted VSMCs correlates with significantly increased migratory persistence. This evidence led us to believe that Rac1 suppression during ageing enhances VSMC persistence, however, subsequent experiments revealed that Rac1 knockdown does not influence the migratory behaviour of MRC-5 fibroblasts. This suggests that other factors are responsible for driving persistent migration in aged VSMCs.

Rho is important for stress fibre formation and regulates the contractile force necessary to drive cell movement.[253] Rho also mediates focal adhesion formation and reduced Rho activity in endothelial cells is associated with the disassembly of focal adhesions and actin stress fibres.[277] Furthermore, knocking down RhoA hinders fibroblast migration and the Rho inhibitor, C3 transferase, causes a loss of stress fibres and impedes VSMC cell migration.[263, 278, 279] Contrary to this, transient Rho inhibition in Swiss 3T3 cells correlates with active cell spreading, an indicative measure of cell migration.[280] In another study, stationary human VSMCs exhibit increased RhoA activity compared with migratory cells, suggesting that cell migration is stimulated by Rho deactivation.[88] In support, cells lacking FAK, which normally inhibits Rho activity, are less migratory.[281] In this study, FAK -/- mouse fibroblasts lack Rho inhibition and adopt a non-polarised, circular shape with increased focal adhesions across their surface. However, FAK+/+ cells have low Rho activity and are elongated with a polygonal morphology. Furthermore, focal adhesions were primarily located at the edges of FAK+/+ cells and exhibited rapid turnover compared with stable focal adhesions in FAK-/- cells. In summary, Rho inhibition promotes focal adhesion dynamics and cell migration which replicates the phenotypic changes associated with presenescent VSMCs in our studies. This suggests that loss of RhoA expression drives VSMC phenotypic switching from contractile to synthetic phenotype and contributes towards age-related changes in cell migration. Moreover, we show that RhoA knockdown enhances fibroblast migration speed and inhibiting ROCK, a downstream effector of RhoA, enhances VSMC migration speed and persistence. A study supporting our findings illustrates that human epithelial cell speed and persistence increases following ROCK inhibition, most likely through reduced myosin II-mediated contractility and increased rear-end stability.[267] This study proposes that producing a ‘drag’ at the cell rear, like a drogue does on a boat, enables cells to control directionality.[267] This led us to speculate that a loss of RhoA/ROCK activity during VSMC presenescent growth reduces cell contractility and stabilises the cell rear to drive persistent cell migration, a theory that will be tested in the future. However, although migrational velocity was enhanced in RhoA-depleted MRC-5 fibroblasts, no change to directional persistence was observed. Other studies also demonstrate that the same ROCK inhibitor hinders VSMC migration and RhoA expression/activity is enhanced in aged rat arteries.[282, 283] Therefore, further work is required to better understand the Rho GTPase changes associated with VSMC ageing. It is possible that other Rac and Rho genes (Rac2/3 and RhoB/C) contribute towards the intrinsic persistence of VSMCs but were not explored in the current study due to time restraints.

3.4.5 Chapter 3 conclusions

This chapter clearly demonstrates that accumulation of the VSMC ageing marker, prelamin A, at the NE alters the cellular morphology and migratory behaviour of VSMCs and MRC-5 fibroblasts. We hypothesise that nuclear lamina disruptions impact upon LINC complex organisation and subsequently drive changes in cell morphology, Rho GTPase activity, focal adhesion formation and cell migration. This is because the LINC complex creates a physically-coupled system throughout the whole cell, allowing nuclear adaptations to be directly transmitted to the actin cytoskeleton and actin-regulated processes. Furthermore, actin tension regulates focal adhesion formation at the cell membrane, which in turn influences Rho GTPase activity. Therefore, we predict that the LINC complex directly and indirectly regulates cell motility via mechanical and biochemical pathways, respectively.

During *in-vitro* VSMC ageing, cell migration speed and persistence peaks at the presenescent growth stage before slowing down when VSMCs become senescent, however, the mechanisms behind this migratory switch remain unclear. Healthy VSMCs normally undergo phenotypic transformation from a contractile to a migratory phenotype in response to vessel damage. Therefore, we speculate that presenescent VSMCs exhibit an enhanced migratory phenotype as a protective repair mechanism prior to the onset of senescence when VSMC migration and proliferation ceases.

3.4.6 Limitations and future work

3.4.6.1 VSMC isolates

The experiments conducted throughout this chapter were performed in triplicate mostly using VSMCs derived from a 35 year old female (35Fs). Due to time restraints and accessibility to precious stocks of primary VSMCs, the results obtained in the current study are limited. In the future, our results will be validated using more VSMC isolates.

3.4.6.2 Ageing model

Throughout this chapter, FACE-1 siRNA was used to model VSMC ageing by artificially accumulating prelamin A in young VSMCs and MRC-5 fibroblasts. However, it would be naïve of us to believe that prelamin A alone is causal for the phenotypic adaptations associated with VSMC ageing. Our studies illustrate that *in-vitro* aged VSMCs have larger, more elongated nuclei than young VSMCs, which is mirrored by

their general cell shape. However, FACE-1 depleted VSMCs exhibit no nuclear size or shape changes and become more elongated but not larger. *In-vitro* aged VSMCs migrate faster and more persistently yet FACE-1 depletion only increases migratory persistence. Despite our model not completely mimicking an aged VSMC, our study specifically focusses on the phenotypic similarities induced by prelamin A accumulation such as cellular elongation, enhanced focal adhesion turnover and increased migratory persistence. The efficacy of siRNA-mediated knockdown also poses another limitation to this work and functional studies in the future will overexpress prelamin A (lentiviral/adenoviral) to support our findings.

3.4.6.3 VSMCs vs fibroblasts

Our studies highlight inconsistencies in the response of VSMCs and MRC-5 fibroblasts to prelamin A accumulation. FACE-1 depletion did not impact on VSMC size, yet MRC-5 cells became significantly smaller following siRNA treatment. Despite both cell types exhibiting similar changes in focal adhesion morphology and turnover, fibroblast migration speed and persistence was enhanced in response to FACE-1 knockdown whereas only slight increases in VSMC persistence were observed. Such discrepancies are unsurprising as VSMCs and fibroblasts exhibit differing functional roles within tissue. Fibroblasts are slow moving cells, possibly enabling small changes in migration to appear more striking against faster-moving VSMCs. Furthermore, we speculate that the LINC complex itself may vary between these cell types in its composition, stability and adaptability to nuclear lamina changes. This is an interesting concept as VSMCs uniquely undergo transient phenotypic switching between a contractile and synthetic phenotype which requires continuous cellular remodelling, most likely dependent on a malleable LINC complex. On the other hand, fibroblasts normally terminally differentiate into myofibroblasts thus reducing their phenotypic plasticity. Therefore, fibroblasts provide a cleaner model system enabling the impact of nuclear lamina disruption upon cellular morphology and motility to be exaggerated.

3.4.6.4 Migrational model

The migratory studies conducted throughout this chapter were performed on 2D rigid glass/plastic surfaces *in-vitro* which do not accurately represent a cells natural environment. Within tissue, cells are normally exposed to simultaneous pro and anti-migratory cues and migratory behaviour is governed by numerous extrinsic factors including diffusible chemokines (chemotaxis), ECM-bound molecules (haptotaxis) or mechanical signals (durotaxis).[284] Ultimately, all of these determinants must be considered when studying cell migration in order to truly reproduce a physiologically

relevant setting. We explored the impact of ageing on intrinsic VSMC migration *in-vitro* but did not consider that *in-vivo* the vessel wall itself will undergo age-related structural and mechanical changes that will influence cell migratory behaviour. Previous studies have demonstrated differences in cell morphology, signalling and migration between 2D and 3D models.[285, 286] Therefore, future studies utilising 3D matrices and confocal microscopy to monitor cell migration will generate more accurate and reliable results. Additionally, aged VSMCs secrete more MMP-2 than those derived from young aorta.[198] MMPs are regulated by Rho GTPases and enhance migration by degrading ECM. Therefore, future work will also assess how VSMC ageing and prelamin A accumulation influence MMP expression/activity using gel zymography.

3.4.6.5 The role of LINC complex in mechanotransduction

To assess the mechanical strength that the LINC complex provides to the cell, future studies will assess the mechano-sensitivity of cells following NE disruption by applying cyclic strain followed by staining for apoptotic, proliferation and differentiation markers. Further work will also investigate how stretch/strain affects the activity of known regulators of mechanotransduction including Rho GTPases and the MAPK family proteins, ERK1/2, JNK1/2 and p38, using GST-pull down assays and phopsho-specific antibodies. Atomic force microscopy (AFM) or optical/magnetic tweezers would also be useful to measure the mechanical strength of cells and determine whether cells are weakened following LINC complex disruption.

Chapter 4: The role of the LINC complex in regulating cell motility

4.1 Introduction

Thus far, the focus of this thesis has been to characterise the impact of the VSMC ageing marker, prelamin A, on cell function. We propose that prelamin A accumulation at the NE drives cellular changes as a result of disrupting the LINC complex. This chapter further investigates the effect of prelamin A on LINC complex organisation, in an attempt to better understand its role as a driving force behind VSMC ageing. We will also explore the importance of other core LINC complex components, including SUN and nesprin proteins, in regulating cell morphology and migration. Current literature presents a LINC complex that is conserved in structure and function throughout different cell types. This chapter tests whether this holds true as we compare the result of LINC complex disruption between VSMCs and MRC-5 fibroblasts.

4.2 Aim of this chapter

This chapter will perform subcellular fractionations and Western blot analysis to specifically determine the impact of VSMC ageing and prelamin A accumulation on individual LINC complex components. We will also explore the role of SUN and nesprins in regulating cell morphology and migration using an siRNA-mediated approach to target these proteins. FRAP will study nesprin-2 mobility/dynamics following nuclear lamina disruption in U2OS cells.

4.3 Results

4.3.1 VSMC ageing alters LINC complex organisation

Firstly, we investigated the impact of *in-vitro* ageing and prelamin A accumulation upon the VSMC LINC complex. Western blot analysis compared proliferative and presenescent whole VSMC lysates and demonstrated an accumulation of prelamin A in the latter. This inversely correlated with SUN2 expression with SUN2 levels diminishing in presenescent cells compared with proliferative cells (**Figure 4.1A**). Nesprin-2 and lamin A/C remained unchanged between proliferative and presenescent growth stages. This experiment was repeated using FACE-1 siRNA and aside from increased prelamin A in FACE-1 depleted VSMCs, all other LINC complex proteins remained unchanged (**Figure 4.1B**).

To further explore the effect of VSMC ageing on LINC complex organisation, subcellular fractionations were performed on early-passage and presenescent VSMCs. Western blotting confirmed that prelamin A accumulated in the nuclear insoluble fraction of presenescent VSMCs (nuclear insoluble fractions contain the NE, nuclear lamina and ER as these are contiguous structures). This corresponded with increased nesprin-2 isoforms and reduced lamin A/C within the same fraction whilst emerin and coomassie loading levels remained unchanged (**Figure 4.2A**). Immunofluorescence microscopy also revealed that nesprin-2, although distributed between the NE and ER of proliferative VSMCs, appeared stabilised at the NE and absent from the ER of presenescent VSMCs (**Figure 4.2B**). These collective data reveal that ageing impinges on nuclear morphology and LINC complex organisation.

4.3.2 Prelamin A accumulation disrupts LINC complex organisation

To specifically establish the impact of prelamin A upon LINC complex organisation, FACE-1 knockdown was performed in VSMCs prior to subcellular fractionation. Western blotting confirmed that FACE-1 depletion was successful as prelamin A accumulated within the nuclear insoluble fraction. Nesprin-2 isoforms and lamin A/C levels also accumulated within this fraction whereas emerin, SUN2 and coomassie staining remained unchanged (**Figure 4.3**). This suggests that prelamin A may be important for stabilising LINC complex components at the NE. Unexpectedly, lamin A also accumulated in the nuclear insoluble fraction which suggests that lamin A is also more stable at the NE in the presence of prelamin A. This finding is difficult to

explain but only highlights the complexity of the LINC complex further. In addition, the control sample in this experiment appears to be different from that in the previous experiment (Figure 4,2). This change can be explained by the different conditions in each experiment prior to fractionation including the presence of Hiperfect and siRNA in the cellular samples.

Furthermore, immunofluorescence microscopy revealed that nesprin-2 was lost from the NE and accumulated at the ER in 46.07 ± 3.679% FACE-1 depleted cells (**Figure 4.4B & D**) whereas nesprin-2 localised at the NE and ER of 78.17 ± 3.940% control cells (**Figure 4.4A & D**). Lamin A siRNA was also used as a positive control and nesprin-2 mislocalised to the ER in 77.87 ± 7.806% lamin A depleted VSMCs (**Figure 4.4C & D**), suggesting that prelamin A accumulation at the NE severs the connection between the nuclear lamina and nesprins on the ONM.

In addition, subcellular fractionations of control and FACE-1 siRNA treated fibroblasts confirmed that prelamin A accumulated in the nuclear insoluble fraction of FACE-1 depleted fibroblasts (**Figure 4.5**) to mimic FACE-1 depleted and *in-vitro* aged VSMCs. This correlated with increased nesprin-2 and lamin A/C levels in the same fraction, whereas emerin and coomassie levels were unchanged. This evidence supports VSMC data and further suggests that prelamin A accumulation at the NE effects LINC complex organisation.

4.3.3 SUN2 is an important regulator of cell morphology and migration

Our data reveal that SUN2 levels were diminished during *in-vitro* VSMC ageing (**Figure 4.1A**) which encouraged us to further explore the role of SUN proteins as regulators of cell morphology and migration. siRNA was used to target SUN1, SUN2 and both proteins together (SUN1/2). Western blotting confirmed SUN2 knockdown in VSMCs but we were unsuccessful in identifying an antibody to detect SUN1 (**Figure 4.6A**). SUN1 and SUN2 depletion had no impact on nesprin-2 protein levels (**Figure 4.6A**) and immunofluorescence microscopy confirmed that nesprin-2 localisation at the NE was retained in these cells to reflect control VSMCs (**Figure 4.6B**).

To establish whether SUN disruption was responsible for driving the *in-vitro* aged VSMC phenotype described in chapter 3, we determined the importance of SUN1/2 proteins in regulating VSMC morphology. Immunofluorescence microscopy captured images of F-actin stained VSMCs following siRNA treatment (**Figure 4.7A**).

Both SUN1 and SUN2 depleted VSMCs were significantly smaller (**Figure 4.7B**) with no change to circularity (**Figure 4.7C**). Nuclear staining with DAPI mirrored the cytoskeletal changes (**Figure 4.7D & E**). Following SUN1 and SUN2 knockdown, VSMCs underwent 16 hours of time-lapse microscopy and random single cell migration was tracked using Image J software (**Figure 4.8A**). Mathematica software analysed VSMC migration to reveal that SUN1 depletion (0.196 ± 0.008 μm/min) did not affect cell migration when compared with control cells (0.196 ± 0.007 μm/min), whereas, SUN2 depletion (0.241 ± 0.010 μm/min) significantly enhanced VSMC velocity (**Figure 4.8B**). No change to migratory persistence was detected between control (0.501 ± 0.023), SUN1 (0.477 ± 0.028), or SUN2 (0.044 ± 0.026) siRNA-treated VSMCs (**Figure 4.8C**).

Fibroblasts were also treated with SUN1 and SUN2 siRNA and knockdown was confirmed using Western blot analysis (**Figure 4.9A & B**). Staining F-actin with rhodamine phalloidin followed by immunofluorescence microscopy revealed that, similarly to VSMCs, SUN1 and SUN2 knockdown reduced cell area but only SUN2 significantly (**Figure 4.9C & D**). Both SUN1 and SUN2 depletion significantly reduced fibroblast circularity (**Figure 4.9C & E**). Furthermore, time-lapse microscopy revealed that migration speed significantly increased in both SUN1 (0.097 ± 0.013 μm/min) and SUN2 (0.125 ± 0.012 μm/min) siRNA-treated fibroblasts compared with control cells (0.065 ± 0.004 μm/min) (**Figure 4.10A**). However, no change to migratory persistence was detected following SUN1 or 2 knockdown (**Figure 4.10B**). Therefore, both VSMC and fibroblast data strongly implicate SUN proteins as key determinants of cell morphology and migrational velocity.

4.3.4: Nesprin knockdown differentially effects VSMC and fibroblast speed

Nesprins mediate an essential link between the nucleus and cell cytoskeleton, play a key role in maintaining cell structure and are believed to be important regulators of cell motility.[151] After studying the effects of nuclear lamina and SUN protein disruption upon cellular morphology and migration, we next progressed to target nesprins on the ONM using an siRNA-mediated approach. Nesprin-1 and nesprin-2 mRNA depletion in VSMCs by 63.42 ± 9.587% and 66.85 ± 9.801%, respectively was confirmed using qPCR (**Figure 4.11A & B**). Time-lapse microscopy captured random VSMC migration over 16 hours and Image J software was used to manually track individual cells (**Figure 4.11C**). Subsequent analysis using Mathematica software revealed that both nesprin-1 (0.147 ± 0.006 μm/min) and nesprin-2 (0.117 ± 0.005

μm/min) depleted VSMCs were significantly slower than control (0.172 ± 0.007 μm/min) VSMCs (**Figure 4.11D**). No change to persistence was detected between control (0.615 ± 0.016), nesprin-1 (0.636 ± 0.020) and nesprin-2 (0.594 ± 0.020) siRNA-treated VSMCs (**Figure 4.11E**). This evidence suggests that nesprins are essential LINC complex components in VSMCs and without nesprins bridging F-actin to the nucleus, cell migration is significantly impaired.

The above experiment was repeated in MRC-5 fibroblasts and nesprin-1/2 knockdown was initially confirmed in these cells by Western blot analysis (**Figure 4.12A & B**). Time-lapse microscopy revealed that both nesprin-1 (0.075 ± 0.005 μm/min) and nesprin-2 (0.086 ± 0.006 μm/min) depleted fibroblasts migrated faster, but only nesprin-2 to a significant extent, compared with control cells (0.065 ± 0.004 μm/min (**Figure 4.12C**). No change to migrational persistence was detected (**Figure 4.12D**). Therefore, nesprins differentially regulate the migratory capacity of VSMCs and MRC-5 fibroblasts.

4.3.5 Nesprin-2 dynamics at the NE following LINC complex disruption

Based on our findings, we speculate that NE changes influence cell motility via nesprin-tethered F-actin. To better understand the importance of nesprin as a LINC complex component, we next studied nesprin-2 dynamics at the NE. Initially, GFP-fused nespin-2 was expressed in U2OS cells. As the nesprin-2 giant is so large (6874 amino acids), we used a shorter artificial construct, GFP-mini-nesprin-2 giant (GFP-mini-N2G) containing an N-terminal actin-binding CH region, 2 adjacent spectrin repeats and C-terminal KASH domain (**Figure 4.13A**). Despite lacking all of the spectrin repeats known to exist within the nesprin-2 giant, this construct specifically localises to the ONM where it retains interactions with F-actin and SUN proteins.[163] GFP-mini-N2G was transfected into U2OS cells where it localised to the NE in low expressing cells and both the NE and cytoplasm when highly expressed (**Figure 4.13 B & C**). FRAP revealed that nesprin-2 was relatively immobile at the NE and was extremely mobile in cytoplasm (**Figure 4.14A & B**). Only low expressing cells with NE staining alone were used to analyse nesprin-2 mobility throughout FRAP experiments and high expressers were used to standardise recovery curves.

To determine the impact of LINC complex disruption upon nesprin-2 mobility, siRNA was used to knock down FACE-1, lamin A, SUN1 and SUN2 in U2OS cells co-transfected with GFP-mini-N2G. This construct localised primarily to the NE of lamin A

and FACE-1 depleted U2OS cells (**Figure 4.15A**). However, GFP-mini-N2G localised to the NE and cytoplasm of SUN1 and SUN2 depleted U2OS cells (**Figure 4.15B**). Therefore, these cells could not be used in FRAP experiments as diffusion from the cytoplasm would provide an inaccurate account of nesprin-2 mobility at the NE.

FRAP studies revealed that control (27.27 ± 2.75%), FACE-1 (28.87 ± 2.01%) and lamin A (26.89 ± 3.23%) siRNA-treated U2OS cells had similar nesprin-2 recovery rates after photobleaching the NE (**Figure 4.16A & B**). These data demonstrate that nuclear lamina disruption did not impact on the diffusional mobility of nesprin-2 at the NE, which was relatively low. FRAP data was further analysed to determine the binding rate kinetics of GFP-mini-N2G following nuclear lamina disruption. Interestingly, the association (K_{on}) and dissociation (K_{off}) of nesprin-2 was significantly higher (1.6 and 1.7-fold increase, respectively) in lamin A depleted U2OS cells. This suggests that lamin A knockdown can potentially reduce the binding affinity of nesprin-2 to the ONM. Although there seemed to be an upwards trend, FACE-1 knockdown did not significantly affect nesprin-2 dynamics at the ONM (**Figure 4.17A & B**).

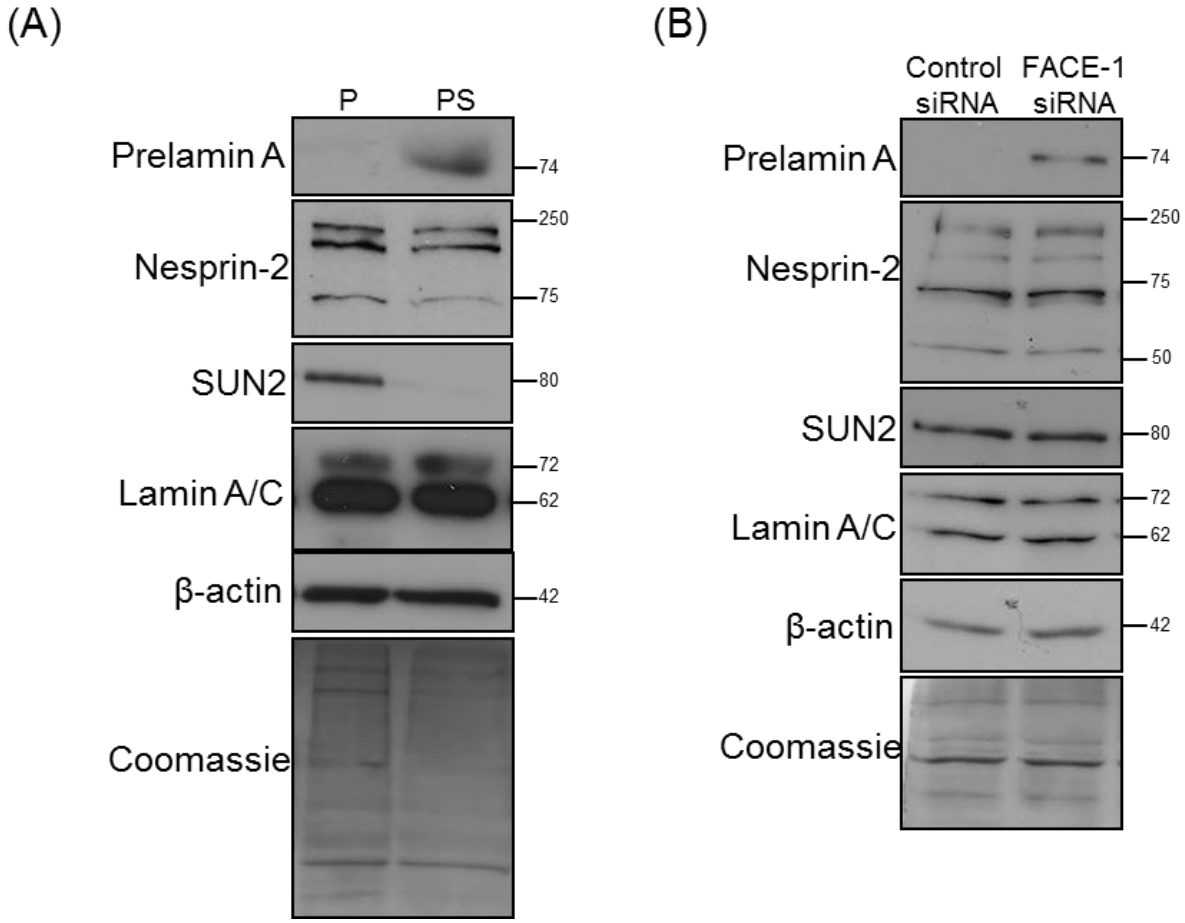

Figure 4.1: The impact of *in-vitro* ageing and prelamin A accumulation upon the LINC complex. (A) Proliferative (P) and presenescent (PS) and **(B)** control and FACE-1 treated 35F VSMC lysates were subjected to Western blot analysis to compare prelamin A, nesprin-2, SUN2 and lamin A/C protein levels. Western blots are representative of 3 independent experiments. β-actin and coomassie stain indicated equal sample loading (20 µg of each protein lysate was loaded).

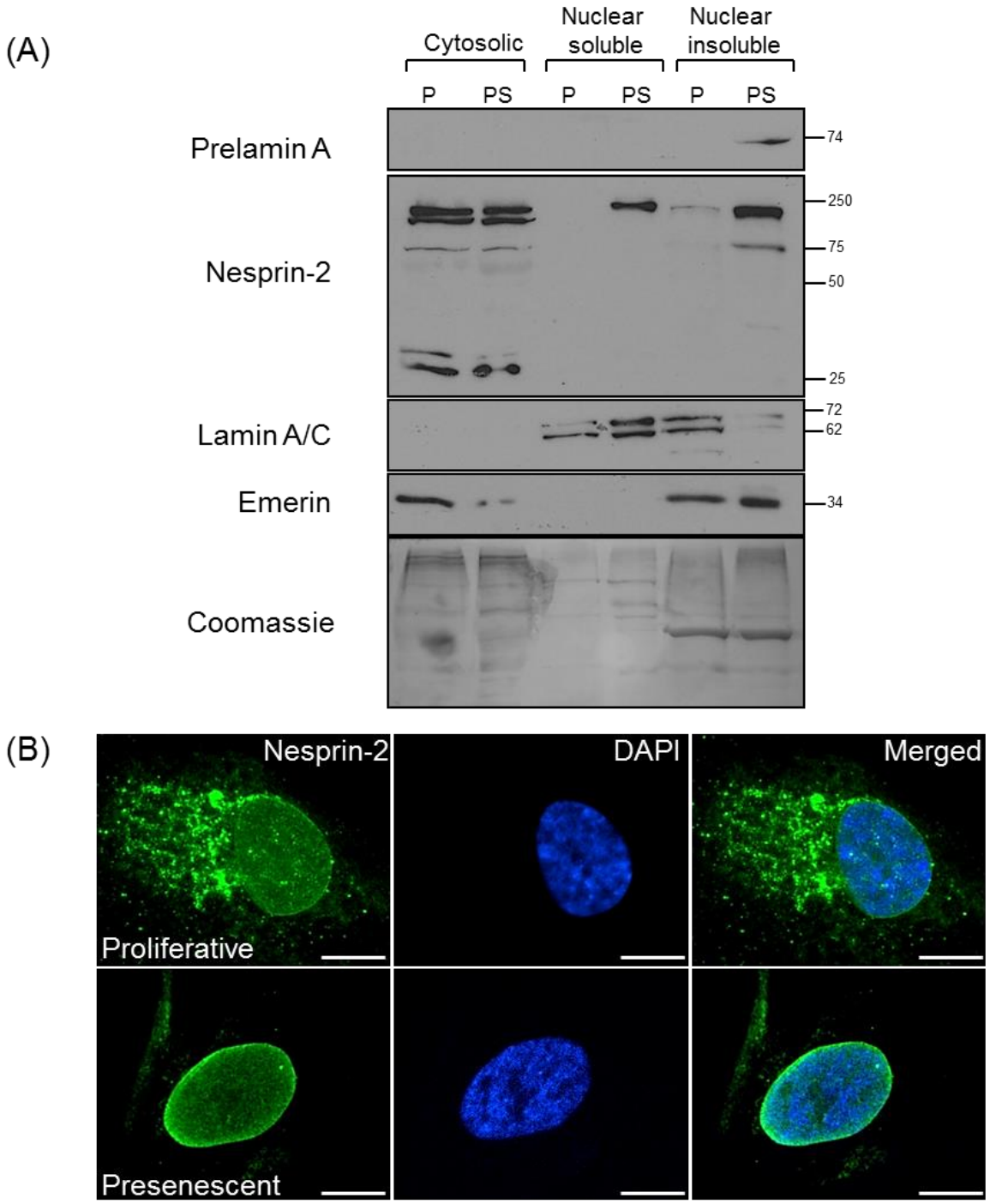

Figure 4.2: Nesprin-2 localises to the NE of aged VSMCs. (A) Subcellular fractionation was performed on presenescent (PS) and proliferative (P) 35F VSMCs. Western blotting determined levels of prelamin A, nesprin-2 and lamin A/C. Emerin and coomassie stain indicated equal loading (20 µg of each protein lysate was loaded).. **(B)** Immunofluorescence images showing nesprin-2 (*green*) localisation in early-passage and presenescent 35F VSMCs. DAPI (*blue*) stained VSMC nuclei. Scale bar represents 10 µm. All images are representative of 3 independent experiments.

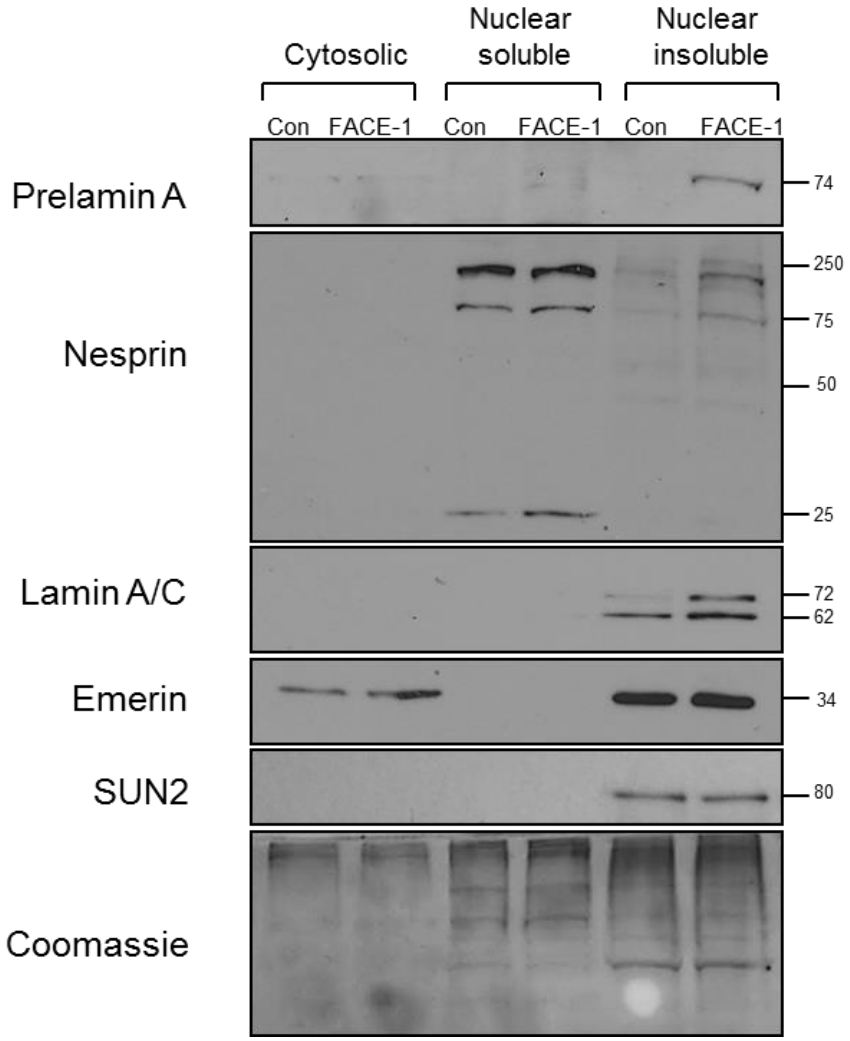

Figure 4.3: FACE-1 knockdown affects nesprin-2 solubility at the NE. Subcellular fractionation was performed on control and FACE-1 siRNA treated 35F VSMCs.. Western blotting determined levels of prelamin A, nesprin-2 and lamin A/C.. . Emerin and coomassie stain indicated equal loading (20 µg of each protein lysate was loaded)..Blots are representative of 3 independent experiments.

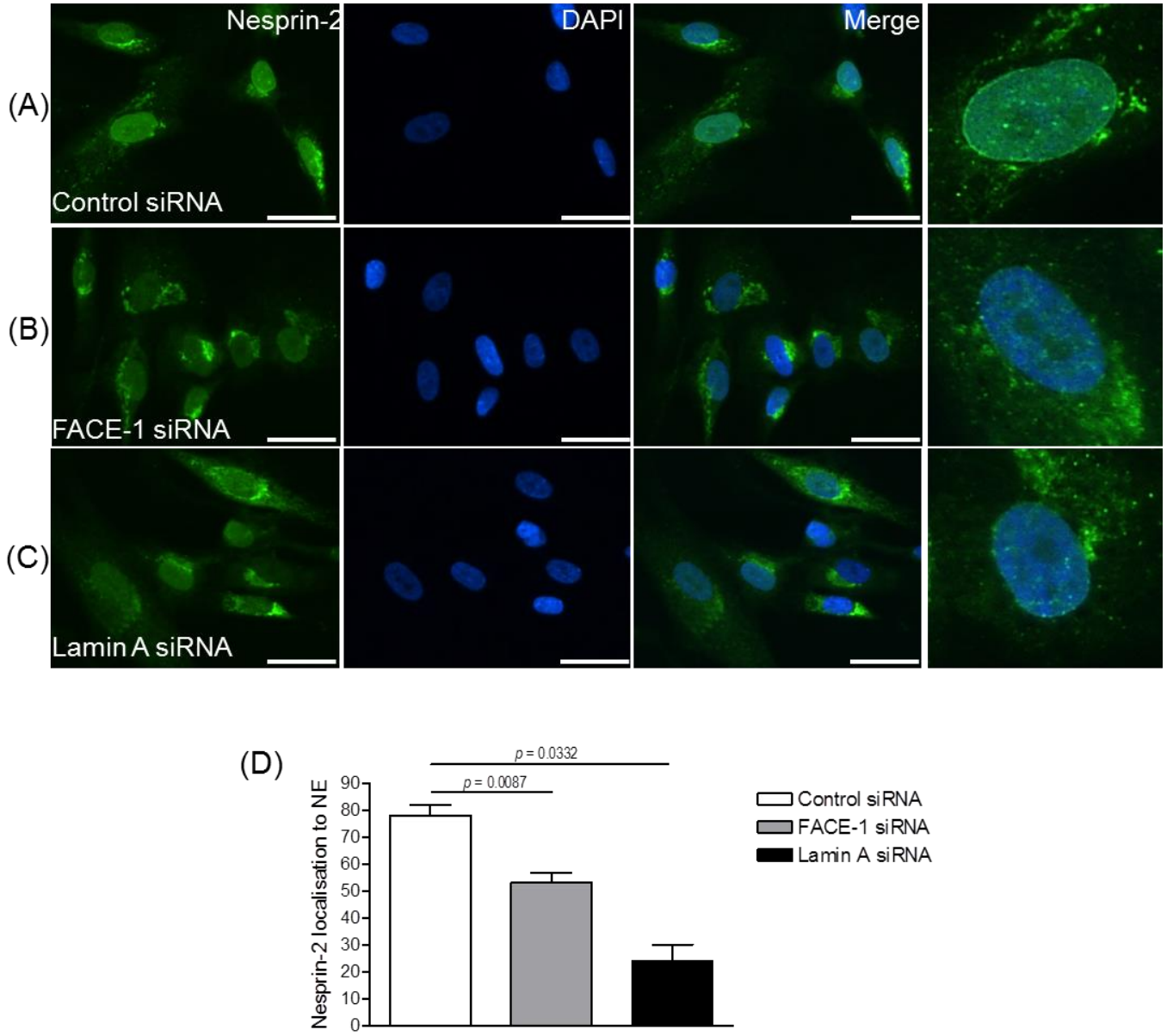

Figure 4.4: Prelamin A accumulation mislocalises nesprin-2 from the NE. Representative immunofluorescence images showing nesprin-2 (*green*) localisation in **(A)** control **(B)** FACE-1 and **(C)** lamin A siRNA treated 35F VSMCs. DAPI (*blue*) stains VSMC nuclei. Scale bar represents 35 µm. Far right panel displays higher magnification images of individual VSMC nuclei. **(D)** The number of cells containing nesprin-2 primarily at the NE were counted. Data are based on >300 cells counted across 3 independent experiments. Statistical significance was calculated using a paired Student's *t* test (control vs treatment).

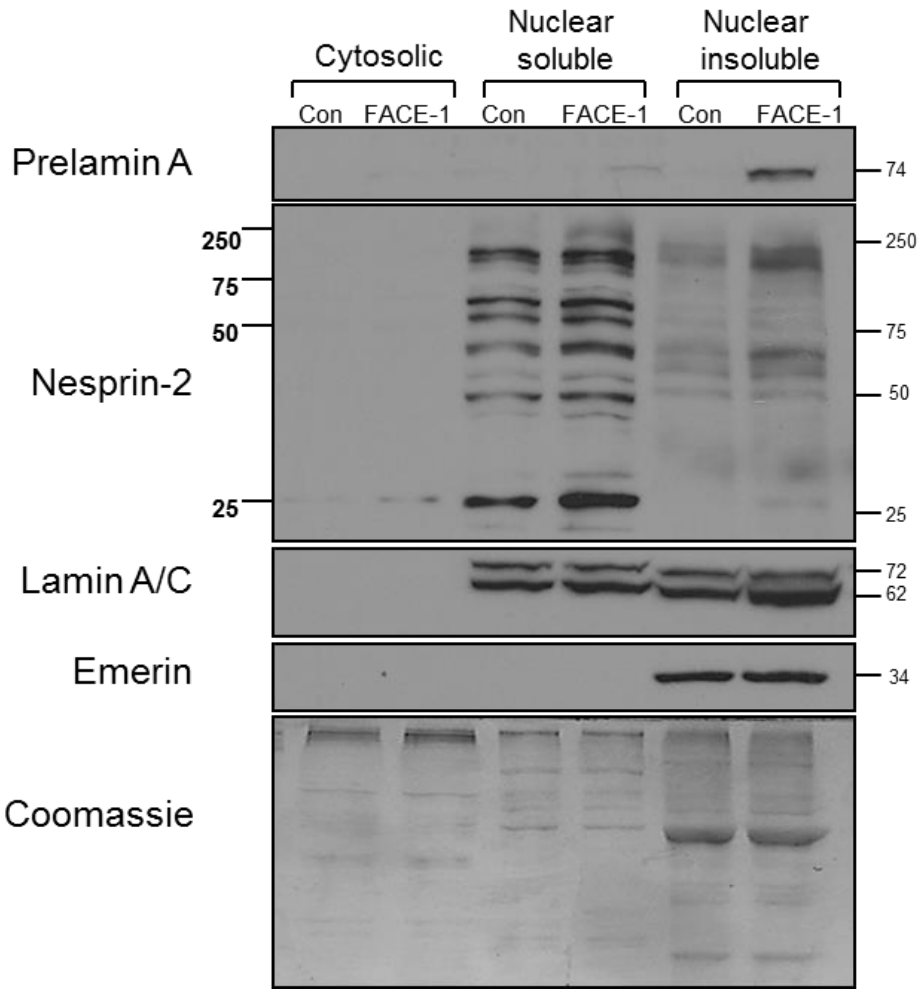

Figure 4.5: FACE-1 knockdown and prelamin A accumulation at the nuclear envelope is associated with LINC complex stabilisation. MRC-5 fibroblasts were treated with control and FACE-1 siRNA for 72 h. Subcellular fractionation was performed on control and FACE-1 siRNA treated fibroblasts. Western blotting determined levels of prelamin A, nesprin-2 and lamin A/C. Emerin and coomassie stain indicated equal loading (20 µg of each protein lysate was loaded). Blots are representative of 3 independent experiments.

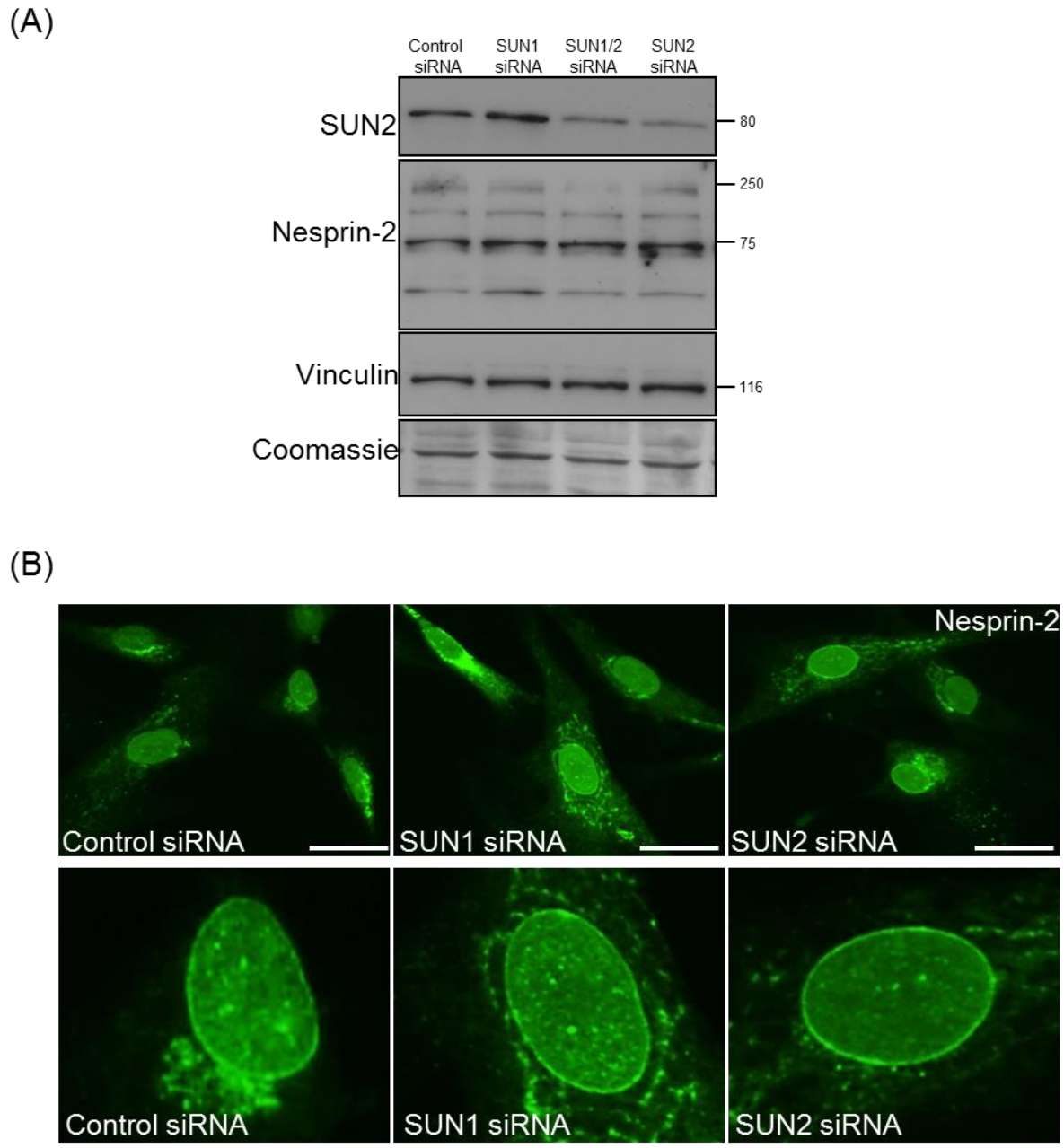

Figure 4.6: The impact ofSUN1/2 knockdown on nesprin-2 localisation in VSMCs. (A) Western blot analysis of SUN2 and nesprin-2 levels following the treatment of 35F VSMCs with control, SUN1, SUN1/2 and SUN2 siRNA. Vinculin and coomassie stain indicate equal protein loading (20 µg of each protein lysate was loaded). **(B)** Representative immunofluorescence images illustrating nesprin-2 (*green*) localisation in SUN1 and SUN2 depleted VSMCs. Scale bars represent 34 µm. Lower panel displays these images at a higher magnification (x5 magnification). Images are representative of 3 independent experiments.

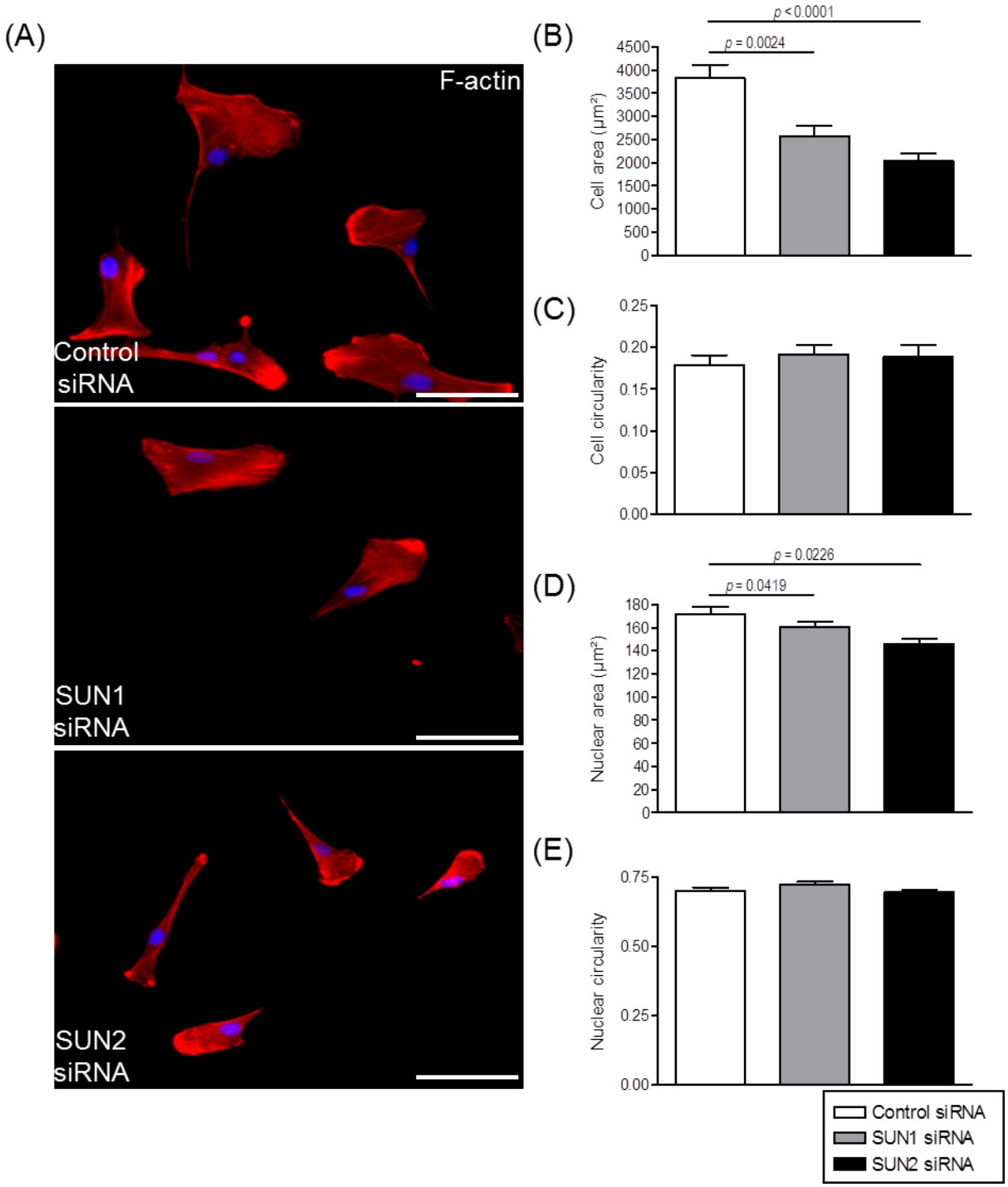

Figure 4.7: SUN1/2 knockdown drives VSMC morphological changes. Representative immunofluorescence images showing 35F VSMCs treated with control, SUN1 and SUN2 siRNA. **(A)** Actin filaments (F-actin) were stained using rhodamine phalloidin (*red*) and DAPI (*blue*) stained VSMC nuclei. Scale bar represents 60 µm. Volocity software was used to measure **(B)** cell area, **(C)** cell circularity, **(D)** nuclear area and **(E)** nuclear circularity in all 3 treatment groups. Data are based on the measurement of 50-100 VSMCs pooled from 3 independent experiments. Statistical significance was calculated using a paired Student's *t* test (control vs treatment).

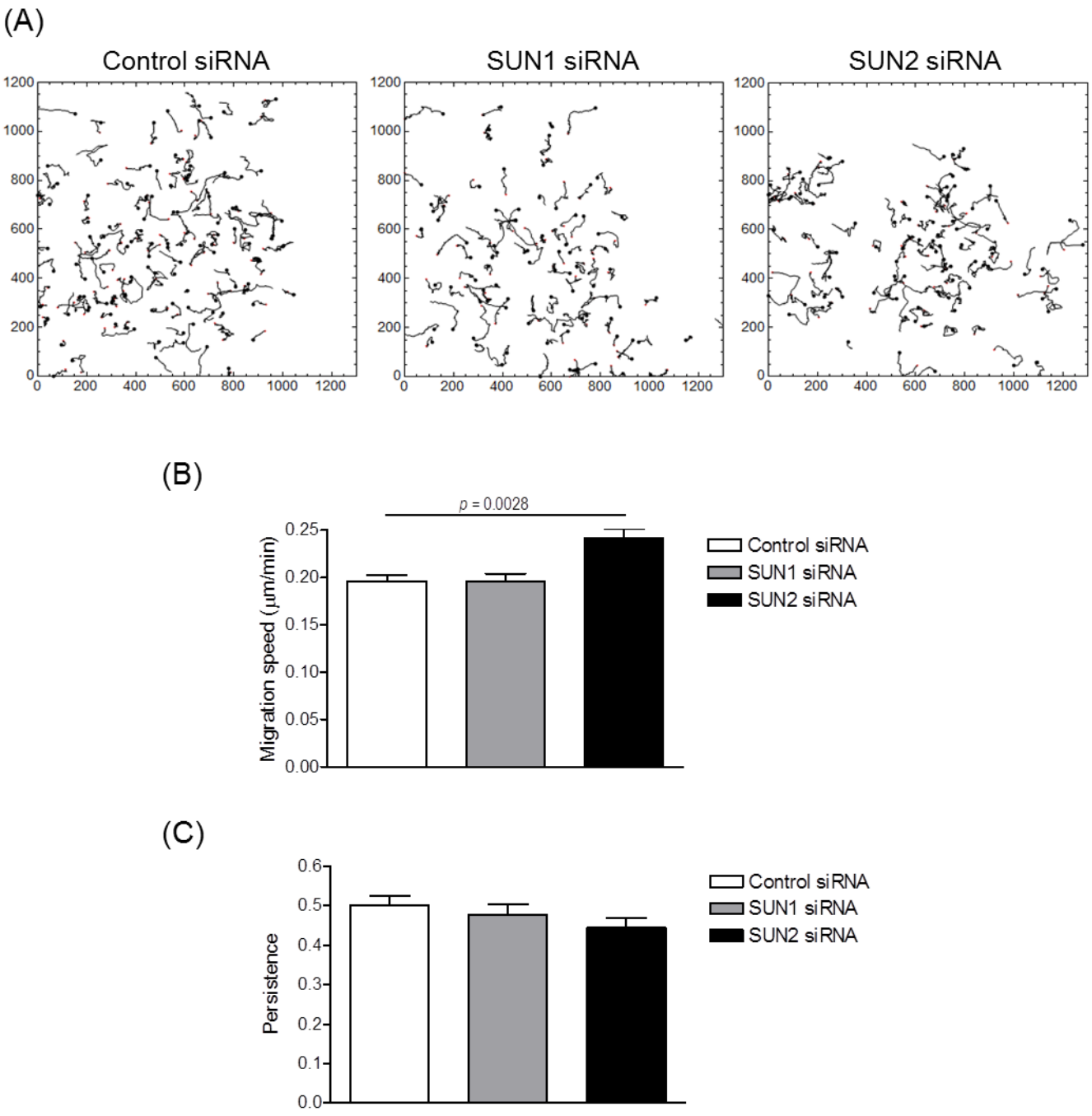

Figure 4.8: SUN2 depletion increases VSMC migration speed. Time-lapse microscopy was used to capture random single cell migration of control, SUN1 and SUN2 siRNA treated VSMCs. Images were captured every 5 min for 16 h and Mathematica software plotted x-y coordinates to provide **(A)** an overlay of individual cell tracks and analysed **(B)** migratory velocity and **(C)** persistence. Data are based on the analysis of 121 (control), 84 (SUN1 siRNA) and 87 (SUN2 siRNA) individually tracked cells pooled from 3 independent experiments. Statistical significance was calculated using a paired Student's *t* test (control vs treatment).

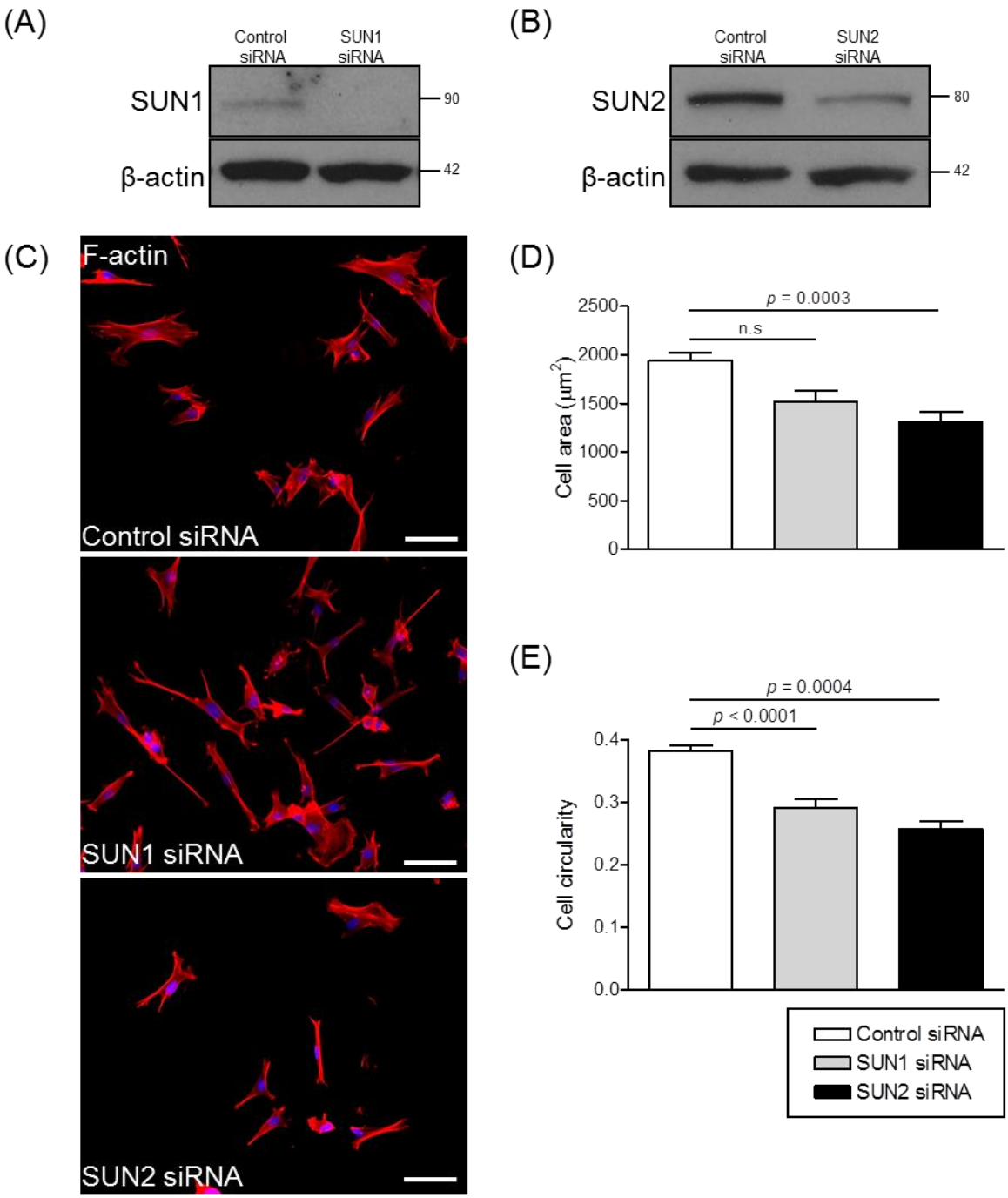

Figure 4.9: SUN knockdown drives actin morphology changes. MRC-5 fibroblasts were treated with control, SUN1 and SUN2 siRNA for 72 h prior to experimentation. Western blot analysis indicated successful **(A)** SUN1 and **(B)** SUN2 knockdown. β-actin indicates equal protein loading (20 µg of each protein lysate was loaded). **(C)** Representative immunofluorescence images of F-actin stained fibroblasts with rhodamine phalloidin (*red*). DAPI (*blue*) stained nuclei. Scale bar represents 30 µm. Volocity software was used to measure **(D)** cell area and **(E)** cell circularity in both SUN1 and SUN2 depleted fibroblasts compared with control cells. Data are based on the measurement of >100 MRC-5 fibroblasts pooled from 3 independent experiments. Statistical significance was calculated using a paired Student's *t* test (control vs treatment).

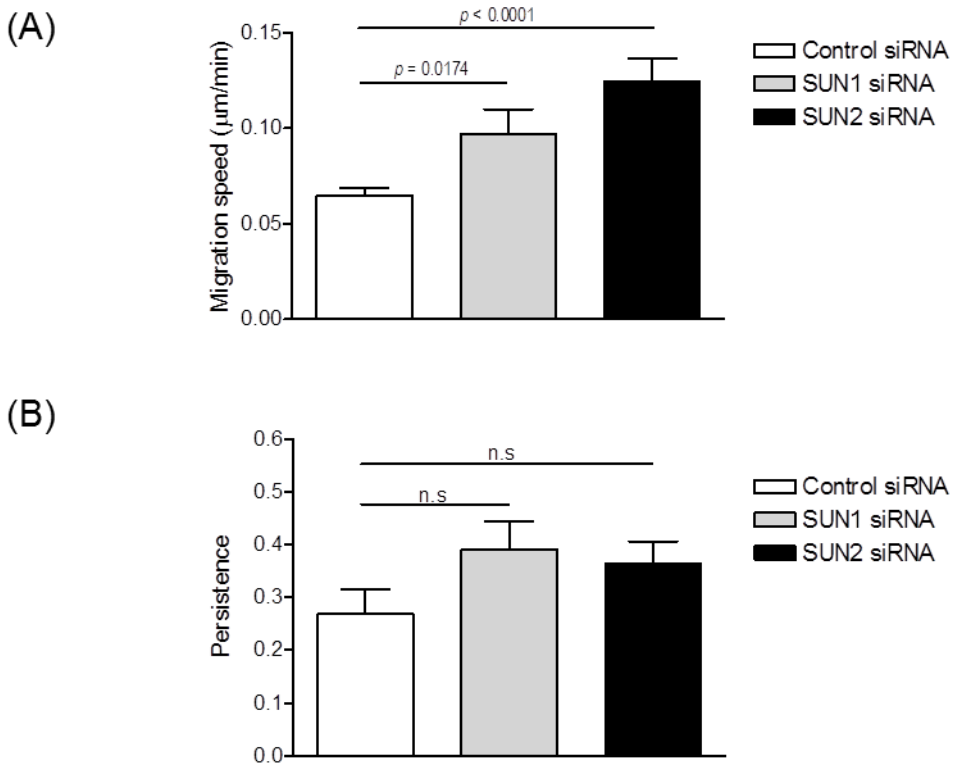

Figure 4.10: SUN knockdown increases fibroblast migration speed. MRC-5 fibroblasts were treated with control, SUN1 and SUN2 siRNA for 72 h prior to experimentation. Images were captured every 5 min for 16 h and Mathematica software plotted x-y coordinates to provide **(A)** an overlay of individual cell tracks and analysed **(B)** migratory velocity and **(C)** persistence.. Data are based on the analysis of 72 (control siRNA) and 47 (SUN1 siRNA) and 67 (SUN2 siRNA) cells pooled from 3 independent experiments. Statistical significance was calculated using a paired Student's *t* test (control vs treatment).

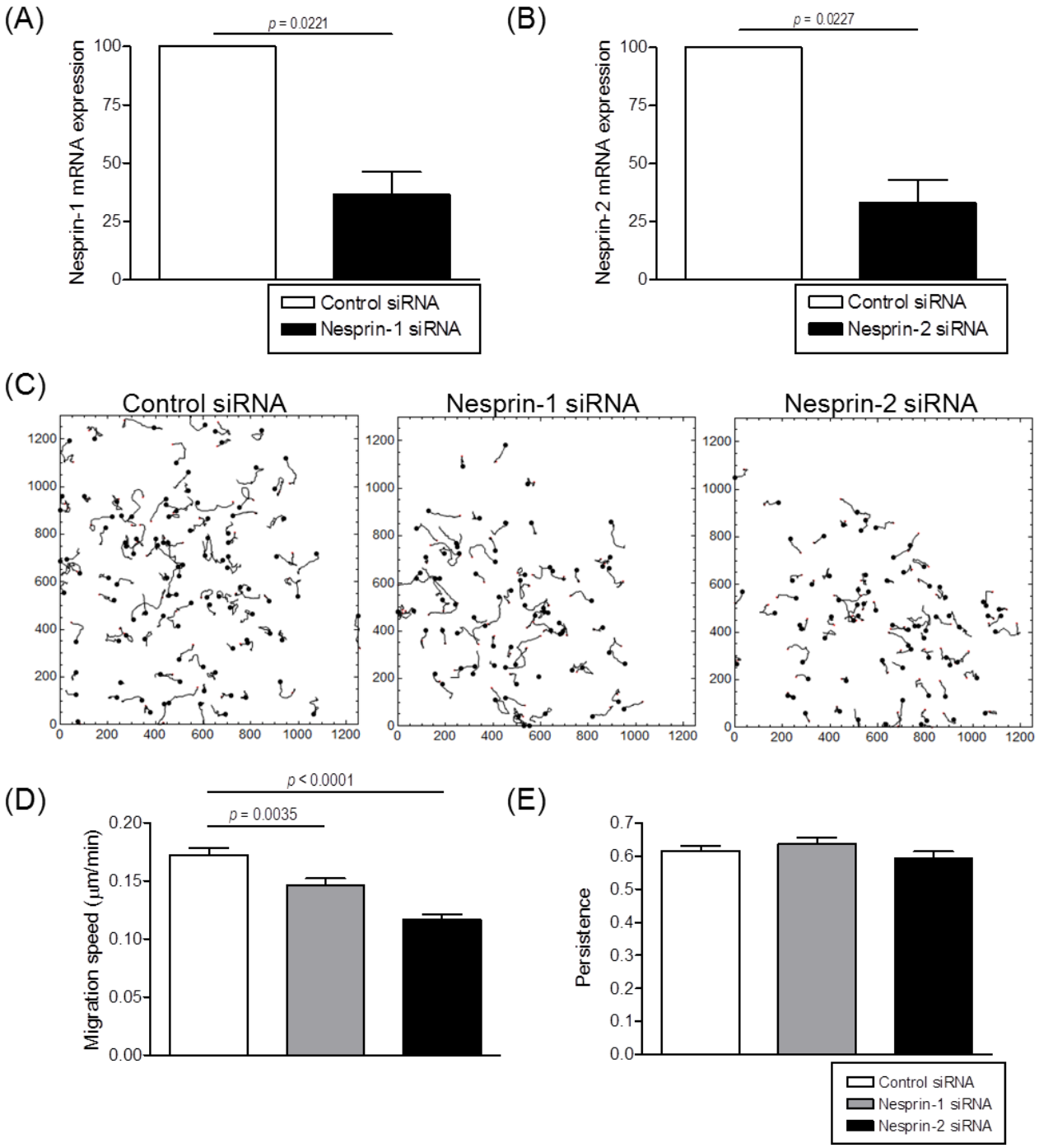

Figure 4.11: Nesprin depletion hinders VSMC migration. VSMCs (35F) were treated with control, nesprin-1 and nesprin-2 siRNA for 72 h prior to experimentation. qPCR analysis indicated successful **(A)** nesprin-1 and **(B)** nesprin-2 knockdown. Time-lapse microscopy captured images of random cell every 5 min for 16 h and Mathematica software plotted x-y coordinates to provide **(C)** an overlay of individual cell tracks and analysed **(D)** migratory velocity and **(E)** persistence. Data are based on the analysis of 106 (control) and 77 (nesprin-1 & 2 siRNA) individually tracked cells pooled from 3 independent experiments. Statistical significance was calculated using a paired Student's *t* test (control vs treatment).

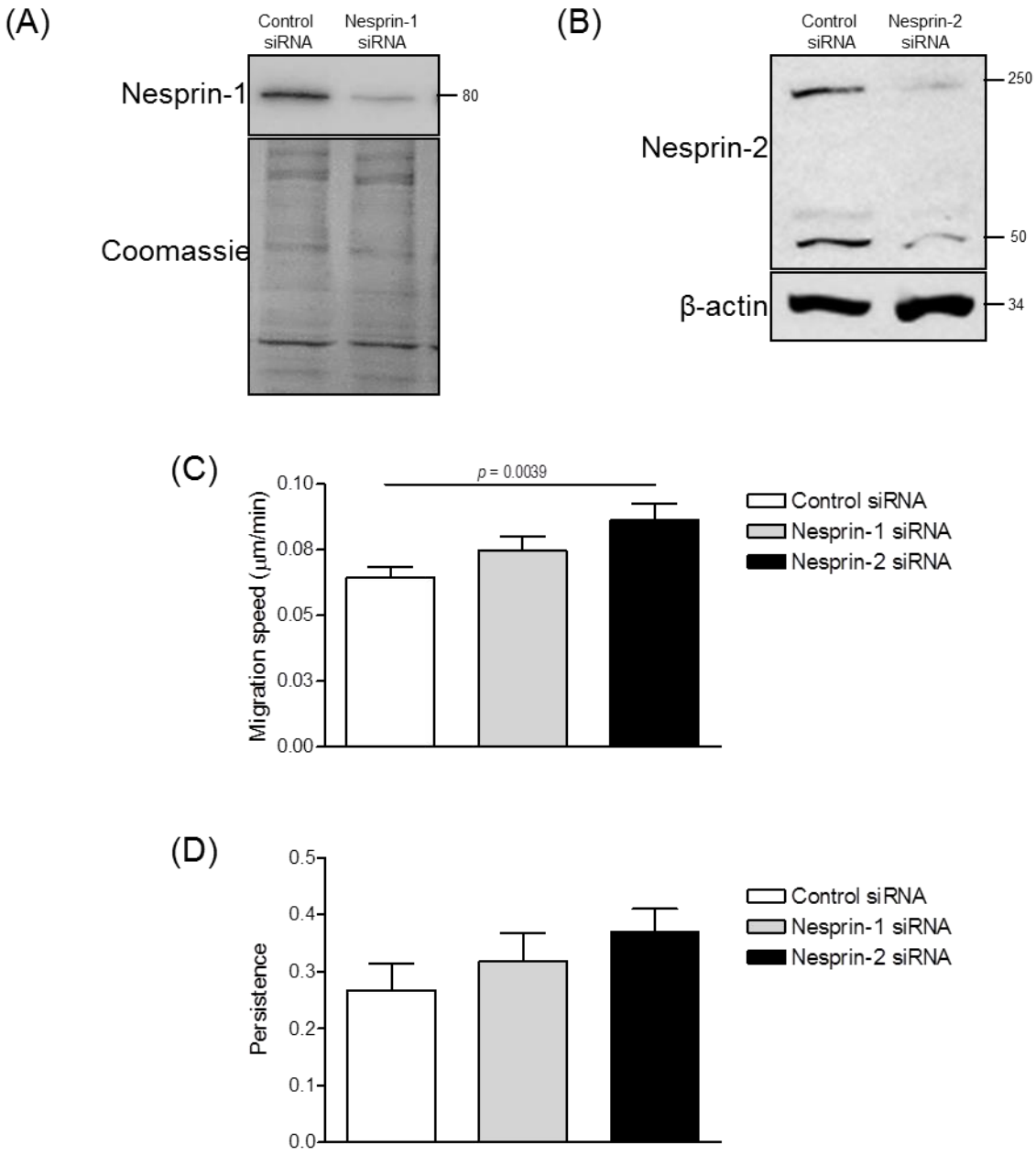

Figure 4.12: Nesprin-2 knockdown increases fibroblast migration speed. MRC-5 fibroblasts were treated with control, nesprin-1 and nesprin-2 siRNA for 72 h prior to experimentation. **(A & B)** Western blot analysis shows nesprin-1 and nesprin-2 levels. Coomassie and β-actin indicate equal protein loading, respectively (20 µg of each protein lysate was loaded). **(C)** Time-lapse microscopy captured images of random cell every 5 min for 16 h and Mathematica software plotted x-y coordinates to provide **(C)** an overlay of individual cell tracks and analysed **(D)** migratory velocity and **(E)** persistence. Data are based on the analysis of 72 (control siRNA), 54 (nesprin-1 siRNA) and 71 (nesprin-2 siRNA) cells pooled from 3 independent experiments. Statistical significance was calculated using a paired Student's *t* test (control vs treatment).

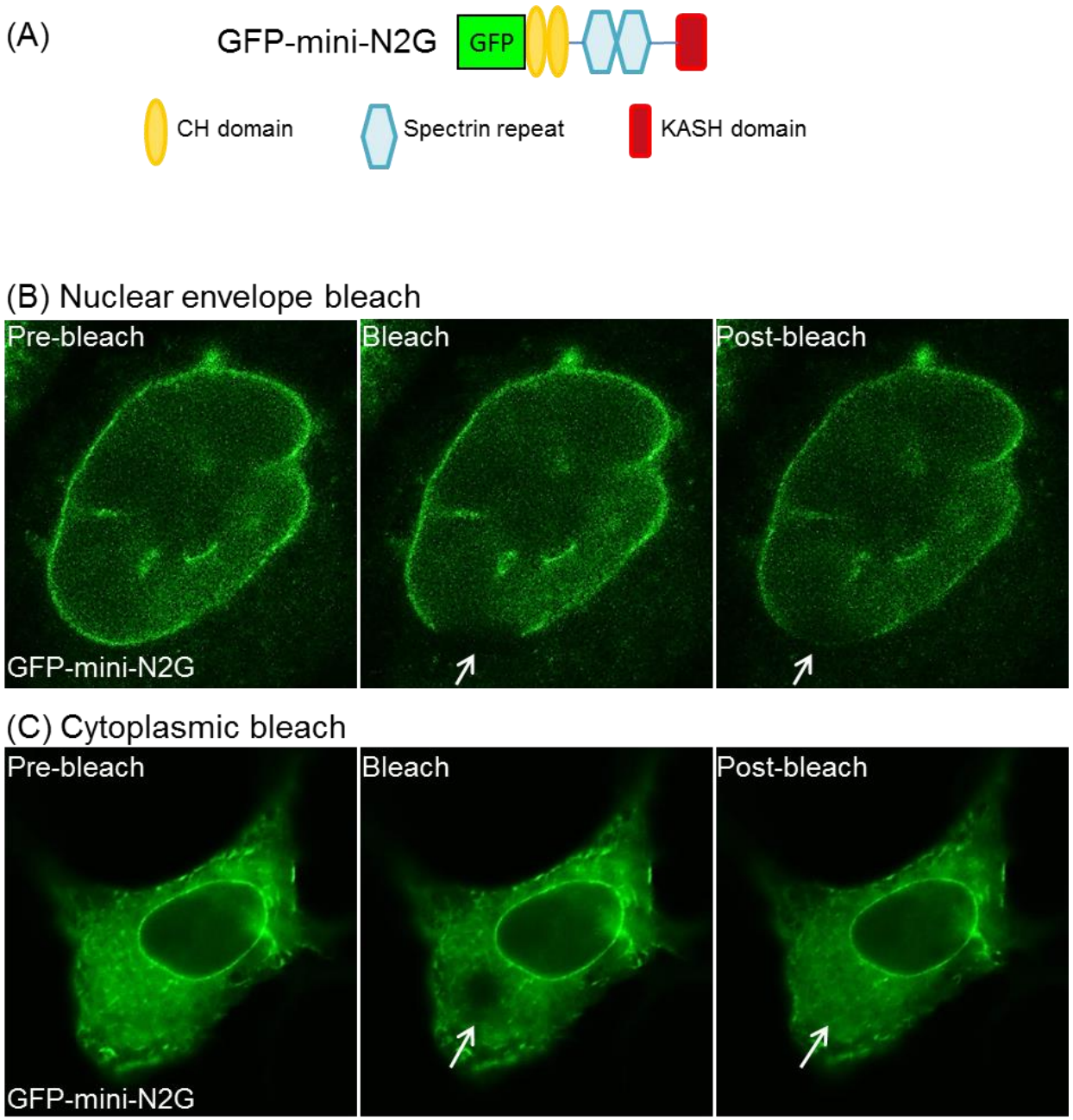

Figure 4.13: GFP-nesprin-2 expression in U2OS cells. (A) A schematic representation of GFP-mini-nesprin-2 giant (GFP-mini-N2G). GFP fuses the N-terminal actin-binding calponin homology (CH) which binds 2 spectrin repeats and a C-terminal NE-targeting KASH domain. U2OS cells were transfected with GFP-mini-N2G and FRAP was performed to determine the recovery of nesprin-2 following photobleaching at **(B)** the NE of low expressing cells and **(C)** the cytoplasm of high expressing U2OS cells. Arrows indicate the bleached ROI. FRAP experiments were performed with the assistance of Daniel Soong, King's College London.

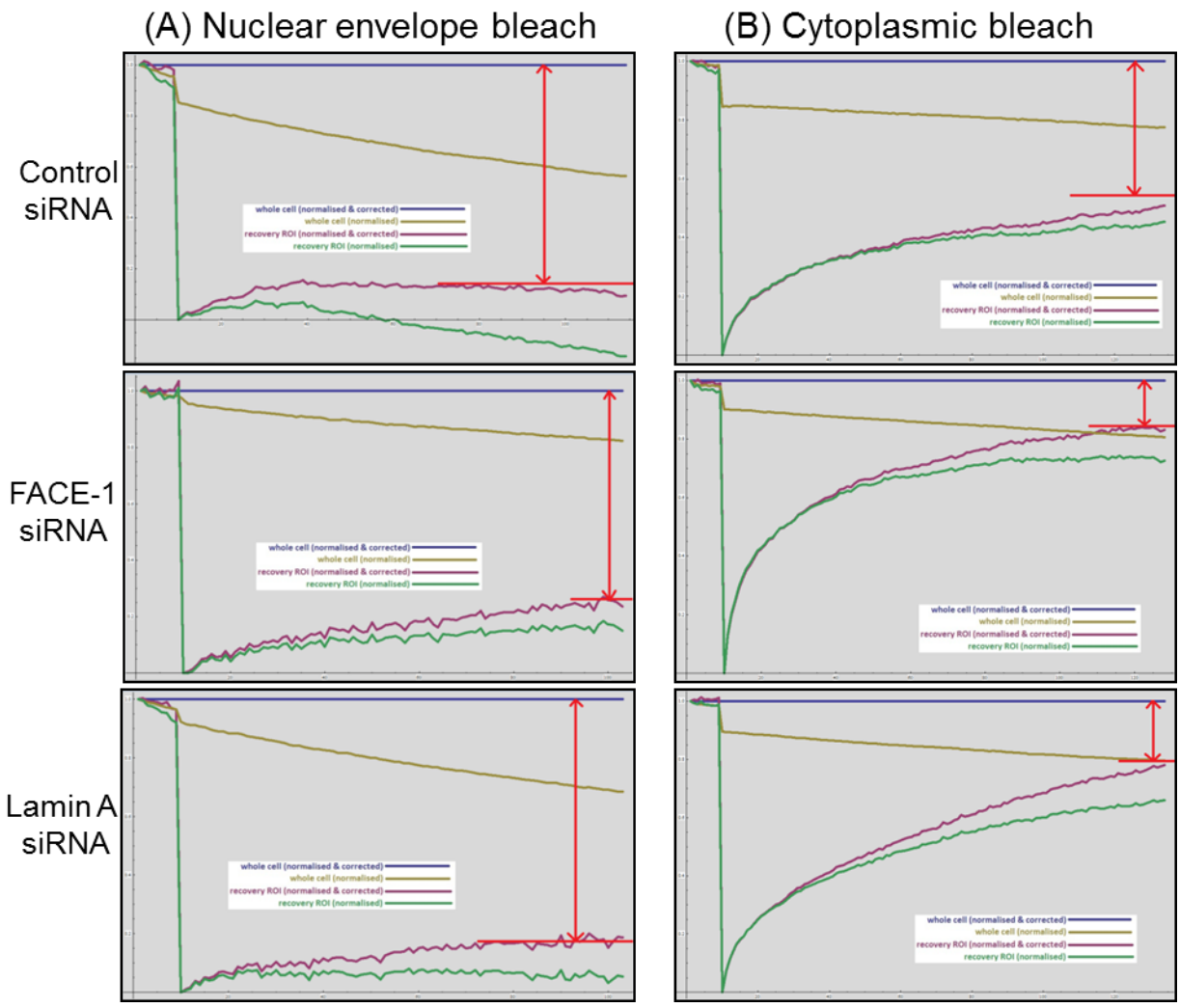

Figure 4.14: GFP-nesprin-2 mobility is low at the NE of U2OS cells. U2OS cells were treated with control, FACE-1 or lamin A siRNA and co-transfected with GFP-mini-nesprin-2 giant (GFP-mini-N2G) before FRAP experiments were performed. Typical profiles of GFP-mini-N2G recovery after photobleaching **(A)** the NE and **(B)** the cytoplasm of control, FACE-1 and lamin A siRNA treated U2OS cells. The x-axis represents the time scale (sec) and the y-axis is mobile fraction. The immobile fraction is highlighted by red arrows. Normalised fluorescence of 1 is the level before bleaching and bleaching occurred at 20 sec. FRAP experiments were performed with the assistance of Daniel Soong, King's College London.

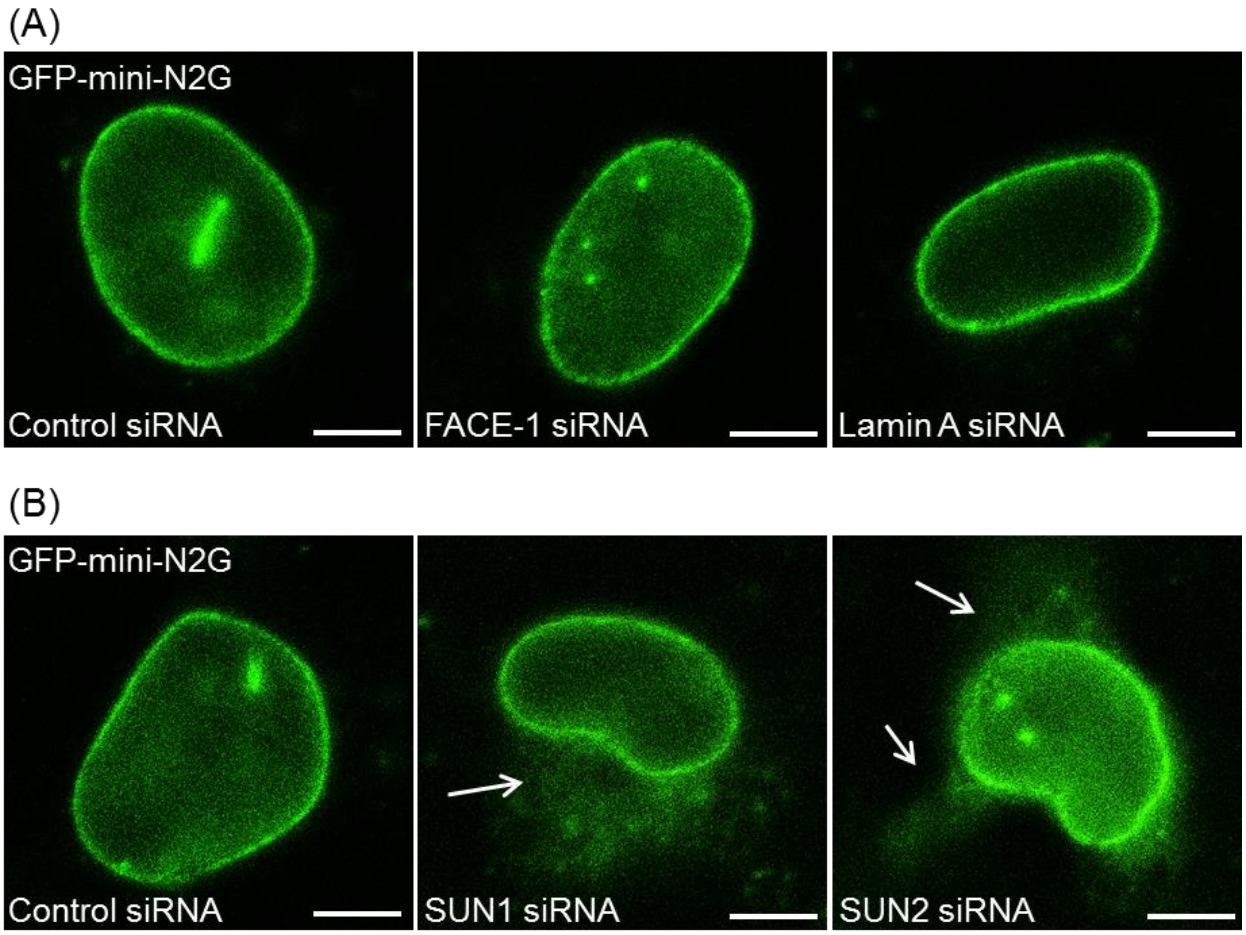

Figure 4.15: GFP-nesprin-2 expression in U2OS cells following LINC complex disruption. U2OS cells were treated with **(A)** control, FACE, lamin A siRNA and **(B)** control, SUN1, SUN2 siRNA before being co-transfected with GFP-mini-nesprin-2 giant (GFP-mini-N2G). Representative immunofluorescent images demonstrate nesprin-2 localisation to the NE in these cells. Arrows indicate nesprin-2 mislocalisation to the ER in SUN1 and 2 depleted U2OS cells. Scale bars represent 10 µm. Intranuclear staining represents invagination of the NE in different focal planes. FRAP experiments were performed with the assistance of Daniel Soong, King's College London.

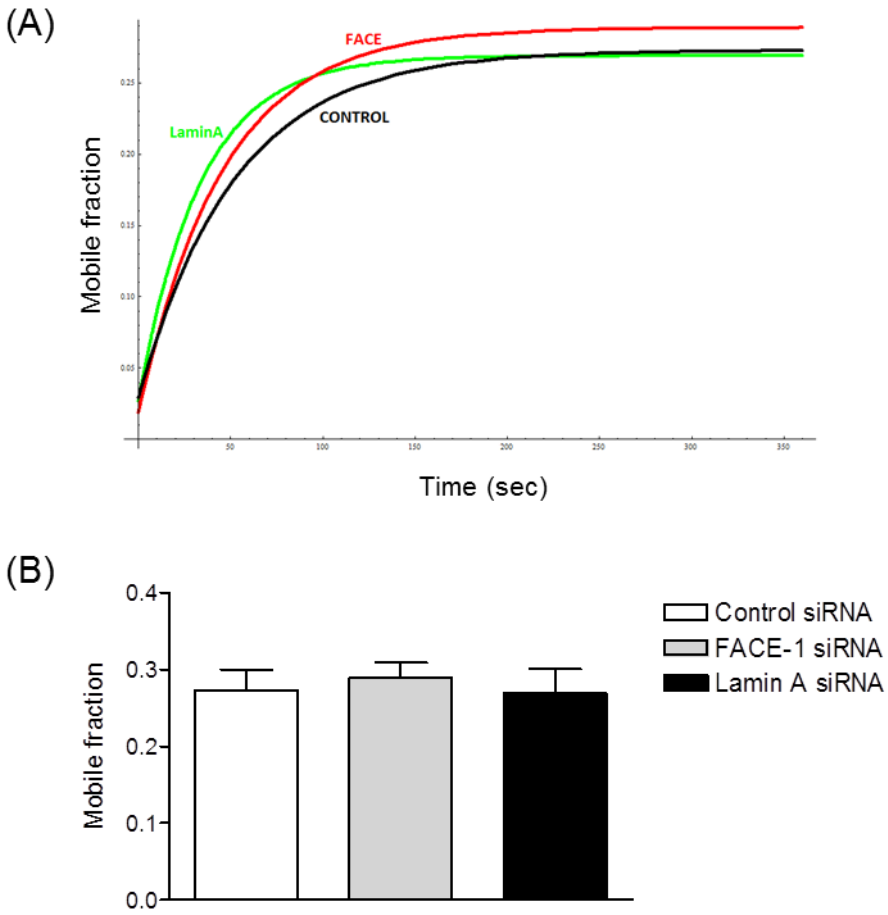

Figure 4.16: GFP-nesprin-2 mobility at the NE is not affected by nuclear lamina disruption. U2OS cells were treated with control, FACE-1 or lamin A siRNA and co-transfected with GFP-mini-nesprin-2 giant (GFP-mini-N2G) before FRAP experiments were performed. **(A)** Normalised average rate plot. **(B)** Mobile fraction of GFP-mini-N2G following photobleaching at the NE of siRNA-treated U2OS cells. Data represent the analysis of 17-20 cells pooled from 4-5 independent experiments. FRAP experiments were performed with the assistance of Daniel Soong, King's College London.

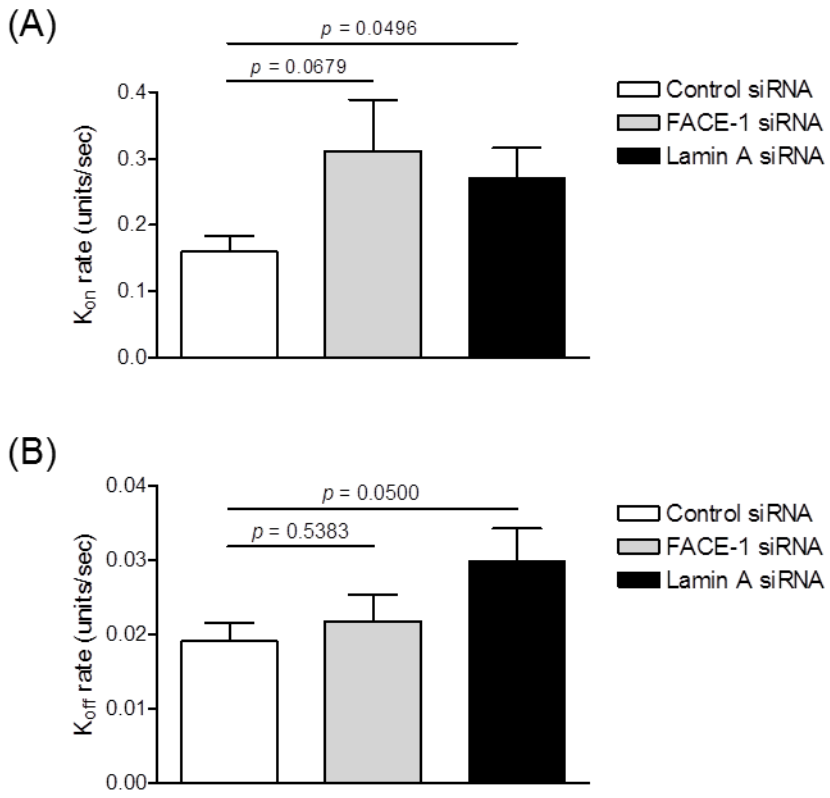

Figure 4.17: GFP-nesprin-2G is more dynamic following lamin A knockdown. U2OS cells were treated with control, FACE-1, lamin A siRNA and co-transfected with GFP-mini-nesprin-2 giant (GFP-mini-N2G) prior to FRAP experiments. **(A)** Association (K_{on}) and **(B)** dissociation (K_{off}) rates of GFP-mini-N2G at the NE. Data represent the analysis of 17-20 cells pooled from 4-5 independent experiments. An unpaired Student's *t* test was used for statistical analysis. FRAP experiments were performed with the assistance of Daniel Soong, King's College London.

4.4 Discussion

This chapter further explored the relationship between LINC complex composition, cellular morphology and migratory behaviour. We also determined whether the role of individual LINC complex components was conserved across different cell types. To achieve this, we investigated the outcome of LINC complex disruption in VSMCs, MRC-5 fibroblasts and U2OS cells. This work provides strength to earlier findings described in chapter 3 to reveal that the LINC complex is an important regulator of cell morphology, focal adhesion organisation and cell migration which undergoes reorganisation at the NE during VSMC ageing.

4.4.1 SUN proteins regulate cellular morphology and migratory behaviour

SUN1/2 proteins are crucial LINC complex constituents as clearly indicated by the dramatic lethality of double knockout SUN1 & 2 mice.[287] SUN1/2 located within the PNS form an integral nuclear-cytoplasmic connection between nesprins located at the ONM and the nuclear lamina.[165] In this chapter, we uncover a striking age-related reduction in VSMC SUN2 expression. This reinforces previous work demonstrating that SUN2 is downregulated in fibroblasts during *in-vitro* passaging and both SUN1/2 are diminished in HGPS fibroblasts.[157, 162] Furthermore, EDMD patients harbour mutations in the SUN1/2 gene and mutant SUN1/2 expression in a human keratinocyte cell line disrupts cell adhesion, migration and nuclear shape.[162] This encouraged us to further study the LINC complex and the importance of SUN proteins in regulating migratory behaviour. We illustrate that silencing SUN1 and SUN2 significantly reduces VSMC size. However, we predict that VSMCs possess little SUN1 as antibodies failed to detect SUN1 in these cells. In addition, SUN2, but not SUN1, depletion significantly enhances VSMC migration speed to reflect that of *in-vitro* aged VSMCs.

Both SUN1 and SUN2 depleted fibroblasts are smaller, more elongated and migrate faster than control cells. Although SUN1 and SUN2 are detectable in MRC-5 fibroblasts, SUN2 is more abundant. Overall, SUN2 depletion has the most dramatic impact on fibroblast and VSMC phenotype, implicating SUN2 as the more important LINC complex component and regulator of cell migration. In support of this theory, studies show that SUN2 depletion increases nesprin-2 mobility at the NE, whereas SUN1 knockdown has no impact.[163] This study speculates that SUN2, but not SUN1, is involved in anchoring nesprin-2 to the ONM and bridging the nuclear exterior and interior.

4.4.2 Nesprins regulate cell migratory speed

After observing the cellular changes associated with nuclear lamina and SUN protein disruption, we finally progressed to the ONM and targeted nesprins-1/2 using siRNA. It is well-established that nesprin-1/2 CH domains at the ONM tether F-actin to the cytoplasmic face of the nucleus and play an important role in regulating actin cytoskeleton organisation.[147, 151] Previous studies demonstrate that a nesprin-2 construct lacking CH is unable to rescue nuclear movement in nesprin-2 depleted cells, highlighting that nesprin-actin interactions are critical for nuclear orientation, cell polarity and cell migration.[288] Our results reinforce this, as we also found VSMC migration to be hindered following nesprin-1/2 depletion. We predict that F-actin uncoupling from the nucleus in these cells prevents the actin reorganisation necessary to drive forwards cell movement. This supports previous data demonstrating that fibroblasts lacking nesprin-2 have impaired cell polarity and migration into a wound.[289]

In contrast, we show that nesprin-2 knockdown significantly enhances MRC-5 fibroblast speed, whereas nesprin-1 has no impact, suggesting that differences lie in LINC complex organisation between these cell types. Furthermore, the diversity of nesprin splice variants could also be producing very different outcomes on cell motility between different cell types. In support of this theory, SUN trimers are able to interact with varying nesprin isoforms to create flexible KASH-SUN assemblies at the NE which could enhance LINC complex versatility across different cell types.[152, 156] Nevertheless, nesprin-2 depletion induces the most dramatic phenotypic change to fibroblasts and VSMCs compared with nesprin-1. Therefore, although the precise function of nesprins in regulating cell migration is not fully understood, nesprin-2 appears to be the most important.

4.4.3 Nuclear lamina disruption affects nesprin-2 dynamics at the ONM

FRAP studies enabled us to explore the importance of the nuclear lamina in regulating nesprin-2 mobility and dynamics at the ONM. Several studies have demonstrated A-type lamins to be essential for nesprin localisation, hence, lamin A/C alterations mislocalise nesprin from the NE to the ER.[154, 290, 291] We also show that nesprin-2 is displaced from the ONM of nuclear lamina disrupted VSMCs following FACE-1 or lamin A depletion. However, we found that nuclear lamina disrupted U2OS cells retain nesprin-2 at the ONM. In fact, we show that both SUN1 and SUN2 are required to tether nesprin-2 in U2OS cells whereas individual SUN1/2 proteins support

nesprin-2 localisation to the ONM in VSMCs. Again, this evidence reiterates that LINC complex organisation and stability varies between cell types.

Interestingly, our FRAP data illustrates that although nesprin-2 localisation and mobility at ONM was unchanged in U2OS cells, its dynamicity was enhanced following lamin A knockdown. This suggests that lamin A is responsible for indirectly maintaining nesprin-2 stability at the ONM, which is most likely mediated via SUN interactions. A more recent study supporting our data reveals that the absence of lamin A does not affect nesprin-2-SUN2 assemblies but makes the LINC complex more unstable and increases the mobile fraction of cytoplasmic actin.[292] Therefore, we predict that nuclear lamina disruptions weaken the LINC complex across the NE, consequently increasing nesprin-2 dynamics, F-actin turnover, cytoskeletal remodelling and cell motility. Conversely, similar FRAP experiments also exploring the importance of lamins in retaining nesprin localisation reveal that GFP-mini-N2G is significantly more mobile in embryonic fibroblasts lacking A-type lamins compared with cells from wild-type mice.[163] However, caution should be taken when interpreting such data as slight GFP-mini-N2G overexpression results in its cytoplasmic localisation and increases its apparent mobility and dynamicity.

4.4.4 Chapter 4 conclusions

This chapter demonstrates that nesprin-2 and SUN2 proteins are important regulators of cellular morphology and motility, however, their specific roles vary between different cell types and remain inconclusive. In particular, we highlight substantial differences in the migratory capacity of fibroblasts and VSMCs following nesprin disruption and both SUN1/2 are essential for nesprin NE localisation in U2OS cells but not VSMCs. Therefore, although the basic elements are conserved, we believe that LINC complexes are specialised within different cell types and their arrangement is specifically adaptable to cell function. We finally progressed to investigate the implications of LINC complex disruption upon nesprin-2 mobility and dynamics using FRAP. Although lamin A depletion increases nesprin-2 dynamics, clearly much more remains to be discovered with regards to the structure, dynamicity and versatility of the LINC complex.

4.4.5 Limitations and future work

4.4.5.1 A plethora of nesprin variants

Recent data indicates that nesprins-1/2 possess multiple alternative start and termination sites throughout their genes, resulting in the production of numerous small nesprin variants.[152] As nesprin-1/2 siRNA specifically targets the N-terminal actin binding region, an obvious limitation of our study is that we did not effectively deplete all nesprin-1 or nesprin-2 isoforms particularly C-terminal KASH variants that may also play a regulatory role in cell morphology and motility (**Figure 2.1**). Due to the plethora of nesprin isoforms that exist, it is also plausible that knocking down nesprin-1/2 results in the upregulation other nesprin variants at the ONM as a compensatory mechanism. Another limitation of our study was that giant nesprin isoforms were not detectable via Western blot analysis using in-house antibodies. Therefore, future studies will specifically determine which nesprins are important for regulating cell migration and isoform-specific siRNA and antibodies will be utilised.

4.4.5.2 The impact of prelamin A on nesprin mobility

Another limitation of this study is that FRAP experiments utilised a GFP-mini-N2G construct lacking spectrin repeats known to exist in the full-length nesprin-2 giant. The spectrin repeat backbone of nesprins normally mediates protein-protein interactions, therefore, the absence of spectrin repeats in GFP-mini-N2G potentially effects its localisation, mobility and dynamic ability. Future studies will use nesprin-2 constructs of differing length and spectrin repeat capacity to better interrogate the role of the LINC complex on nesprin-2 mobility and dynamics. Due to time constraints, FRAP experiments were only performed in U2OS cells. As previously described, the LINC complex appears to be utilised differently between cell types and enhanced nesprin dynamics in response to NE adaptations in U2OS cells are not necessarily reflected in other cell types. Therefore, this experiment will also be repeated in VSMCs and MRC-5 fibroblasts in the future.

Chapter 5: Characterising the role of cell traces in VSMC migration

5.1 Introduction

As cells migrate, cell membrane protrusions at the leading edge attach to the underlying ECM via focal adhesion complexes.[28] These traction sites are continuously assembled at the leading edge and dissembled at the trailing end to facilitate forward movement.[29] To date, much of the literature focusses on the leading edge processes that drive migration, with little interest on the cell rear. Although the rate of rear-end detachment is thought to determine migration speed, the mechanisms of detachment and its involvement in regulating migrational behaviour are yet to be clearly defined.[293] A combination of force driven by actin-myosin contraction and proteolytic cleavage by calpains and matrix metalloproteinases (MMPs) are required for cell detachment.[30] This was originally thought to not result in the loss of any cell material, however, more recent evidence illustrates that cell debris is released at the rear of migrating cells, forming characteristic tracks that map cell migration.[294] Although believed to be an artefact of *in-vitro* migration, studies describe the release of cellular material or 'cell traces' in numerous cell types, including fibroblasts, mammalian thymoma and sarcoma cells, cytotoxic T-lymphocytes and primary chondrocytes.[295] As cell traces can only be visualised using high magnification techniques, the physiological relevance of these structures in cell migration has yet to be fully explored

5.2 Aim of this chapter

This chapter utilised IRM and time-lapse microscopy to closely study rear-end detachment and the release of cellular material from of migrating VSMCs. We aimed to determine whether cell traces are an *in-vitro* artefact or play a physiological role in VSMC migration.

5.3 Results

5.3.1 Migrating VSMCs *in-vitro* release traces at their trailing end

A number of studies describe the phenomenon of various cell types releasing cell traces at their rear during migration *in-vitro.*[294-296] Such studies speculate a physiological role for cell traces, however, no specific function has yet been identified. We used IRM to capture high magnification images of randomly migrating VSMCs *in-vitro.* Cell traces were visible at the trailing end of VSMCs using this technique which were not detectable using phase-contrast time-lapse microscopy.

VSMC cell traces were long (often tripling the length of the host cell), branched structures that adumbrated the path of cell migration (**Figure 5.1A i & ii**). Because cell traces are thought to reflect a cells migrational capacity, IRM compared presenescent (91.9 ± 4.236%) VSMC traces with those derived from slower-moving proliferative (90.47 ± 4.767%) and senescent (82.40 ± 4.034%) VSMCs to reveal that almost every single VSMC presented similar trace formation during all 3 stages of VSMC growth (**Figure 5.1B**).[294] Control (90 ± 3.841%), FACE-1 (92 ± 3.432%) and lamin A (82 ± 2.500%) siRNA treated VSMCs also deposited traces at the rear (**Figure 5.1C**). This suggests that the release of cell material is a common occurrence during VSMC migration *in-vitro* and does not reflect migratory changes associated with ageing or nuclear lamina disruption.

After studying the captured IRM images in more detail we detected that long, branched traces often terminated in bead-like structures (**Figure 5.2A**). As IRM is an established method of observing adhesion dynamics, we predicted these punctate structures to be focal adhesions retained at the cell rear. Immunofluorescent staining of VSMCs with anti-vinculin and rhodamine phalloidin revealed that focal adhesions were present in areas where a defined actin cytoskeleton was no longer visible and only a few fine actin filaments remained (**Figure 5.2B**). This implies that adhesions were released from the cell rear and retained on the substrate whilst the donor cell continued migrating.

5.3.2 VSMCs migrate over pre-laid cell-derived traces

For the first time, we provide strong evidence that VSMCs release traces during *in-vitro* migration similarly to those previously detected in fibroblasts and other cell

types.[294] IRM and time-lapse microscopy were further utilised to determine whether cell traces exhibit a physiological role in cell migration. For example, IRM imaged a single migrating VSMC with a clear leading edge and cell traces detectable at its trailing end (**Figure 5.3**). Within 10 min, the leading edge started to retract and at 20 min cell traces at the rear were used to form a new leading edge. At 30 min, the original leading edge at 0 min was completely replaced by cell traces and the leading edge was re-established, creating a change in VSMC direction. Therefore, VSMCs migrate towards and over their own traces and appear to be essential for aiding cell directionality. Furthermore, pre-laid traces derived from migrating VSMCs were sensed by proximal VSMCs leading to reorientation of their leading edge and direction of travel (**Figure 5.4**). Therefore, cell traces at the trailing end of a migrating VSMC appear to play an important role in guiding the migration of neighbouring cells. To support this theory, an IRM movie captured a migrating VSMC releasing traces that outlined a path from which another VSMC started to follow (**Figure 5.5**). Furthermore, time-lapse microscopy showed that, despite the absence of chemoattractant gradient, a leading VSMC released cellular material on the underlying substrate which a neighbouring cell migrated directly towards (**Figure 5.6**).

5.3.3 Cell traces provide a cell-derived matrix to assist VSMC migration

To better understand the importance of cell traces in VSMC migration, I attempted to reproduce cell traces in culture. VSMCs were seeded and cultured for 24 hours before being sheared (cells were scraped from the culture flask using a cell scraper) to remove the cell body whilst retaining cell traces on the underlying substratum. This technique aimed to mimic the 'ripping' motion by actin-myosin-generated force that normally detaches focal adhesions from the cell cytoskeleton, leaving integrins on the surface behind.[30] Although a crude method, staining with rhodamine phalloidin and anti-vinculin revealed no remnants of cytoskeletal filaments, whereas, vinculin mirrored the appearance of previously stained traces (**Figure 5.7A**).

To compare cell traces derived from proliferative and presenescent VSMCs, these cells were cultured for 24 hours and sheared before healthy VSMCs were seeded on top. Time-lapse microscopy recorded VSMC migration over cell-derived traces to reveal no change in migration speed (**Figure 5.7B**) or persistence (**Figure 5.7C**) between cells migrating over proliferative (0.250 ± 0.013 μm/min) or presenescent VSMC-derived traces (0.257 ± 0.013 μm/min). However, VSMC speed significantly increased when seeded onto cell-derived traces in general (proliferative

and presenescent traces) compared with those migrating on plastic (control; 0.198 ± 0.012 μm/min). Cell traces did not impact on migratory persistence.

To test that enhanced VSMC speed was specifically a result of VSMC traces and not secreted ECM proteins, we compared VSMC migration over cell-derived traces with migration over collagen I, a known physiological ECM component within the vessel wall. As predicted, collagen I (0.192 ± 0.008 μm/min) significantly increased VSMC migration speed compared with VSMCs seeded onto plastic (control; 0.139 ± 0.006 μm/min). However, VSMCs seeded onto cell-derived traces (0.240 ± 0.009 μm/min) were significantly faster than those on plastic and rat tail collagen I matrix (**Figure 5.8A**). No change in migrational persistence was detected between VSMCs seeded onto plastic, collagen I or cell-derived traces (**Figure 5.8B**). Therefore, VSMCs release cell traces *in-vitro* which are important for cell migration, most probably by laying down a distinctive cell-derived matrix to aid the migration of neighbouring cells.

5.3.4 The impact of ROCK inhibition on VSMC migration

As ROCK is essential for focal adhesion disassembly and generating the contractile force required for rear-end retraction, a ROCK inhibitor (Y-27632) was used to explore its impact on VSMC trace formation.[114] IRM captured the effect of ROCK inhibition and illustrated that within as little as 10 min, VSMCs could not retract properly and exhibited exaggerated cell traces at the rear with no distinct leading edge (**Figure 5.9**). This phenotype change was also detected using time-lapse microscopy up to 12 h following Y-27632 treatment. VSMCs became elongated and branched by extending long, narrow protrusions in multiple directions from the cell body (**Figure 5.10A**). Measurement of tail length was significantly increased following Y-27632 treatment (62.09 ± 4.486 μm^2) when compared with control VSMC tail length (41.4 ± 2.081 μm^2) (**Figure 5.10B**). Although ROCK-inhibited VSMCs produced cell traces at the rear, these appeared to be extensions of the trailing end that couldn't detach due to lack of retraction force.

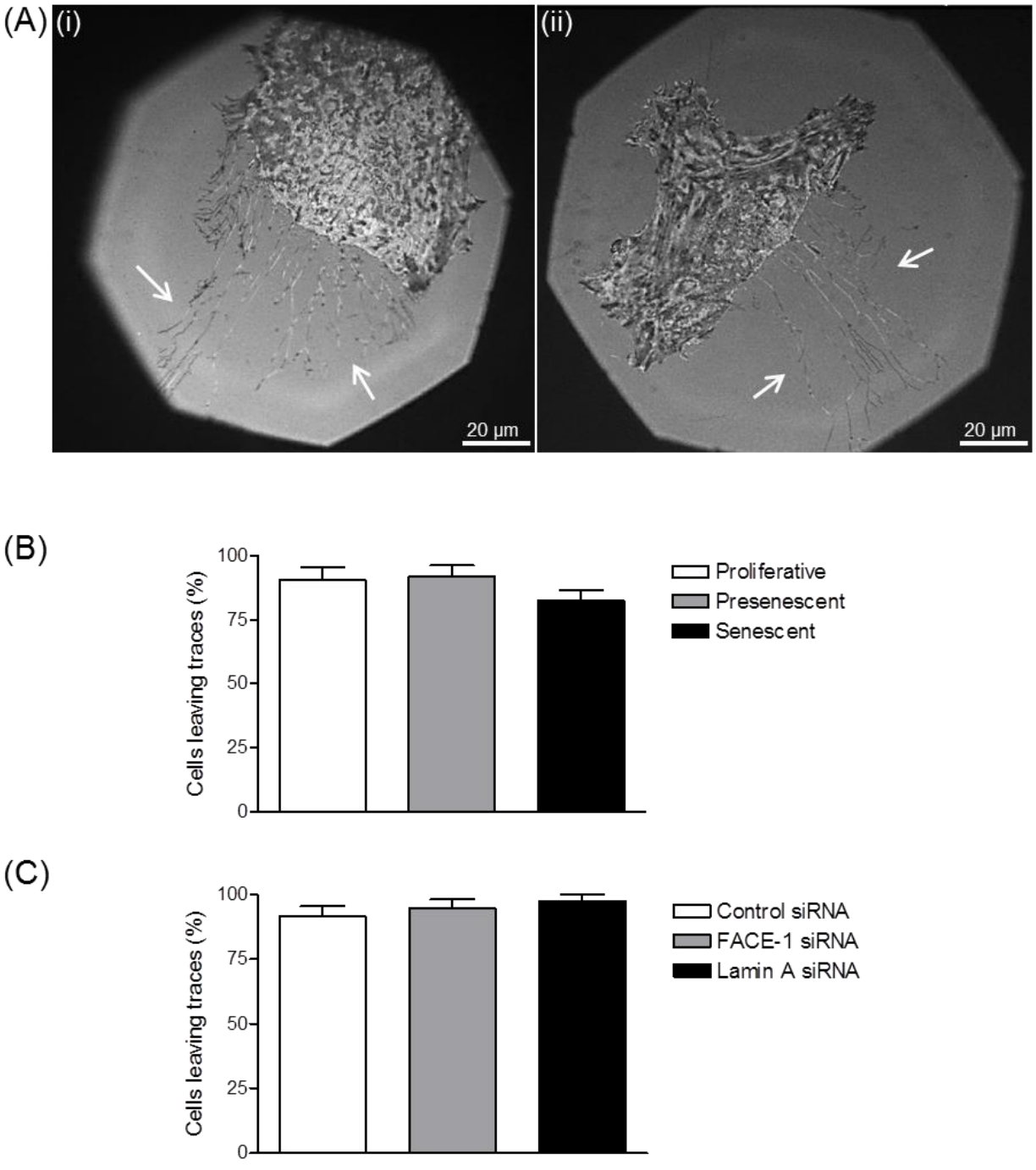

Figure 5.1: Migrating VSMCs leave traces at their trailing end. **(A)** Representative interference reflection microscopy (IRM) images of VSMC (35F) migration *in-vitro* following 1 h timelapse. Cell traces at the rear of migrating VSMCs are indicated by *arrows* **(i & ii)**. **(B)** The number of proliferative, presenescent, senescent and **(C)** control, FACE-1 and lamin A siRNA treated 35F VSMCs releasing cell traces at their trailing end during migration were counted. Data are based on counting 20 cells per group from 3 independent experiments.

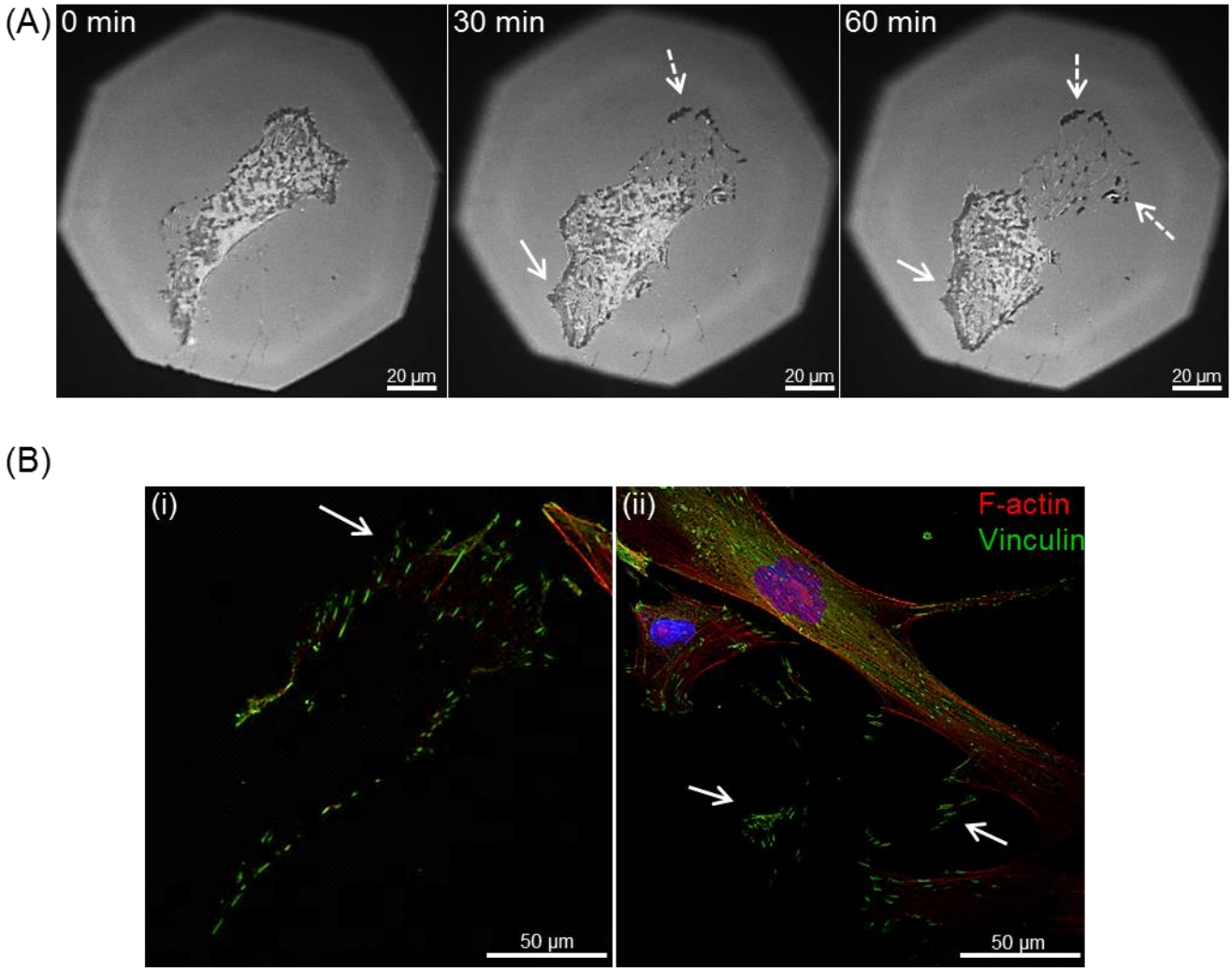

Figure 5.2: Migrating VSMCs leave adhesions at their trailing end. (A) Sequential images of a migrating VSMC (35F) *in-vitro* captured using IRM at 0, 30 and 60 min. *Solid arrows* indicate the leading edge and *dashed arrows* show adhesions at the trailing end of the VSMC. **(B)** Confocal images of VSMCs immunofluorescently stained for vinculin (*green*) and F-actin (*red*). *Arrows* indicate vinculin staining in areas where the actin cytoskeleton was not detectable.

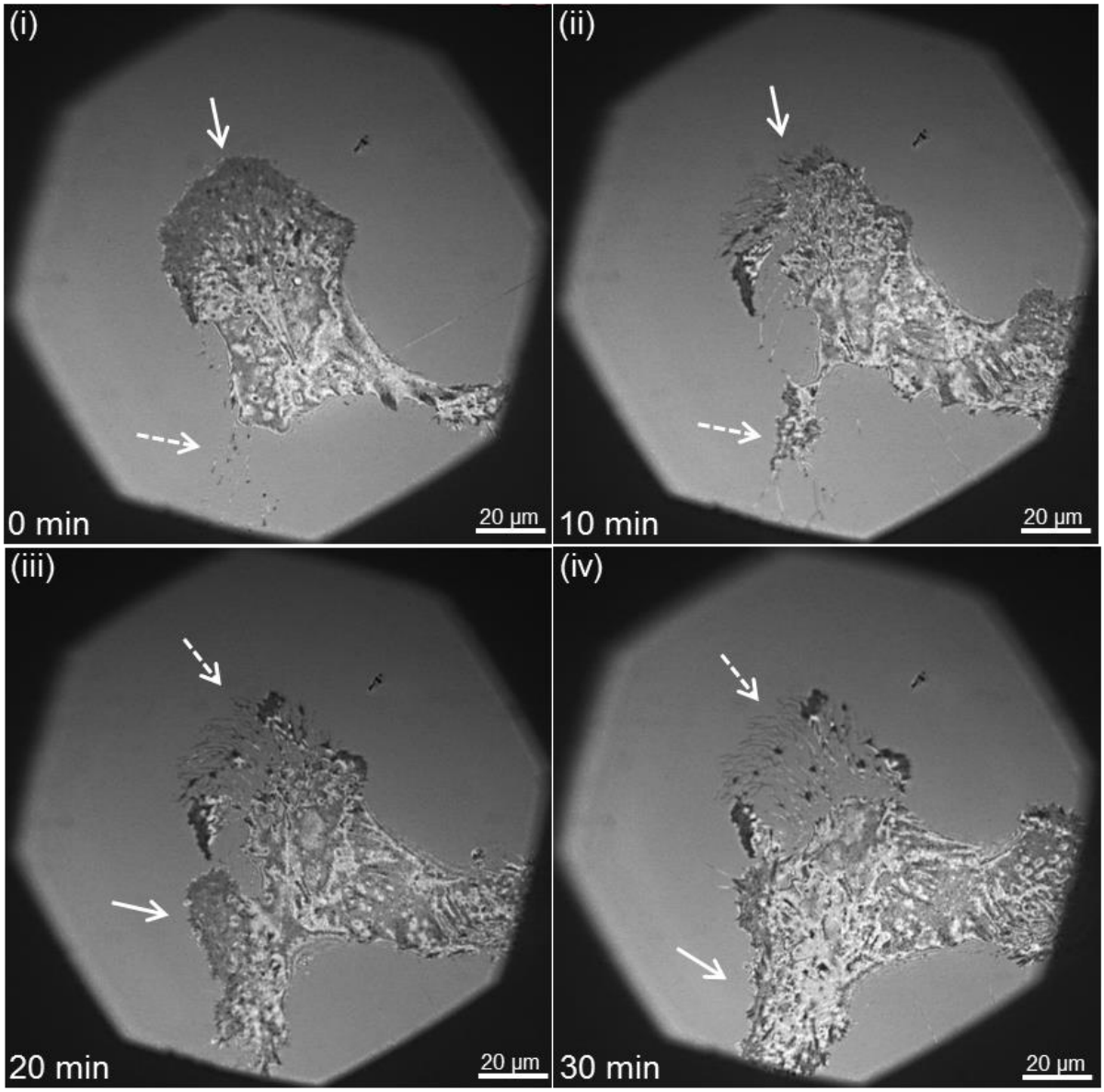

Figure 5.3: Cell-derived traces assist leading edge formation. Sequential images of a VSMC (35F) migrating *in-vitro* captured during 30 min IRM. *Solid arrows* indicate the cell leading edge and *dashed arrows* indicate cell traces at the trailing end. At 0 min **(i)** a clear leading edge was visible with traces detectable at the rear. Over the next 20 min, the leading edge retracted and traces were used to establish a new leading edge **(ii & iii)**. At 30 min **(iv)** cell traces outlined the original leading edge.

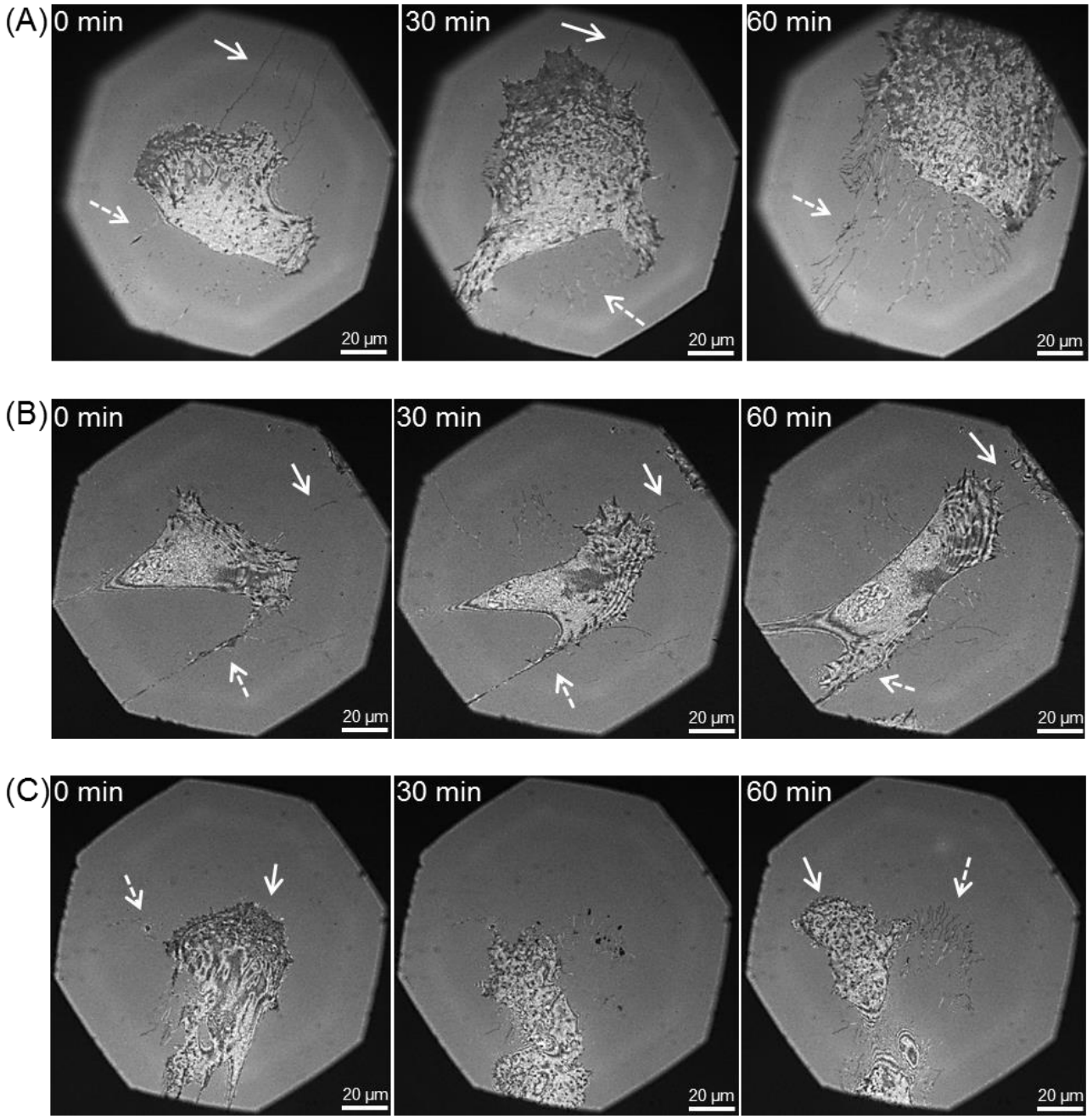

Figure 5.4: Cell traces aid the direction of VSMC migration. Sequential images of *in-vitro* VSMC migration captured over 1 h IRM. 3 examples represent VSMCs (35F) migrating towards traces derived from neighbouring cells. **(A)** *Solid arrow* indicates pre-laid traces in front of the leading edge (0 min). The VSMC migrated directionally towards these traces (30 min). *Dashed arrow* highlights traces at the trailing end of the VSMC (60 min). **(B)** Both *solid* and *dashed arrows* show 2 areas of pre-laid traces (0 min) and migration occurred towards these traces (30 & 60 min). **(C)** At 0 min the *solid arrow* represents the cell leading and the *dashed arrow* indicates pre-laid cell traces. The VSMC reoriented itself towards the traces (30 min), leading to re-establishment of its leading edge (*solid arrow*; 60 min). The *dashed arrow* at 60 min shows traces left behind.

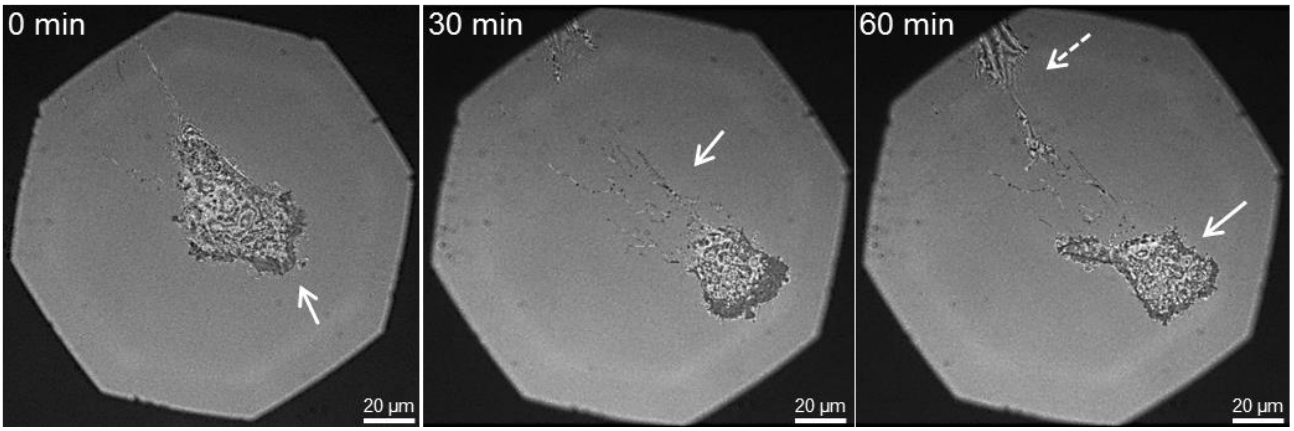

Figure 5.5: VSMCs follow traces derived from neighbouring cells. Representative IRM images of VSMC (35F) migration *in-vitro*. *Solid arrow* shows the cell leading edge (0 min) and cell traces left behind following migration (30 min). At 60 min, a neighbouring cell (*dashed arrow*) migrated directly towards the traces released by the leading cell (*solid arrow*).

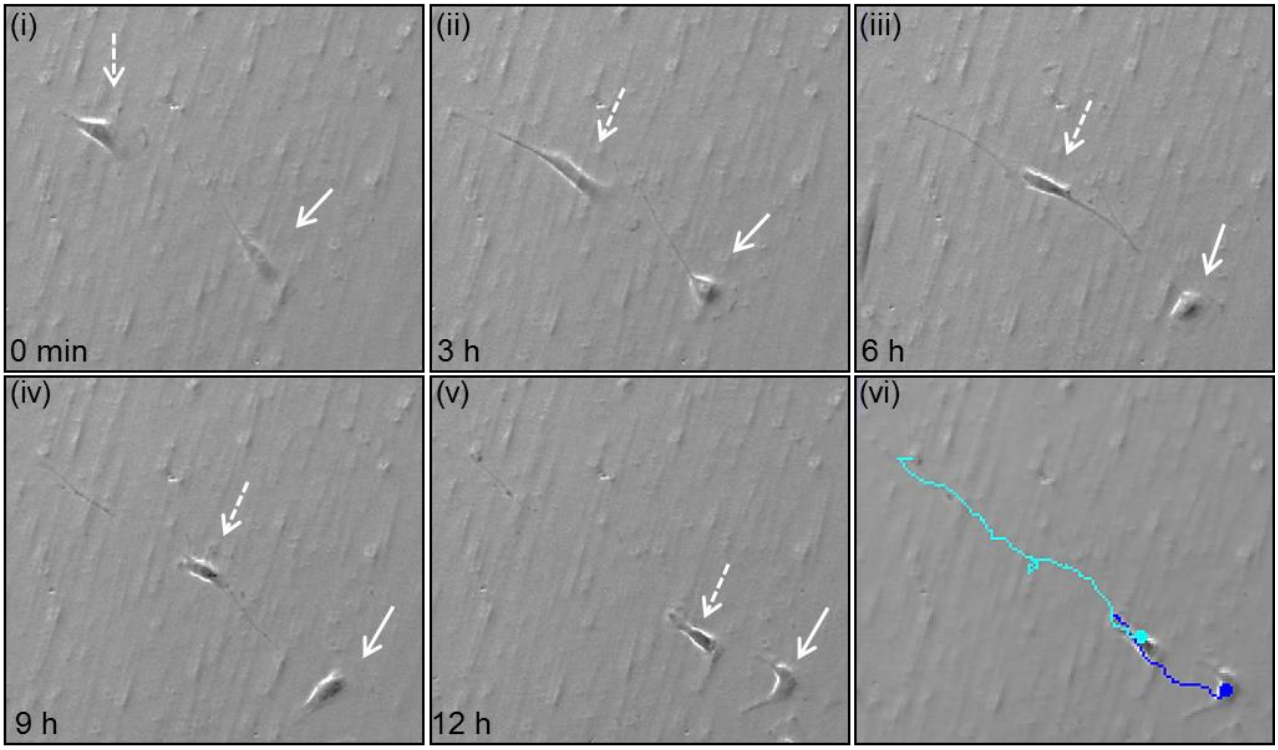

Figure 5.6: VSMC sense and migrate towards neighbouring cells. Random VSMC (35F) migration was recorded over 12 h using time-lapse microscopy and sequential images **(i – v)** illustrate VSMC (*dashed arrows*) migration directly towards a neighbouring cell (*solid arrows*). The final image **(vi)** illustrates the migrational tracks of both cells that were generated using Image J tracking software.

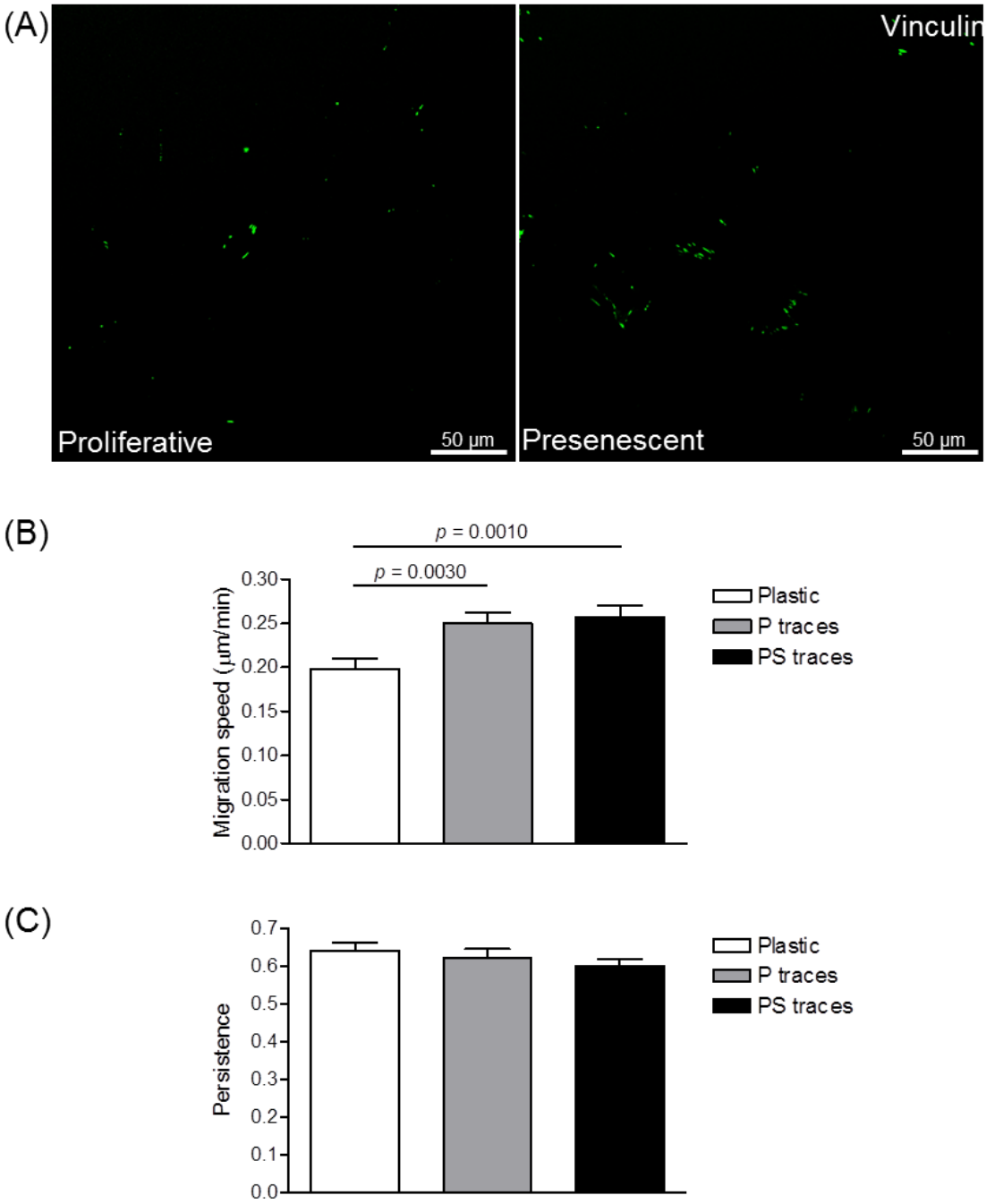

Figure 5.7: Proliferative and presenescent VSMC traces aid VSMC migration. Proliferative and presenescent 35F VSMCs were cultured for 24 h before cells were sheared and stained for F-actin (*red*) and vinculin (*green*). **(A)** Representative immunofluorescence images show vinculin patches on the surface post scraping. Proliferative 35F VSMCs were seeded sparsely on top of the cell-derived matrix and time-lapse microscopy captured random single cell migration for 16 h. Individual cells were tracked using Image J software and Mathematica analysed **(B)** the speed and **(C)** persistence of VSMC migration over proliferative (P) and presenescent (PS) cell traces compared with cells seeded on to plastic (control). Data are based on the analysis of 94 (control), 100 (proliferative cell traces) and 106 (presenescent cell traces) individually tracked cells pooled from 3 independent experiments. Statistical significance was calculated using a paired Student's *t* test.

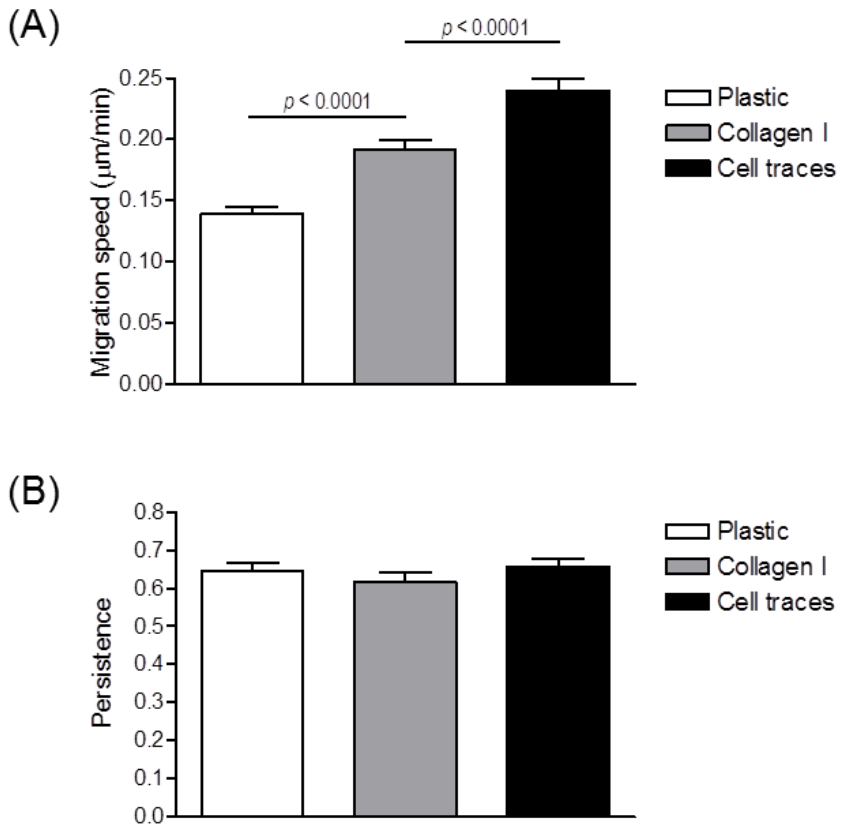

Figure 5.8: A cell-derived matrix supports VSMC migration. Time-lapse microscopy recorded random migration of VSMCs (35F) seeded on to plastic (control), collagen I-coated plastic or a cell-derived matrix (cell traces). Images were captured for 16 h and individual cells were tracked using Image J tracking software. Mathematica analysed the speed **(A)** and persistence **(B)** of VSMC migration on the 3 different matrices. Data presented are based on >100 VSMCs tracked per group and pooled from 3 independent experiments. Statistical significance was calculated using a paired Student's *t* test

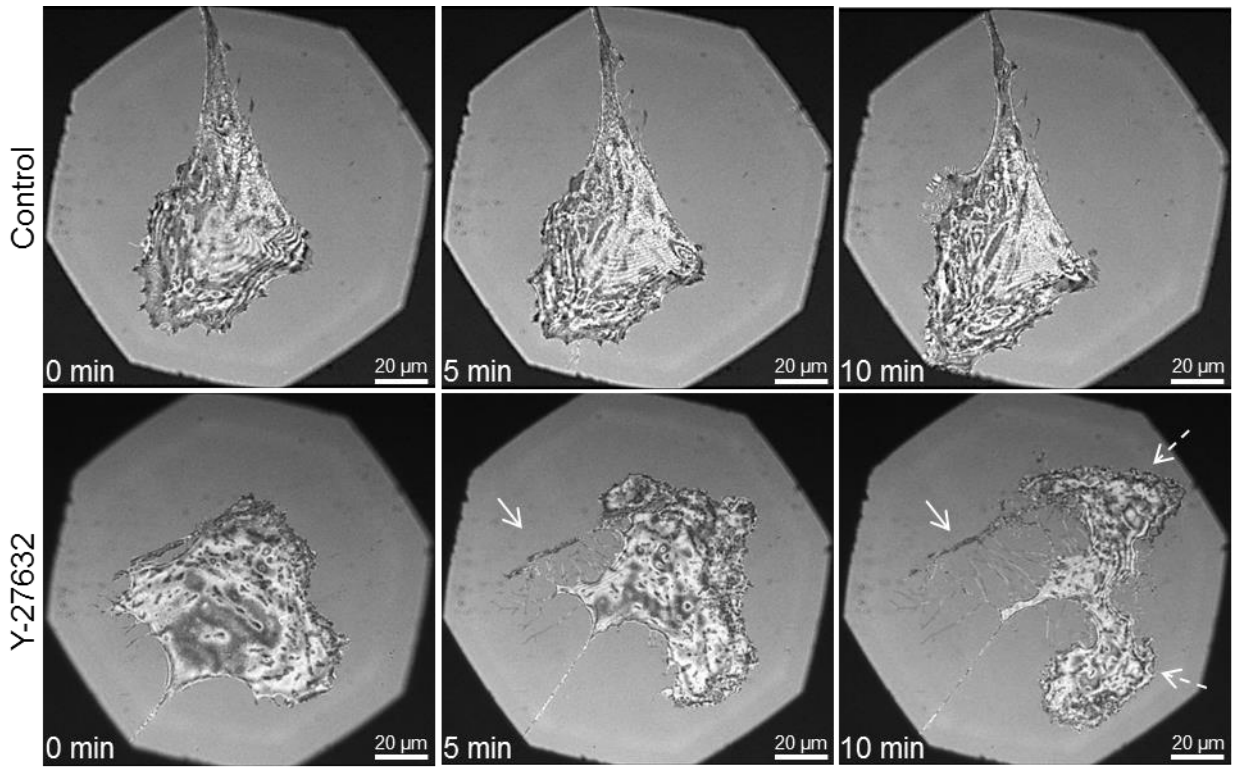

Figure 5.9: The impact of ROCK inhibition on VSMC migration. Representative IRM images of VSMC (35F) migration following Y-27632 (10 µM) treatment.at 3 separate time points (0, 5, 10 min). *Solid arrows* represent cell traces at the trailing edge and *dashed arrows* show leading edge protrusions.

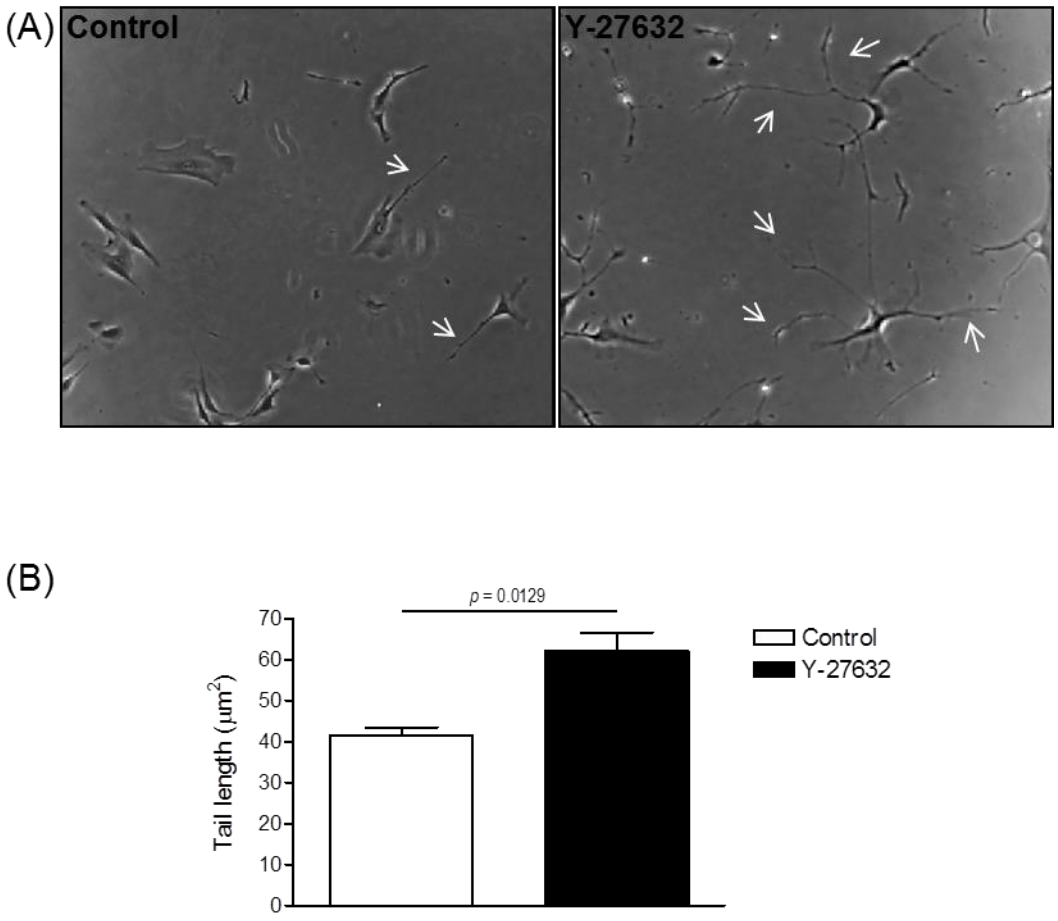

Figure 5.10: ROCK inhibition prevents rear-end VSMC retraction. (A) Representative phase contrast images of VSMCs (35F) following 12 h Y-27632 (10 µM) treatment. *Arrows* indicate the rear end 'tails' of migrating VSMCs. **(B)** Tail length of ROCK-treated and control VSMCs was measured using Volocity software. Data are based on the measurement of >30 cell tails pooled from 3 independent experiments. Statistical significance was calculated using a paired Student's *t* test (control vs treatment).

5.4: Discussion

The aim of this chapter was to utilise specialised imaging techniques such as IRM to investigate the physiological role of cell-derived traces in VSMC migration. The release of traces at the cell rear has been previously described in many cell types, however, we are the first to describe this phenomenon in VSMCs.

5.4.1 VSMCs release traces at the rear during migration

The term 'cell traces' describes the release of cellular material at the rear of migrating cells that is retained on the underlying substrate.[293] [297] Because cell traces are difficult to detect under a light microscope the purpose of cell traces has not been fully explored. Using high magnification IRM, cell traces were detectable at the rear of migrating VSMCs, which have never been previously described in these cells. Similarly to other cell types, cell traces in VSMCs vary between long, parallel and short, branched structures. VSMC traces are distinct from the cell body with a pattern adumbrating their migratory path. Although our studies were performed *in-vitro* on an artificial surface, earlier evidence illustrates that cell traces are also released in a more physiological context, such as from cells migrating over cartilage or surface of other cells.[296]

Earlier work states that cell traces are not identical with focal adhesion structure but can include focal adhesion components.[294] The presence of vinculin in VSMC cell traces fits with previous studies demonstrating that membrane 'ripping' at the cell rear releases retraction fibres high in integrin that form characteristic migrational tracks.[30] Others also show integrin patches retained on the substratum following tail detachment of skeletal muscle fibroblasts as well as remnants of cytoplasmic material such as F-actin and tubulin.[294, 295] Therefore, further investigation of VSMC trace composition is required to better understand their physiological relevance.

Despite been disregarded in the past as artefact or result of experimental stress, cell traces derived from fibroblasts, macrophages and cancer cell lines provide information about the activity of the donor cell, including its migrational velocity and direction of movement.[294] Our data illustrates numerous examples of VSMCs using their own traces to assist and direct migration as well as following traces derived from neighbouring VSMCs. We speculate that focal adhesion components, including vinculin, are retained on the substrate at the rear of migrating VSMCs following

inefficient breakage of cell membrane-ECM contacts. These are clearly not redundant as this well-organised cell trace structure appears to form a path or 'breadcrumbs' for neighbouring cells to follow. We hypothesise that cell-derived traces dictate VSMC migration via a method of haptotaxis; directional cell migration towards an adhesion gradient formed by insoluble substratum-bound material in the ECM.[284] In support of our hypothesis, earlier work demonstrates that VSMCs migrate in a concentration-dependent manner towards gradients of substratum-bound vitronectin, a multifunctional glycoprotein found to be localised in atherosclerotic lesions.[298] This study predicts that vitronectin deposition in the intima is important for recruiting VSMCs from the media. Therefore, cell trace formation may be fundamental for directing and assisting VSMCs to sites of injury or disease sites such as atherosclerotic plaques. Moreover, cell traces themselves could also be important in repair and possess wound healing properties.

5.4.2 Recreating cell-derived traces

To better understand the impact of cell-derived traces on a cells migratory capacity, we attempted to recreate traces *in-vitro*. A shearing method was used to mimic the 'ripping' motion that detaches the cell body from the substrate. Our evidence shows that cell-derived traces support VSMC migration more efficiently than collagen, the most abundant ECM protein of the vessel wall that is normally synthesised and secreted by VSMCs during cell migration.[265] An earlier study used similar principals to investigate the role of fibroblast-generated 'tracks' (traces) in cancer cell invasion. Fibroblasts were cultured overnight to produce tracks before they were killed using puromycin or detergent extraction and cancer cells seeded on top. This work revealed that fibroblast-derived matrix supports cancer cell invasion and supports our notion that cell-derived traces provide a unique platform over which the host cell and neighbouring cells can migrate.[299]

Despite using a crude shearing technique to reproduce cell traces, the resulting cell material reflected that of cell traces and vinculin was retained on the substratum. Alternative techniques described in the literature involve the application of harsh detergents or freeze-fracture to physically break cell-ECM connections.[300] Increasingly more studies now use micropatterned substrates to better mimic a tissue-like environment *in-vitro*. Lithography is used to create micropatterned surfaces and this technique was used in an earlier study to reconstruct cell traces.[296] In this study, micropatterned surfaces were able to dictate the direction and path of cell migration.

Therefore, utilising this technique would be beneficial in future studies to manipulate VSMC migration and better understand the physiological function of cell traces.

5.4.3 ROCK inhibition prevents rear-end retraction of VSMCs

ROCK promotes actin-myosin force generation and is an important regulator of cell contractility, adhesion and migration.[113, 114] Therefore, ROCK inhibition exaggerates VSMC trace formation most likely due to loss of actin-myosin crosslinking and force necessary to efficiently sever cell body-ECM connections. This results in impaired rear-end retraction and formation of heavily-branched VSMCs, implying that trace generation is dependent on the contractile force generated by the host cell.

5.4.4 Chapter 5 conclusions

This chapter clearly demonstrates that VSMCs release traces of cellular material at the rear during migration. Our preliminary data reveal that VSMC-derived traces provide migratory paths that appear to assist and direct the migration of proximal cells in a haptotactic manner (**Figure 5.11**). We predict that that this is a novel mechanism of collective cell migration important for facilitating VSMC migration within the vessel to sites of damage.

5.4.5 Limitations and future work

Future work will investigate how cell traces are released from cells and determine their composition using immunofluorescence microscopy in combination with a proteomics approach. We will also investigate whether migration over pre-laid tracks involves the uptake of any cellular material that could further enhance cell migration. The use of more advanced microscopy including scanning electron microscopy (SEM), that was particularly useful in earlier cell trace studies, will enable us to better observe VSMC-derived traces in more physiologically relevant settings.[296] Aforementioned, reproducing cell traces on micropatterned substrates is our ultimate goal in determining their specific role in VSMC migration.

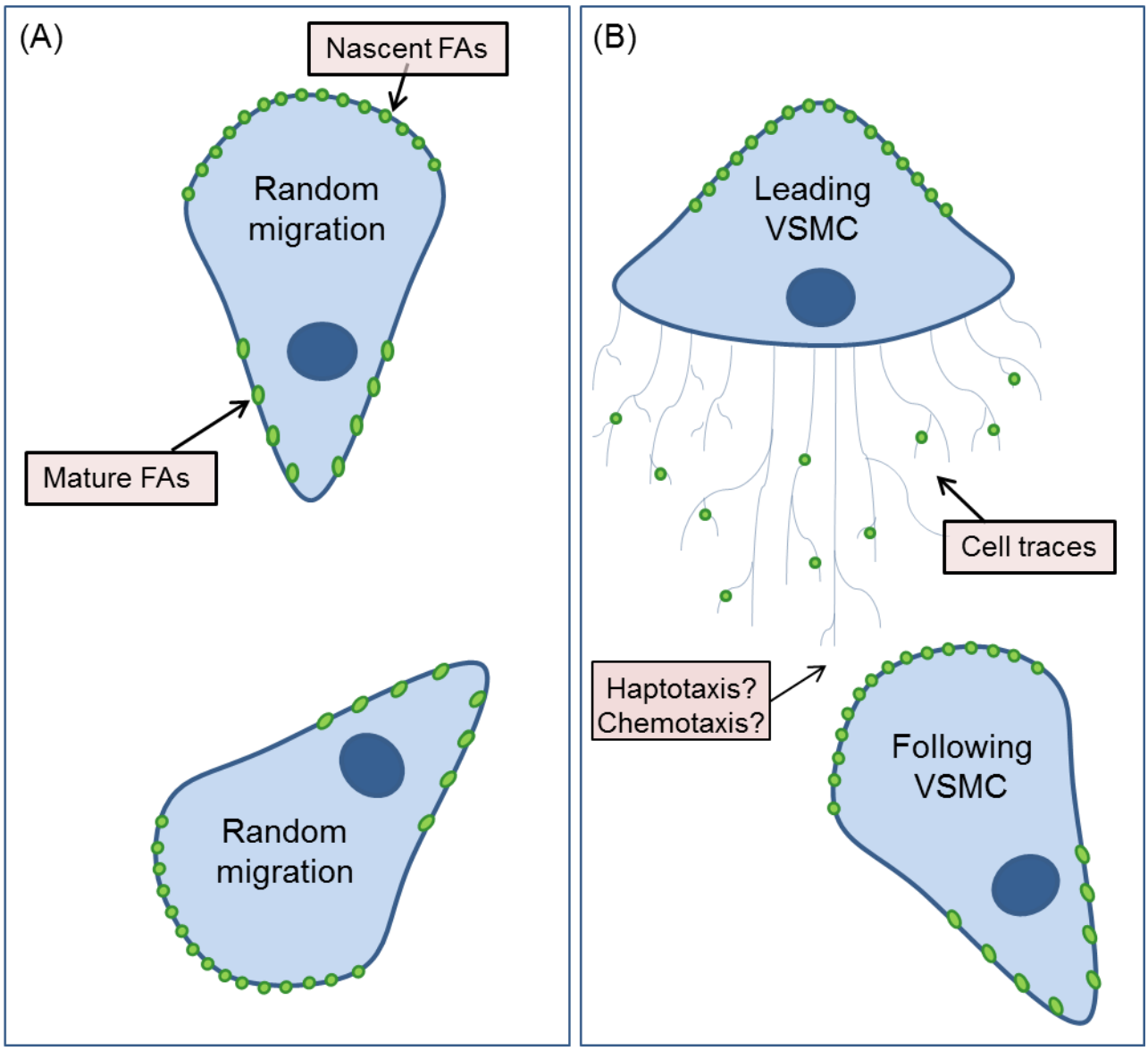

Figure 5.11: Cell-derived traces aid the migration of neighbouring cells. This schematic provides a working model of the results summarised within this chapter. **(A)** During migration small nascent focal adhesions form at the cell leading edge which mature over time and form stable anchors with underlying ECM. VSMCs migrate randomly in the absence of a chemotactic gradient. **(B)** As migrating VSMCS retract they release cell traces behind them that form a skeleton of cell membrane and focal adhesion components. This adumbrates the migratory path of a leading VSMC and allows proximal VSMCs to follow. We speculate that cell traces aid collective migration by creating either a haptotactic or chemotactic gradient.

Chapter 6: General Discussion & Conclusions

6.1 Ageing and NE remodelling impacts on cell migration

Directional cell migration is fundamental for tissue development and wound healing responses to injury and disease. During cell migration, Rho GTPases and their numerous downstream signalling targets regulate actin cytoskeleton remodelling, cell shape, adhesion and motility.[23, 34] However, the LINC complex has recently emerged as a novel regulator of cytoskeletal organisation and cell motility as it physically tethers F-actin to the nucleus via nesprin-SUN-nuclear lamina interactions across the NE.[127-130] The LINC complex is an integral multi-protein complex that supports cell architecture and maintains structural tension throughout the cell.[301] This is important as mechanical forces transmitted through a pre-stressed (tense) cytoskeleton are significantly faster (30msec/50µm) than the rate-limited diffusion of biochemical cascades (10sec/50µm).[164, 302] Previous studies describe physical linkage between the cell surface, cytoskeleton and nucleus which is crucial for effective mechanotransduction signalling between the cell interior and local surroundings.[186, 189, 197] It has also been reported that cell surface deformations (stretch/compression) influence nuclear morphology and gene transcription which is suppressed following LINC complex disruption.[165, 186, 189, 197, 246, 303] Interestingly, our work demonstrates that focal adhesion formation is defined at a nuclear level as nuclear lamina disruptions subsequently alter focal adhesion organisation and dynamics at the cell membrane. We speculate that this is mediated by the LINC complex which extends beyond the NE to physically connect the nucleus, actin cytoskeleton and focal adhesion components. This mechanically-coupled system throughout the cell would facilitate force transmission between the nucleus and cell membrane, ultimately modifying the cellular tension required for focal adhesion assembly/disassembly (**Figure 6.1**). As focal adhesion components regulate Rho GTPase activity, this also implicates a role of the LINC complex in Rho GTPase signalling.[281] Therefore, our working model predicts that the LINC complex regulates cell migration via a combination of biophysical and biochemical mechanisms.

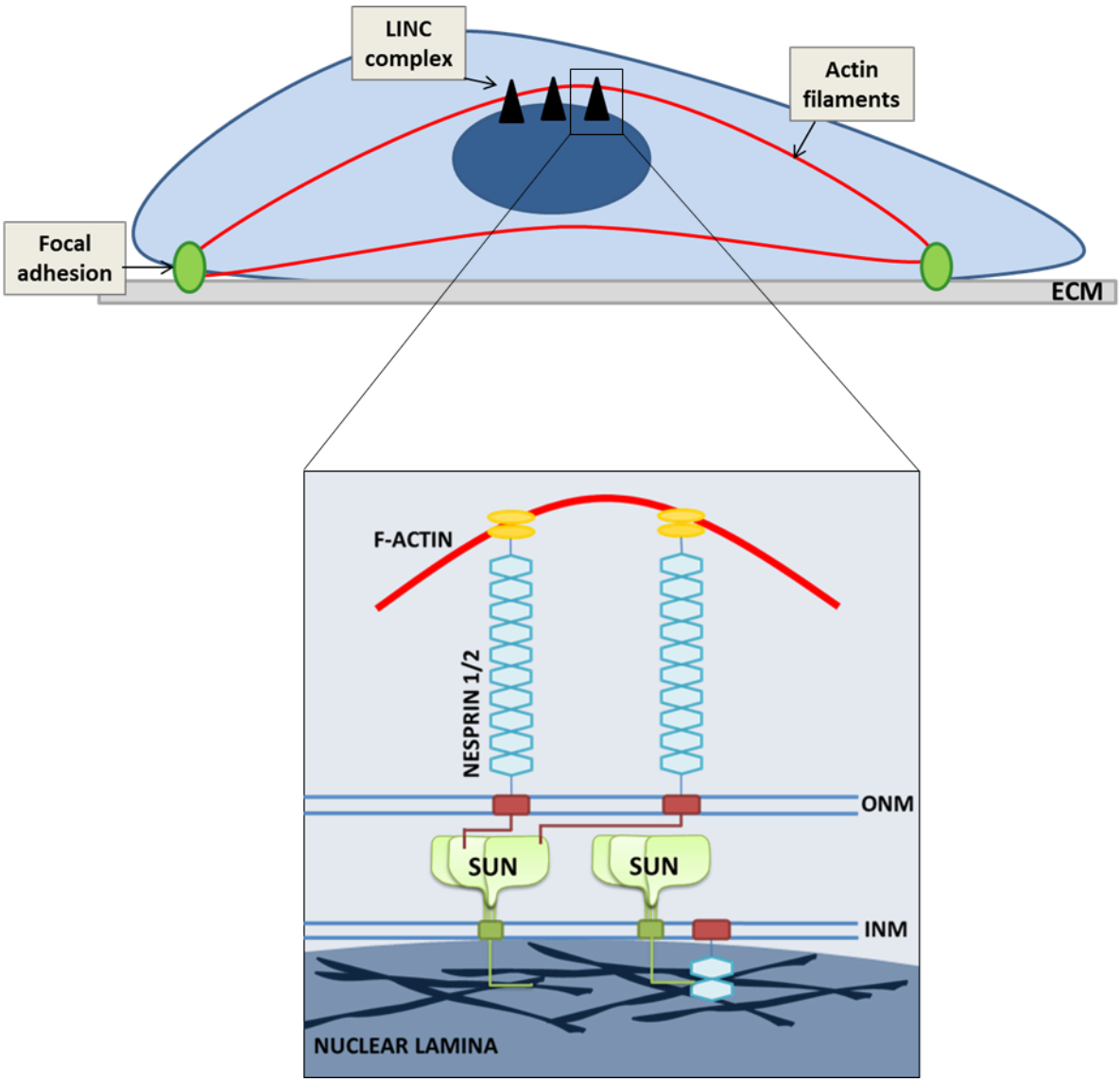

Figure 6.1: The LINC complex creates a mechanically-coupled system throughout the cell. Working model of the LINC complex based on our findings that nuclear lamina alterations impact on focal adhesion organisation/dynamics at the cell membrane. The nuclear lamina at the INM is indirectly connected to focal adhesions via LINC complex components spanning the NE (nuclear lamin-SUN-nesprin) and actin filaments bridging the nucleus and cell membrane.

The original aim of this thesis was to further explore the role of prelamin A, a novel biomarker of VSMC ageing in cell motility.[204] Prelamin A accumulates at the NE where it uncouples lamin A from the nuclear lamina, however, until now the precise mechanisms of how this affects LINC complex function were undefined.[138, 227] Previous studies show that lamin A/C deficient cells exhibit defective cytoskeletal organisation, cell adhesion, polarisation and motility.[172, 186, 187, 196] In support, we demonstrate that age-associated prelamin A accumulation disrupts LINC complex organisation, drives cell elongation and focal adhesion reorganisation. We also reveal that *in-vitro* aged VSMCs exhibit faster migration rates and are more persistent during presenescent growth when prelamin A begins to accumulate. Artificially inducing prelamin A accumulation by FACE-1 knockdown also drives similar migratory changes in fibroblasts. However, FACE-1 depletion enhances VSMC persistence but is not causal for the enhanced speed associated with VSMC ageing. This led us to further explore the importance of other LINC complex components in regulating VSMC migration.

Excitingly, this is the first study to reveal an age-related reduction in SUN2 expression. Similarly to *in-vitro* aged VSMCs, SUN2 depleted VSMCs retain nesprin-2 at the NE, which was mislocalised to the ER in nuclear lamina disrupted VSMCs. Furthermore, knocking down SUN2 reproduced the increased migration speed observed in presenescent VSMCs, suggesting that prelamin A accumulation combined with SUN2 attenuation brings about the migratory phenotype reflective of VSMC ageing (**Figure 6.2**). We speculate that NE remodelling during VSMC ageing uncouples nuclear lamina-SUN interactions leading to unstable SUN2 recruitment to the NE and its subsequent degradation. This is plausible as studies have shown that SUN2 localisation is dependent on lamin A/C whereas SUN1 possesses other nuclear binding partners, namely emerin and nucleoplasmic nesprin isoforms.[128, 157, 158] However, our studies reveal that prelamin A accumulation following FACE-1 knockdown does not directly impact on SUN2 expression, suggesting that SUN2 stability is regulated by other factors. Despite SUN1 and SUN2 exhibiting similar affinities for nesprin-2, other studies have illustrated that SUN2 knockdown, but not SUN1, enhances nesprin-2 mobility at the ONM.[163] Our data also show that SUN2 is more abundant than SUN1 in VSMCs, therefore, SUN2 is potentially the dominant SUN protein in LINC complex coupling of the nuclear lamina to nesprins and cytoskeletal networks. In summation, our data indicate that the accumulation of prelamin A and loss of SUN2 at the NE induce age-associated LINC complex alterations that compromise cell migration. However, FACE-1 and SUN2 depletion induce different morphological changes to *in-vitro* aged VSMCs. Presenescent VSMCs are large and elongated, whereas prelamin A

elongates but does not affect VSMC size and SUN2 depleted VSMCs are smaller with no overall change to cell shape. Therefore, targeting individual LINC complex components induces varying morphologies and suggests that numerous factors, not only prelamin A and SUN2, are responsible for defining VSMC phenotype during ageing.

The overall findings in this thesis reveal that the LINC complex is a dynamic structure with a composition uniquely adaptable to specific cell requirements. We envisage that individually disrupting LINC complex proteins, the nuclear lamina (FACE-1 or lamin A/C), nesprins or SUN proteins mechanically weakens this biophysical network and consequently impinges on actin-regulated processes including cell morphology, focal adhesion organisation/turnover and cell motility. Therefore, we emphasise that the LINC complex as a whole is an important regulator of cell phenotype and our work sheds light on how the LINC complex aberrations associated with nuclear envelopathies and premature ageing diseases are characterised by abnormal cell functions. It is now well-established that prelamin A normally accumulates in VSMCs during ageing and we show that prelamin A impacts on cellular morphology and migratory capacity. As cell migration is essential for normal tissue repair and homeostasis, any defects in these processes will accelerate tissue degeneration and ageing. In agreement with this, mutant prelamin A accumulates in the premature ageing syndrome, HGPS. However, the full extent of the NE in regulating actin organisation and cell motility during tissue homeostasis remains to be defined.

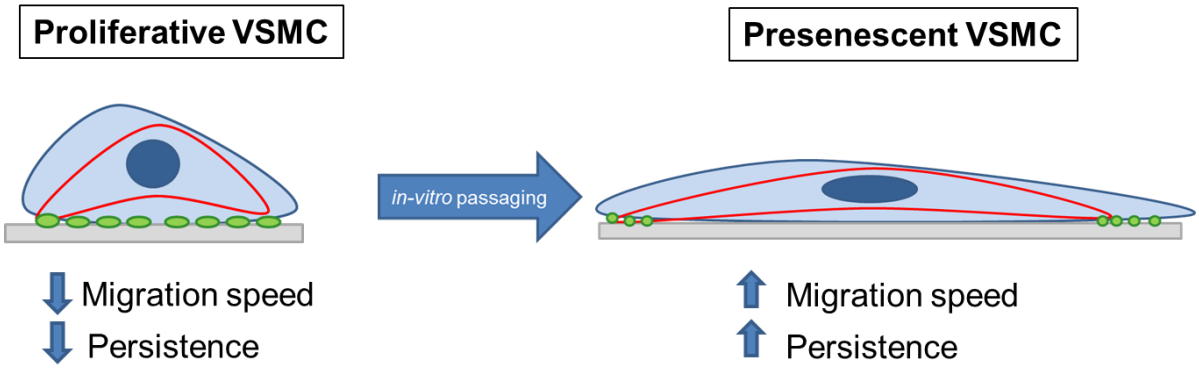

	Proliferative VSMC	Presenescent VSMC
FACE-1	High	Low
Prelamin A	Low	High
SUN2	High	Low
Nesprin-2	No change	No change
Lamin A/C	No change	No change
Rac1	High	Low
RhoA	High	Low

Figure 6.2: Comparison of proliferative and presenescent VSMCs. (A) This model provides an overview of the phenotypic differences between proliferative and presenescent VSMCs that were characterised following *in-vitro* passaging. Proliferative VSMCs adopt a small, circular morphology with a high number of large focal adhesions distributed across the cell surface. Presenescent VSMCs are larger and spindle-like with fewer focal adhesions primarily localised to the cell periphery. These focal adhesions are small and rounded, correlating with enhanced focal adhesion turnover in presenescent VSMCs. Presenescent VSMCs also migrate faster and more persistently than proliferative VSMCs. **(B)** VSMC ageing is associated with a reduction in FACE-1 expression which correlates with prelamin A accumulation. We are the first study to describe an age-related attenuation of SUN2 as well as Rac1 and RhoA expression in VSMCs. Total levels of lamin A/C and nesprin-2 remained unchanged.

6.2 Pathological VSMC migration

Despite previous studies indicating that cell migration is impaired during ageing, our work reveals that VSMC migration *in-vitro* increases progressively with age until a peak is reached at presenescent growth, after which migration subsides.[218, 219] This supports recent data demonstrating that VSMCs undergo age-associated phenotypic switching and become dedifferentiated with diminished cytoskeletal myocitic markers and enhanced proliferation and migration rates.[217] Efficient VSMC migration is fundamental for vessel development and repair. Moreover, VSMCs are a prominent cell-type at atherosclerotic sites where they aid the formation of a protective cap to stabilise rupture-prone lesions.[12, 14] However, increased VSMC migration and proliferation also drives vessel remodelling and intimal thickening which are major pathogenic factors in atherosclerosis and restenosis.[9, 215, 216] Current literature is divided as to whether VSMCs are beneficial or detrimental to vessel health, therefore, their role in atherosclerotic development remains undefined.

Our findings demonstrate that presenescent VSMCs innately migrate more rapidly and persistently than their early-passage predecessors, which is believed to represent precise and efficient directional migration.[260] We also demonstrate that presenescent VSMCs retain their chemotactic ability, suggesting that VSMCs at this growth stage are still recruited to areas of vessel damage and atherosclerotic plaques. However, we predict that age-related changes to migratory phenotype may ultimately lead to inefficient vessel repair and contribute towards inappropriate remodelling of the vasculature. Faster VSMC migration, coupled with enhanced ECM deposition would cause intimal thickening, a preferable site for atherosclerotic plaque development.[215, 216] Ageing also induces the VSMC secretion of chemokines including interleukins, monocyte chemotactic protein-1 and tumour necrosis factor-α, leading to chronic vessel inflammation.[304] Furthermore, recent evidence specifically demonstrates that prelamin A-containing presenescent VSMCs exhibit a heightened inflammatory profile.[305] This pro-inflammatory phenotype may further enhance presenescent VSMC recruitment to wound sites, thus exacerbating the inflammatory response that underlies numerous vascular pathologies. We hypothesise that the age-related enhancement of VSMC migration is primarily a protective mechanism allowing presenescent VSMCs a final attempt to repair vessel damage with a migratory ‘boost’ before they become senescent. However, the inability of presenescent VSMCs to switch back to a differentiated phenotype once their synthetic function is complete, i.e. vessel damage repair or atherosclerotic cap formation, drives pathological vessel remodelling and atherogenesis. Ultimately, when VSMCs reach senescence, we reveal that migration

and proliferation ceases and VSMCs lose their chemotactic responses. The loss of VSMCs recruitment to wound sites would result in inefficient atherosclerotic cap formation, inevitably leading to plaque instability and rupture (**Figure 6.3**).

At present, the literature describing the impact of ageing on cell migration is confusing and undefined. Our work highlights a clear explanation for these conflicting results as VSMC ageing appears to be associated with a progressive surge in migration speed and persistence during presenescence, prior to halting when cells become senescent. Our results provide an important insight into *in-vitro* VSMC ageing, however, repeating these experiments in VSMCs isolated from aged donors and aged-related diseases would apply better physiological relevance to these findings.

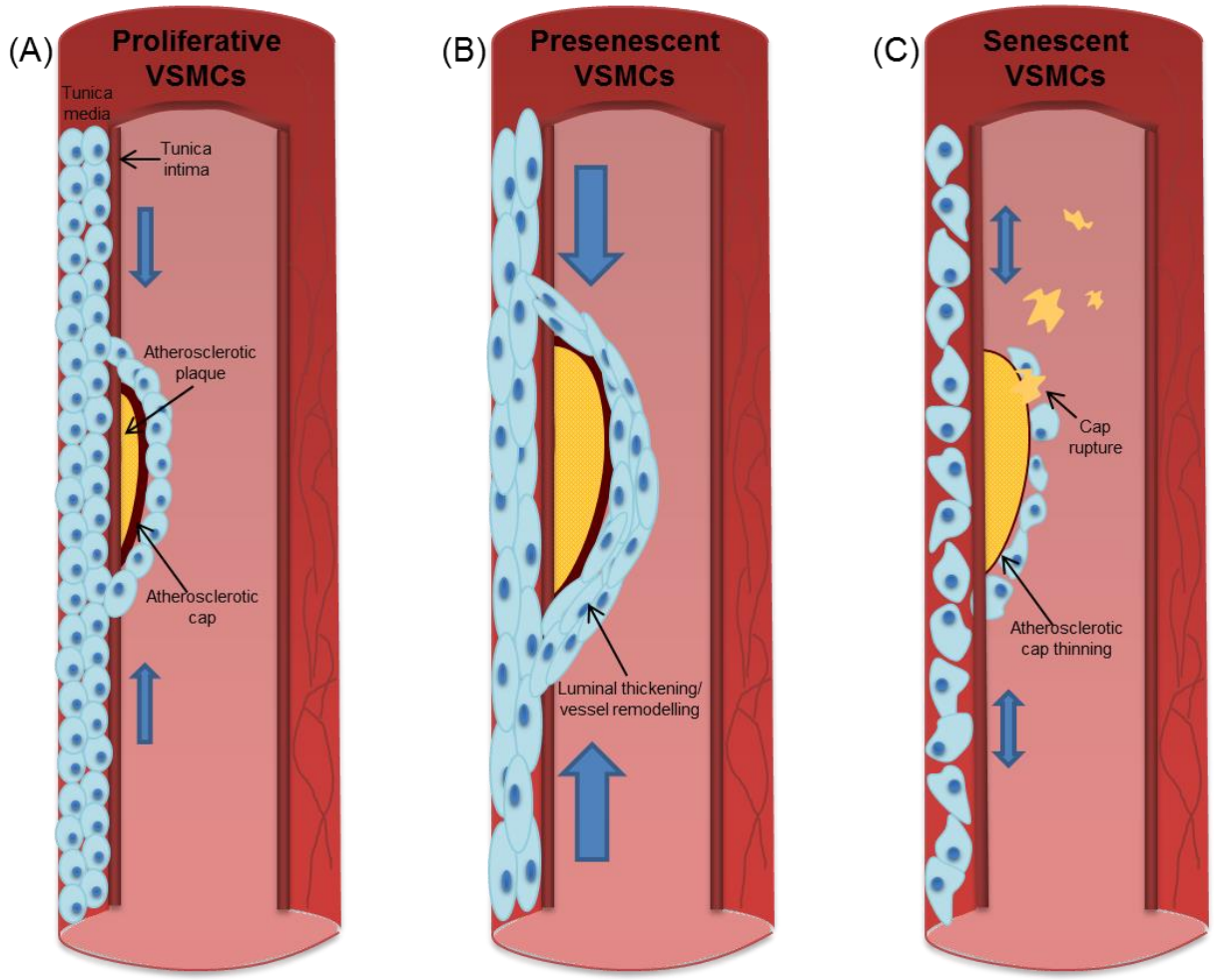

Figure 6.3: Atherosclerosis at differing stages of VSMC growth. Working model demonstrating how VSMCs of different growth stages are involved in vessel repair and atherosclerotic cap formation. **(A)** Young and healthy VSMCs have a small and rounded morphology with relatively slow migration rates from the media to the intima in response to chemotactic cues. Intimal VSMCs are highly proliferative and directionally migrate towards atherosclerotic lesions or sites of vessel damage where they generate a uniform protective cap to stabilise atherosclerotic plaques and repair vessel damage. **(B)** Presenescent VSMCs are large and elongated with relatively fast migration speeds and high persistence. Increased VSMC migration towards the intima is potentially a protective mechanism that enhances atherosclerotic cap formation. However, exaggerated migration consequently leads to intimal thickening, vessel remodelling and exacerbated inflammatory responses that drive atherogenesis. **(C)** Senescent VSMCs have increasing levels of prelamin A at the NE and have a large, flattened appearance. These cells migrate slowly, lack persistence and cannot respond to chemotactic or haptotactic cues. This creates an unstable plaque and consequently leads to plaque rupture, myocardial infarction and strokes, all of which are prevalent age-related disorders. Blue arrows indicate direction of VSMC migration.

6.3 Cell-derived traces

Originally the deposition of cellular material, known as cell traces, during migration were believed to occur as a result of experimental stress with no known function. However, increasing evidence suggests that cell traces are physiologically relevant and have been identified in numerous cell types.[294, 296] Our data suggest that cell-derived traces play a regulatory role in VSMC migration. We show that VSMCs deposit long, branched structures of cell traces at the rear during migration which adumbrates their migratory path. We predict that cell traces result from the inefficient breakage of cell-ECM contacts and are composed of cell membrane and focal adhesion constituents that are retained on the underlying substrate. Even in sparsely-seeded cultures, proximal cells sense and migrate directly towards these adhesion-like molecules in a haptotactic-like manner. Haptotaxis is defined by directional cell migration towards an adhesion gradient formed by insoluble ECM-bound molecules.[284] Therefore, cell-derived traces are clearly not redundant and act as migratory 'footprints' or 'breadcrumbs' to outline a path for neighbouring cells to follow in a novel form of collective migration. The notion that 'leader' cells guide 'follower' cells has been previously described in endothelial and epithelial cell migration, whereby leading cells display distinct polarised morphologies, sense directional cues and induce collective, sheet-like migration of multiple rows of successive cells.[77, 306]

Collective cell migration underlies tissue development and repair as well as contributing towards tumour cell metastasis.[85] It is defined by 2 distinct modalities; i) multicellular clusters that maintain strong cell-cell contact and migrate together in sheets or, ii) chain-like streaming of cells in single file that requires unstable cell-cell contact.[75-77, 79, 80] The mode of VSMC migration we typically observed was similar to collective cell streaming, however, it will be interesting to test this in denser VSMC populations and *in-vivo* settings. Neural crest cells are commonly used to model cell streaming as they migrate over long distances in spatially segregated chain-like patterns or 'streams' during which loose cell-cell connections are retained by long, thin filopodia.[92] These cellular extensions form a path to facilitate cell migration and can induce directional changes similarly to that observed by VSMC-derived traces in our studies. Furthermore, cell streaming is crucial for the *in-vivo* migration of human breast tumour cells and is more efficient than random migration as it facilitates higher velocity rates and further net travel.[307] This leads us to speculate that cell-derived traces are a form of cell-cell contact that maintain communication between neighbouring cells and provide a guidance mechanism for long-range collective cell migration.

It is well-established that cell migration requires structural modifications to surrounding ECM, including clearing of a migratory track by MMPs and deposition of ECM proteins to generate a basement membrane for cells to follow.[85] It is suggested that migrational tracks do not only directionally guide cell migration but, owing to their structural and molecular properties, could serve additional physiological functions. For example, newly secreted basement membrane might provide a smooth scaffold to assist cell migration into tissue in a collective and continuous manner.[308] We demonstrate that VSMCs release vinculin-containing traces at the rear during migration whose specific role is currently unidentified. An earlier study illustrates that fibroblasts release migratory tracks or trails of fibronectin and tenascin-c within the ECM to enhance collective cancer cell invasion into connective tissue independently of soluble factors.[299] This emerging evidence supports our hypothesis that cell-derived traces form physical tracks in the substrate that promote and support cell migration.

Another mechanism of cell traces aiding collective cell migration potentially involves the release of soluble molecules to attract proximal cells via chemotaxis. A chemoattractant source directly influences cell polarisation, orientation and promotes directional persistence towards the chemotactic gradient. Work in dictystelium cells illustrates that this is coupled by the synthesis and secretion of additional chemoattractant which is packaged into cell-derived vesicles, also termed exosomes, which fuse to the rear membrane before their content is released.[309] This release forms tracks at the rear of migrating cells which are important for amplifying chemotaxis by stimulating the migration of proximal cells in a positive feedback mechanism. This mode of migration has also been described in tumour cells that release cell fragments behind during migration which further stimulates the chemotaxis of neighbouring cells via streaming.[310] Endothelial cells also secrete exosomes as well as capturing exosomes from proximal cells.[311-313] A recent *in-vitro* study demonstrates that endothelial cell-derived exosomes are important mediators of cell-cell communication as they transfer signalling molecules to recipient endothelial cells to influence their migratory behaviour such as stimulation of movement into a wound.[314] During wound healing or at infection sites, macrophages synthesise chemotactic factors to recruit other blood cells and more recent work reveals that macrophages also release epidermal growth factor (EGF) to promote tumour cell invasion and metastasis.[315] Based on this body of evidence, we speculate that cell traces serve as vehicles of exosome delivery and chemoattractant release into the extracellular environment during cell migration.

Our studies demonstrate that VSMC ageing does not impact on cell trace formation. In support, recent evidence reveals that ageing does not affect VSMC exosome release but is in fact associated with changes in exosomal content.[305] Furthermore, *in-vitro* VSMC passaging or prelamin A overexpression induces changes in the expression of chemokines, growth factors and proteases, which may contribute to the age-related alterations we detect in VSMC adhesion and migration.[305] Future work will benefit from testing exosome-mediated signalling between VSMCs by harvesting VSMC-derived exosomes and resuspending increasing levels into culture medium. Alternatively, established exosome inhibitors could be used to determine the impact of exosomes on cell migration.

Overall, we hypothesise that VSMC-derived traces guide neighbouring VSMCs and other cell types by laying down a migratory path through tissue and complex ECM. This potentially supports cell migration during development and to sites of injury including atherosclerotic plaques where VSMCs are heavily implicated. Furthermore, cell traces themselves could be important in vessel repair and atherosclerotic cap formation.

6.4 Final conclusions

Cell migration underlies many biological processes chiefly tissue development, maintenance and regeneration. The LINC complex has recently emerged as a critical regulator of cytoskeletal organisation and our data elaborates upon this to demonstrate that cellular morphology, focal adhesion formation, Rho GTPase activity and cell migration are also defined by the LINC complex. Moreover, we reveal that LINC complex disruption by prelamin A accumulation and attenuated SUN2 expression, hallmarks of VSMC ageing, increases VSMC migration speed and persistence. This exaggerated VSMC phenotype may ultimately drive inappropriate vascular remodelling and contribute towards the pathogenesis of age-related vascular disease. Therefore, improved knowledge of the processes involved in prelamin A and SUN2 regulation may highlight new strategies to counteract the age-related vessel reorganisation that accelerates atherosclerosis.

Reference list

1. Sun D, Huang A, Recchia FA, Cui Y, Messina EJ, Koller A, Kaley G. Nitric oxide-mediated arteriolar dilation after endothelial deformation. *Am J Physiol Heart Circ Physiol*. 2001;280:H714-721
2. Martinez-Lemus LA. The dynamic structure of arterioles. *Basic & clinical pharmacology & toxicology*. 2012;110:5-11
3. Rhodin JA. The ultrastructure of mammalian arterioles and precapillary sphincters. *Journal of ultrastructure research*. 1967;18:181-223
4. Haurani MJ, Pagano PJ. Adventitial fibroblast reactive oxygen species as autacrine and paracrine mediators of remodeling: Bellwether for vascular disease? *Cardiovasc Res*. 2007;75:679-689
5. Di Wang H, Ratsep MT, Chapman A, Boyd R. Adventitial fibroblasts in vascular structure and function: The role of oxidative stress and beyond. *Canadian journal of physiology and pharmacology*. 2010;88:177-186
6. Hinz B. Formation and function of the myofibroblast during tissue repair. *J Invest Dermatol*. 2007;127:526-537
7. Renna NF, de Las Heras N, Miatello RM. Pathophysiology of vascular remodeling in hypertension. *International journal of hypertension*. 2013;2013:808353
8. Gibbons GH, Dzau VJ. The emerging concept of vascular remodeling. *N Engl J Med*. 1994;330:1431-1438
9. Louis SF, Zahradka P. Vascular smooth muscle cell motility: From migration to invasion. *Experimental and clinical cardiology*. 2010;15:e75-85
10. Lusis AJ. Atherosclerosis. *Nature*. 2000;407:233-241
11. Hürlimann D, Ruschitzka F, Lüscher TF. The relationship between the endothelium and the vessel wall. *Eur Heart J*. 2002;4:A1–A7
12. Dickson BC, Gotlieb AI. Towards understanding acute destabilization of vulnerable atherosclerotic plaques. *Cardiovasc Pathol*. 2003;12:237-248
13. Gorenne I, Kavurma M, Scott S, Bennett M. Vascular smooth muscle cell senescence in atherosclerosis. *Cardiovasc Res*. 2006;72:9-17
14. Naghavi M, Libby P, Falk E, Casscells SW, Litovsky S, Rumberger J, Badimon JJ, Stefanadis C, Moreno P, Pasterkamp G, Fayad Z, Stone PH, Waxman S, Raggi P, Madjid M, Zarrabi A, Burke A, Yuan C, Fitzgerald PJ, Siscovick DS, de Korte CL, Aikawa M, Airaksinen KE, Assmann G, Becker CR, Chesebro JH, Farb A, Galis ZS, Jackson C, Jang IK, Koenig W, Lodder RA, March K, Demirovic J, Navab M, Priori SG, Rekhter MD, Bahr R, Grundy SM, Mehran R, Colombo A, Boerwinkle E, Ballantyne C, Insull W, Jr., Schwartz RS, Vogel R, Serruys PW, Hansson GK, Faxon DP, Kaul S, Drexler H, Greenland P, Muller JE, Virmani R, Ridker PM, Zipes DP, Shah PK, Willerson JT. From vulnerable plaque to vulnerable patient: A call for new definitions and risk assessment strategies: Part ii. *Circulation*. 2003;108:1772-1778
15. Burleigh MC, Briggs AD, Lendon CL, Davies MJ, Born GV, Richardson PD. Collagen types i and iii, collagen content, gags and mechanical strength of human atherosclerotic plaque caps: Span-wise variations. *Atherosclerosis*. 1992;96:71-81
16. Owens GK. Regulation of differentiation of vascular smooth muscle cells. *Physiol Rev*. 1995;75:487-517
17. Rensen SS, Doevendans PA, van Eys GJ. Regulation and characteristics of vascular smooth muscle cell phenotypic diversity. *Neth Heart J*. 2007;15:100-108
18. Owens GK, Kumar MS, Wamhoff BR. Molecular regulation of vascular smooth muscle cell differentiation in development and disease. *Physiol Rev*. 2004;84:767-801

19. Raftopoulou M, Hall A. Cell migration: Rho gtpases lead the way. *Dev Biol*. 2004;265:23-32
20. Pasterkamp G, Schoneveld AH, Hijnen DJ, de Kleijn DP, Teepen H, van der Wal AC, Borst C. Atherosclerotic arterial remodeling and the localization of macrophages and matrix metalloproteases 1, 2 and 9 in the human coronary artery. *Atherosclerosis*. 2000;150:245-253
21. Faxon DP, Creager MA, Smith SC, Jr., Pasternak RC, Olin JW, Bettmann MA, Criqui MH, Milani RV, Loscalzo J, Kaufman JA, Jones DW, Pearce WH. Atherosclerotic vascular disease conference: Executive summary: Atherosclerotic vascular disease conference proceeding for healthcare professionals from a special writing group of the american heart association. *Circulation*. 2004;109:2595-2604
22. http://www.nhs.uk/conditions/atherosclerosis/Pages/Introduction.aspx. National health service: The public health impact of atherosclerosis. *Atherosclerosis*. 2012
23. Fletcher DA, Mullins RD. Cell mechanics and the cytoskeleton. *Nature*. 2010;463:485-492
24. Venticinque L, Jamieson KV, Meruelo D. Interactions between laminin receptor and the cytoskeleton during translation and cell motility. *PLoS One*. 2011;6:e15895
25. dos Remedios CG, Chhabra D, Kekic M, Dedova IV, Tsubakihara M, Berry DA, Nosworthy NJ. Actin binding proteins: Regulation of cytoskeletal microfilaments. *Physiol Rev*. 2003;83:433-473
26. Pollard TD, Borisy GG. Cellular motility driven by assembly and disassembly of actin filaments. *Cell*. 2003;112:453-465
27. Small JV, Rottner K, Kaverina I, Anderson KI. Assembling an actin cytoskeleton for cell attachment and movement. *Biochim Biophys Acta*. 1998;1404:271-281
28. Ananthakrishnan R, Ehrlicher A. The forces behind cell movement. *Int J Biol Sci*. 2007;3:303-317
29. Broussard JA, Webb DJ, Kaverina I. Asymmetric focal adhesion disassembly in motile cells. *Curr Opin Cell Biol*. 2008;20:85-90
30. Kirfel G, Rigort A, Borm B, Herzog V. Cell migration: Mechanisms of rear detachment and the formation of migration tracks. *Eur J Cell Biol*. 2004;83:717-724
31. Lee J, Ishihara A, Oxford G, Johnson B, Jacobson K. Regulation of cell movement is mediated by stretch-activated calcium channels. *Nature*. 1999;400:382-386
32. Yoshinaga-Ohara N, Takahashi A, Uchiyama T, Sasada M. Spatiotemporal regulation of moesin phosphorylation and rear release by rho and serine/threonine phosphatase during neutrophil migration. *Exp Cell Res*. 2002;278:112-122
33. Chrzanowska-Wodnicka M, Burridge K. Rho-stimulated contractility drives the formation of stress fibers and focal adhesions. *J Cell Biol*. 1996;133:1403-1415
34. Hall A, Nobes CD. Rho gtpases: Molecular switches that control the organization and dynamics of the actin cytoskeleton. *Philos Trans R Soc Lond B Biol Sci*. 2000;355:965-970
35. Carragher NO, Levkau B, Ross R, Raines EW. Degraded collagen fragments promote rapid disassembly of smooth muscle focal adhesions that correlates with cleavage of pp125(fak), paxillin, and talin. *J Cell Biol*. 1999;147:619-630
36. Dourdin N, Bhatt AK, Dutt P, Greer PA, Arthur JS, Elce JS, Huttenlocher A. Reduced cell migration and disruption of the actin cytoskeleton in calpain-deficient embryonic fibroblasts. *J Biol Chem*. 2001;276:48382-48388
37. Amano M, Chihara K, Kimura K, Fukata Y, Nakamura N, Matsuura Y, Kaibuchi K. Formation of actin stress fibers and focal adhesions enhanced by rho-kinase. *Science*. 1997;275:1308-1311

38. Bershadsky AD, Balaban NQ, Geiger B. Adhesion-dependent cell mechanosensitivity. *Annu Rev Cell Dev Biol*. 2003;19:677-695
39. Zaidel-Bar R, Itzkovitz S, Ma'ayan A, Iyengar R, Geiger B. Functional atlas of the integrin adhesome. *Nat Cell Biol*. 2007;9:858-867
40. Turner CE. Paxillin interactions. *J Cell Sci*. 2000;113 Pt 23:4139-4140
41. Zamir E, Geiger B. Molecular complexity and dynamics of cell-matrix adhesions. *J Cell Sci*. 2001;114:3583-3590
42. Wehrle-Haller B, Imhof B. The inner lives of focal adhesions. *Trends Cell Biol*. 2002;12:382-389
43. Pelham RJ, Jr., Wang Y. Cell locomotion and focal adhesions are regulated by substrate flexibility. *Proc Natl Acad Sci U S A*. 1997;94:13661-13665
44. Hu P, Luo BH. Integrin bi-directional signaling across the plasma membrane. *J Cell Physiol*. 2013;228:306-312
45. Hall A. Rho gtpases and the control of cell behaviour. *Biochem Soc Trans*. 2005;33:891-895
46. Geiger B, Bershadsky A. Assembly and mechanosensory function of focal contacts. *Curr Opin Cell Biol*. 2001;13:584-592
47. Gardel ML, Schneider IC, Aratyn-Schaus Y, Waterman CM. Mechanical integration of actin and adhesion dynamics in cell migration. *Annu Rev Cell Dev Biol*. 2010;26:315-333
48. Ciobanasu C, Faivre B, Le Clainche C. Actin dynamics associated with focal adhesions. *Int J Cell Biol*. 2012;2012:941292
49. Chen CS, Tan J, Tien J. Mechanotransduction at cell-matrix and cell-cell contacts. *Annu Rev Biomed Eng*. 2004;6:275-302
50. Phillips DR, Nannizzi-Alaimo L, Prasad KS. Beta3 tyrosine phosphorylation in alphaiibbeta3 (platelet membrane gp iib-iiia) outside-in integrin signaling. *Thromb Haemost*. 2001;86:246-258
51. Miyamoto S, Akiyama SK, Yamada KM. Synergistic roles for receptor occupancy and aggregation in integrin transmembrane function. *Science*. 1995;267:883-885
52. Schwartz MA, Ginsberg MH. Networks and crosstalk: Integrin signalling spreads. *Nat Cell Biol*. 2002;4:E65-68
53. Brown MC, Turner CE. Paxillin: Adapting to change. *Physiol Rev*. 2004;84:1315-1339
54. Humphries JD, Wang P, Streuli C, Geiger B, Humphries MJ, Ballestrem C. Vinculin controls focal adhesion formation by direct interactions with talin and actin. *J Cell Biol*. 2007;179:1043-1057
55. Hynes RO. Integrins: Versatility, modulation, and signaling in cell adhesion. *Cell*. 1992;69:11-25
56. Zhang X, Jiang G, Cai Y, Monkley SJ, Critchley DR, Sheetz MP. Talin depletion reveals independence of initial cell spreading from integrin activation and traction. *Nat Cell Biol*. 2008;10:1062-1068
57. Rao SS, Winter JO. Adhesion molecule-modified biomaterials for neural tissue engineering. *Frontiers in neuroengineering*. 2009;2:6
58. Grashoff C, Hoffman BD, Brenner MD, Zhou R, Parsons M, Yang MT, McLean MA, Sligar SG, Chen CS, Ha T, Schwartz MA. Measuring mechanical tension across vinculin reveals regulation of focal adhesion dynamics. *Nature*. 2010;466:263-266
59. Ziegler WH, Liddington RC, Critchley DR. The structure and regulation of vinculin. *Trends Cell Biol*. 2006;16:453-460
60. Carisey A, Ballestrem C. Vinculin, an adapter protein in control of cell adhesion signalling. *Eur J Cell Biol*. 2011;90:157-163
61. Mierke CT. The role of vinculin in the regulation of the mechanical properties of cells. *Cell Biochem Biophys*. 2009;53:115-126
62. Xu W, Baribault H, Adamson ED. Vinculin knockout results in heart and brain defects during embryonic development. *Development*. 1998;125:327-337

63. Alenghat FJ, Fabry B, Tsai KY, Goldmann WH, Ingber DE. Analysis of cell mechanics in single vinculin-deficient cells using a magnetic tweezer. *Biochem Biophys Res Commun*. 2000;277:93-99
64. Mierke CT, Kollmannsberger P, Zitterbart DP, Smith J, Fabry B, Goldmann WH. Mechano-coupling and regulation of contractility by the vinculin tail domain. *Biophys J*. 2008;94:661-670
65. le Duc Q, Shi Q, Blonk I, Sonnenberg A, Wang N, Leckband D, de Rooij J. Vinculin potentiates e-cadherin mechanosensing and is recruited to actin-anchored sites within adherens junctions in a myosin ii-dependent manner. *J Cell Biol*. 2010;189:1107-1115
66. Coll JL, Ben-Ze'ev A, Ezzell RM, Rodriguez Fernandez JL, Baribault H, Oshima RG, Adamson ED. Targeted disruption of vinculin genes in f9 and embryonic stem cells changes cell morphology, adhesion, and locomotion. *Proc Natl Acad Sci U S A*. 1995;92:9161-9165
67. Volberg T, Geiger B, Kam Z, Pankov R, Simcha I, Sabanay H, Coll JL, Adamson E, Ben-Ze'ev A. Focal adhesion formation by f9 embryonal carcinoma cells after vinculin gene disruption. *J Cell Sci*. 1995;108 (Pt 6):2253-2260
68. Saunders RM, Holt MR, Jennings L, Sutton DH, Barsukov IL, Bobkov A, Liddington RC, Adamson EA, Dunn GA, Critchley DR. Role of vinculin in regulating focal adhesion turnover. *Eur J Cell Biol*. 2006;85:487-500
69. Deakin NO, Turner CE. Paxillin comes of age. *J Cell Sci*. 2008;121:2435-2444
70. Schaller MD. Paxillin: A focal adhesion-associated adaptor protein. *Oncogene*. 2001;20:6459-6472
71. Sai X, Naruse K, Sokabe M. Activation of pp60(src) is critical for stretch-induced orienting response in fibroblasts. *J Cell Sci*. 1999;112 (Pt 9):1365-1373
72. Tomar A, Schlaepfer DD. Focal adhesion kinase: Switching between gaps and gefs in the regulation of cell motility. *Current Opinion in Cell Biology*. 2009;21:676-683
73. Iqbal J, Zaidi M. Molecular regulation of mechanotransduction. *Biochem Biophys Res Commun*. 2005;328:751-755
74. Friedl P, Wolf K. Plasticity of cell migration: A multiscale tuning model. *J Cell Biol*. 2010;188:11-19
75. Christiansen JJ, Rajasekaran AK. Reassessing epithelial to mesenchymal transition as a prerequisite for carcinoma invasion and metastasis. *Cancer Res*. 2006;66:8319-8326
76. Friedl P, Noble PB, Walton PA, Laird DW, Chauvin PJ, Tabah RJ, Black M, Zanker KS. Migration of coordinated cell clusters in mesenchymal and epithelial cancer explants in vitro. *Cancer Res*. 1995;55:4557-4560
77. Farooqui R, Fenteany G. Multiple rows of cells behind an epithelial wound edge extend cryptic lamellipodia to collectively drive cell-sheet movement. *J Cell Sci*. 2005;118:51-63
78. Arrieumerlou C, Meyer T. A local coupling model and compass parameter for eukaryotic chemotaxis. *Dev Cell*. 2005;8:215-227
79. Ridley AJ, Schwartz MA, Burridge K, Firtel RA, Ginsberg MH, Borisy G, Parsons JT, Horwitz AR. Cell migration: Integrating signals from front to back. *Science*. 2003;302:1704-1709
80. Friedl P, Weigelin B. Interstitial leukocyte migration and immune function. *Nat Immunol*. 2008;9:960-969
81. Friedl P, Borgmann S, Brocker EB. Amoeboid leukocyte crawling through extracellular matrix: Lessons from the dictyostelium paradigm of cell movement. *J Leukoc Biol*. 2001;70:491-509
82. Lammermann T, Sixt M. Mechanical modes of 'amoeboid' cell migration. *Curr Opin Cell Biol*. 2009;21:636-644
83. Kaye GI, Siegel LF, Pascal RR. Cell replication of mesenchymal elements in adult tissues. I. The replication and migration of mesenchymal cells in the adult rabbit dermis. *Anat Rec*. 1971;169:593-611

84. Grinnell F. Fibroblast mechanics in three-dimensional collagen matrices. *Journal of bodywork and movement therapies*. 2008;12:191-193
85. Friedl P, Gilmour D. Collective cell migration in morphogenesis, regeneration and cancer. *Nat Rev Mol Cell Biol*. 2009;10:445-457
86. Koutsouki E, Beeching CA, Slater SC, Blaschuk OW, Sala-Newby GB, George SJ. N-cadherin-dependent cell-cell contacts promote human saphenous vein smooth muscle cell survival. *Arterioscler Thromb Vasc Biol*. 2005;25:982-988
87. Lyon CA, Koutsouki E, Aguilera CM, Blaschuk OW, George SJ. Inhibition of n-cadherin retards smooth muscle cell migration and intimal thickening via induction of apoptosis. *J Vasc Surg*. 2010;52:1301-1309
88. Blindt R, Bosserhoff AK, Dammers J, Krott N, Demircan L, Hoffmann R, Hanrath P, Weber C, Vogt F. Downregulation of n-cadherin in the neointima stimulates migration of smooth muscle cells by rhoa deactivation. *Cardiovasc Res*. 2004;62:212-222
89. Lois C, Garcia-Verdugo JM, Alvarez-Buylla A. Chain migration of neuronal precursors. *Science*. 1996;271:978-981
90. McLennan R, Kulesa PM. In vivo analysis reveals a critical role for neuropilin-1 in cranial neural crest cell migration in chick. *Dev Biol*. 2007;301:227-239
91. Davis EM, Trinkaus JP. Significance of cell-to cell contacts for the directional movement of neural crest cells within a hydrated collagen lattice. *J Embryol Exp Morphol*. 1981;63:29-51
92. Teddy JM, Kulesa PM. In vivo evidence for short- and long-range cell communication in cranial neural crest cells. *Development*. 2004;131:6141-6151
93. Schultz J, Milpetz F, Bork P, Ponting CP. Smart, a simple modular architecture research tool: Identification of signaling domains. *Proc Natl Acad Sci U S A*. 1998;95:5857-5864
94. Van Aelst L, D'Souza-Schorey C. Rho gtpases and signaling networks. *Genes Dev*. 1997;11:2295-2322
95. Kjoller L, Hall A. Signaling to rho gtpases. *Exp Cell Res*. 1999;253:166-179
96. Lamarche N, Hall A. Gaps for rho-related gtpases. *Trends Genet*. 1994;10:436-440
97. Schmidt A, Hall A. Guanine nucleotide exchange factors for rho gtpases: Turning on the switch. *Genes Dev*. 2002;16:1587-1609
98. Moon SY, Zheng Y. Rho gtpase-activating proteins in cell regulation. *Trends Cell Biol*. 2003;13:13-22
99. Bishop AL, Hall A. Rho gtpases and their effector proteins. *Biochem J*. 2000;348 Pt 2:241-255
100. Schliwa M, Euteneuer U, Graf R, Ueda M. Centrosomes, microtubules and cell migration. *Biochem Soc Symp*. 1999;65:223-231
101. Etienne-Manneville S, Hall A. Rho gtpases in cell biology. *Nature*. 2002;420:629-635
102. Goley ED, Welch MD. The arp2/3 complex: An actin nucleator comes of age. *Nat Rev Mol Cell Biol*. 2006;7:713-726
103. Mullins RD, Heuser JA, Pollard TD. The interaction of arp2/3 complex with actin: Nucleation, high affinity pointed end capping, and formation of branching networks of filaments. *Proc Natl Acad Sci U S A*. 1998;95:6181-6186
104. Miki H, Sasaki T, Takai Y, Takenawa T. Induction of filopodium formation by a wasp-related actin-depolymerizing protein n-wasp. *Nature*. 1998;391:93-96
105. Machesky LM, Mullins RD, Higgs HN, Kaiser DA, Blanchoin L, May RC, Hall ME, Pollard TD. Scar, a wasp-related protein, activates nucleation of actin filaments by the arp2/3 complex. *Proc Natl Acad Sci U S A*. 1999;96:3739-3744
106. Mogilner A, Keren K. The shape of motile cells. *Curr Biol*. 2009;19:R762-771
107. Edwards DC, Sanders LC, Bokoch GM, Gill GN. Activation of lim-kinase by pak1 couples rac/cdc42 gtpase signalling to actin cytoskeletal dynamics. *Nat Cell Biol*. 1999;1:253-259

108. Kordowska J, Hetrick T, Adam LP, Wang CL. Phosphorylated l-caldesmon is involved in disassembly of actin stress fibers and postmitotic spreading. *Exp Cell Res*. 2006;312:95-110
109. Webb BA, Zhou S, Eves R, Shen L, Jia L, Mak AS. Phosphorylation of cortactin by p21-activated kinase. *Arch Biochem Biophys*. 2006;456:183-193
110. Romero S, Le Clainche C, Didry D, Egile C, Pantaloni D, Carlier MF. Formin is a processive motor that requires profilin to accelerate actin assembly and associated atp hydrolysis. *Cell*. 2004;119:419-429
111. Xu Y, Moseley JB, Sagot I, Poy F, Pellman D, Goode BL, Eck MJ. Crystal structures of a formin homology-2 domain reveal a tethered dimer architecture. *Cell*. 2004;116:711-723
112. Okada K, Bartolini F, Deaconescu AM, Moseley JB, Dogic Z, Grigorieff N, Gundersen GG, Goode BL. Adenomatous polyposis coli protein nucleates actin assembly and synergizes with the formin mdia1. *J Cell Biol*. 2010;189:1087-1096
113. Kawano Y, Fukata Y, Oshiro N, Amano M, Nakamura T, Ito M, Matsumura F, Inagaki M, Kaibuchi K. Phosphorylation of myosin-binding subunit (mbs) of myosin phosphatase by rho-kinase in vivo. *J Cell Biol*. 1999;147:1023-1038
114. Clark K, Langeslag M, Figdor CG, van Leeuwen FN. Myosin ii and mechanotransduction: A balancing act. *Trends in Cell Biology*. 2007;17:178-186
115. Van Eyk JE, Arrell DK, Foster DB, Strauss JD, Heinonen TY, Furmaniak-Kazmierczak E, Cote GP, Mak AS. Different molecular mechanisms for rho family gtpase-dependent, ca2+-independent contraction of smooth muscle. *J Biol Chem*. 1998;273:23433-23439
116. Maekawa M, Ishizaki T, Boku S, Watanabe N, Fujita A, Iwamatsu A, Obinata T, Ohashi K, Mizuno K, Narumiya S. Signaling from rho to the actin cytoskeleton through protein kinases rock and lim-kinase. *Science*. 1999;285:895-898
117. Feng J, Ito M, Kureishi Y, Ichikawa K, Amano M, Isaka N, Okawa K, Iwamatsu A, Kaibuchi K, Hartshorne DJ, Nakano T. Rho-associated kinase of chicken gizzard smooth muscle. *J Biol Chem*. 1999;274:3744-3752
118. Araki S, Ito M, Kureishi Y, Feng J, Machida H, Isaka N, Amano M, Kaibuchi K, Hartshorne DJ, Nakano T. Arachidonic acid-induced ca2+ sensitization of smooth muscle contraction through activation of rho-kinase. *Pflugers Arch*. 2001;441:596-603
119. Kitazawa T, Eto M, Woodsome TP, Brautigan DL. Agonists trigger g protein-mediated activation of the cpi-17 inhibitor phosphoprotein of myosin light chain phosphatase to enhance vascular smooth muscle contractility. *J Biol Chem*. 2000;275:9897-9900
120. Koyama M, Ito M, Feng J, Seko T, Shiraki K, Takase K, Hartshorne DJ, Nakano T. Phosphorylation of cpi-17, an inhibitory phosphoprotein of smooth muscle myosin phosphatase, by rho-kinase. *FEBS Lett*. 2000;475:197-200
121. Kaneko T, Amano M, Maeda A, Goto H, Takahashi K, Ito M, Kaibuchi K. Identification of calponin as a novel substrate of rho-kinase. *Biochem Biophys Res Commun*. 2000;273:110-116
122. Dessy C, Kim I, Sougnez CL, Laporte R, Morgan KG. A role for map kinase in differentiated smooth muscle contraction evoked by alpha-adrenoceptor stimulation. *The American journal of physiology*. 1998;275:C1081-1086
123. Bhattacharya B, Roberts RE. Enhancement of alpha2-adrenoceptor-mediated vasoconstriction by the thromboxane-mimetic u46619 in the porcine isolated ear artery: Role of the erk-map kinase signal transduction cascade. *Br J Pharmacol*. 2003;139:156-162
124. Florian JA, Watts SW. Integration of mitogen-activated protein kinase kinase activation in vascular 5-hydroxytryptamine2a receptor signal transduction. *The Journal of pharmacology and experimental therapeutics*. 1998;284:346-355

125. Roberts RE. Role of the extracellular signal-regulated kinase (erk) signal transduction cascade in alpha(2) adrenoceptor-mediated vasoconstriction in porcine palmar lateral vein. *Br J Pharmacol*. 2001;133:859-866
126. Morgan KG, Gangopadhyay SS. Invited review: Cross-bridge regulation by thin filament-associated proteins. *Journal of applied physiology*. 2001;91:953-962
127. Zhou Z, Du X, Cai Z, Song X, Zhang H, Mizuno T, Suzuki E, Yee MR, Berezov A, Murali R, Wu SL, Karger BL, Greene MI, Wang Q. Structure of sad1-unc84 homology (sun) domain defines features of molecular bridge in nuclear envelope. *J Biol Chem*. 2012;287:5317-5326
128. Crisp M, Liu Q, Roux K, Rattner JB, Shanahan C, Burke B, Stahl PD, Hodzic D. Coupling of the nucleus and cytoplasm: Role of the linc complex. *J Cell Biol*. 2006;172:41-53
129. Starr DA, Fischer JA. Kash 'n karry: The kash domain family of cargo-specific cytoskeletal adaptor proteins. *Bioessays*. 2005;27:1136-1146
130. Haque F, Lloyd DJ, Smallwood DT, Dent CL, Shanahan CM, Fry AM, Trembath RC, Shackleton S. Sun1 interacts with nuclear lamin a and cytoplasmic nesprins to provide a physical connection between the nuclear lamina and the cytoskeleton. *Mol Cell Biol*. 2006;26:3738-3751
131. Banes AJ, Link GW, Jr., Gilbert JW, Tran Son Tay R, Monbureau O. Culturing cells in a mechanically active environment. *Am Biotechnol Lab*. 1990;8:12-22
132. Katsumi A, Orr AW, Tzima E, Schwartz MA. Integrins in mechanotransduction. *J Biol Chem*. 2004;279:12001-12004
133. Salina D, Bodoor K, Enarson P, Raharjo WH, Burke B. Nuclear envelope dynamics. *Biochem Cell Biol*. 2001;79:533-542
134. Schirmer EC, Florens L, Guan T, Yates JR, 3rd, Gerace L. Nuclear membrane proteins with potential disease links found by subtractive proteomics. *Science*. 2003;301:1380-1382
135. Holmer L, Worman HJ. Inner nuclear membrane proteins: Functions and targeting. *Cellular and molecular life sciences : CMLS*. 2001;58:1741-1747
136. Lusk CP, Blobel G, King MC. Highway to the inner nuclear membrane: Rules for the road. *Nat Rev Mol Cell Bio*. 2007;8:414-420
137. Ohba T, Schirmer EC, Nishimoto T, Gerace L. Energy- and temperature-dependent transport of integral proteins to the inner nuclear membrane via the nuclear pore. *Journal of Cell Biology*. 2004;167:1051-1062
138. Young SG, Fong LG, Michaelis S. Prelamin a, zmpste24, misshapen cell nuclei, and progeria--new evidence suggesting that protein farnesylation could be important for disease pathogenesis. *J Lipid Res*. 2005;46:2531-2558
139. Rusinol AE, Sinensky MS. Farnesylated lamins, progeroid syndromes and farnesyl transferase inhibitors. *J Cell Sci*. 2006;119:3265-3272
140. Corrigan DP, Kuszczak D, Rusinol AE, Thewke DP, Hrycyna CA, Michaelis S, Sinensky MS. Prelamin a endoproteolytic processing in vitro by recombinant zmpste24. *Biochem J*. 2005;387:129-138
141. Kudlow BA, Kennedy BK, Monnat RJ, Jr. Werner and hutchinson-gilford progeria syndromes: Mechanistic basis of human progeroid diseases. *Nat Rev Mol Cell Biol*. 2007;8:394-404
142. Abrantes AM, Serra ME, Goncalves AC, Rio J, Oliveiros B, Laranjo M, Rocha-Gonsalves AM, Sarmento-Ribeiro AB, Botelho MF. Hypoxia-induced redox alterations and their correlation with 99mtc-mibi and 99mtc-hl-91 uptake in colon cancer cells. *Nucl Med Biol*. 2010;37:125-132
143. Dechat T, Pfleghaar K, Sengupta K, Shimi T, Shumaker DK, Solimando L, Goldman RD. Nuclear lamins: Major factors in the structural organization and function of the nucleus and chromatin. *Genes Dev*. 2008;22:832-853
144. Shanahan CM, Weissberg PL, Metcalfe JC. Isolation of gene markers of differentiated and proliferating vascular smooth muscle cells. *Circ Res*. 1993;73:193-204

145. Zhang Q, Skepper JN, Yang F, Davies JD, Hegyi L, Roberts RG, Weissberg PL, Ellis JA, Shanahan CM. Nesprins: A novel family of spectrin-repeat-containing proteins that localize to the nuclear membrane in multiple tissues. *J Cell Sci*. 2001;114:4485-4498
146. Rajgor D, Shanahan CM. Nesprins: From the nuclear envelope and beyond. *Expert reviews in molecular medicine*. 2013;15:e5
147. Zhang Q, Ragnauth C, Greener MJ, Shanahan CM, Roberts RG. The nesprins are giant actin-binding proteins, orthologous to drosophila melanogaster muscle protein msp-300. *Genomics*. 2002;80:473-481
148. Wilhelmsen K, Litjens SH, Kuikman I, Tshimbalanga N, Janssen H, van den Bout I, Raymond K, Sonnenberg A. Nesprin-3, a novel outer nuclear membrane protein, associates with the cytoskeletal linker protein plectin. *J Cell Biol*. 2005;171:799-810
149. Roux KJ, Crisp ML, Liu Q, Kim D, Kozlov S, Stewart CL, Burke B. Nesprin 4 is an outer nuclear membrane protein that can induce kinesin-mediated cell polarization. *Proc Natl Acad Sci U S A*. 2009;106:2194-2199
150. Zhang Q, Bethmann C, Worth NF, Davies JD, Wasner C, Feuer A, Ragnauth CD, Yi Q, Mellad JA, Warren DT, Wheeler MA, Ellis JA, Skepper JN, Vorgerd M, Schlotter-Weigel B, Weissberg PL, Roberts RG, Wehnert M, Shanahan CM. Nesprin-1 and -2 are involved in the pathogenesis of emery dreifuss muscular dystrophy and are critical for nuclear envelope integrity. *Hum Mol Genet*. 2007;16:2816-2833
151. Mellad JA, Warren DT, Shanahan CM. Nesprins linc the nucleus and cytoskeleton. *Curr Opin Cell Biol*. 2011;23:47-54
152. Rajgor D, Mellad JA, Autore F, Zhang Q, Shanahan CM. Multiple novel nesprin-1 and nesprin-2 variants act as versatile tissue-specific intracellular scaffolds. *PLoS One*. 2012;7:e40098
153. Dawe HR, Adams M, Wheway G, Szymanska K, Logan CV, Noegel AA, Gull K, Johnson CA. Nesprin-2 interacts with meckelin and mediates ciliogenesis via remodelling of the actin cytoskeleton. *J Cell Sci*. 2009;122:2716-2726
154. Zhang Q, Ragnauth CD, Skepper JN, Worth NF, Warren DT, Roberts RG, Weissberg PL, Ellis JA, Shanahan CM. Nesprin-2 is a multi-isomeric protein that binds lamin and emerin at the nuclear envelope and forms a subcellular network in skeletal muscle. *J Cell Sci*. 2005;118:673-687
155. Mislow JMK, Holaska JM, Kim MS, Lee KK, Segura-Totten M, Wilson KL, McNally EM. Nesprin-1 alpha self-associates and binds directly to emerin and lamin a in vitro. *Febs Letters*. 2002;525:135-140
156. Sosa BA, Rothballer A, Kutay U, Schwartz TU. Linc complexes form by binding of three kash peptides to domain interfaces of trimeric sun proteins. *Cell*. 2012;149:1035-1047
157. Haque F, Mazzeo D, Patel JT, Smallwood DT, Ellis JA, Shanahan CM, Shackleton S. Mammalian sun protein interaction networks at the inner nuclear membrane and their role in laminopathy disease processes. *J Biol Chem*. 2010;285:3487-3498
158. Padmakumar VC, Libotte T, Lu W, Zaim H, Abraham S, Noegel AA, Gotzmann J, Foisner R, Karakesisoglou I. The inner nuclear membrane protein sun1 mediates the anchorage of nesprin-2 to the nuclear envelope. *J Cell Sci*. 2005;118:3419-3430
159. Schmitt J, Benavente R, Hodzic D, Hoog C, Stewarts CL, Alsheimer M. Transmembrane protein sun2 is involved in tethering mammalian meiotic telomeres to the nuclear envelope. *P Natl Acad Sci USA*. 2007;104:7426-7431
160. Xiong HJ, Rivero F, Euteneuer U, Mondal S, Mana-Capelli S, Larochelle D, Vogel A, Gassen B, Noegel AA. Dictyostelium sun-1 connects the centrosome to chromatin and ensures genome stability. *Traffic*. 2008;9:708-724

161. Poh YC, Shevtsov SP, Chowdhury F, Wu DC, Na S, Dundr M, Wang N. Dynamic force-induced direct dissociation of protein complexes in a nuclear body in living cells. *Nat Commun*. 2012;3:866
162. Taranum S, Vaylann E, Meinke P, Abraham S, Yang L, Neumann S, Karakesisoglou I, Wehnert M, Noegel AA. Linc complex alterations in dmd and edmd/cmt fibroblasts. *Eur J Cell Biol*. 2012;91:614-628
163. Ostlund C, Folker ES, Choi JC, Gomes ER, Gundersen GG, Worman HJ. Dynamics and molecular interactions of linker of nucleoskeleton and cytoskeleton (linc) complex proteins. *J Cell Sci*. 2009;122:4099-4108
164. Wang N, Tytell JD, Ingber DE. Mechanotransduction at a distance: Mechanically coupling the extracellular matrix with the nucleus. *Nat Rev Mol Cell Biol*. 2009;10:75-82
165. Lombardi ML, Jaalouk DE, Shanahan CM, Burke B, Roux KJ, Lammerding J. The interaction between nesprins and sun proteins at the nuclear envelope is critical for force transmission between the nucleus and cytoskeleton. *J Biol Chem*. 2011;286:26743-26753
166. Padmakumar VC, Abraham S, Braune S, Noegel AA, Tunggal B, Karakesisoglou I, Korenbaum E. Enaptin, a giant actin-binding protein, is an element of the nuclear membrane and the actin cytoskeleton. *Exp Cell Res*. 2004;295:330-339
167. Zhen YY, Libotte T, Munck M, Noegel AA, Korenbaum E. Nuance, a giant protein connecting the nucleus and actin cytoskeleton. *J Cell Sci*. 2002;115:3207-3222
168. Lu WS, Schneider M, Neumann S, Jaeger VM, Taranum S, Munck M, Cartwright S, Richardson C, Carthew J, Noh K, Goldberg M, Noegel AA, Karakesisoglou I. Nesprin interchain associations control nuclear size. *Cellular and Molecular Life Sciences*. 2012;69:3493-3509
169. Randles KN, Lam le T, Sewry CA, Puckelwartz M, Furling D, Wehnert M, McNally EM, Morris GE. Nesprins, but not sun proteins, switch isoforms at the nuclear envelope during muscle development. *Dev Dyn*. 2010;239:998-1009
170. Puckelwartz MJ, Kessler E, Zhang YA, Hodzic D, Randles KN, Morris G, Earley JU, Hadhazy M, Holaska JM, Mewborn SK, Pytel P, McNally EM. Disruption of nesprin-1 produces an emery dreifuss muscular dystrophy-like phenotype in mice. *Human Molecular Genetics*. 2009;18:607-620
171. Somech R, Shaklai S, Amariglio N, Rechavi G, Simon AJ. Nuclear envelopathies--raising the nuclear veil. *Pediatr Res*. 2005;57:8R-15R
172. Hale CM, Shrestha AL, Khatau SB, Stewart-Hutchinson PJ, Hernandez L, Stewart CL, Hodzic D, Wirtz D. Dysfunctional connections between the nucleus and the actin and microtubule networks in laminopathic models. *Biophys J*. 2008;95:5462-5475
173. Merideth MA, Gordon LB, Clauss S, Sachdev V, Smith AC, Perry MB, Brewer CC, Zalewski C, Kim HJ, Solomon B, Brooks BP, Gerber LH, Turner ML, Domingo DL, Hart TC, Graf J, Reynolds JC, Gropman A, Yanovski JA, Gerhard-Herman M, Collins FS, Nabel EG, Cannon RO, 3rd, Gahl WA, Introne WJ. Phenotype and course of hutchinson-gilford progeria syndrome. *N Engl J Med*. 2008;358:592-604
174. Eriksson M, Brown WT, Gordon LB, Glynn MW, Singer J, Scott L, Erdos MR, Robbins CM, Moses TY, Berglund P, Dutra A, Pak E, Durkin S, Csoka AB, Boehnke M, Glover TW, Collins FS. Recurrent de novo point mutations in lamin a cause hutchinson-gilford progeria syndrome. *Nature*. 2003;423:293-298
175. Gordon LB, Brown WT, Collins FS. Hutchinson-gilford progeria syndrome. In: Pagon RA, Adam MP, Bird TD, Dolan CR, Fong CT, Stephens K, eds. *Genereviews*. Seattle (WA); 1993.
176. Chen L, Lee L, Kudlow BA, Dos Santos HG, Sletvold O, Shafeghati Y, Botha EG, Garg A, Hanson NB, Martin GM, Mian IS, Kennedy BK, Oshima J. Lmna mutations in atypical werner's syndrome. *Lancet*. 2003;362:440-445

177. Doh YJ, Kim HK, Jung ED, Choi SH, Kim JG, Kim BW, Lee IK. Novel lmna gene mutation in a patient with atypical werner's syndrome. *The Korean journal of internal medicine*. 2009;24:68-72
178. Helbling-Leclerc A, Bonne G, Schwartz K. Emery-dreifuss muscular dystrophy. *Eur J Hum Genet*. 2002;10:157-161
179. Raffaele Di Barletta M, Ricci E, Galluzzi G, Tonali P, Mora M, Morandi L, Romorini A, Voit T, Orstavik KH, Merlini L, Trevisan C, Biancalana V, Housmanowa-Petrusewicz I, Bione S, Ricotti R, Schwartz K, Bonne G, Toniolo D. Different mutations in the lmna gene cause autosomal dominant and autosomal recessive emery-dreifuss muscular dystrophy. *American journal of human genetics*. 2000;66:1407-1412
180. Bonne G, Di Barletta MR, Varnous S, Becane HM, Hammouda EH, Merlini L, Muntoni F, Greenberg CR, Gary F, Urtizberea JA, Duboc D, Fardeau M, Toniolo D, Schwartz K. Mutations in the gene encoding lamin a/c cause autosomal dominant emery-dreifuss muscular dystrophy. *Nature genetics*. 1999;21:285-288
181. Brodsky GL, Muntoni F, Miocic S, Sinagra G, Sewry C, Mestroni L. Lamin a/c gene mutation associated with dilated cardiomyopathy with variable skeletal muscle involvement. *Circulation*. 2000;101:473-476
182. Puckelwartz MJ, Kessler EJ, Kim G, Dewitt MM, Zhang Y, Earley JU, Depreux FF, Holaska J, Mewborn SK, Pytel P, McNally EM. Nesprin-1 mutations in human and murine cardiomyopathy. *J Mol Cell Cardiol*. 2010;48:600-608
183. Fatkin D, MacRae C, Sasaki T, Wolff MR, Porcu M, Frenneaux M, Atherton J, Vidaillet HJ, Jr., Spudich S, De Girolami U, Seidman JG, Seidman C, Muntoni F, Muehle G, Johnson W, McDonough B. Missense mutations in the rod domain of the lamin a/c gene as causes of dilated cardiomyopathy and conduction-system disease. *N Engl J Med*. 1999;341:1715-1724
184. Hegele RA, Cao H, Frankowski C, Mathews ST, Leff T. Pparg f388l, a transactivation-deficient mutant, in familial partial lipodystrophy. *Diabetes*. 2002;51:3586-3590
185. Shackleton S, Lloyd DJ, Jackson SN, Evans R, Niermeijer MF, Singh BM, Schmidt H, Brabant G, Kumar S, Durrington PN, Gregory S, O'Rahilly S, Trembath RC. Lmna, encoding lamin a/c, is mutated in partial lipodystrophy. *Nature genetics*. 2000;24:153-156
186. Lammerding J, Schulze PC, Takahashi T, Kozlov S, Sullivan T, Kamm RD, Stewart CL, Lee RT. Lamin a/c deficiency causes defective nuclear mechanics and mechanotransduction. *J Clin Invest*. 2004;113:370-378
187. Lee JS, Hale CM, Panorchan P, Khatau SB, George JP, Tseng Y, Stewart CL, Hodzic D, Wirtz D. Nuclear lamin a/c deficiency induces defects in cell mechanics, polarization, and migration. *Biophys J*. 2007;93:2542-2552
188. Emerson LJ, Holt MR, Wheeler MA, Wehnert M, Parsons M, Ellis JA. Defects in cell spreading and erk1/2 activation in fibroblasts with lamin a/c mutations. *Biochim Biophys Acta*. 2009;1792:810-821
189. Broers JL, Peeters EA, Kuijpers HJ, Endert J, Bouten CV, Oomens CW, Baaijens FP, Ramaekers FC. Decreased mechanical stiffness in lmna-/- cells is caused by defective nucleo-cytoskeletal integrity: Implications for the development of laminopathies. *Hum Mol Genet*. 2004;13:2567-2580
190. Zhang JL, Felder A, Liu YJ, Guo LT, Lange S, Dalton ND, Gu YS, Peterson KL, Mizisin AP, Shelton GD, Lieber RL, Chen J. Nesprin 1 is critical for nuclear positioning and anchorage. *Human Molecular Genetics*. 2010;19:329-341
191. Stewart-Hutchinson PJ, Hale CM, Wirtz D, Hodzic D. Structural requirements for the assembly of linc complexes and their function in cellular mechanical stiffness. *Exp Cell Res*. 2008;314:1892-1905
192. Olson EN, Nordheim A. Linking actin dynamics and gene transcription to drive cellular motile functions. *Nat Rev Mol Cell Biol*. 2010;11:353-365

193. Ho CY, Jaalouk DE, Vartiainen MK, Lammerding J. Lamin a/c and emerin regulate mkl1-srf activity by modulating actin dynamics. *Nature*. 2013;497:507-511
194. Khatau SB, Hale CM, Stewart-Hutchinson PJ, Patel MS, Stewart CL, Searson PC, Hodzic D, Wirtz D. A perinuclear actin cap regulates nuclear shape. *Proc Natl Acad Sci U S A*. 2009;106:19017-19022
195. Kim DH, Khatau SB, Feng Y, Walcott S, Sun SX, Longmore GD, Wirtz D. Actin cap associated focal adhesions and their distinct role in cellular mechanosensing. *Scientific reports*. 2012;2:555
196. Houben F, Willems CH, Declercq IL, Hochstenbach K, Kamps MA, Snoeckx LH, Ramaekers FC, Broers JL. Disturbed nuclear orientation and cellular migration in a-type lamin deficient cells. *Biochim Biophys Acta*. 2009;1793:312-324
197. Maniotis AJ, Chen CS, Ingber DE. Demonstration of mechanical connections between integrins, cytoskeletal filaments, and nucleoplasm that stabilize nuclear structure. *Proc Natl Acad Sci U S A*. 1997;94:849-854
198. Lakatta EG. Arterial and cardiac aging: Major shareholders in cardiovascular disease enterprises: Part iii: Cellular and molecular clues to heart and arterial aging. *Circulation*. 2003;107:490-497
199. Wissler RW, Robert L. Aging and cardiovascular disease: A summary of the eighth munster international arteriosclerosis symposium. *Circulation*. 1996;93:1608-1612
200. Yang XP, Pei ZH, Ren J. Making up or breaking up: The tortuous role of platelet-derived growth factor in vascular ageing. *Clin Exp Pharmacol Physiol*. 2009;36:739-747
201. Kirkwood TB. Understanding the odd science of aging. *Cell*. 2005;120:437-447
202. Dyer CA, Sinclair AJ. The premature ageing syndromes: Insights into the ageing process. *Age Ageing*. 1998;27:73-80
203. Hayflick L. Current theories of biological aging. *Fed Proc*. 1975;34:9-13
204. Ragnauth CD, Warren DT, Liu Y, McNair R, Tajsic T, Figg N, Shroff R, Skepper J, Shanahan CM. Prelamin a acts to accelerate smooth muscle cell senescence and is a novel biomarker of human vascular aging. *Circulation*. 2010;121:2200-2210
205. Minamino T, Komuro I. Vascular cell senescence: Contribution to atherosclerosis. *Circ Res*. 2007;100:15-26
206. Liu GH, Barkho BZ, Ruiz S, Diep D, Qu J, Yang SL, Panopoulos AD, Suzuki K, Kurian L, Walsh C, Thompson J, Boue S, Fung HL, Sancho-Martinez I, Zhang K, Yates J, 3rd, Izpisua Belmonte JC. Recapitulation of premature ageing with ipscs from hutchinson-gilford progeria syndrome. *Nature*. 2011;472:221-225
207. Kovacic JC, Moreno P, Hachinski V, Nabel EG, Fuster V. Cellular senescence, vascular disease, and aging: Part 1 of a 2-part review. *Circulation*. 2011;123:1650-1660
208. O'Brien ER, Alpers CE, Stewart DK, Ferguson M, Tran N, Gordon D, Benditt EP, Hinohara T, Simpson JB, Schwartz SM. Proliferation in primary and restenotic coronary atherectomy tissue. Implications for antiproliferative therapy. *Circ Res*. 1993;73:223-231
209. Saito H, Papaconstantinou J. Age-associated differences in cardiovascular inflammatory gene induction during endotoxic stress. *J Biol Chem*. 2001;276:29307-29312
210. Yamamoto K, Takeshita K, Shimokawa T, Yi H, Isobe K, Loskutoff DJ, Saito H. Plasminogen activator inhibitor-1 is a major stress-regulated gene: Implications for stress-induced thrombosis in aged individuals. *P Natl Acad Sci USA*. 2002;99:890-895
211. Zeng GY, McCue HM, Mastrangelo L, Millis AJT. Endogenous tgf-beta activity is modified during cellular aging: Effects on metalloproteinase and timp-1 expression. *Experimental Cell Research*. 1996;228:271-276

212. Wilkinson IB, McEniery CM. Arterial stiffness, endothelial function and novel pharmacological approaches. *Clin Exp Pharmacol Physiol*. 2004;31:795-799
213. Lee HW, Karam J, Hussain B, Winer N. Vascular compliance in hypertension: Therapeutic implications. *Current diabetes reports*. 2008;8:208-213
214. Kalra SS, Shanahan CM. Vascular calcification and hypertension: Cause and effect. *Annals of medicine*. 2012;44 Suppl 1:S85-92
215. Izzo JL, Jr., Shykoff BE. Arterial stiffness: Clinical relevance, measurement, and treatment. *Rev Cardiovasc Med*. 2001;2:29-34, 37-40
216. Orlandi A, Marcellini M, Spagnoli LG. Aging influences development and progression of early aortic atherosclerotic lesions in cholesterol-fed rabbits. *Arterioscler Thromb Vasc Biol*. 2000;20:1123-1136
217. Ferlosio A, Arcuri G, Doldo E, Scioli MG, De Falco S, Spagnoli LG, Orlandi A. Age-related increase of stem marker expression influences vascular smooth muscle cell properties. *Atherosclerosis*. 2012;224:51-57
218. Ruiz-Torres A, Lozano R, Melon J, Carraro R. Age-dependent decline of in vitro migration (basal and stimulated by igf-1 or insulin) of human vascular smooth muscle cells. *J Gerontol A Biol Sci Med Sci*. 2003;58:B1074-1077
219. Werth D, Grassi G, Konjer N, Dapas B, Farra R, Giansante C, Kandolf R, Guarnieri G, Nordheim A, Heidenreich O. Proliferation of human primary vascular smooth muscle cells depends on serum response factor. *Eur J Cell Biol*. 2010;89:216-224
220. Li ZH, Cheng HP, Lederer WJ, Froehlich J, Lakatta EG. Enhanced proliferation and migration and altered cytoskeletal proteins in early passage smooth muscle cells from young and old rat aortic explants. *Exp Mol Pathol*. 1997;64:1-11
221. Moon SK, Cha BY, Kim CH. In vitro cellular aging is associated with enhanced proliferative capacity, g1 cell cycle modulation, and matrix metalloproteinase-9 regulation in mouse aortic smooth muscle cells. *Arch Biochem Biophys*. 2003;418:39-48
222. McCaffrey TA, Nicholson AC, Szabo PE, Weksler ME, Weksler BB. Aging and arteriosclerosis. The increased proliferation of arterial smooth muscle cells isolated from old rats is associated with increased platelet-derived growth factor-like activity. *J Exp Med*. 1988;167:163-174
223. Bochaton-Piallat ML, Gabbiani F, Ropraz P, Gabbiani G. Age influences the replicative activity and the differentiation features of cultured rat aortic smooth muscle cell populations and clones. *Arteriosclerosis and thrombosis : a journal of vascular biology / American Heart Association*. 1993;13:1449-1455
224. Gennaro G, Menard C, Giasson E, Michaud SE, Palasis M, Meloche S, Rivard A. Role of p44/p42 map kinase in the age-dependent increase in vascular smooth muscle cell proliferation and neointimal formation. *Arterioscler Thromb Vasc Biol*. 2003;23:204-210
225. Ross R. Atherosclerosis is an inflammatory disease. *Am Heart J*. 1999;138:S419-420
226. Gruenbaum Y, Margalit A, Goldman RD, Shumaker DK, Wilson KL. The nuclear lamina comes of age. *Nat Rev Mol Cell Biol*. 2005;6:21-31
227. De Sandre-Giovannoli A, Bernard R, Cau P, Navarro C, Amiel J, Boccaccio I, Lyonnet S, Stewart CL, Munnich A, Le Merrer M, Levy N. Lamin a truncation in hutchinson-gilford progeria. *Science*. 2003;300:2055
228. Denecke J, Brune T, Feldhaus T, Robenek H, Kranz C, Auchus RJ, Agarwal AK, Marquardt T. A homozygous zmpste24 null mutation in combination with a heterozygous mutation in the lmna gene causes hutchinson-gilford progeria syndrome (hgps): Insights into the pathophysiology of hgps. *Hum Mutat*. 2006;27:524-531
229. Shackleton S, Smallwood DT, Clayton P, Wilson LC, Agarwal AK, Garg A, Trembath RC. Compound heterozygous zmpste24 mutations reduce prelamin a processing and result in a severe progeroid phenotype. *Journal of medical genetics*. 2005;42:e36

230. Goldman RD, Shumaker DK, Erdos MR, Eriksson M, Goldman AE, Gordon LB, Gruenbaum Y, Khuon S, Mendez M, Varga R, Collins FS. Accumulation of mutant lamin a causes progressive changes in nuclear architecture in hutchinson-gilford progeria syndrome. *Proc Natl Acad Sci U S A*. 2004;101:8963-8968
231. Scaffidi P, Misteli T. Reversal of the cellular phenotype in the premature aging disease hutchinson-gilford progeria syndrome. *Nat Med*. 2005;11:440-445
232. Huang S, Risques RA, Martin GM, Rabinovitch PS, Oshima J. Accelerated telomere shortening and replicative senescence in human fibroblasts overexpressing mutant and wild-type lamin a. *Experimental Cell Research*. 2008;314:82-91
233. Dimauro T, David G. Chromatin modifications: The driving force of senescence and aging? *Aging (Albany NY)*. 2009;1:182-190
234. Dechat T, Shimi T, Adam SA, Rusinol AE, Andres DA, Spielmann HP, Sinensky MS, Goldman RD. Alterations in mitosis and cell cycle progression caused by a mutant lamin a known to accelerate human aging. *Proc Natl Acad Sci U S A*. 2007;104:4955-4960
235. Yang SH, Bergo MO, Toth JI, Qiao X, Hu Y, Sandoval S, Meta M, Bendale P, Gelb MH, Young SG, Fong LG. Blocking protein farnesyltransferase improves nuclear blebbing in mouse fibroblasts with a targeted hutchinson-gilford progeria syndrome mutation. *P Natl Acad Sci USA*. 2005;102:10291-10296
236. McClintock D, Gordon LB, Djabali K. Hutchinson-gilford progeria mutant lamin a primarily targets human vascular cells as detected by an anti-lamin a g608g antibody. *Proc Natl Acad Sci U S A*. 2006;103:2154-2159
237. Varga R, Eriksson M, Erdos MR, Olive M, Harten I, Kolodgie F, Capell BC, Cheng J, Faddah D, Perkins S, Avallone H, San H, Qu X, Ganesh S, Gordon LB, Virmani R, Wight TN, Nabel EG, Collins FS. Progressive vascular smooth muscle cell defects in a mouse model of hutchinson-gilford progeria syndrome. *Proc Natl Acad Sci U S A*. 2006;103:3250-3255
238. Olive M, Harten I, Mitchell R, Beers J, Djabali K, Cao K, Erdos MR, Blair C, Funke B, Smoot L, Gerhard-Herman M, Machan JT, Kutys R, Virmani R, Collins FS, Wight TN, Nabel EG, Gordon LB. Cardiovascular pathology in hutchinson-gilford progeria: Correlation with the vascular pathology of aging. *Arterioscler Thromb Vasc Biol*. 2010
239. Bergo MO, Gavino B, Ross J, Schmidt WK, Hong C, Kendall LV, Mohr A, Meta M, Genant H, Jiang YB, Wisner ER, van Bruggen N, Carano RAD, Michaelis S, Griffey SM, Young SG. Zmpste24 deficiency in mice causes spontaneous bone fractures, muscle weakness, and a prelamin a processing defect. *P Natl Acad Sci USA*. 2002;99:13049-13054
240. Jackson AL, Burchard J, Leake D, Reynolds A, Schelter J, Guo J, Johnson JM, Lim L, Karpilow J, Nichols K, Marshall W, Khvorova A, Linsley PS. Position-specific chemical modification of sirnas reduces "off-target" transcript silencing. *Rna*. 2006;12:1197-1205
241. Brown D, Byrom M, Krebs J, Kelnar K, Jarvis R, Campbell A, Ford L. Screening with small interfering rnas (sirnas) is an important method for identifying genes involved in biological pathways. 2014;2014
242. Verschueren H. Interference reflection microscopy in cell biology: Methodology and applications. *J Cell Sci*. 1985;75:279-301
243. Holt MR, Calle Y, Sutton DH, Critchley DR, Jones GE, Dunn GA. Quantifying cell-matrix adhesion dynamics in living cells using interference reflection microscopy. *J Microsc*. 2008;232:73-81
244. Zicha D, Dunn G, Jones G. Analyzing chemotaxis using the dunn direct-viewing chamber. *Methods Mol Biol*. 1997;75:449-457
245. Sprague BL, Pego RL, Stavreva DA, McNally JG. Analysis of binding reactions by fluorescence recovery after photobleaching. *Biophys J*. 2004;86:3473-3495

246. Rothballer A, Schwartz TU, Kutay U. Lincing complex functions at the nuclear envelope: What the molecular architecture of the linc complex can reveal about its function. *Nucleus*. 2013;4:29-36
247. Yang L, Munck M, Swaminathan K, Kapinos LE, Noegel AA, Neumann S. Mutations in lmna modulate the lamin a - nesprin-2 interaction and cause linc complex alterations. *PLoS One*. 2013;8:e71850
248. Parsons JT, Horwitz AR, Schwartz MA. Cell adhesion: Integrating cytoskeletal dynamics and cellular tension. *Nat Rev Mol Cell Biol*. 2010;11:633-643
249. Uehata M, Ishizaki T, Satoh H, Ono T, Kawahara T, Morishita T, Tamakawa H, Yamagami K, Inui J, Maekawa M, Narumiya S. Calcium sensitization of smooth muscle mediated by a rho-associated protein kinase in hypertension. *Nature*. 1997;389:990-994
250. Ishizaki T, Uehata M, Tamechika I, Keel J, Nonomura K, Maekawa M, Narumiya S. Pharmacological properties of y-27632, a specific inhibitor of rho-associated kinases. *Mol Pharmacol*. 2000;57:976-983
251. Tian Y, Autieri MV. Cytokine expression and aif-1-mediated activation of rac2 in vascular smooth muscle cells: A role for rac2 in vsmc activation. *Am J Physiol Cell Physiol*. 2007;292:C841-849
252. Rao KM, Cohen HJ. Actin cytoskeletal network in aging and cancer. *Mutat Res*. 1991;256:139-148
253. Hall A. Rho gtpases and the actin cytoskeleton. *Science*. 1998;279:509-514
254. Mayanagi T, Sobue K. Diversification of caldesmon-linked actin cytoskeleton in cell motility. *Cell adhesion & migration*. 2011;5:150-159
255. Ilic D, Furuta Y, Kanazawa S, Takeda N, Sobue K, Nakatsuji N, Nomura S, Fujimoto J, Okada M, Yamamoto T. Reduced cell motility and enhanced focal adhesion contact formation in cells from fak-deficient mice. *Nature*. 1995;377:539-544
256. Beningo KA, Dembo M, Kaverina I, Small JV, Wang YL. Nascent focal adhesions are responsible for the generation of strong propulsive forces in migrating fibroblasts. *J Cell Biol*. 2001;153:881-888
257. Hellstrom M, Kalen M, Lindahl P, Abramsson A, Betsholtz C. Role of pdgf-b and pdgfr-beta in recruitment of vascular smooth muscle cells and pericytes during embryonic blood vessel formation in the mouse. *Development*. 1999;126:3047-3055
258. Ferns GA, Raines EW, Sprugel KH, Motani AS, Reidy MA, Ross R. Inhibition of neointimal smooth muscle accumulation after angioplasty by an antibody to pdgf. *Science*. 1991;253:1129-1132
259. Pickering JG, Uniyal S, Ford CM, Chau T, Laurin MA, Chow LH, Ellis CG, Fish J, Chan BM. Fibroblast growth factor-2 potentiates vascular smooth muscle cell migration to platelet-derived growth factor: Upregulation of alpha2beta1 integrin and disassembly of actin filaments. *Circ Res*. 1997;80:627-637
260. Yin H, van der Veer E, Frontini MJ, Thibert V, O'Neil C, Watson A, Szasz P, Chu MW, Pickering JG. Intrinsic directionality of migrating vascular smooth muscle cells is regulated by nad(+) biosynthesis. *J Cell Sci*. 2012;125:5770-5780
261. Petrie RJ, Doyle AD, Yamada KM. Random versus directionally persistent cell migration. *Nat Rev Mol Cell Biol*. 2009;10:538-549
262. Moissoglu K, Schwartz MA. Integrin signalling in directed cell migration. *Biology of the cell / under the auspices of the European Cell Biology Organization*. 2006;98:547-555
263. Pankov R, Endo Y, Even-Ram S, Araki M, Clark K, Cukierman E, Matsumoto K, Yamada KM. A rac switch regulates random versus directionally persistent cell migration. *J Cell Biol*. 2005;170:793-802
264. Reed MJ, Ferara NS, Vernon RB. Impaired migration, integrin function, and actin cytoskeletal organization in dermal fibroblasts from a subset of aged human donors. *Mech Ageing Dev*. 2001;122:1203-1220

265. Rocnik EF, Chan BM, Pickering JG. Evidence for a role of collagen synthesis in arterial smooth muscle cell migration. *J Clin Invest*. 1998;101:1889-1898
266. Li S, Chow LH, Pickering JG. Cell surface-bound collagenase-1 and focal substrate degradation stimulate the rear release of motile vascular smooth muscle cells. *J Biol Chem*. 2000;275:35384-35392
267. Theisen U, Straube E, Straube A. Directional persistence of migrating cells requires kif1c-mediated stabilization of trailing adhesions. *Dev Cell*. 2012;23:1153-1166
268. Arnesen SM, Lawson MA. Age-related changes in focal adhesions lead to altered cell behavior in tendon fibroblasts. *Mech Ageing Dev*. 2006;127:726-732
269. Li Z, Froehlich J, Galis ZS, Lakatta EG. Increased expression of matrix metalloproteinase-2 in the thickened intima of aged rats. *Hypertension*. 1999;33:116-123
270. Nikkari ST, Koistinaho J, Jaakkola O. Changes in the composition of cytoskeletal and cytocontractile proteins of rat aortic smooth muscle cells during aging. *Differentiation; research in biological diversity*. 1990;44:216-221
271. Orlandi A, Bochaton-Piallat ML, Gabbiani G, Spagnoli LG. Aging, smooth muscle cells and vascular pathobiology: Implications for atherosclerosis. *Atherosclerosis*. 2006;188:221-230
272. Jaffe AB, Hall A. Rho gtpases: Biochemistry and biology. *Annu Rev Cell Dev Biol*. 2005;21:247-269
273. Boureux A, Vignal E, Faure S, Fort P. Evolution of the rho family of ras-like gtpases in eukaryotes. *Mol Biol Evol*. 2007;24:203-216
274. Ridley AJ. Rho gtpases and cell migration. *J Cell Sci*. 2001;114:2713-2722
275. Tapon N, Hall A. Rho, rac and cdc42 gtpases regulate the organization of the actin cytoskeleton. *Curr Opin Cell Biol*. 1997;9:86-92
276. Glogauer M, Marchal CC, Zhu F, Worku A, Clausen BE, Foerster I, Marks P, Downey GP, Dinauer M, Kwiatkowski DJ. Rac1 deletion in mouse neutrophils has selective effects on neutrophil functions. *J Immunol*. 2003;170:5652-5657
277. Wickstrom SA, Alitalo K, Keski-Oja J. Endostatin associates with lipid rafts and induces reorganization of the actin cytoskeleton via down-regulation of rhoa activity. *J Biol Chem*. 2003;278:37895-37901
278. Ai S, Kuzuya M, Koike T, Asai T, Kanda S, Maeda K, Shibata T, Iguchi A. Rho-rho kinase is involved in smooth muscle cell migration through myosin light chain phosphorylation-dependent and independent pathways. *Atherosclerosis*. 2001;155:321-327
279. Aktories K, Just I. Clostridial rho-inhibiting protein toxins. *Curr Top Microbiol Immunol*. 2005;291:113-145
280. Ren XD, Kiosses WB, Schwartz MA. Regulation of the small gtp-binding protein rho by cell adhesion and the cytoskeleton. *EMBO J*. 1999;18:578-585
281. Ren XD, Kiosses WB, Sieg DJ, Otey CA, Schlaepfer DD, Schwartz MA. Focal adhesion kinase suppresses rho activity to promote focal adhesion turnover. *J Cell Sci*. 2000;113 (Pt 20):3673-3678
282. Kishi H, Bao J, Kohama K. Inhibitory effects of ml-9, wortmannin, and y-27632 on the chemotaxis of vascular smooth muscle cells in response to platelet-derived growth factor-bb. *J Biochem*. 2000;128:719-722
283. Miao L, Calvert JW, Tang J, Parent AD, Zhang JH. Age-related rhoa expression in blood vessels of rats. *Mech Ageing Dev*. 2001;122:1757-1770
284. Carter SB. Principles of cell motility: The direction of cell movement and cancer invasion. *Nature*. 1965;208:1183-1187
285. Beningo KA, Dembo M, Wang YL. Responses of fibroblasts to anchorage of dorsal extracellular matrix receptors. *Proc Natl Acad Sci U S A*. 2004;101:18024-18029
286. McLennan R, Dyson L, Prather KW, Morrison JA, Baker RE, Maini PK, Kulesa PM. Multiscale mechanisms of cell migration during development: Theory and experiment. *Development*. 2012;139:2935-2944

287. Lei K, Zhang X, Ding X, Guo X, Chen M, Zhu B, Xu T, Zhuang Y, Xu R, Han M. Sun1 and sun2 play critical but partially redundant roles in anchoring nuclei in skeletal muscle cells in mice. *Proc Natl Acad Sci U S A*. 2009;106:10207-10212
288. Luxton GW, Gomes ER, Folker ES, Vintinner E, Gundersen GG. Linear arrays of nuclear envelope proteins harness retrograde actin flow for nuclear movement. *Science*. 2010;329:956-959
289. Luke Y, Zaim H, Karakesisoglou I, Jaeger VM, Sellin L, Lu W, Schneider M, Neumann S, Beijer A, Munck M, Padmakumar VC, Gloy J, Walz G, Noegel AA. Nesprin-2 giant (nuance) maintains nuclear envelope architecture and composition in skin. *J Cell Sci*. 2008;121:1887-1898
290. Muchir A, van Engelen BG, Lammens M, Mislow JM, McNally E, Schwartz K, Bonne G. Nuclear envelope alterations in fibroblasts from lgmd1b patients carrying nonsense y259x heterozygous or homozygous mutation in lamin a/c gene. *Exp Cell Res*. 2003;291:352-362
291. Libotte T, Zaim H, Abraham S, Padmakumar VC, Schneider M, Lu WS, Munck M, Hutchison C, Wehnert M, Fahrenkrog B, Sauder U, Aebi U, Noegel AA, Karakesisoglou L. Lamin a/c-dependent localization of nesprin-2, a giant scaffolder at the nuclear envelope. *Molecular Biology of the Cell*. 2005;16:3411-3424
292. Folker ES, Ostlund C, Luxton GW, Worman HJ, Gundersen GG. Lamin a variants that cause striated muscle disease are defective in anchoring transmembrane actin-associated nuclear lines for nuclear movement. *Proc Natl Acad Sci U S A*. 2011;108:131-136
293. Chen WT. Mechanism of retraction of the trailing edge during fibroblast movement. *J Cell Biol*. 1981;90:187-200
294. Fuhr G, Richter E, Zimmermann H, Hitzler H, Niehus H, Hagedorn R. Cell traces--footprints of individual cells during locomotion and adhesion. *Biol Chem*. 1998;379:1161-1173
295. Palecek SP, Schmidt CE, Lauffenburger DA, Horwitz AF. Integrin dynamics on the tail region of migrating fibroblasts. *J Cell Sci*. 1996;109 (Pt 5):941-952
296. Zimmermann H, Richter A, Reichle C, Geggier P, Rehn U, Rogaschewski S, Bleili W, Fuhr GR. Mammalian cell traces - morphology, molecular composition, artificial guidance and biotechnological relevance as a new type of 'bionanotube'. *Appled Physics A*. 2001;73:11-26
297. Bereiter-Hahn J, Voth M. Ionic control of locomotion and shape of epithelial cells: Ii. Role of monovalent cations. *Cell Motil Cytoskeleton*. 1988;10:528-536
298. Naito M, Hayashi T, Funaki C, Kuzuya M, Asai K, Yamada K, Kuzuya F. Vitronectin-induced haptotaxis of vascular smooth muscle cells in vitro. *Exp Cell Res*. 1991;194:154-156
299. Gaggioli C, Hooper S, Hidalgo-Carcedo C, Grosse R, Marshall JF, Harrington K, Sahai E. Fibroblast-led collective invasion of carcinoma cells with differing roles for rhogtpases in leading and following cells. *Nat Cell Biol*. 2007;9:1392-1400
300. Baetscher M, Pumplin DW, Bloch RJ. Vitronectin at sites of cell-substrate contact in cultures of rat myotubes. *J Cell Biol*. 1986;103:369-378
301. Ingber DE. Tensegrity ii. How structural networks influence cellular information processing networks. *J Cell Sci*. 2003;116:1397-1408
302. Na S, Collin O, Chowdhury F, Tay B, Ouyang M, Wang Y, Wang N. Rapid signal transduction in living cells is a unique feature of mechanotransduction. *Proc Natl Acad Sci U S A*. 2008;105:6626-6631
303. Anno T, Sakamoto N, Sato M. Role of nesprin-1 in nuclear deformation in endothelial cells under static and uniaxial stretching conditions. *Biochem Biophys Res Commun*. 2012;424:94-99
304. Csiszar A, Sosnowska D, Wang M, Lakatta EG, Sonntag WE, Ungvari Z. Age-associated proinflammatory secretory phenotype in vascular smooth muscle

cells from the non-human primate macaca mulatta: Reversal by resveratrol treatment. *J Gerontol A Biol Sci Med Sci*. 2012;67:811-820
305. Liu Y, Drozdov I, Shroff R, Beltran LE, Shanahan CM. Prelamin a accelerates vascular calcification via activation of the DNA damage response and senescence-associated secretory phenotype in vascular smooth muscle cells. *Circ Res*. 2013;112:e99-109
306. Vitorino P, Meyer T. Modular control of endothelial sheet migration. *Genes Dev*. 2008;22:3268-3281
307. Patsialou A, Bravo-Cordero JJ, Wang Y, Entenberg D, Liu H, Clarke M, Condeelis J. Intravital multiphoton imaging reveals multicellular streaming as a crucial component of in vivo cell migration in human breast tumors. *IntraVital*. 2013;2
308. Ilina O, Friedl P. Mechanisms of collective cell migration at a glance. *J Cell Sci*. 2009;122:3203-3208
309. Kriebel PW, Barr VA, Rericha EC, Zhang G, Parent CA. Collective cell migration requires vesicular trafficking for chemoattractant delivery at the trailing edge. *J Cell Biol*. 2008;183:949-961
310. Mayer C, Maaser K, Daryab N, Zanker KS, Brocker EB, Friedl P. Release of cell fragments by invading melanoma cells. *Eur J Cell Biol*. 2004;83:709-715
311. Zhan R, Leng X, Liu X, Wang X, Gong J, Yan L, Wang L, Wang Y, Wang X, Qian LJ. Heat shock protein 70 is secreted from endothelial cells by a non-classical pathway involving exosomes. *Biochem Biophys Res Commun*. 2009;387:229-233
312. Hood JL, Pan H, Lanza GM, Wickline SA, Consortium for Translational Research in Advanced I, Nanomedicine. Paracrine induction of endothelium by tumor exosomes. *Lab Invest*. 2009;89:1317-1328
313. Sheldon H, Heikamp E, Turley H, Dragovic R, Thomas P, Oon CE, Leek R, Edelmann M, Kessler B, Sainson RC, Sargent I, Li JL, Harris AL. New mechanism for notch signaling to endothelium at a distance by delta-like 4 incorporation into exosomes. *Blood*. 2010;116:2385-2394
314. van Balkom BW, de Jong OG, Smits M, Brummelman J, den Ouden K, de Bree PM, van Eijndhoven MA, Pegtel DM, Stoorvogel W, Wurdinger T, Verhaar MC. Endothelial cells require mir-214 to secrete exosomes that suppress senescence and induce angiogenesis in human and mouse endothelial cells. *Blood*. 2013;121:3997-4006, S3991-3915
315. Wyckoff J, Wang W, Lin EY, Wang Y, Pixley F, Stanley ER, Graf T, Pollard JW, Segall J, Condeelis J. A paracrine loop between tumor cells and macrophages is required for tumor cell migration in mammary tumors. *Cancer Res*. 2004;64:7022-7029